THE UNIVERSITY *of* EDINBURGH

Measurement of the CP violating phase ϕ_s using $B_s^0 \to J/\psi K^+ K^-$ decays at the LHCb Experiment

Jennifer Zonneveld

Doctor of Philosophy
The University of Edinburgh
April 2020

Abstract

The LHCb experiment at the Large Hadron Collider (LHC) at CERN is designed to search for indirect evidence of physics beyond the Standard Model (SM) in *CP* violation and rare decays of beauty and charm hadrons. One of the key measurements is the *CP* violating phase ϕ_s, that arises from the interference between the decay of B_s^0 mesons into *CP* eigenstates directly and via $B_s^0 - \overline{B}_s^0$ mixing.

In this thesis, the phase ϕ_s is measured in the $B_s^0 \to J/\psi K^+ K^-$ decay channel using 1.9 fb^{-1} of proton-proton collisions collected at a centre-of-mass energy of $\sqrt{s} = 13$ TeV. Other parameters that are measured are the average decay width of the B_s^0 meson with respect to that of the B_d^0 meson, $\Gamma_s - \Gamma_d$, the difference in decay widths of the heavy and light mass eigenstates of the $B_s^0 - \overline{B}_s^0$ system, $\Delta\Gamma_s$, and a further parameter that describes the *CP* violation in interference between mixing and decay, $|\lambda|$. The following results are obtained:

$$\begin{aligned} \phi_s &= -0.080 \pm 0.041 \pm 0.006 \text{ rad} \\ \Gamma_s - \Gamma_d &= -0.0041 \pm 0.0024 \pm 0.0015 \text{ ps}^{-1} \\ \Delta\Gamma_s &= 0.0764 \pm 0.0077 \pm 0.0026 \text{ ps}^{-1} \\ |\lambda| &= 1.014 \pm 0.016 \pm 0.006 \end{aligned} \tag{1}$$

These are the most precise measurements using a single decay channel. Combining this analysis with other decay channels measured at the LHCb experiment that are sensitive to ϕ_s yields the most precise measurements to date:

$$\begin{aligned} \phi_s &= -0.042 \pm 0.025 \text{ rad} \\ \Gamma_s &= 0.6566 \pm 0.0021 \text{ ps}^{-1} \\ \Delta\Gamma_s &= 0.0811 \pm 0.0048 \text{ ps}^{-1} \\ |\lambda| &= 0.993 \pm 0.010 \end{aligned} \tag{2}$$

Lay Summary

The Universe that we observe today is predominantly made out of matter, there is only a small amount of antimatter. The Standard Model of particle physics includes a matter-antimatter asymmetry due to a difference in behaviour between particles and antiparticles, a process called *CP* violation. However, the amount of asymmetry predicted by the Standard Model only accounts for a very small fraction of the observed abundance. The LHCb experiment at the Large Hadron Collider at CERN is designed to search for indirect evidence of physics beyond the Standard Model in *CP* violation.

The analysis presented in this thesis focuses on the decay of a b-hadron, the B_s^0 meson. By measuring the decay properties, unexpected differences between matter and antimatter could be observed. One of the properties is a *CP* violating parameter that is precisely predicted by the Standard Model and a significant deviation would be a hint for yet unknown physics phenomena. Previous measurements are in agreement with the prediction, however a lot is yet to gain in the experimental precision. This thesis uses data collected by the LHCb experiment in the years 2015 and 2016 to measure the B_s^0 meson decay. A combination with previously conducted analyses will drive the experimental precision towards the theoretical prediction.

Declaration

I declare that this thesis was composed by myself, that the work contained herein is my own except where explicitly stated otherwise in the text, and that this work has not been submitted for any other degree or professional qualification except as specified.

Parts of this work have been published in [1].

(*Jennifer Zonneveld, April 2020*)

Acknowledgements

First and foremost, I would like to thank my supervisor Pete Clarke for his guidance and expertise throughout my entire PhD. His constructive feedback and support in any situation meant a great deal to me. I am grateful for Franz Muheim his support to do my PhD at the Edinburgh PPE group, leading to great unexpected experiences. The group has been invaluable to my PhD both on a scientific and social level. In particular I want to express my gratitude towards Konstantin Gizdov, who always helped me when needed throughout my PhD, and Emmy Gabriel for being the best office partner I could imagine. I also thank Greig Cowan, Silvia Gambetta and Rob Currie for sharing their knowledge to guide me. A special thanks to Yanyan Gao and Gary Robertson for keeping me sane throughout the thesis writing.

Next, I want to thank Francesca, Veronika, Sevda, Katya, Diego, Simon, Gerard, Liming, Miriam and Wenhua for the fruitful collaboration during the research. As well as all of the other great physicists that I have met and worked with throughout my PhD. Thanks to the LHCb collaboration and CERN for providing the recourses to make my research possible.

The four years I spent working towards this PhD have been an unforgettable experience. It would not have been the same without the friends that I have made along the way both inside and outside the world of physics. Finally, but by no means least, I would like to express my gratitude towards my family and friends for their support, energy and patience. Especially towards my parents who have always been just a phone call away when needed.

Contents

List of Figures

List of Tables

Chapter 1

Introduction

The behaviour of nature is summarised in a single theory: the Standard Model of elementary particle physics. It describes the interaction between the building blocks of our world as well as three of the four fundamental forces: the strong, weak, and electromagnetic interaction. The SM has successfully explained almost all experimental results and precisely predicted a wide variety of phenomena. However, it is unable to resolve some of the ongoing mysteries in the Universe. First, the fourth fundamental force, gravity, is not included in this framework. Moreover, the matter-antimatter asymmetry is too small to explain the matter abundance. The SM does not include dark matter and dark energy, which, through observations, is found to make up about 95% of the Universe [2]. Because of these, and more unexplained puzzles, the SM is considered as a low-energy effective description of a more complete, but unknown, theory of particle physics. Direct and indirect searches for New Physics (NP) beyond the SM will provide insights into the properties of this more complete theory.

The Universe as we observe it today is predominantly made out of matter, there is only a small amount of antimatter. A particle and its anti-particle have the same mass and opposite charge (colour charge, weak isospin and electric charge), and, normally when they meet, they annihilate. A very small fraction of the matter abundance observed in the Universe can be explained by the processes that are known today. Hunts for as yet unknown physical behaviours are being pursued to discover the source of the large matter-antimatter asymmetry.

The matter abundance observed in our Universe is believed to originate from the first few moments after the Big Bang. After approximately 10^{-6} s, a

quark-gluon plasma was present where unbound quarks and gluons were moving with relativistic velocities. Particle-antiparticle pairs were continuously created and annihilated, and hence the abundance was equal. At some point, while temperature was decreasing, processes occurred that led to a difference in the interactions of matter with respect to antimatter. This is called *baryogenesis*, and caused more matter than antimatter to be created.

In 1967 Sakharov identified three requirements to cause the different behaviour between matter and antimatter [3]: there must be a process that violates conservation of baryon number, the Universe must be out of thermal equilibrium, and there must be processes with a difference in the rate of decay to particles and to antiparticles. The last requirement is known as CP violation; it is a violation of the combined symmetry of charge (C) conjugation and space inversion or parity (P) operation.

CP violation was first detected in the weak decay of neutral kaon mesons in 1964 by Cronin and Fitch [4]. This observation was a big surprise, as it could not be explained by the existing theories based on the three quarks types that were known at the time: up, down and strange. In 1973, the Cabibbo-Kobayashi-Maskawa (CKM) quark mixing matrix included CP violation in the SM, which led to the proposed and subsequent discovery of the third family of quarks [5]. The CKM matrix includes an irreducible non-trivial complex phase, and could therefore introduce differences in the weak transitions of particles and antiparticles. The kaon system shows matter-antimatter asymmetry effects of about 10^{-3}, however, in weak transitions involving bottom quarks the asymmetries can become much larger. These transitions can be studied in B-meson decays, which provide an improved testing ground for the SM and CKM mechanism.

In 1999 BaBar at the PEP-II collider and Belle at the KEK-B collider started their b-physics studies by asymmetrically accelerating electrons and positrons. The Babar experiment used beam energies for the electrons of 9 GeV and positrons of 3.1 GeV, while the Belle experiment accelerated electrons to 8 GeV and positrons to 3.5 GeV [6]. These accelerators are known as B-factories, since they operated at a centre-of-mass energy tuned to the $\Upsilon(4S)$ resonance, a $b\bar{b}$ meson which predominantly decays into a B^+B^- or $B^0\bar{B}^0$ pair. At the same time, the CDF and DØ experiments at the Tevatron collider were studying b-physics by taking data of proton-antiproton ($p\bar{p}$) collisions with collision energies up to 2 TeV [7]. Due to the hadronic environment heavier particles as B_s^0, B_c^+ and b-baryons could

be produced. In the meantime the LHCb detector was being build at the LHC with the same purpose, to study b-physics and CP violation, in proton-proton (pp) collisions at higher energies up to 14 TeV, and started operating in 2010. LHCb has further sharpened the picture of the SM flavour sector and will continue doing so in the years to come.

1.1 Thesis Outline

The outline of this thesis is the following. Chapter 2 gives an overview of the theoretical background and motivation behind the analysis, covering the SM, CKM matrix, CP violation, the decay mode of interest $B_s^0 \to J/\psi K^+K^-$, and the phase ϕ_s. Chapter 3 discusses the LHC and the LHCb experiment, covering all sub-detectors separately and additionally the trigger system. Chapter 4 then focuses on the event selection of the signal and control channels. Decision Trees are discussed in detail. Chapter 5 describes the experimental effects that have to be taken into account in the analysis to determine ϕ_s. Chapter 6 explains the maximum-likelihood fit to data performed using the `RapidFit` framework, and presents the final results. Chapter 7 summarises the systematic uncertainties. The analysis of 2015 and 2016 data has been published and yields the most precise single measurement of ϕ_s. Chapter 8 covers the combination with other analyses at LHCb that are sensitive to ϕ_s and the inclusion of correlations between them. A summary and outlook is discussed in Chapter 9.

Chapter 2

Theory

2.1 The Standard Model

The Standard Model of elementary particle physics is a theoretical framework that describes the current knowledge of the fundamental particles and the forces through which particles interact. During the 1960s and early 1970s descriptions were formulated of the strong interaction by *Quantum Chromodynamics* (QCD) [8], and of the electromagnetic and weak forces in a theory of *electroweak interactions* [9]. Both theories are based on Quantum Field Theory (QFT), in which quarks and leptons are described as fermionic fields that interact via bosonic fields, and are unified in the SM [10]. The observation of the predicted missing three particles - the top quark (1995 [11, 12]), tau neutrino (2000 [13]) and the Higgs boson (2012 [14, 15]) - have led to strong credence in the SM.

Figure 2.1 shows the particle content of the SM. It describes twelve fermion fields (quarks and leptons), twelve gauge bosons fields (eight g, W^+, W^-, Z^0 and γ), and a complex scalar doublet field (the Higgs boson). The gluons are the mediators of the strong interaction, the W and Z bosons of the weak interaction, and the photon of the electromagnetic interaction. The Higgs field causes particles to acquire mass via the *Brout-Englert-Higgs mechanism* [16]. Quarks and leptons are divided into three generations, based on similar physical behaviour.

The strong interaction combines quarks into hadrons and nucleons into nuclei. Its charge is referred to as *colour*, which can be red (R), green (G) or blue (B) for quarks, and antired ($\bar{R}$), antiblue ($\bar{B}$) or antigreen ($\bar{G}$) for antiquarks. The

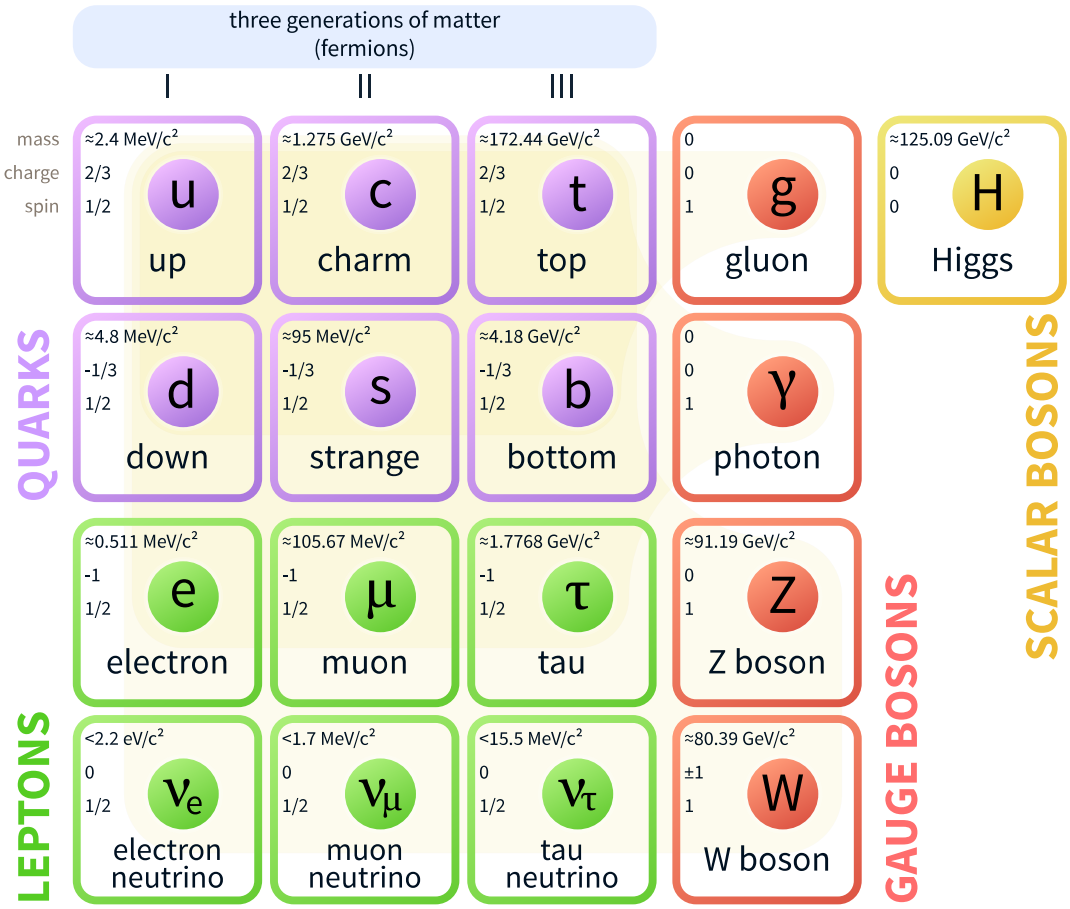

Figure 2.1 *The Standard Model with its particle content [17].*

quarks are bound into neutral combinations of colours as (e.g.):

$$R\bar{R} = G\bar{G} = B\bar{B} = RGB = \bar{R}\bar{G}\bar{B} = 0 \text{ [18]}. \tag{2.1}$$

Eight massless vector boson fields (the gluons) mediate the interaction with coupling strength g_s. They are electrically neutral, have zero weak isospin and carry combinations of colour and anticolour. The strong force increases in strength with decreasing distance. This makes it impossible to completely separate coloured particles. Consequently, quarks and gluons are *confined* within colour-neutral objects, such as hadrons. Interestingly enough, experiments have shown that when quarks are probed at very short distances, quarks seem to move almost freely, which is referred to as *asymptotic freedom*. The theory of QCD describes this behaviour and the colour fields. There are six *flavours* of quarks, categorised into three generations. The lightest generation, the up (u) and down (d) quarks, makes up protons and neutrons. The second and third pair, the

charm (c) and strange (s) quarks and the top (t) and bottom (b) quarks, follow in order of mass and time of discovery. Of each combination one quark has electric charge $+2/3$ and weak isospin $+1/2$ (u, c, t), and its partner electric charge $-1/3$ and weak isospin $-1/2$ (d, s, b).

The electromagnetic force carrier is the massless, colour and electrically neutral photon which interacts with coupling strength $\sqrt{\alpha}$. The photon couples to electrically charged particles with an infinite range. The massive W^+, W^- and Z^0 bosons are the carriers of the weak interaction, a short-range force. For the decay of a (heavy) quark or lepton the transition to one of the lighter quarks or leptons is required. In the SM, this *flavour change* is only possible in a weak interaction that is mediated by the $W^\pm$ boson. The interaction is similar to that of the electromagnetic force, except the coupling strength is given by the weak charge, $\sqrt{\alpha_W}$. The mixing of quark flavours is discussed in more detail in Section 2.2.

S. Weinberg [19] and A. Salam [20] proposed the existence of the weak bosons in 1967, and combined the electromagnetic and weak forces into a single theory. The *electroweak* theory postulates that both forces become equivalent at very high energies. The so-called electroweak force is mediated by four massless spin-1 particles, a triplet W (W^1, W^2 and W^3) and a singlet B. The particles couple with strength g and g', respectively. At lower energy, the electroweak gauge symmetry is spontaneously broken by the *Higgs mechanism*. As a result, the weak and electromagnetic neutral bosons (Z^0 and γ) are a linear combination of W^3 and B, and $W^\pm$ of W^1 and W^2. The Higgs mechanism predicts the massive spin-0 Higgs boson, H, and generates masses for the massive particles in the SM, i.e. the $W^\pm$ and Z^0 bosons, but also for the fermions and quarks via the Yukawa terms in the SM Lagrangian.

The charged weak force carriers only couple to left-handed particle states and right-handed antiparticle states. A charge conjugation transforms the particle into its antiparticle, and parity conjugation inverts spatial coordinates, which transforms left-handed states into right-handed states. The majority of SM interactions are invariant under the combined CP operation, treating matter and antimatter the same way. The only CP violating processes involve the flavour changing weak interaction. Hence they provide a test of the matter-antimatter asymmetry in the SM. The flavour changing weak interaction will be discussed in the following section.

2.2 Quark Mixing

In the SM, *CP* violation is induced by a complex phase in the CKM matrix [5, 21]. This matrix originates from the Yukawa couplings of the quarks to the Higgs field in the SM Lagrangian from which quarks acquire their masses. The CKM matrix is chosen, by convention, to be a rotation between the flavour and mass eigenstates of the down type quarks (d, s, b) as follows:

$$\begin{pmatrix} d' \\ s' \\ b' \end{pmatrix} = \begin{pmatrix} V_{ud} & V_{us} & V_{ub} \\ V_{cd} & V_{cs} & V_{cb} \\ V_{td} & V_{ts} & V_{tb} \end{pmatrix} \begin{pmatrix} d \\ s \\ b \end{pmatrix}. \tag{2.2}$$

The CKM matrix is based on the fact that quark mass eigenstates are superpositions of the flavour eigenstates. The definition of the CKM matrix implies that the mass eigenstates of the up-type quarks are identical to the flavour eigenstates. As a result, there is a certain chance for an up-type quark to transform into any of the down-type quarks. The probability of such a transition is governed by the respective CKM element:

$$P(i \to j) \propto |V_{ij}|^2. \tag{2.3}$$

The CKM matrix is a 3×3 unitary matrix, and has therefore three mixing angles and one complex phase. The Wolfenstein parametrisation [22] is a commonly used approximation, because it includes valuable experimental information. It represents the CKM terms in three real parameters (λ, A, ρ) and an imaginary one ($i\eta$) as follows:

$$V_{CKM} = \begin{pmatrix} 1 - \frac{1}{2}\lambda^2 & \lambda & A\lambda^3(\rho - i\eta) \\ -\lambda & 1 - \frac{1}{2}\lambda^2 & A\lambda^2 \\ A\lambda^3(1 - \rho - i\eta) & -A\lambda^2 & 1 \end{pmatrix} + \mathcal{O}(\lambda^4). \tag{2.4}$$

The four parameters are of the same order ($\lambda \approx 0.23$, $A \approx 0.81$, $\rho \approx 0.14$, $\eta \approx 0.35$), hence it is trivial to estimate the magnitude of each element from the number of powers of λ. The CKM matrix has a *hierarchical* structure: the elements on the diagonal - the coupling between up-type and down-type quarks of the same generation - are close to unitary and the strength decreases for elements further from the diagonal. This suppression between generations is called *Cabibbo suppression*. Nine unitary relationships can be constructed from the CKM matrix, six of which sum to zero and can therefore be represented as *unitary triangles* in

the complex plane. By convention, these unitary triangles are normalised such that one side has unit length and points along the real axis. Each of the six triangles has a different shape, but have the same area. Two of the relations are of main interest for LHCb, since they govern the dynamics in the B^0 and B_s^0 meson systems:

$$B^0 : V_{ud}V_{ub}^* + V_{cd}V_{cb}^* + V_{td}V_{tb}^* = 0, \tag{2.5}$$

$$B_s^0 : V_{us}V_{ub}^* + V_{cs}V_{cb}^* + V_{ts}V_{tb}^* = 0. \tag{2.6}$$

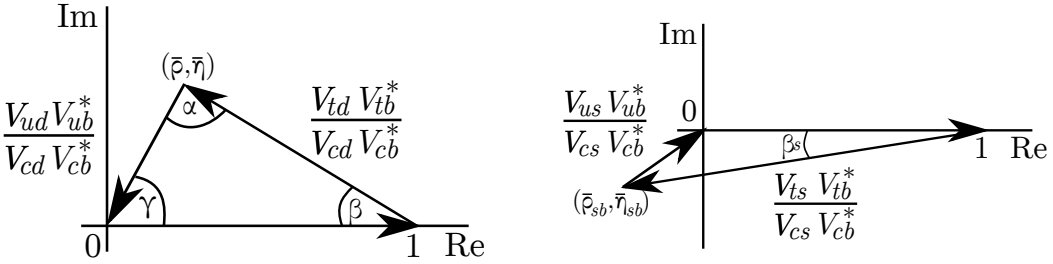

Figure 2.2 *CKM unitarity triangles for the B^0 (left) and the B_s^0 (right) mesons. Note the triangles are not drawn to scale.*

The corresponding triangles are shown in Figure 2.2, after dividing the relations by $V_{cd}V_{cb}^*$ and $V_{cs}V_{cb}^*$ for the B^0 and B_s^0 meson, respectively. From the triangles the angles in Equation 2.7 can be defined, which can be measured experimentally.

$$\begin{aligned} \alpha = \left(-\frac{V_{td}V_{tb}^*}{V_{ud}V_{ub}^*} \right), \quad \beta = \left(-\frac{V_{cd}V_{cb}^*}{V_{td}V_{tb}^*} \right), \quad \gamma = \left(-\frac{V_{ud}V_{ub}^*}{V_{cd}V_{cb}^*} \right), \\ \beta_s = \left(-\frac{V_{ts}V_{tb}^*}{V_{cs}V_{cb}^*} \right). \end{aligned} \tag{2.7}$$

All three sides of the B^0 triangle are of similar length, leading to large angles. The complex phase for the B_s^0 relation is present in the V_{ts} term. It only arises for higher orders, as the phase is only apparent at $\mathcal{O}(\lambda^4)$, leading to a very small value for β_s. The complex phase β_s is of one of the main interests in this thesis. The decay mode $B_s^0 \to J/\psi(\to \mu^+\mu^-)\phi(\to K^+K^-)$ is one of the channels in which this phase can be probed.

The observed hierarchy of the CKM elements is still a mystery. One of the main goals of flavour physics is to confirm the CKM picture. Measurements of different parameters of flavour physics lead to constraints on the CKM unitarity triangles, as presented in Figure 2.3. The location of the apexes of the B^0 and B_s^0 unitarity

triangles lead by definition to:

$$\bar{\rho} + i\bar{\eta} = -\frac{V_{ud}V_{ub}^*}{V_{cd}V_{cb}^*}, \qquad \bar{\rho}_{sb} + i\bar{\eta}_{sb} = -\frac{V_{us}V_{ub}^*}{V_{cs}V_{cb}^*}. \tag{2.8}$$

The flavour physics parameter $\sin(2\beta)$ related to CP violation in the B-system leads to a constraint on one of the angles, ϵ_K is a measure of the CP violation in the K system and provides a constraint on the position of the apex, the CKM element $|V_{ub}|$ constrains one side of the triangles, and the mass difference Δm in the B^0 and B_s^0 mixing constrains another side. In the SM, the curves should be consistent with the position of the apexes of the unitarity triangles. The CKMfitter group performs a global fit to the measurements to test the internal consistency of the SM [23].

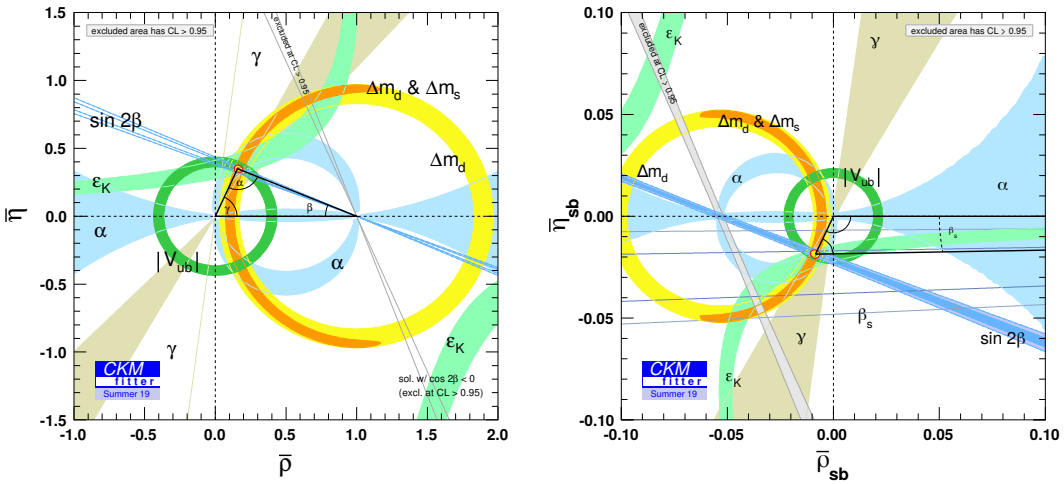

Figure 2.3 *The current (Summer 2019) constraints on the B^0 (left) and B_s^0 (right) unitarity triangle from experiments [23]. The coloured bands correspond to constraints on $\bar{\rho}$ and $\bar{\eta}$ ($\bar{\rho}_{sb}$ and $\bar{\eta}_{sb}$) from various measurements. α, β and γ (β_s) are the three (one) angles that arise in the B^0 (B_s^0) unitary triangle shown in the centre. Δm_s and Δm_d are the mass differences from $B_{s,d}^0$ mixing. ε_K is a CP violating parameter from the kaon sector.*

2.3 Neutral Meson Mixing and Decay

The neutral B_s^0 and $\overline{B}_s^0$ mesons have common mass and opposite flavour content: they contain the quarks $\bar{b}s$ and $b\bar{s}$, respectively. The B_s^0 system has two mass eigenstates, the heavy (B_H) and light (B_L) mass eigenstates. They have almost

the same masses and lifetimes of approximately 1.5×10^{-12} s. The mass eigenstates can be written as a linear combination of the flavour eigenstates:

$$\begin{aligned} |B_H\rangle &= p|B_s^0\rangle + q|\overline{B}_s^0\rangle \\ |B_L\rangle &= p|B_s^0\rangle - q|\overline{B}_s^0\rangle, \end{aligned} \tag{2.9}$$

where p and q are complex parameters that are normalised:

$$|p^2| + |q^2| = 1. \tag{2.10}$$

The time evolution of the mass eigenstates is given by the following simplified formalism in terms of their masses (m_H, m_L) and decay widths (Γ_H, Γ_L) [24]:

$$\begin{aligned} |B_H(t)\rangle &= e^{-im_H t - \frac{1}{2}\Gamma_H t}|B_H(0)\rangle \\ |B_L(t)\rangle &= e^{-im_L t - \frac{1}{2}\Gamma_L t}|B_L(0)\rangle. \end{aligned} \tag{2.11}$$

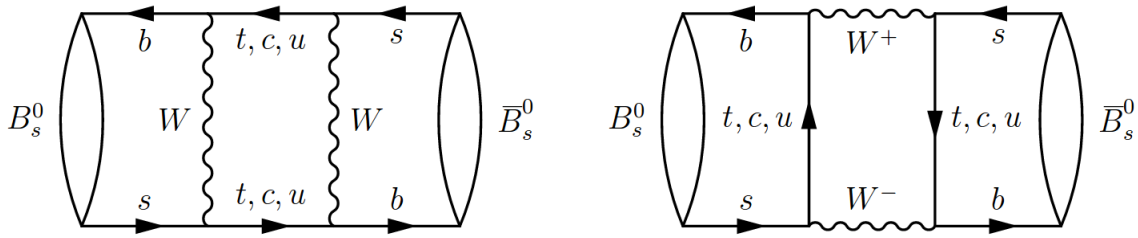

Figure 2.4 *Feynman diagrams for $B_s^0 - \overline{B}_s^0$ mixing within the SM.*

Quark mixing allows the flavour eigenstates of weakly decaying neutral mesons, i.e. K^0 ($\bar{s}d$), D^0 ($c\bar{u}$), B^0 ($\bar{b}d$) and B_s^0, to oscillate into their own antiparticle without violating conservation laws. This process can be illustrated by the Feynman diagrams in Figure 2.4. The internal quark contribution is dominated by the top quark, so one of the main factors for the B_s^0 mixing is $V_{ts}^2 \propto \lambda^2$, which for example explains the much faster oscillation rate than that of the B^0 mixing which is mainly influenced by $V_{td}^2 \propto \lambda^3$. From Equations 2.9 and 2.11, the time evolution of a B_s^0 meson produced in a particular flavour eigenstate at $t = 0$ is:

$$\begin{aligned} |B_s^0(t)\rangle &= g_+(t)|B_s^0(0)\rangle + \frac{q}{p}g_-(t)|\overline{B}_s^0(0)\rangle \\ |\overline{B}_s^0(t)\rangle &= \frac{p}{q}g_-(t)|B_s^0(0)\rangle + g_+(t)|\overline{B}_s^0(0)\rangle, \end{aligned} \tag{2.12}$$

with

$$g_\pm(t) = \frac{1}{2}(e^{-im_H t - \frac{1}{2}\Gamma_H t} \pm e^{-im_L t - \frac{1}{2}\Gamma_L t}). \tag{2.13}$$

The time evolution expressions of initially pure B_s^0 and $\overline{B}_s^0$ can be translated into the probability that the initial meson decays to a final state f at time t, defined as the time-dependent decay rate. The following will describe a simple case, corresponding to the central decay mode in this thesis $B_s^0 \to J/\psi(\to \mu^+\mu^-)\phi(\to K^+K^-)$ - from now on referred to as $B_s^0 \to J/\psi K^+K^-$-, where the final state can be obtained from the decay of both the B_s^0 and $\overline{B}_s^0$ meson. In this case the final state is a CP eigenstate with eigenvalue $\eta_f = \pm 1$:

$$CP|f_{CP}\rangle = \eta_f|f_{CP}\rangle. \tag{2.14}$$

The decay amplitudes of the B_s^0 and $\overline{B}_s^0$ into final state f are described as:

$$\begin{aligned} A_f(t) &= |\langle f|\mathcal{H}|B_s^0(t)\rangle|, A_f = |\langle f|\mathcal{H}|B_s^0(0)\rangle|, \\ \bar{A}_f(t) &= |\langle f|\mathcal{H}|\overline{B}_s^0(t)\rangle|, \bar{A}_f = |\langle f|\mathcal{H}|\overline{B}_s^0(0)\rangle|. \end{aligned} \tag{2.15}$$

The decay amplitudes squared provide the decay rates. By using the time evolution expressions in Equation 2.12, the following time-dependent decay rates are obtained for the B_s^0 and $\overline{B}_s^0$ meson:

$$\begin{aligned} \Gamma(B_s^0(t) \to f) &= |A_f|^2\left[|g_+(t)|^2 + \left|\frac{q}{p}\frac{\bar{A}_f}{A_f}\right|^2 |g_-(t)|^2 + 2\Re\left(\frac{q}{p}\frac{\bar{A}_f}{A_f}g_+^*(t)g_-(t)\right)\right], \\ \Gamma(\overline{B}_s^0(t) \to f) &= |A_f|^2\left|\frac{p}{q}\right|^2\left[|g_-(t)|^2 + \left|\frac{q}{p}\frac{\bar{A}_f}{A_f}\right|^2 |g_+(t)|^2 + 2\Re\left(\frac{q}{p}\frac{\bar{A}_f}{A_f}g_+(t)g_-^*(t)\right)\right]. \end{aligned} \tag{2.16}$$

The first term, proportional to $|A_f|^2$, is associated with a decay that occurred without oscillation; the second term is associated with a decay following a net oscillation; the third term is associated to the interference between the two cases. We introduce the complex parameter λ_f, which is used to parametrise one type of CP violation (see next section):

$$\lambda_f \equiv \frac{q}{p}\frac{\bar{A}_f}{A_f}. \tag{2.17}$$

From Equation 2.14 it follows that $\bar{A}_f = \eta_f \bar{A}_{\bar{f}}$, hence the complex parameter depends on the CP eigenvalue as:

$$\lambda_f = \eta_f \frac{q}{p}\frac{\bar{A}_{\bar{f}}}{A_f} \tag{2.18}$$

We furthermore derive the following from Equation 2.13:

$$
\begin{aligned}
|g_{\pm}(t)|^2 &= \frac{e^{-\Gamma_s t}}{2}\Big(\cosh(\tfrac{1}{2}\Delta\Gamma_s t) \pm \cos(\Delta m_s t)\Big) \\
g_{+}^{*}(t)g_{-}(t) &= \frac{e^{-\Gamma_s t}}{2}\Big(\sinh(\tfrac{1}{2}\Delta\Gamma_s t) + i\sin(\Delta m_s t)\Big) \\
g_{+}(t)g_{-}^{*}(t) &= \frac{e^{-\Gamma_s t}}{2}\Big(\sinh(\tfrac{1}{2}\Delta\Gamma_s t) - i\sin(\Delta m_s t)\Big),
\end{aligned}
\tag{2.19}
$$

where $\Gamma_s = (\Gamma_H + \Gamma_L)/2$, $\Delta\Gamma_s = \Gamma_H - \Gamma_L$ and $\Delta m_s = m_H - m_L$. These parameters are important observables of the $B_s^0 - \overline{B}_s^0$ system, and refer to the average decay width and the difference in decay width and mass between the two mass eigenstates, respectively. Note that the decay widths are the inverse of the corresponding lifetimes, $\Gamma = 1/\tau$. Substituting Equation 2.18 and 2.19 into 2.16 leads to the following master equations for the decay rates for neutral B_s^0 mesons:

$$
\begin{aligned}
\Gamma(B_s^0(t) \to f) &= |A_f|^2(1 + |\lambda_f|^2)\frac{e^{-\Gamma_s t}}{2}\times \\
&\qquad \Big(\cosh(\tfrac{1}{2}\Delta\Gamma_s t) + D\sinh(\tfrac{1}{2}\Delta\Gamma_s t) + C(\cos\Delta m_s t) - S\sin(\Delta m_s t)\Big), \\
\Gamma(\overline{B}_s^0(t) \to f) &= |A_f|^2\left|\frac{p}{q}\right|^2(1 + |\lambda_f|^2)\frac{e^{-\Gamma_s t}}{2}\times \\
&\qquad \Big(\cosh(\tfrac{1}{2}\Delta\Gamma_s t) + D\sinh(\tfrac{1}{2}\Delta\Gamma_s t) - C(\cos\Delta m_s t) + S\sin(\Delta m_s t)\Big),
\end{aligned}
\tag{2.20}
$$

with the following observables:

$$
D = -\frac{2\Re(\lambda_f)}{1 + |\lambda_f|^2}, \qquad C = \frac{1 - |\lambda_f|^2}{1 + |\lambda_f|^2}, \qquad S = \frac{2\Im(\lambda_f)}{1 + |\lambda_f|^2}. \tag{2.21}
$$

Here $C^2 + S^2 + D^2 = 1$.

2.4 *CP* Violation

The decay rate of a B-meson can differ from that of the *CP* conjugated process. *CP* violation can be categorised in the following three classifications:

1. ***CP* violation in decay** (direct *CP* violation). This type of *CP* violation happens when the decay rate of the B-meson to a final state f differs from

the decay rate of a $\overline{B}$-meson to the *CP* conjugated final state $\bar{f}$, meaning:

$$\left|\frac{\bar{A}_{\bar{f}}}{A_f}\right| \neq 1. \tag{2.22}$$

Experimentally, direct *CP* violation can be measured by the quantity A_{CP} defined in terms of the time-independent decay rates:

$$A_{CP} = \frac{\Gamma(B \to f) - \Gamma(\overline{B} \to \bar{f})}{\Gamma(B \to f) + \Gamma(\overline{B} \to \bar{f})} \tag{2.23}$$

2. ***CP* violation in mixing** (indirect *CP* violation). This implies that the oscillation from meson to antimeson is different from the oscillation from antimeson to meson. The quantity $\frac{q}{p}$ is the one related to oscillation, also referred to as mixing. *CP* violation in mixing is satisfied if:

$$\left|\frac{q}{p}\right| \neq 1. \tag{2.24}$$

3. ***CP* violation in interference between mixing and decay**. This form of *CP* violation is the one common for B^0 and B_s^0 mesons where the final state is a *CP* eigenstate, hence $f = \bar{f}$. In this case two amplitudes will contribute to the transition amplitude from the initial state $|B_s^0\rangle$ to a final state f, namely the one for direct decay, $A(B_s^0 \to f)$, and decay via mixing, $A(B_s^0 \to \overline{B}_s^0 \to f)$. Interference between the two paths leads to *CP* violation, and the *CP* asymmetry can be measured by the difference in the time-dependent decay rates:

$$A_{CP}(t) = \frac{\Gamma(B_s^0(t) \to f) - \Gamma(\overline{B}_s^0(t) \to f)}{\Gamma(B_s^0(t) \to f) + \Gamma(\overline{B}_s^0(t) \to f)}. \tag{2.25}$$

CP might be violated through interference even if it is not individually violated in decay or mixing, for which $|\lambda_f| = 1$. Using the decay rates defined in Equation 2.20, this leads to the following:

$$A_{CP}(t) = \frac{-\Im(\lambda_f)\sin(\Delta m_s t)}{\cosh(\frac{1}{2}\Delta\Gamma_s t) - \Re(\lambda_f)\sinh(\frac{1}{2}\Delta\Gamma_s t)}. \tag{2.26}$$

Hence, *CP* can still be violated if λ_f has a non-zero imaginary part. The

weak phase ϕ_s is defined to address the amount of *CP* violation:

$$\phi_s \equiv -\arg(\lambda_f) = -\arg\left(\eta_f \frac{q}{p}\frac{\bar{A}_f}{A_f}\right) \neq 0. \tag{2.27}$$

The decay mode $B_s^0 \to J/\psi K^+K^-$, which is central in this thesis, is subject to the third type of *CP* violation, and measuring the phase ϕ_s will be of special interest.

2.5 The Decay $B_s^0 \to J/\psi K^+K^-$ and Phase ϕ_s

As discussed in the previous section, *CP* violation is present for $B_s^0 \to J/\psi K^+K^-$ due to the phase that arises from interference between the two possible decay paths. The $B_s^0 \to J/\psi K^+K^-$ decay occurs in the SM via a $\bar{b} \to \bar{c}c\bar{s}$ transition predominantly at tree level as presented in Figure 2.5. As mentioned before, the neutral B_s^0 meson has the possibility to first oscillate into its antiparticle via the mixing diagram in Figure 2.4, and subsequently decay into the same final state. The direct decay gives rise to the weak phase $\phi_D = \arg(V_{cs}V_{cb}^*)$, while

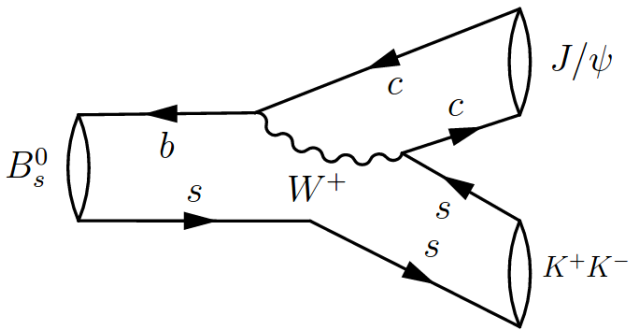

Figure 2.5 *Feynman diagram of the $B_s^0 \to J/\psi K^+K^-$ decay at tree level, the main contribution in the SM.*

the mixing process results in a mixing phase which is mainly dominated by the top quark exchange, $\phi_M = \arg[(V_{ts}V_{tb}^*)^2]$. The difference in phase between the two available paths shown in Figure 2.6 gives rise to the *CP* violating phase ϕ_s. Assuming the *CP* violation predicted by the SM and ignoring sub-leading penguin contributions, ϕ_s is directly related to the CKM angle β_s, which is previously

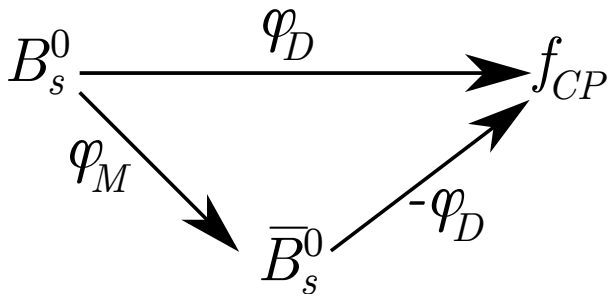

Figure 2.6 *Origin of the phase ϕ_s, which arises from the weak phase difference between the decay to the final state directly and via mixing.*

introduced in Equation 2.7:

$$\phi_s^{SM} = \phi_M - 2\phi_D = \arg[(V_{ts}V_{tb}^*)^2] - 2\arg(V_{cs}V_{cb}^*) = 2\arg\left(\frac{V_{ts}V_{tb}^*}{V_{cs}V_{cb}^*}\right) \equiv -2\beta_s. \tag{2.28}$$

The measurement of this phase is one of the main goals of this thesis. By performing a global fit to experimental data, assuming unitarity of the CKM matrix, the CKMfitter group determines this parameter to be $-2\beta_s = -0.0369^{+0.0010}_{-0.0007}$ rad [23]. This precise determination within the SM makes the measurement of ϕ_s very interesting since New Physics (NP) processes could modify the phase if new particles were to contribute to the $B_s^0 - \overline{B}_s^0$ box diagrams. Though the phase ϕ_s can be measured in additional $\bar{b} \to \bar{c}c\bar{s}$ transition decays, $B_s^0 \to J/\psi\ K^+K^-$ is considered to be the golden decay because it is relatively free from any theoretical uncertainty and unknown strong interaction phases, and it is experimentally interesting due to its high yield and easily recognisable signature in the detector.

Other important parameters that can be measured using the $B_s^0 \to J/\psi\ K^+K^-$ channel are the average decay width, Γ_s, and the difference in decay width between the two mass eigenstates, $\Delta\Gamma_s$, observables related to the $B_s^0 - \overline{B}_s^0$ system. In the SM precise predictions can be determined for these parameters [25]. Especially the lifetime or decay width ratios between different B-mesons have accurate values, due to the cancellation of common uncertainties. The following values are predicted:

$$\begin{aligned} (\Gamma_s/\Gamma_d)^{SM} &= 1.0006 \pm 0.0025\ [26] \\ \Delta\Gamma_s^{SM} &= 0.088 \pm 0.020\,\text{ps}^{-1}\ [27]. \end{aligned} \tag{2.29}$$

The high theoretical precisions make these quantities excellent testing cases of

the SM.

2.6 Polarisation Amplitudes

The decay of $B_s^0 \to J/\psi K^+K^-$ proceeds predominantly via $B_s^0 \to J/\psi\phi$ with the ϕ meson subsequently decaying into K^+K^-. In this case, the K^+K^- pair is in a P-wave configuration. Additionally, the K^+K^- pair can be in an S-wave state. The total decay amplitude of $B_s^0 \to J/\psi K^+K^-$ can be split into four independent amplitudes, where three originate from the P-wave state, as will be explained below, and one from the S-wave.

Three different amplitudes contribute to the $B_s^0 \to J/\psi\phi$ channel. The B_s^0 meson is a pseudo-scalar (spin 0), while the intermediate J/ψ and ϕ are both vector particles (spin 1). The polarisation vector of the vector particles can be pointing longitudinal, parallel or perpendicular to each other, resulting in three different polarisation amplitudes: A_0, $A_\parallel$ and $A_\perp$, respectively (see Figure 2.7). The total

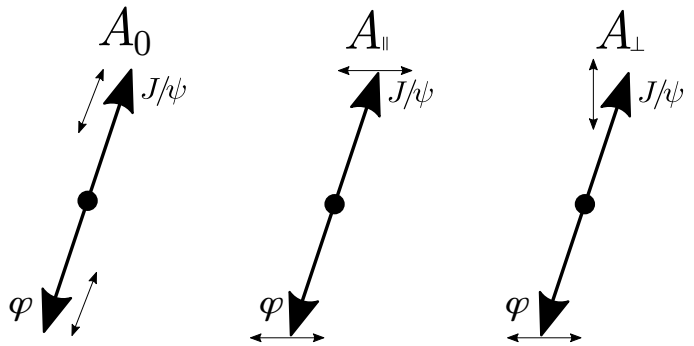

Figure 2.7 *The three different polarisations of the vector mesons for the different amplitudes contributing to the P-wave final state. A_0, $A_\parallel$ and $A_\perp$ represent the longitudinal, parallel and perpendicular polarisation, respectively. The small arrow represents the polarisation vector orientation of the meson.*

angular momentum (j) is zero before decay, hence should also be zero for the final state due to momentum conservation. The total angular momentum is the result of combining the orbital angular momentum (l) and spin (s). As a consequence, the A_0, $A_\parallel$ amplitudes can be in orbital angular momentum 0 or 2 states, and the $A_\perp$ can be in orbital angular momentum 1 state. This leads to the following

CP eigenvalues:

$$CP|J/\psi K^+K^-\rangle = \eta_f|J/\psi K^+K^-\rangle = (-1)^l|J/\psi K^+K^-\rangle, \tag{2.30}$$

resulting in CP-even ($l = 0, 2$) and CP-odd ($l = 1$) final states. The S-wave final state is a purely CP-odd state, and has amplitude A_S. Each of the four polarisation amplitudes - A_0, $A_\parallel$, $A_\perp$ and A_S - has an associated complex strong phase, which are δ_0, $\delta_\parallel$, $\delta_\perp$, and δ_S, respectively.

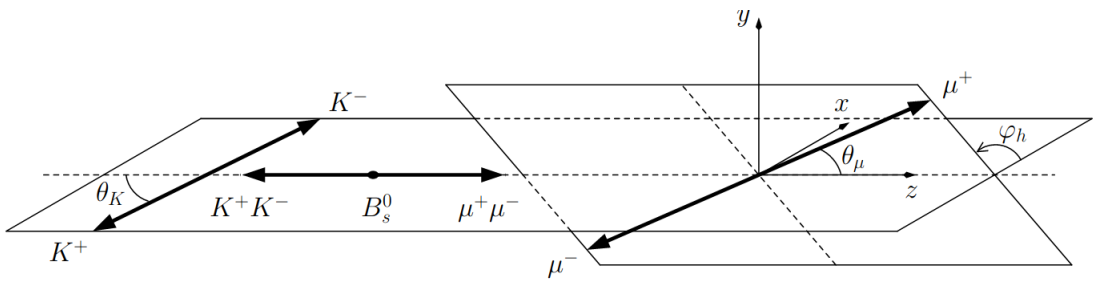

Figure 2.8 *Definition of helicity angles θ_K, θ_μ and ϕ_h as discussed in the text.*

Since the CP eigenvalue is $+1$ for the CP-even and -1 for the CP-odd components, the amplitude of the CP asymmetry in Equation 2.26 would be diluted depending on the relative fraction of the states. In order to optimally measure ϕ_s, the CP-even and CP-odd amplitudes have to be disentangled, which is done by analysing the distribution of the reconstructed decay angles of the final state. The decay angles are defined in the helicity basis as shown in Figure 2.8 and the helicity angles are denoted by $\vec{\Omega} = \{\cos\ \theta_K, \cos\ \theta_\mu, \phi_h\}$. Starting from the rest frame of the B_s^0, the helicity axis is defined by the directions of the K^+K^- and $\mu^+\mu^-$ momenta. The two polar angles θ_K and θ_μ are defined in the K^+K^- and $\mu^+\mu^-$ rest frames, respectively. The angle θ_K (θ_μ) is defined as the angle between the K^+ (μ^+) direction and the helicity axis. The azimuthal angle ϕ_h specifies the relative orientation of the K^+K^- and $\mu^+\mu^-$ decay planes. It is defined as the angle between the K^- side of the K^+K^- plane and the μ^+ side of the $\mu^+\mu^-$ plane. The rotation is positive in the direction of the $\mu^+\mu^-$ pair momentum.

2.7 Time- and Angular-dependent Decay Rate

By decomposing the time-dependent decay rate for the B_s^0 meson in Equation 2.20 in the P-wave and S-wave polarisations, its full time- and angular-dependent

differential decay rate can be expressed as a sum of ten terms, due to the four squared amplitudes and their interference terms [28]:

$$\frac{\mathrm{d}^4\Gamma(B_s^0 \to J/\psi K^+K^-)(t,\vec{\Omega})}{\mathrm{d}t\mathrm{d}\vec{\Omega}} \propto \sum_{k=1}^{10} h_k(t) f_k(\vec{\Omega}), \tag{2.31}$$

where the decay-time-dependent functions $h_k(t)$ are given as:

$$h_k(t) = N_k e^{-\Gamma_s t}\left[a_k \cosh\frac{\Delta\Gamma_s t}{2} + b_k \sinh\frac{\Delta\Gamma_s t}{2} + c_k \cos(\Delta m_s t) + d_k \sin(\Delta m_s t)\right]. \tag{2.32}$$

For an initial $\overline{B}_s^0$ at production, the signs of c_k and d_k should be reversed. The angular functions $f_k(\vec{\Omega})$ and coefficients N_k are given in Table 2.1, where the first are expressed in the helicity angles, and the latter in terms of the amplitudes. The coefficients a_k, b_k, c_k and d_k in the time-dependent functions $h_k(t)$ are defined

k	$f_k(\vec{\Omega})$	N_k
1	$2\cos^2\theta_K \sin^2\theta_\mu$	$\lvert A_0\rvert^2$
2	$\sin^2\theta_K(1-\sin^2\theta_\mu\cos^2\phi_h)$	$\lvert A_\parallel\rvert^2$
3	$\sin^2\theta_K(1-\sin^2\theta_\mu\sin^2\phi_h)$	$\lvert A_\perp\rvert^2$
4	$\sin^2\theta_K\sin^2\theta_\mu\sin 2\phi_h$	$\lvert A_\parallel A_\perp\rvert$
5	$\frac{1}{2}\sqrt{2}\sin 2\theta_K\sin 2\theta_\mu\cos\phi_h$	$\lvert A_0 A_\parallel\rvert$
6	$-\frac{1}{2}\sqrt{2}\sin 2\theta_K\sin 2\theta_\mu\sin\phi_h$	$\lvert A_0 A_\perp\rvert$
7	$\frac{2}{3}\sin^2\theta_\mu$	$\lvert A_S\rvert^2$
8	$\frac{1}{3}\sqrt{6}\sin\theta_K\sin 2\theta_\mu\cos\phi_h$	$\lvert A_S A_\parallel\rvert$
9	$-\frac{1}{3}\sqrt{6}\sin\theta_K\sin 2\theta_\mu\sin\phi_h$	$\lvert A_S A_\perp\rvert$
10	$\frac{4}{3}\sqrt{3}\cos\theta_K\sin^2\theta_\mu$	$\lvert A_S A_0\rvert$

Table 2.1 *Definitions of the angular components and amplitudes in the differential decay rate of* $B_s^0 \to J/\psi K^+K^-$.

in Table 2.2 which depend on the strong phases - δ_0, $\delta_\perp$, $\delta_\parallel$, δ_S - and the *CP* violating parameter λ_f following the representations in Equation 2.21. The real component in D is defined as $\Re(\lambda_f) = |\lambda_f|\cos(-\phi_s)$ and the imaginary component in S as $\Im(\lambda_f) = |\lambda_f|\sin(-\phi_s)$. The following conventions are adopted: $\delta_0 = 0$ and $|A_0|^2+|A_\perp|^2+|A_\parallel|^2 = 1$, and the S-wave fraction is defined as $F_S = |A_S|^2/(|A_S|^2+|A_0|^2+|A_\perp|^2+|A_\parallel|^2) = |A_S|^2/(|A_S|^2+1)$.

The representation above assumes the same *CP* violation for each of the polarisation amplitudes. However, NP models could lead to differences in *CP* asymmetry between the different polarisation states [29]. To test this, an alternative parametrisation is defined, which includes different *CP* violating

k	a_k	b_k	c_k	d_k
1	1	D	C	$-S$
2	1	D	C	$-S$
3	1	$-D$	C	S
4	$C\sin(\delta_\perp - \delta_\parallel)$	$S\cos(\delta_\perp - \delta_\parallel)$	$\sin(\delta_\perp - \delta_\parallel)$	$D\cos(\delta_\perp - \delta_\parallel)$
5	$\cos(\delta_\parallel - \delta_0)$	$D\cos(\delta_\parallel - \delta_0)$	$C\cos(\delta_\parallel - \delta_0)$	$-S\cos(\delta_\parallel - \delta_0)$
6	$C\sin(\delta_\perp - \delta_0)$	$S\cos(\delta_\perp - \delta_0)$	$\sin(\delta_\perp - \delta_0)$	$D\cos(\delta_\perp - \delta_0)$
7	1	D	C	$-S$
8	$C\cos(\delta_\parallel - \delta_S)$	$S\sin(\delta_\parallel - \delta_S)$	$\cos(\delta_\parallel - \delta_S$	$D\sin(\delta_\parallel - \delta_S)$
9	$\sin(\delta_\perp - \delta_S)$	$-D\sin(\delta_\perp - \delta_S)$	$C\sin(\delta_\perp - \delta_S)$	$S\sin(\delta_\perp - \delta_S)$
10	$C\cos(\delta_0 - \delta_S)$	$S\sin(\delta_0 - \delta_S)$	$\cos(\delta_0 - \delta_S)$	$D\sin(\delta_0 - \delta_S)$

Table 2.2 *Definitions of the coefficients in the time-dependent functions of the differential decay rate of $B_s^0 \to J/\psi K^+K^-$. D, C and S are defined in Equation 2.21.*

parameters and phases for each amplitude, $|\lambda_p|$ and ϕ_p, where $p \in \{0, \perp, \|\}$ for every polarisation and $p = S$ for the S-wave component [30]. The coefficients in the time-dependent functions are then expressed as in Table 2.3, and allows for a test of polarisation-dependent CP violation.

k	a_k	b_k	c_k	d_k
1	1	$\frac{2\lvert\lambda_0\rvert}{1+\lvert\lambda_0\rvert^2}\cos(\phi_0)$	$\frac{1-\lvert\lambda_0\rvert^2}{1+\lvert\lambda_0\rvert^2}$	$\frac{2\lvert\lambda_0\rvert}{1+\lvert\lambda_0\rvert^2}\sin(\phi_0)$
2	1	$\frac{2\lvert\lambda_\parallel\rvert}{1+\lvert\lambda_\parallel\rvert^2}\cos(\phi_\parallel)$	$\frac{1-\lvert\lambda_\parallel\rvert^2}{1+\lvert\lambda_\parallel\rvert^2}$	$\frac{2\lvert\lambda_\parallel\rvert}{1+\lvert\lambda_\parallel\rvert^2}\sin(\phi_\parallel)$
3	1	$-\frac{2\lvert\lambda_\perp\rvert}{1+\lvert\lambda_\perp\rvert^2}\cos(\phi_\perp)$	$\frac{1-\lvert\lambda_\perp\rvert^2}{1+\lvert\lambda_\perp\rvert^2}$	$-\frac{2\lvert\lambda_\perp\rvert}{1+\lvert\lambda_\perp\rvert^2}\sin(\phi_\perp)$
4	$\frac{1}{2}[\sin(\delta_\perp - \delta_\parallel) - \lvert\lambda_\perp\lambda_\parallel\rvert$ $\sin(\delta_\perp - \delta_\parallel - \phi_\perp + \phi_\parallel)]$	$-\frac{1}{2}[\lvert\lambda_\perp\rvert\sin(\delta_\perp - \delta_\parallel - \phi_\perp)$ $+\lvert\lambda_\parallel\rvert\sin(\delta_\parallel - \delta_\perp - \phi_\parallel)]$	$\frac{1}{2}[\sin(\delta_\perp - \delta_\parallel) + \lvert\lambda_\perp\lambda_\parallel\rvert$ $\sin(\delta_\perp - \delta_\parallel - \phi_\perp + \phi_\parallel)]$	$-\frac{1}{2}[\lvert\lambda_\perp\rvert\cos(\delta_\perp - \delta_\parallel - \phi_\perp)$ $+\lvert\lambda_\parallel\rvert\cos(\delta_\parallel - \delta_\perp - \phi_\parallel)]$
5	$\frac{1}{2}[\cos(\delta_0 - \delta_\parallel) + \lvert\lambda_0\lambda_\parallel\rvert$ $\cos(\delta_0 - \delta_\parallel - \phi_0 + \phi_\parallel)]$	$\frac{1}{2}[\lvert\lambda_0\rvert\cos(\delta_0 - \delta_\parallel - \phi_0)$ $+\lvert\lambda_\parallel\rvert\cos(\delta_\parallel - \delta_0 - \phi_\parallel)]$	$\frac{1}{2}[\cos(\delta_0 - \delta_\parallel) - \lvert\lambda_0\lambda_\parallel\rvert$ $\cos(\delta_0 - \delta_\parallel - \phi_0 + \phi_\parallel)]$	$-\frac{1}{2}[\lvert\lambda_0\rvert\sin(\delta_0 - \delta_\parallel - \phi_0)$ $+\lvert\lambda_\parallel\rvert\sin(\delta_\parallel - \delta_0 - \phi_\parallel)]$
6	$-\frac{1}{2}[\sin(\delta_0 - \delta_\perp) - \lvert\lambda_0\lambda_\perp\rvert$ $\sin(\delta_0 - \delta_\perp - \phi_0 + \phi_\perp)]$	$-\frac{1}{2}[\lvert\lambda_0\rvert\sin(\delta_0 - \delta_\perp - \phi_0)$ $+\lvert\lambda_\perp\rvert\sin(\delta_\perp - \delta_0 - \phi_\perp)]$	$-\frac{1}{2}[\sin(\delta_0 - \delta_\perp) + \lvert\lambda_0\lambda_\perp\rvert$ $\sin(\delta_0 - \delta_\perp - \phi_0 + \phi_\perp)]$	$-\frac{1}{2}[\lvert\lambda_0\rvert\cos(\delta_0 - \delta_\perp - \phi_0)$ $+\lvert\lambda_\perp\rvert\cos(\delta_\perp - \delta_0 - \phi_\perp)]$
7	1	$-\frac{2\lvert\lambda_S\rvert}{1+\lvert\lambda_S\rvert^2}\cos(\phi_S)$	$\frac{1-\lvert\lambda_S\rvert^2}{1+\lvert\lambda_S\rvert^2}$	$-\frac{2\lvert\lambda_S\rvert}{1+\lvert\lambda_S\rvert^2}\sin(\phi_S)$
8	$\frac{1}{2}[\cos(\delta_S - \delta_\parallel) - \lvert\lambda_S\lambda_\parallel\rvert$ $\cos(\delta_S - \delta_\parallel - \phi_S + \phi_\parallel)]$	$-\frac{1}{2}[\lvert\lambda_S\rvert\cos(\delta_S - \delta_\parallel - \phi_S)$ $-\lvert\lambda_\parallel\rvert\cos(\delta_\parallel - \delta_S - \phi_\parallel)]$	$\frac{1}{2}[\cos(\delta_S - \delta_\parallel) + \lvert\lambda_S\lambda_\parallel\rvert$ $\cos(\delta_S - \delta_\parallel - \phi_S + \phi_\parallel)]$	$\frac{1}{2}[\lvert\lambda_S\rvert\sin(\delta_S - \delta_\parallel - \phi_S)$ $-\lvert\lambda_\parallel\rvert\sin(\delta_\parallel - \delta_S - \phi_\parallel)]$
9	$-\frac{1}{2}[\sin(\delta_S - \delta_\perp) + \lvert\lambda_S\lambda_\perp\rvert$ $\sin(\delta_S - \delta_\perp - \phi_S + \phi_\perp)]$	$\frac{1}{2}[\lvert\lambda_S\rvert\sin(\delta_S - \delta_\perp - \phi_S)$ $-\lvert\lambda_\perp\rvert\sin(\delta_\perp - \delta_S - \phi_\perp)]$	$-\frac{1}{2}[\sin(\delta_S - \delta_\perp) - \lvert\lambda_S\lambda_\perp\rvert$ $\sin(\delta_S - \delta_\perp - \phi_S + \phi_\perp)]$	$-\frac{1}{2}[-\lvert\lambda_S\rvert\cos(\delta_S - \delta_\perp - \phi_S)$ $+\lvert\lambda_\perp\rvert\cos(\delta_\perp - \delta_S - \phi_\perp)]$
10	$\frac{1}{2}[\cos(\delta_S - \delta_0) - \lvert\lambda_S\lambda_0\rvert$ $\cos(\delta_S - \delta_0 - \phi_S + \phi_0)]$	$-\frac{1}{2}[\lvert\lambda_S\rvert\cos(\delta_S - \delta_0 - \phi_S)$ $-\lvert\lambda_0\rvert\cos(\delta_0 - \delta_S - \phi_0)]$	$\frac{1}{2}[\cos(\delta_S - \delta_0) + \lvert\lambda_S\lambda_0\rvert$ $\cos(\delta_S - \delta_0 - \phi_S + \phi_0)]$	$\frac{1}{2}[\lvert\lambda_S\rvert\sin(\delta_S - \delta_0 - \phi_S)$ $-\lvert\lambda_0\rvert\sin(\delta_0 - \delta_S - \phi_0)]$

Table 2.3 *Coefficients of the time-dependent terms in the differential decay rate of $B_s^0 \to J/\psi K^+K^-$ in a polarisation-dependent representation.*

2.8 Penguin Contributions

As mentioned in Section 2.5 the $B_s^0 \to J/\psi K^+K^-$ decay proceeds predominantly via the tree level diagram. Additionally, the decay can occur at loop level which is shown in Figure 2.9. This type of diagram is referred to as a *penguin diagram*.

The penguin contribution to the B_s^0 decay of interest is highly suppressed in the SM, however, as the experimental uncertainty on ϕ_s is decreasing with more data added, it will become important in the future to consider the penguin contribution as well. A shift of the experimental result from the SM prediction could namely be misinterpreted as NP, if this contribution is not properly estimated. By including

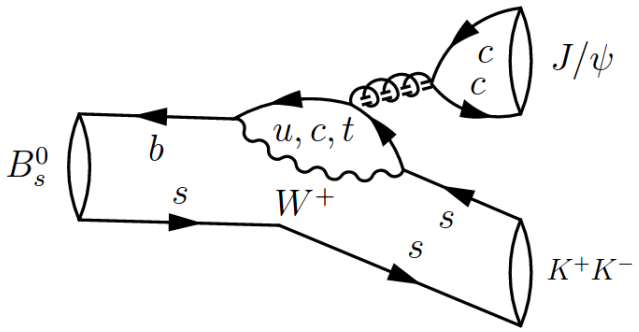

Figure 2.9 *Feynman diagram of the $B_s^0 \to J/\psi K^+K^-$ decay at loop level which is suppressed in the SM.*

penguin diagrams the $\bar{b} \to \bar{c}c\bar{s}$ amplitude becomes:

$$\begin{aligned} A &= V_{cs}V_{cb}^* T + V_{cs}V_{cb}^* P_c + V_{us}V_{ub}^* P_u + V_{ts}V_{tb}^* P_t \\ &= V_{cs}V_{cb}^*(T + P_c - P_t) + V_{us}V_{ub}^*(P_u - P_t), \end{aligned} \tag{2.33}$$

where T represents the tree level and P_i the penguin contributions with $i \in \{u, c, t\}$. Assuming the unitarity of the CKM matrix, the second line in Equation 2.33 is reached for which $V_{ts}V_{tb}^* = -V_{us}V_{ub}^* - V_{cs}V_{cb}^*$ holds. In the CKM matrix $|V_{cs}V_{cb}^*| \approx \lambda^2$ and $|V_{us}V_{ub}^*| \approx \lambda^4$, hence the second term on the right-hand side is much smaller than the first.

To estimate the size of the penguin contribution, similar decay channels can be studied. The authors of Ref. [31] have proposed the use of the alternative decay $B_s^0 \to J/\psi K^{*0}$ to measure the size while exploiting the s-d flavour symmetry. Its amplitude can be derived from Equation 2.33 by replacing all s indices with d:

$$A = V_{cd}V_{cb}^*(T + P_c - P_t) + V_{ud}V_{ub}^*(P_u - P_t). \tag{2.34}$$

Both terms on the right-hand side of Equation 2.34 are of equal size because they are of order λ^3, allowing the measurement of the penguin contribution. Results of $B_s^0 \to J/\psi K^{*0}$ are combined with constraints from a similar $\bar{b} \to \bar{c}c\bar{d}$ transition decay, $B^0 \to J/\psi\rho$, to calculate the predicted penguin phase shift for

each polarisation state of $B_s^0 \to J/\psi\phi$ [32]:

$$\begin{aligned}
\Delta\phi_{s,0}^{J/\psi\phi} &= 0.000^{+0.009}_{-0.011}(\text{stat})^{+0.004}_{-0.009}(\text{syst}) \text{ rad}, \\
\Delta\phi_{s,\parallel}^{J/\psi\phi} &= 0.001^{+0.010}_{-0.014}(\text{stat}) \pm 0.008(\text{syst}) \text{ rad}, \\
\Delta\phi_{s,\perp}^{J/\psi\phi} &= 0.003^{+0.010}_{-0.014}(\text{stat}) \pm 0.008(\text{syst}) \text{ rad}.
\end{aligned} \tag{2.35}$$

These results show that penguin pollution in the determination of ϕ_s is small within a precision of ~ 10 mrad. If the experimental value reaches this accuracy, it will be fundamental to update these results and potentially include penguin contributions in the ϕ_s analysis.

Chapter 3

The LHCb Detector at the Large Hadron Collider

The analysis described in this thesis uses data recorded by the LHCb detector. The LHCb experiment is one of the four main experiments at the Large Hadron Collider (LHC). Its main goal is to search for indirect evidence of NP in *CP* violation and rare decays of beauty and charm hadrons. This chapter will first discuss the LHC, and then move on to the LHCb detector, covering its sub-detectors and trigger system. The detector is able to accurately measure the decay of interest - $B_s^0 \to J/\psi K^+ K^-$ - due to its ability to track the relatively large flight distance of the B_s^0 meson and to identify the charged final state particles using information from various sub-detectors.

3.1 The Large Hadron Collider

The Large Hadron Collider (LHC) is the current world's largest and highest energy particle collider. It is the final part of a chain of particle accelerators hosted by the European Organisation for Nuclear Research (CERN) to study processes taking place in *pp* collisions at record high energies. The LHC is also capable of accelerating heavy ion beams, e.g. lead, which is done at the end of a data-taking year, making heavy ion physics studies possible. The LHC is built in a 27 km long circular tunnel, located 100 m under Swiss and French ground.

Figure 3.1 shows the multiple components of CERN that the protons have

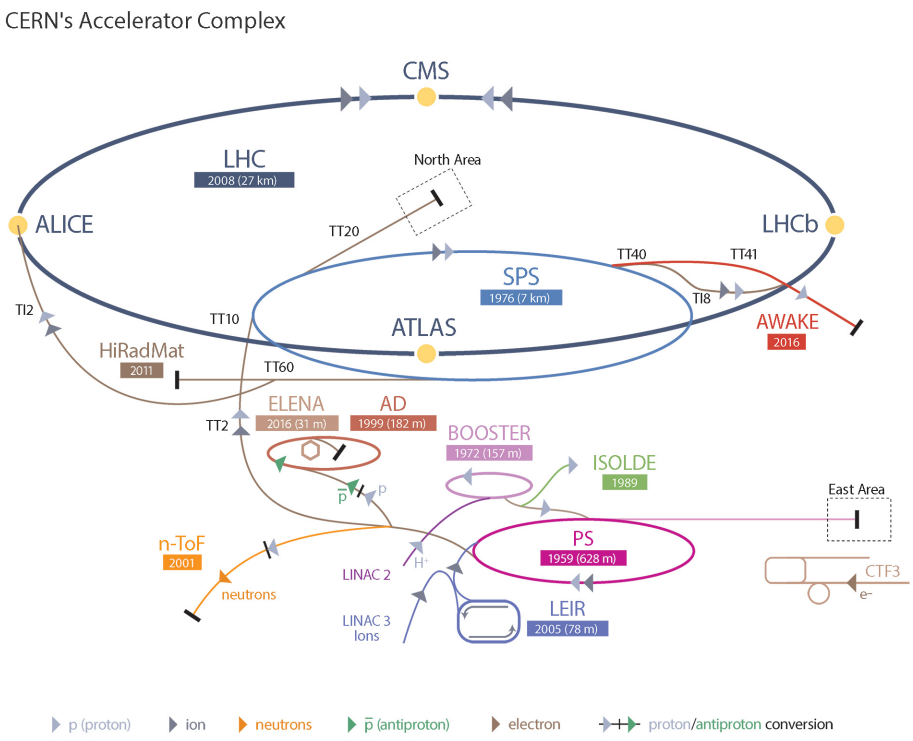

Figure 3.1 *The particle accelerators and detectors at CERN. Figure taken from Ref. [33].*

to pass through before they are accelerated to the desired energy. Protons are obtained from hydrogen gas, which are then accelerated to an energy of 50 MeV by a linear collider (LINAC2). Next, the protons are accelerated to 1.4 GeV by the Proton Synchroton Booster (BOOSTER), then to 25 GeV by the Proton Synchroton (PS), and afterwards to 450 GeV by the Super Proton Synchrotron (SPS). The protons are thereafter injected into the LHC in two beams circulating in opposite directions. The beams are accelerated to the desired centre-of-mass energy for the pp collisions. The LHC started operating in 2010. Run 1 refers to the data-taking years 2011 and 2012, in which the protons collided at a centre-of-mass energy of $\sqrt{s} = 7$ TeV and $\sqrt{s} = 8$ TeV, respectively. During Long Shutdown 1 (LS1) the LHC was prepared to operate at $\sqrt{s} = 13$ TeV during Run 2, covering the years from 2015 until 2018, after which Long Shutdown 2 (LS2) started in December 2018. The protons in the accelerator are grouped together in bunches of about 10^{11} particles per bunch to ensure optimal acceleration. In Run 1 the bunches were 50 ns apart, which was reduced to 25 ns during Run 2. The LHC achieved a peak instantaneous luminosity during Run 2 of $\mathcal{L} = 2 \times 10^{34}$ cm^{-2}s^{-1}, twice its design value. It is designed to have centre-of-mass energy of $\sqrt{s} = 14$ TeV, with a maximum of

2808 bunches per beam, corresponding to a bunch crossing rate of 40 MHz. The design centre-of-mass energy will be reached when Run 3 starts in 2021. This thesis will focus on the analysis of data recorded in the years 2015 and 2016.

The two beams are magnetically forced to follow an almost circular trajectory. Where the four main experiments at the LHC are located, the protons are brought into collision. Two experiments are general purpose detectors studying a wide range of particle phycis, ATLAS [34] and CMS [35], whereas LHCb [36] and ALICE [37] are dedicated to the study of flavour and heavy ion physics, respectively. It can take up to several hours before the protons - after extraction from the hydrogen - reach the LHC. The protons are injected into the LHC, then ramped up from 450 GeV to the desired centre-of-mass energy, and finally brought into collision. Every step requires the handshake confirmation from each experiment within a grace period of 5 minutes. A data-taking period can last up to 36 hours, until the collision rate is too low and a new fill is requested. On average a fill only lasts for about 12 hours, as a lot can go wrong during this period both at the LHC or at one of the (sub-)detectors, causing a beam dump before the scheduled dump. For each dump a request is send to all experiments to make sure the detectors are ready for the next physics state.

3.2 The LHCb Detector

The LHCb detector is a single-arm forward spectrometer that focuses on decays originating from b- and c-hadrons [36]. At the interaction point of the LHCb, the beam is de-focussed to ensure the events are dominated by a single pp interaction per bunch crossing, $<\mu>= 1.1$ in Run 2 [38]. This reduces the occupancy, making the events easier to reconstruct and allowing for more precise measurements. The luminosity at the LHCb interaction point is as a result levelled at $\mathcal{L} = 4 \times 10^{32}$ cm^{-2}s^{-1}. The cumulative integrated luminosity recorded by LHCb is shown in Figure 3.2. The physics program covers many topics, such as the following:

- Rare b- and c-hadron decays
- CP violation
- CKM parameters
- Spectroscsopy

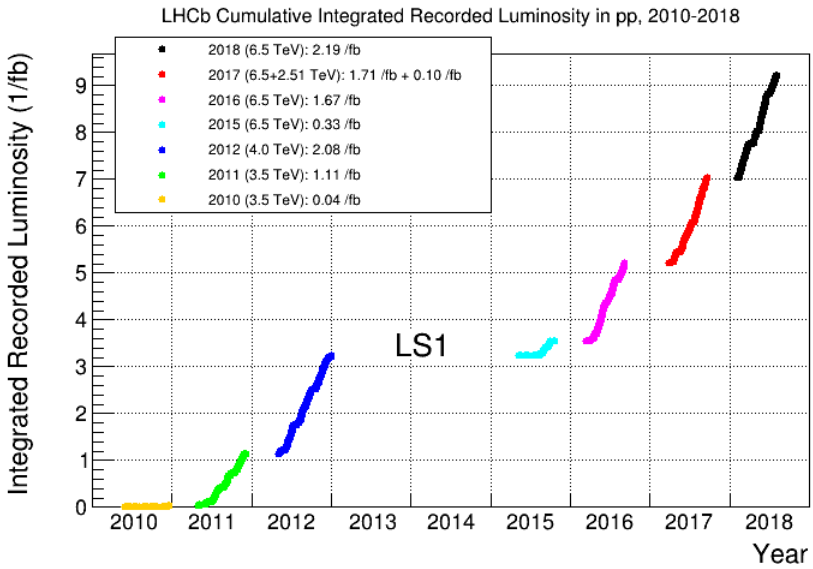

Figure 3.2 *The evolution of the integrated luminosity recorded at the LHCb detector. The legend displays the colours, centre-of-mass energies and integrated luminosities for each year. Figure taken from Ref. [39].*

- Soft QCD
- Heavy ion physics

The detector is located at Intersection Point 8 of the LHC and uses the cavern of the former LEP experiment DELPHI. It has a right-handed coordinate system and is designed to cover the region from approximately 10 mrad to 300 (250) mrad in the $x - z$ ($x - y$) plane. This can be translated into the *pseudorapidity* range $2 < \eta < 5$. The pseudorapidity is defined as:

$$\eta = -\log\tan(\theta/2), \tag{3.1}$$

where θ is the angle between the particle momentum and the beam axis. A side-view of the LHCb detector can be found in Figure 3.3. The design of the acceptance is based on the trajectory of b-hadrons at high energies, which is mainly along the direction of the beam pipe. In Figure 3.4 the distribution of $b\bar{b}$ pairs produced in the pp interaction can be seen. They are produced forward or backward, and on average one out of four produced $b\bar{b}$ pairs lies in the LHCb detector acceptance, indicated in red. Additionally, the heavy quarks in the forward region have a large boost, leading to a flight distance in the detector. B-mesons for example typically travel about 1 cm after production due to their long lifetimes of approximately 1.5×10^{-12} s. The LHCb detector is therefore

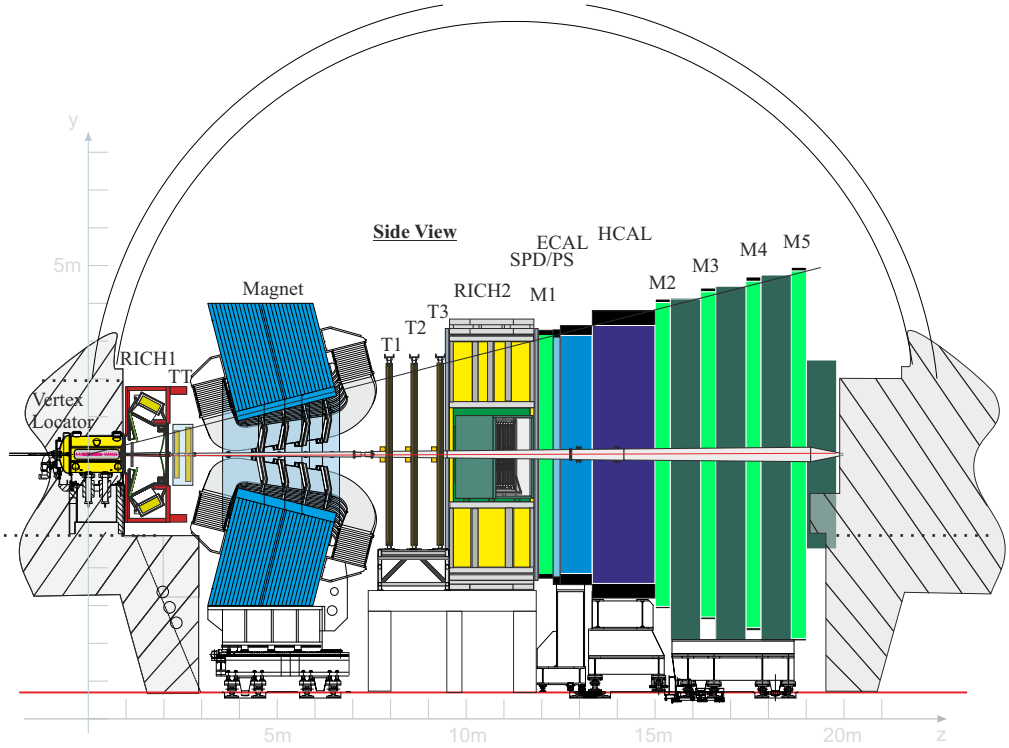

Figure 3.3 *A side-view of the LHCb detector in the $y-z$ plane, illustrating the different sub-detectors.*

able to distinguish decay products of secondary particles from particles produced in the initial pp collision.

To be able to reconstruct the b- and c-hadron decays in a variety of leptonic, semileptonic and hadronic final states the detector is made out of several specialised components that can be divided into the tracking system and the particle identification system. A detailed description of the sub-detectors can be found in Ref. [36], and will be summarised in the following.

3.3 Front-end Electronics

The LHCb sub-detectors are exposed to signals at the 40 MHz bunch crossing rate, after which a hardware-based first level trigger (Level-0 or L0) makes required trigger decisions to reduce the event rate by about a factor 10 with a trigger rate up to 1 MHz. This is the maximum rate manageable by the data acquisition system (DAQ) and readout links. Figure 3.5 shows the DAQ with the data flow

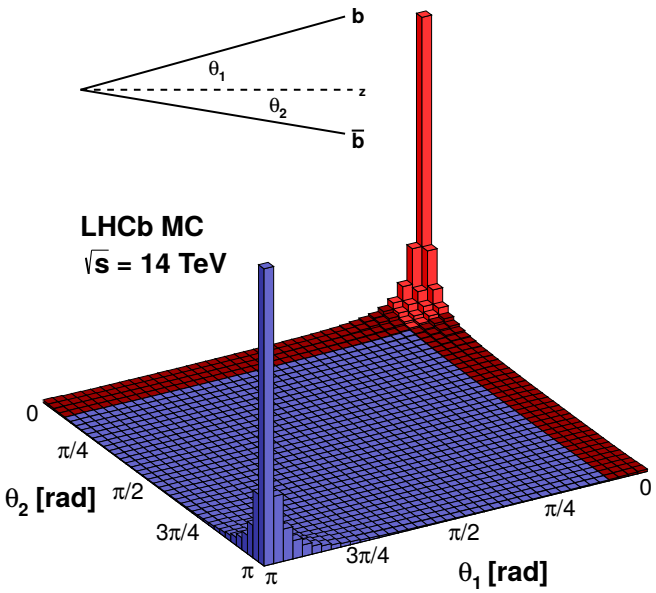

Figure 3.4 *Polar angle distribution of $b\bar{b}$ pairs produced in pp interactions. The LHCb detector acceptance is shown in red. Figure taken from Ref. [40].*

and the front-end architecture. The front-end system refers to the processing and buffering of all detector signals before it is passed to the DAQ. A limited set of readout links is exploited to transfer the analogue signals that have been amplified, digitised and selected by a positive trigger decision. Only one signal sample is extracted by the analog detector from one bunch crossing within 25 ns. The Trigger and Timing Control (TTC) system uses optical fibres to keep the front-end synchronised to the bunch crossings at the LHC, and the separate front-end modules and delivery of trigger decisions synchronised to each other. The supervision of calibration, debugging or normal data-taking in the front-end system is governed by the Experimental Control System (ECS). The ECS also controls the DAQ and trigger system. In general one local controller per sub-detector regulates the front-end electronics, which can communicate to higher levels via the ECS. The DAQ processes the received data by exploiting the High Level Trigger (HLT) using a shared CPU farm. Details of the trigger system is described in Chapter 3.6.

Bunch crossings within the LHCb bunch structure are identified by a bunch ID. At three different stages of the data flow in the front-ends the bunch ID can be added: directly at the input of the L0 pipeline buffer, at the input of the L0 derandomiser buffer, or when transferred to the L1 front-end electronics. Another identification number is the L0 event ID, the event number in the sequence of positive L0 triggers. This can only be added at the input of the L0 derandomiser

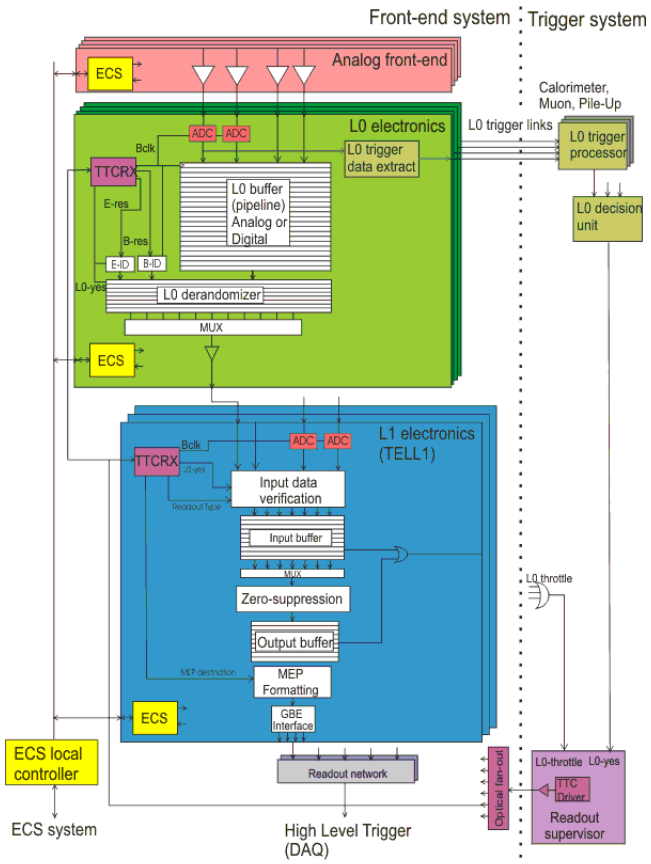

Figure 3.5 *Front-end architecture and data flow at the LHCb detector.*

buffer or at the input of the L1 electronics. Monitoring the pair of bunch ID and event ID of the data in the front-end or DAQ system allows the ECS to verify the synchronisation of the data stream. The L1 electronics perform a first basic validation of the collected data followed by event formatting to send it to the DAQ system. Almost all sub-detectors use so-called TELL1 modules for the L1, except for the RICH detector, which uses UKL1 boards instead.

3.4 Tracking System

The purpose of the tracking system is to reconstruct the charged particles traversing the detector. The tracking system includes the Vertex Locator (VELO) around the interaction point, the Tracker Turicensis (TT) located upstream of the dipole magnet and tracking stations (T1 - T3) located downstream of the magnet. The positions of interactions between charged particles and the tracking system are employed to reconstruct the trajectories (tracks). The angle of deflection through the magnetic field is used to determine the particle's momentum -

important information that can be used for the identification of the particle's type. Special care has been taken to make optimal use of the varying particle density in the LHCb detector coverage and to reduce the detector material budget.

3.4.1 Dipole Magnet

The tracks of charged particles are bent in the LHCb detector by a dipole magnet located 5 m behind the interaction point. The magnetic field is created by two identical mirror-symmetrically placed saddle-shaped coils. Each coil consists of fifteen layers of hollow aluminium conductor with a central cooling system. The coils are attached on a window-frame yoke centred in the $x-y$ plane with sloping poles to establish the required detector acceptance. Laminated low-carbon steel plates of each 100 mm thick and a maximum weight of 25 tons make up the bottom, top and vertical parts of the magnetic yoke. A perspective view can be seen in Figure 3.6.

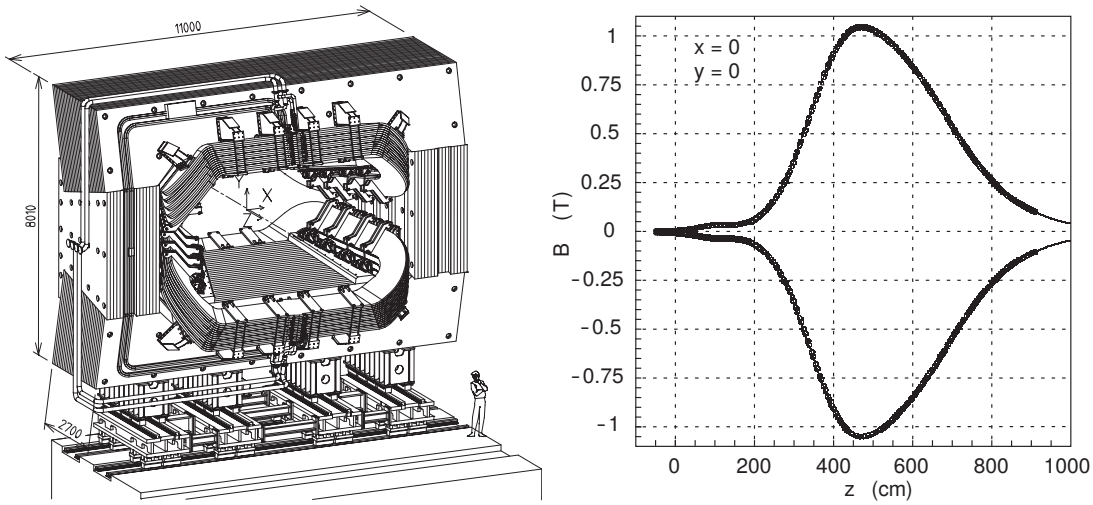

Figure 3.6 *Perspective view of the LHCb dipole magnet which is centred in the $x-y$ plane (left) and the magnetic field as a function of position along the z-axis (right).*

Particles that travel the full length of the detector of 10 m experience a total integrated magnetic field of 4 Tm. The integrated magnetic field can be known with a relative precision of about 10^{-4}, to allow the required momentum resolution of $\Delta p/p$ of 0.5% at low momentum to 1.0% at 200 GeV/c^2. Figure 3.6 shows the varying magnetic field as a function of position in z for the two magnet polarities. During the operation of the LHC the magnet polarity is changed after every two

weeks of data-taking to reduce detector asymmetries originating from the different datasets.

3.4.2 Vertex Locator

The Vertex Locator makes up the most inner part of the LHCb detector, with an inner radius of 8.2 mm. Due to its position, the VELO is able to precisely measure the particle trajectories close to the beam axis, and therefore provides accurate determination of the locations of pp collisions (primary vertices (PVs)) and heavy hadron decays (secondary vertices (SVs)). It has to cover the angular acceptance of the downstream detectors, i.e. detect particles with a pseudorapidity in the range $1.6 < \eta < 4.9$ and particles coming from PVs in the range $|z| < 10.6$ cm. The VELO consists of a series of silicon modules, arranged along the beam direction, and measures in R and ϕ coordinates for fast pattern recognition, as shown in Figure 3.7). The R-sensor consists of circular strips to measure hits in the R direction, the ϕ-sensor comprises radial strips measuring the azimuthal ϕ hit position.

During the LHC operation protons are injected and accelerated with a distance between the two proton beams larger than the VELO radius. To avoid damaging the sensor, the sub-detector is able to retract up to 30 mm from the centre of the beam. The VELO is kept open until the LHC reaches the collision state and data-taking can start. The VELO is split vertically into two halves, each consisting of 21 modules positioned perpendicular to the beam. The two halves are separated from the LHC primary vacuum to shield them from possible radio-frequency (RF) pick-up from the proton beams. A 300 μm thick aluminium foil (RF-foil) is used for this purpose.

3.4.3 Silicon Tracker

Because of the significantly higher density of charged particle tracks closer to the beam, the Silicon Tracker (ST) is installed close to the beam pipe. This includes the TT upstream of the magnet and the Inner Tracker (IT) downstream which forms the inner part of the three tracking stations T1-T3. Silicon ensures a good hit resolution and fast response time, necessary to operate in regions of high track density and radiation levels. Silicon micro strip sensors with a strip pitch of about

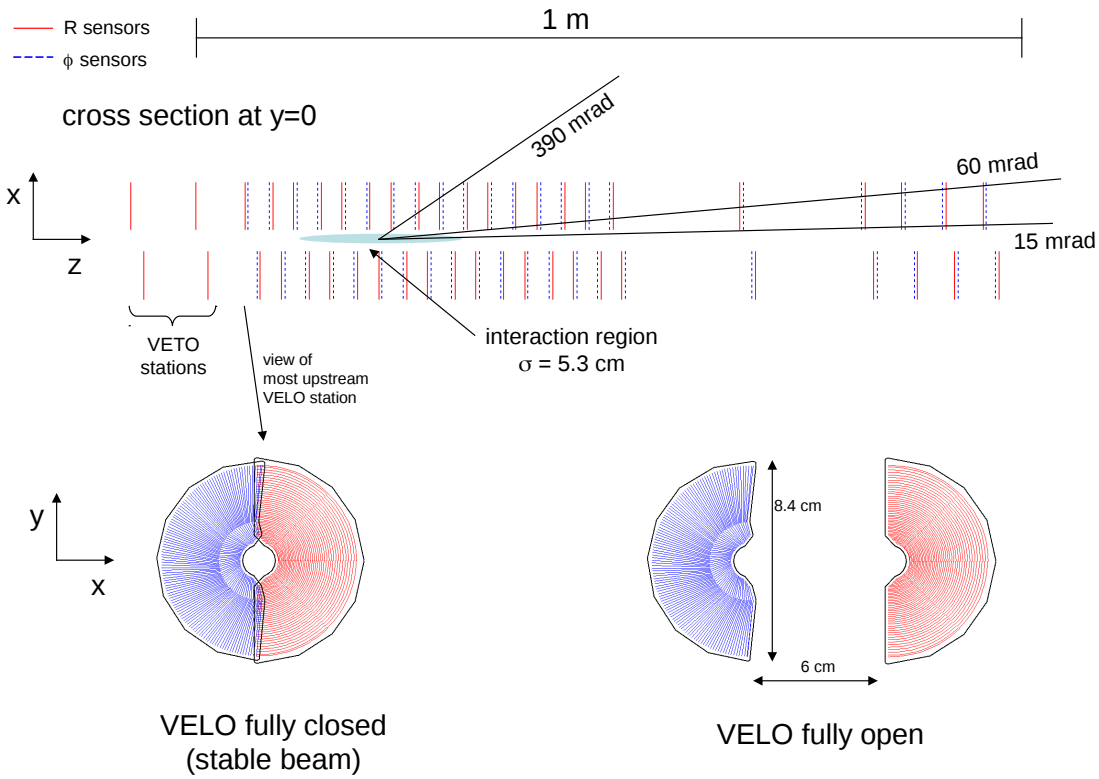

Figure 3.7 *Cross section of the VELO showing the silicon modules along the beam axis (up) together with the layout of the R and ϕ sensors in closed (bottom left) and open (bottom right) positions. The minimal (15 mrad) and maximal (390 mrad) angles for crossing at least 3 VELO stations are indicated.*

200 μm make up both trackers. Each station is composed of four layers in an $(x-u-v-x)$ arrangement with vertical strips in the first and last layer and strips tilted in a -5° and +5° angle in the second and third layer, respectively.

The TT is installed to improve the momentum estimate and to detect decay products of long lived neutral particles that decay outside the VELO (e.g. the K_S^0 and Λ mesons). Figure 3.8 shows the layout for one of the layers. The TT dimensions are chosen to cover the full detector acceptance (130 cm high and 150 cm wide). The goal of the IT is to improve the invariant mass and decay-time resolutions due to accurate momentum determination. The three IT stations are arranged in a box shape around the beam pipe, which all contain the previously mentioned four layers of detector. The boxes are each 40 cm high and 120 cm wide, see Figure 3.8. The spacial resolution is about 50 μm and 60 μm for the TT and IT, respectively.

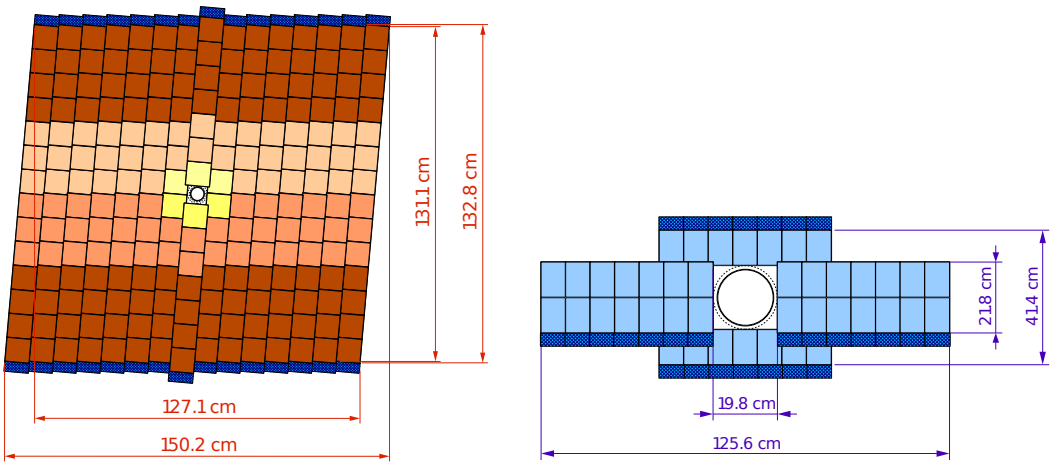

Figure 3.8 *The second layer, u, of the TT at an angle of +5° (left) and one of the IT boxes indicating the orientation around the beam pipe (right).*

3.4.4 Outer Tracker

To keep the costs low, the IT is enclosed by the Outer Tracker (OT), which is a large area straw-tube detector, and detects about 70% of the charged particles tracks that are produced inside the LHCb acceptance. It has a lower granularity than the ST due to the lower activity in the outer regions. Same as the ST it consists of four layers in an $(x - u - v - x)$ arrangement. The OT provides excellent momentum resolution which is necessary for the precise determination of the invariant mass of the reconstructed b-hadrons. The front-end electronics measure drift times of ionisation clusters produced by charged particles traversing the straw tubes, which is translated into hit position. Figure 3.9 shows the three OT stations which comprise two layers of circular straws with an inner diameter of 4.9 mm. The straws are filled with a mixture of Argon (70%), CO_2 (28.5%) and O_2 (1.5%) to ensure a fast drift time below 50 ns and a sufficient drift-coordinate resolution (200 μm).

3.4.5 Track Reconstruction

Tracks are reconstructed from hits in the VELO, TT and T detectors. Tracks are classified based upon the sub-detectors they traverse, as illustrated in Figure 3.10. These include the following [42]:

- VELO tracks: tracks that only traverse the VELO

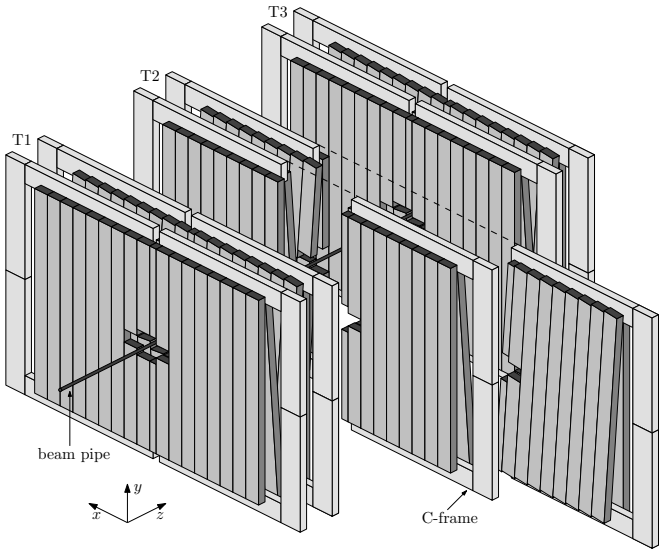

Figure 3.9 *Arrangement of the OT straw-tube modules in layers and stations [41].*

- Long tracks: tracks that traverse the VELO, and the IT or the OT
- Upstream tracks: tracks that traverse the VELO and the TT, but neither the IT nor the OT
- Downstream tracks: tracks that are produced outside the VELO but traverse the TT, and the IT or the OT
- T tracks: tracks that solely traverse either the IT or the OT

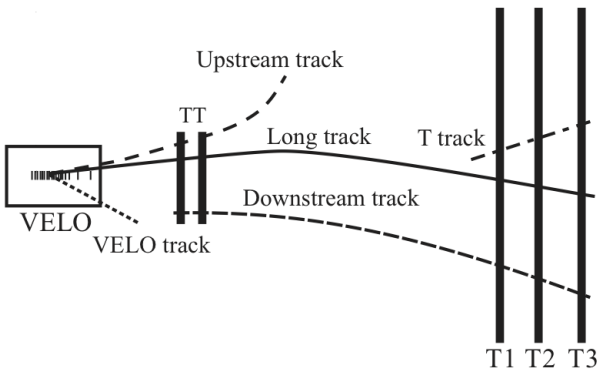

Figure 3.10 *Classification of tracks based on the tracking system components they pass through.*

This analysis uses long tracks exclusively to detect the muon tracks originating from the B_s^0 meson decay within the VELO. Additionally, it ensures a high momentum resolution for the final state kaons. The following describes the construction of long tracks. First, VELO tracks are reconstructed from the

particle trajectories by requiring hits in at least three R and three ϕ sensors in the VELO for each of the tracks. Then, information from TT and T stations is added which is determined by 'forward tracking' and 'track matching' algorithms. The forward tracking first combines the hits in the VELO with information from a single T station for a determination of the momentum and trajectory of the particles. The algorithm then looks for hits along each trajectory in other T stations to determine the optimal set of hits that describe the long tracks. The track matching, on the other hand, combines the VELO tracks with hits after the magnet in the T stations by applying a standalone track finding algorithm. Each trajectory is required to have hits for each of the three T stations in one of the x layers and in one of the tilted layers. The information from both algorithms is combined, while discarding duplicates, for the final set of long tracks that can be used in analyses. Finally, the hit trajectories are extrapolated to the TT to find consistent hits for an improvement of the momentum determination. The final step includes a Kalman-fitter [43] that fits to the tracks and takes into account multiple scattering and corrects for energy loss due to ionisation. The quality of each established trajectory is defined by the χ^2 per degree of freedom.

Mis-reconstructed (*ghost*) tracks do not agree with the trajectory of a real charged particle. They mostly arise from wrong associations between the VELO and T tracks which is caused by the large extrapolation distance when traversing the magnet. A neural network classifier is exploited to decrease the number of ghost tracks by exploiting the information coming from the track fit, the track kinematics, and the number of measured hits in the tracking stations versus the number of expected hits.

3.5 Particle Identification System

The purpose of the particle identification (PID) system is to identify the different particle species that travel through the LHCb detector. In pp collisions at the LHC predominantly pions are produced, hence it is crucial to distinguish them from the other particle types. Information from the Ring Imaging Cherenkov detectors is used to distinguish the charged final state hadrons - kaons, pions, and protons. The calorimeters provide information to identify and measure the energy of photons, electrons and hadrons. The muon detectors are employed to detect and measure muons.

3.5.1 Ring Imaging Cherenkov Detectors

The Ring Imaging Cherenkov (RICH) detectors provide information which is crucial to determine the species of the charged hadrons in the final state. To cover the full momentum spectrum of particles that traverse the detector, LHCb uses information from two RICH detectors: RICH1 upstream of the magnet between the VELO and TT, and RICH 2 downstream of the magnet before the muon stations. RICH1 covers the low momentum range ($1 - 60$ GeV/c^2) and consists of aerogel and C_4F_{10} radiators. RICH2 covers the high momentum range (15 GeV/c^2 up to and beyond 100 GeV/c^2) and consists of CF_4 radiators. Figure 3.11 shows schematic illustrations of both RICH detectors. The angular coverage of RICH1 is from 25 mrad to 250 mrad in the vertical plane and 300 mrad in the horizontal, while the RICH2 coverage is 15 mrad to 100 mrad in the vertical plane and 120 mrad in the horizontal.

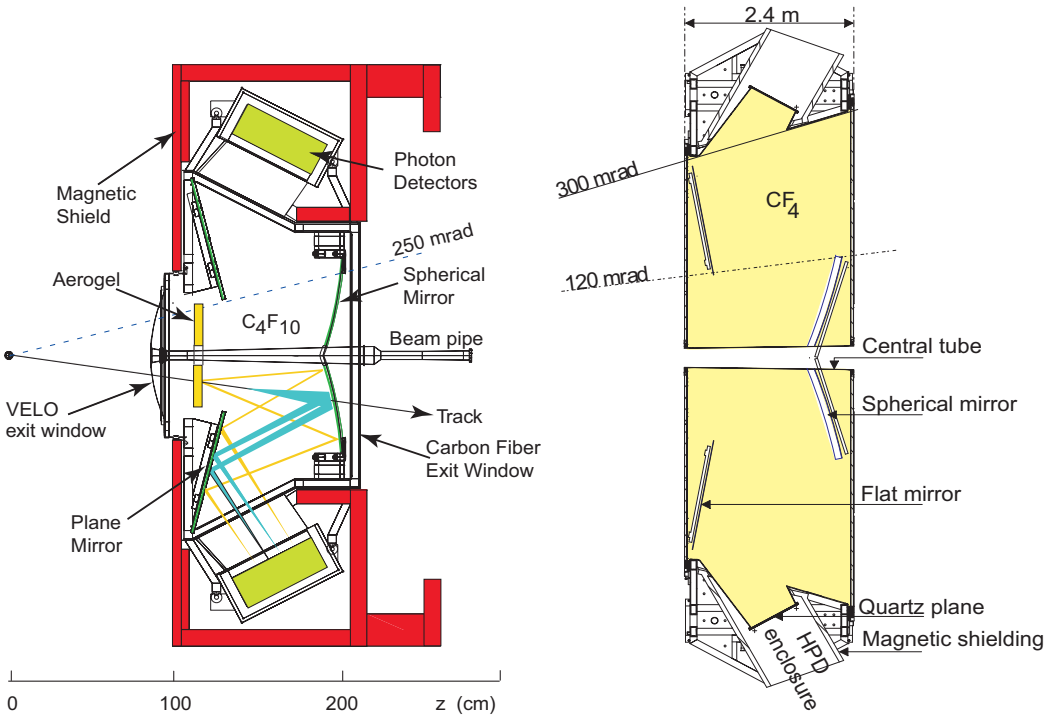

Figure 3.11 *Side view schematic layout of the RICH1 detector showing the path of Cherenkov light (left) and top-down view schematic of the RICH2 detector (right).*

The same principal is exploited by both detectors: charged particles that travel through a medium with a speed, $\beta = v/c$, greater than the macroscopic speed of light in the same medium emit Cherenkov radiation in the shape of a cone. The refractive index of the medium, n, is inversely proportional to the speed of light,

$1/n$. The travelling particle emits Cherenkov radiation at a constant polar angle from its trajectory. This angle is referred to as the Cherenkov angle, θ_c, and can be determined by the following relation:

$$\cos(\theta_c) = \frac{1}{n\beta} \tag{3.2}$$

From the combination of the Cherenkov angle with the momentum information coming from the tracking system the particle's mass and type can be determined. Figure 3.12 shows the distinct Cherenkov angle versus momenta distributions of the charged particles that travel through the RICH.

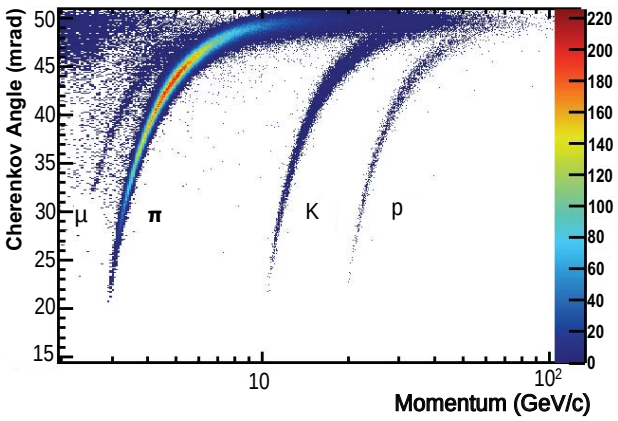

Figure 3.12 *Cherenkov angle (θ_c) plotted against the particle's momentum. Particle types are determined from the combination of information from the RICH system with the tracking system. Figure taken from Ref. [44]*

Spherical and flat mirrors inside RICH1 and RICH2 reflect the cones of emitted Cherenkov radiation. Hybrid Photon Detectors (HPDs) are placed outside of the detector acceptance to detect the circular projections of the reflected cones. Figure 3.13 shows a diagram of an HPD. It is a vacuum photon detector with silicon pixels positioned at the anode side. First, Cherenkov photons reach with a wavelength of about $200 - 600$ nm the spherically shaped piece of quartz coated with a multi-alkali photocatode. Photoelectrons are created and accelerated by an applied high voltage of about $10 - 20$ kV. Finally, the photoelectrons hit the pixel sensor and electron-hole pairs are created with an average yield of one for every 3.6 eV of deposited energy.

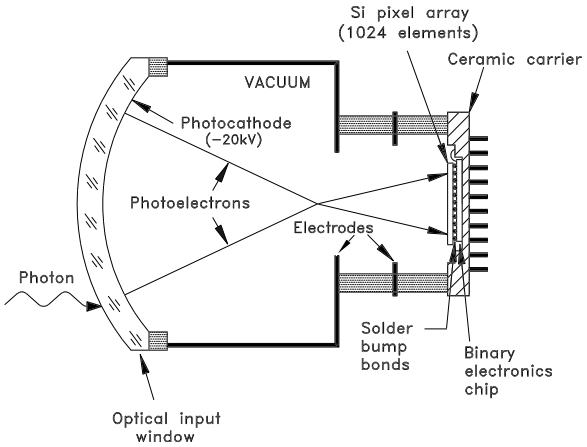

Figure 3.13 *Schematic view of an HPD.*

3.5.2 Calorimeters

The calorimeter system (CALO) includes four components: the Scintillating Pad Detector (SPD), the Pre-Shower (PS) detector, the Electromagnetic Calorimeter (ECAL) and the Hadronic Calorimeter (HCAL). Its main task is to discriminate hadrons, electrons and photons, and to measure their energies and positions. The CALO also provides important transverse energy measurements for the Level-0 trigger described in Section 3.6. The system is positioned downstream of the magnet after RICH2. All four detectors are based on alternating layers of absorber - either lead or iron - and scintillating material. When particles interact with the absorber material, showers of charged particles and photons are generated. These showers are converted into photons inside the scintillator layers, which are then transmitted to photomultipliers. The number of detected photons is proportional to the original particle's energy.

The choice of absorption material and thickness of the sub-detectors is optimised for their purpose. The absorber material for the ECAL is lead and the total thickness is designed to be 25 radiation lengths in order to fully absorb the energy of photons and electrons. The HCAL consists of iron absorber layers to detect and measure the energy of hadrons for which a good resolution is not needed, hence it only has a thickness of 5.6 interaction lengths to minimise the occupied space. The SPD and PS are directly positioned after the first muon station, and both consist of rectangular scintillating pads. A thin layer of lead, with a thickness of 2.5 radiation lengths, is positioned between the two pads to initiate a photon shower and improve the separation of electrons and photons. Only charged particles will induce a signal in the SPD, hence it allows to distinguish

between showers created by electrons and photons. The PS helps to distinguish electrons from the large background of charged and neutral pions as hadrons initiate only small showers in the lead material.

Figure 3.14 shows the segmentation separately for the ECAL and HCAL. The segmentation of the PS and SPD match the ECAL segmentation. Since the hit density falls off as a function of distance from the beam pipe, the calorimeter sub-detectors have variable segmentation, with smaller cells closer to the inner region. The HCAL has larger cells to accommodate for the wider hadron

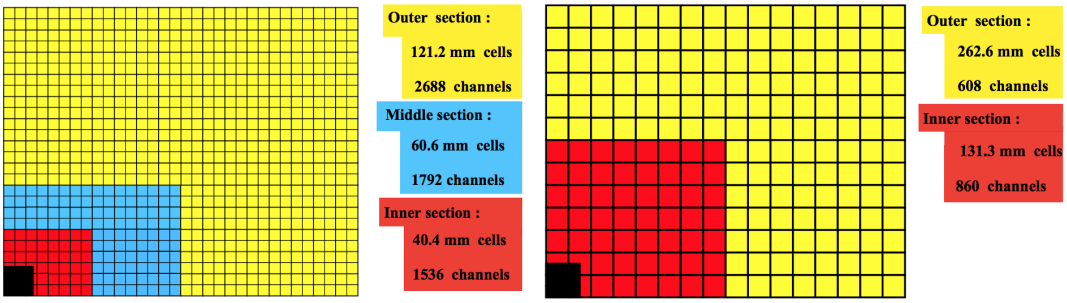

Figure 3.14 *Segmentation of the LHCb calorimeter system with the ECAL shown on the left and the HCAL on the right.*

showers. The angular coverage of the calorimeters span from 25 mrad to 250 mrad in the vertical plane and to 300 mrad in the horizontal, matching the RICH1 coverage. The produced light in the scintillators is transmitted through wavelength-shifting (WLS) fibres to the photomultipliers. The ECAL and HCAL use Photo-Multipliers (PMTs), which are mounted directly on the scintillator modules. The SPD and PS cells are read out using multi-anode Photo-Multipliers (MaPMTs) that are positioned outside the acceptance of the detector inside magnetic shielding.

3.5.3 Muon Stations

Muon triggering and identification is crucial for the LHCb physics program. The muon system provides fast information for the high-p_T muon trigger at the Level-0 stage and muon identification for the High Level Trigger discussed in Section 3.6 and offline analysis. It comprises five stations (M1-M5) of rectangular shape placed along the beam axis. A total of 1380 chambers makes up the muon system which covers an area of 435 m^2.

The first station, M1, is positioned between the RICH2 and the calorimeter

system to significantly improve the p_T measurement in the trigger. Stations M2-M5 are placed downstream of the calorimeters with iron absorbers between each station of a thickness of 80 cm to stop high energy hadrons that might pass the CALO. The muons will have passed most of the detector without depositing much energy, and afterwards traverse the downstream muon stations. The stations mostly consist of Multi-wire Proportional Chambers (MWPCs), except for the inner-most region of M1 where triple gas electron multipliers (GEMs) are used to cope with the high occupancy. Charged particles ionise the gas inside the chambers, from which the produced charge is collected and amplified.

The minimum energy for a muon to travel through all five stations is 6 GeV/c due to the total absorber thickness of about 20 interaction lengths. As illustrated in Figure 3.15 the muon stations are divided into four regions (R1-R4) with increasing distance from the beam axis. To have an similar particle flux and channel occupancy over the four regions a segmentation scale ratio of 1:2:4:8 is chosen. Stations M1-M3 provide high spatial resolution along the x coordinate

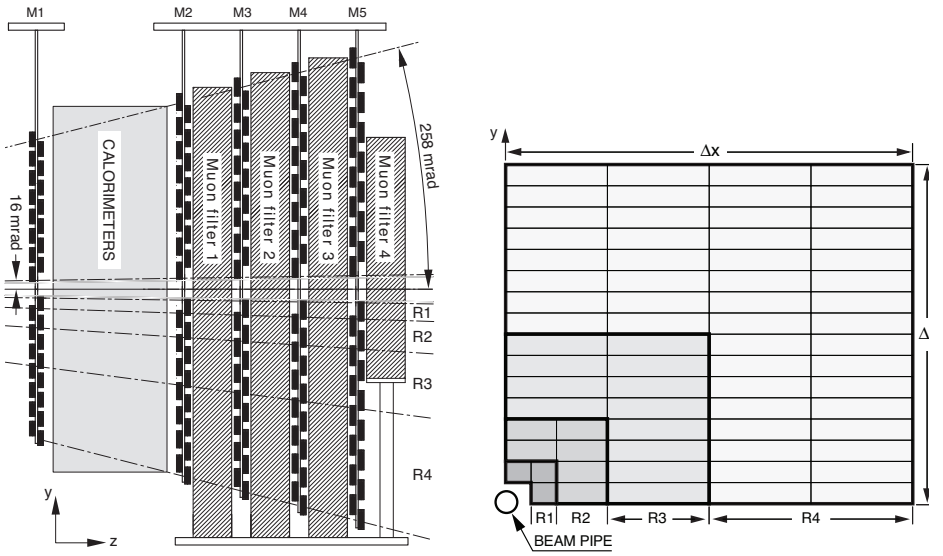

Figure 3.15 *Layout of the muon system (left) and the segmentation of the muon stations (right).*

(bending plane), from which track direction and p_T of the candidate muon can be determined with good accuracy. Station M4 and M5 have limited spatial resolution and are mainly used for the identification of false muon candidates.

3.5.4 Particle Identification Variables

The information of the PID sub-detectors - RICH detectors, CALO and muon stations - is combined to provide optimal identification for charged particle types: K, π, p, e, μ. For each track, the probability of a certain particle hypothesis, x, is computed by associating a likelihood value, $\mathcal{L}(x)$. It is determined by linearly adding the likelihood information produced by each sub-system. To discriminate between species, the likelihood for the respective particle hypothesis x is calculated with respect to the pion hypothesis, as this is most abundant particle type produced in the pp collisions at the LHCb detector. The ratio of log-likelihoods - delta log-likelihood (DLL) - can be used in analyses to improve the selection of certain particle types:

$$\Delta\ln\mathcal{L}_{x\pi} = \ln\mathcal{L}(x) - \ln(\pi) = \ln\frac{\mathcal{L}(x)}{\mathcal{L}(\pi)}. \tag{3.3}$$

A larger difference corresponds to a higher probability of the particle to be of type x than to be a pion. To select pions, the DLL for a certain particle type x is required to be small or negative.

Another set of PID variables is based on machine learning and employs a multivariate analysis, a technique that will be discussed in Section 4.2. The information from the PID sub-detectors is combined with information from the tracking system, and additionally the correlations between the detector systems. For each particle hypothesis a single probability value is computed, labelled as `ProbNN`x, where x represents the particle's type.

3.6 LHCb Trigger

The LHCb experiment is designed to allow data-taking at the bunch crossing rate of the LHC of 40 MHz, however the trigger system that is implemented in Run 2 allows a maximum rate of 12.5 kHz at which events can be written to storage. The essential reduction is achieved in two stages: the online hardware Level-0 (L0) and the offline software High Level Trigger (HLT). The L0 trigger uses custom made electronics and runs synchronously with the 40 MHz bunch crossing frequency, while the HLT runs asynchronously on a processor farm. The L0 applies a quick preliminary selection based on the information from only the

fastest sub-detectors. The output L0 rate of 1 MHz is then sent to the HLT farm where first a fast reconstruction is performed by HLT1 to reduce the rate by a factor of 10. This information is passed to HLT2, where a full event reconstruction is performed after which the desired rate of 12.5 kHz is achieved. The events that survive are written to storage for offline analysis. The trigger system is designed to keep the most relevant pp interactions for subsequent analysis. As LHCb is mainly focused on heavy flavour physics, the trigger system is optimised to select on decays with high transverse momentum (p_T) tracks, high transverse energy (E_T), and displaced vertices.

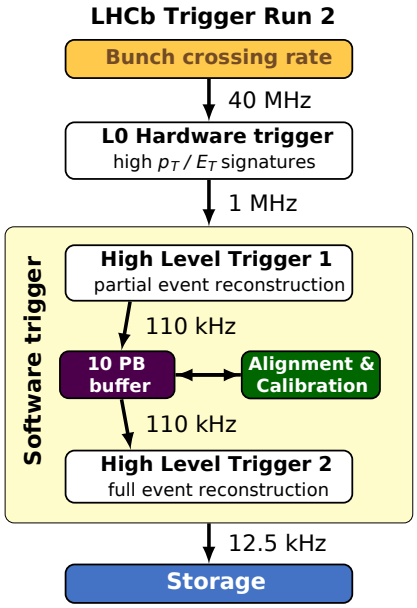

Figure 3.16 *Overview of LHCb trigger system in Run 2.*

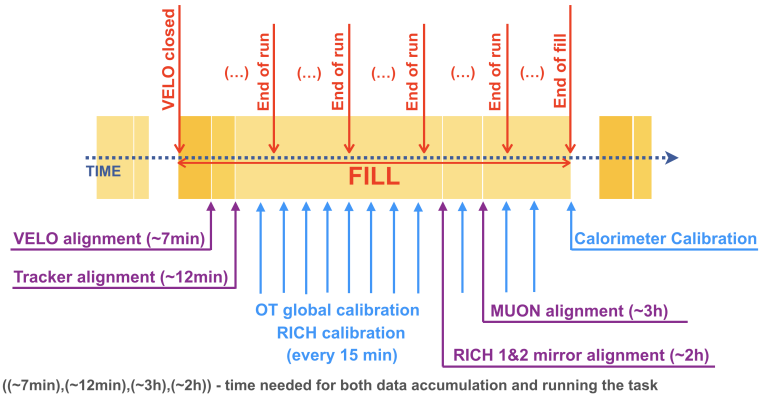

Figure 3.17 *Alignment and calibration procedure from the start of each fill with the time needed to perform each task, as used for 2018 data-taking.*

Figure 3.16 shows the design of the trigger system as used in Run 2 [38]. It was re-designed during LS1 to perform the full offline event reconstruction, which greatly increases the efficiency to select c- and s-hadrons. Information from the trigger system is used directly to enable real-time detector alignment and calibration. This avoids the need to correct for differences between online and offline reconstruction. Figure 3.17 shows the alignment and calibration steps from the start of each fill with the time that each task takes. Each fill is divided into runs which take up to one hour. The events passing HLT1 are buffered to disk, which allows storage for up to two weeks. In parallel, the HLT1 saves dedicated samples to perform the alignment and calibration and the resulting constants are only updated if they differ significantly from the current values. Next, the data is combined with the detector alignment and calibration information on a per run basis, and then passed to HLT2 where a full event reconstruction is performed.

3.6.1 Level-0 Trigger

After the pp interaction there is a time period available of 4 μs before the L0 decision will reach the FE electronics. Considering the time-of-flight of the particles, cable delays and all delays in the FE electronics, 2 μs is left for the L0 to process the data and reach a decision. In case a positive decision is triggered, the event is passed to the next trigger level, and otherwise cleared from memory. Decisions are determined for the `L0Calorimeter` and the `L0Muon` systems, which use information coming from the SPD, PS, ECAL and HCAL sub-detectors and the muon stations, respectively. They evaluate different *trigger lines*, each with a unique collection of selection criteria. The `L0Calorimeter` system classifies a candidate either as hadron, photon or electron depending on which calorimeter system the particle leaves its energy. The `L0Muon` system evaluates the trigger lines `L0Muon`, high p_T `L0Muon` and `L0DiMuon`. Information of the position of the track in the first two muon stations allows a p_T estimate. A threshold is set on the E_T of each candidate in the L0 to select events of interest. A limit on the number of hits in the SPD removes events with high-multiplicity that would take too long to process in the HLT.

3.6.2 High Level Trigger

The High Level Trigger (HLT) evaluates all events that pass the L0 trigger on the Event Filter Farm (EFF), which is a cluster of CPUs running in the radiation shielded part of the LHCb cavern. The HLT is split into two stages, HLT1 and HLT2, to optimise the time consumption. At the first stage, the trajectories of charged particles traversing the LHCb tracking system are reconstructed. In addition, a precise reconstruction of the PV is performed. Due to tight timing constraints in HLT1, the only identification algorithm that can be performed is the muon identification, profiting from the clean signature the muons provide in the detector. The HLT1 lowers the rate of accepted events by imposing selections on track variables, such as the number of VELO hits, track p, and track fit quality. The HLT1 algorithms distribute candidates over four categories: single, high-quality displaced tracks; dimuon candidates; high-energy photon and electrons; and candidates for luminosity and monitoring purposes.

The combined output rate of the HLT1 algorithms is low enough for HLT2 to run a full offline event reconstruction. All tracks that traverse the magnet are reconstructed, which is followed by inclusive and exclusive selections with additional particle identification. Inclusive trigger lines target b-hadron decays with at least two charged particles in the final state and a displaced decay vertex. Exclusive trigger lines target specific final states of c-hadron decays and require all final state particles to be reconstructed. The reason for the tighter cuts used in charm trigger lines is the higher rate of visible production of $c\bar{c}$ than that of $b\bar{b}$. Decays with muons in the final state, as $B_s^0 \to J/\psi K^+K^-$, are most efficiently selected by one of the inclusive dimuon triggers. Dimuon candidates are selected if their invariant mass is compatible with a particular other particle's mass (J/ψ in this case). There are about 20 HLT1 and 500 HLT2 trigger lines. The ones used for this analysis will be discussed in Section 4.1.

3.7 LHCb Software

The LHCb software consists of several stages for the processing of data [45]. The Monte Carlo (MC) simulation samples are processed in a similar way to data. Gaudi [46] is the framework that is used for simulation, reconstruction, analysis, and the steps in between, and is illustrated in Figure 3.18.

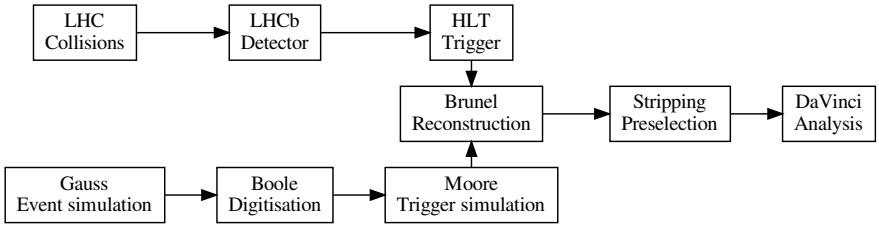

Figure 3.18 *Infrastructure of the different LHCb software stages in the Gaudi framework [47].*

The different applications are explained below:

- Gauss [48] - MC simulation. `Pythia` [49, 50] generates pp collisions, `EvtGen` [51] describes the decay of simulated b- and c-hadrons, and `Geant4` [52, 53] simulates the propagation and interaction of particles through and with the detector. The output is 'hits' in the sub-detector sections.

- Boole - digitises the simulated sub-detector hits to the same output format as the readout electronics and adds L0 decisions.

- Moore [54] - adds HLT decisions to the event information by running the same applications used during real data-taking.

- Brunel - reconstructs raw data to transform detector hits into objects such as tracks and clusters. The output is stored in Data Summary Tape (DST).

- DaVinci [54] - offline physics selection framework, the so-called *stripping*. Events are separated into different physics streams so that they can be used in different analyses. The application reconstructs primary vertices, assigns particle identification hypotheses to tracks and calorimeter events, and stores the output also in DST files. The application provides several tools that can be used for analysis, e.g. constrained vertex fitting, determination of the signal flavour, and calculation of decay angles.

The LHCb software also makes extensive use of the ROOT framework [55], which provides a large set of libraries that can be used for data analysis, simulation and presentation. Datasets that are used in the main physics analysis are selected from the DST output of the relevant stripping line, and are stored in ROOT file

format. The next chapter will discuss the selection process that is applied for this thesis.

Chapter 4

Event Selection

This chapter will cover the event selection strategy to select $B_s^0 \to J/\psi K^+K^-$ signal, which is based on previous studies that used Run 1 data [56]. The collision data sample used for this thesis includes 1.9 fb^{-1} of pp collisions collected at a centre-of-mass energy $\sqrt{s} = 13$ TeV by the LHCb detector during 2015 (0.3 fb^{-1}) and 2016 (1.6 fb^{-1}), referred to as the 'full' dataset in the following. An improved strategy to select the decay mode has been developed for this dataset. A set of trigger lines is required as well as a stripping selection developed for the B_s^0 decay of interest. After applying additional preselection *cuts*, a multivariate algorithm is trained to discriminate between signal and background. Vetoes are implemented to reject similar decays that are present in the signal mass region. The remaining background is statistically subtracted. Corrections to the simulation data sample are discussed as well as the control channels used in this analysis. This work has been performed as part of a team for the most part, whilst the selection of the control channels is my own work.

4.1 Candidate Sample

To obtain a sample of $B_s^0 \to J/\psi K^+K^-$ candidates in data for the analysis, the signal is isolated by performing a selection which discards decays with similar topology. Variables are studied for which the signal and background distributions differ, so that they can be separated. As a first step information at the trigger level is exploited. The presence of high momentum muons in the decay provides

a clear signature in the detector, which can be used to reduce the amount of background significantly. A small set of trigger lines is required, which are chosen based on their preservation of the number of signal events. At the hardware stage all events that pass any of the L0 trigger lines are considered (`B_L0Global`). This means that they will have either a muon with high p_T or a hadron, photon or electron with high energy deposit in the calorimeters.

As mentioned in Section 3.6, at the first software stage a complete reconstruction of the tracks is performed, and additionally of the PV, allowing more distinct information related to individual particles. Figure 4.1 provides a schematic view of the $B_s^0 \to J/\psi K^+K^-$ decay at track level. Due to the short lifetime of the J/ψ and ϕ mesons, they immediately decay in the detector at the secondary vertex.

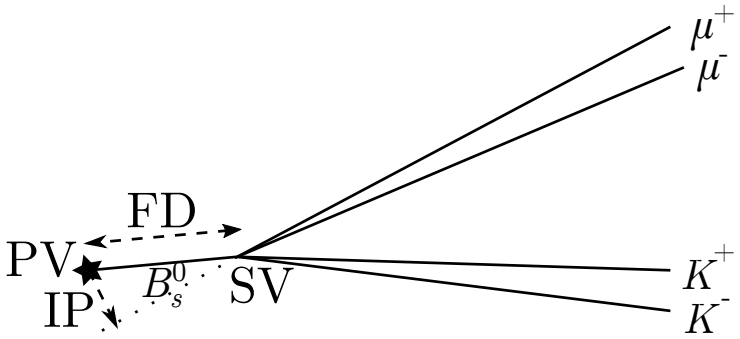

Figure 4.1 *Schematic view of the $B_s^0 \to J/\psi K^+K^-$ decay chain. The signal meson is produced at the interaction point - PV -, and the intermediate particles - J/ψ and ϕ - immediately decay at the SV into the final state particles.*

The $B_s^0 \to J/\psi K^+K^-$ candidate events have to pass one out of three HLT1 trigger lines. These lines can be split into two categories based on whether they introduce a non-uniform efficiency as a function of the B_s^0 decay-time. First, among other conditions, two well-identified oppositely charged muons with invariant mass larger than 2700 MeV/c^2 are required by the `Jpsi_Hlt1DiMuonHighMass` line. Due to its almost uniform efficiency as a function of decay-time, this line is called *unbiased*. The other two lines select on, amongst other conditions, events for which at least one muon track has a large impact parameter (IP) significance, $\chi^2_{\rm IP}$, with respect to any of the PVs. The impact parameter is defined as the distance of closest approach (DOCA) of the reconstructed track to the PV. The significance is determined by the difference in the vertex-fit χ^2 of the PV fitted with and without the considered track. This introduces a non-uniform efficiency

as a function of decay-time, and therefore biases the measured lifetime, hence the trigger lines `B_Hlt1TrackMuon` and `B_Hlt1TwoTrackMVA` are referred to as *biased*. The second trigger line has an extra requirement of a significant displacement from the PV for candidates that form a two-track good-quality secondary vertex. Section 5.2 will cover the correction for the decay-time *acceptance*.

At the second software stage the low rate allows a nearly complete reconstruction of the events, among which the J/ψ. The HLT2 line `Jpsi_Hlt2DiMuonDetachedJPsi` selects on events that have a $J/\psi \to \mu^+\mu^-$ pair with an invariant mass within 120 MeV/c^2 of the J/ψ mass as determined by the Particle Data Group [24], and which form a good-quality vertex that is significantly displaced from the PV. A lower limit on the flight distance (FD) significance of $\mathrm{FD}/\sigma_{\mathrm{FD}} > 3$ enforces a separation between the J/ψ and PV, and these candidates are said to be *detached*. This requirement introduces another small decay-time bias. In case multiple PVs are reconstructed in the event, the PV with the minimum value of χ^2_{IP} is considered.

The second step of the selection is to use the $B^0_s \to J/\psi K^+K^-$ stripping line. At the stripping stage, a full event reconstruction is repeated, which includes the reconstruction of tracks, particle identification and PVs (as mentioned in Section 3.7). Then a set of cuts are imposed that are tight enough to limit the amount of data which has to be stored, but loose enough to keep the selection efficiency high. Table 4.1 summarises the cuts that are applied by the $B^0_s \to J/\psi K^+K^-$ stripping line. These are imposed on the B^0_s decay, but also on the intermediate states in the decay chain and the final state particles.

To select the final state muons and kaons, the PID variables $\Delta\ln\mathcal{L}_{\mu\pi}$ ($\mu^\pm$) and $\Delta\ln\mathcal{L}_{K\pi}$ ($K^\pm$) are used, which are defined in Equation 3.3. They represent the difference between the log-likelihood of the muon and kaon hypothesis and the log-likelihood of the pion hypothesis. The cuts on transverse momentum (p_T) reduce the background due to *prompt* muons and hadrons. Prompt events originate directly from the pp collision. The decay is isolated by requiring the $\mu^+\mu^-$ and K^+K^- invariant mass to be around the J/ψ and ϕ mass [24], respectively. The $m(K^+K^-)$ window does not guarantee that the two kaons originate from the decay of the intermediate particle ϕ, but also allows the K^+K^- S-wave state. An upper limit on the DOCA χ^2 is required for the J/ψ and the K^+K^- pair. Only kaons with a good track goodness-of-fit (χ^2_{track}/nDoF, track χ^2 per number of degrees of freedom) are kept, to eliminate tracks that are reconstructed from a fake set of hits in the detector (ghosts). The upper limit is a common value used

	Variable	Stripping	Preselection
$J/\psi \to \mu^+\mu^-$	$\Delta\ln\mathcal{L}_{\mu\pi}$ $(\mu^\pm)$	> 0	–
	p_T $(\mu^\pm)$	$> 500\,\mathrm{MeV}/c^2$	–
	χ^2_{DOCA}	< 20	–
	$\chi^2_{\mathrm{vtx}}/\mathrm{nDoF}$	< 16	–
	$m(\mu^+\mu^-)$	$\in [3020, 3170]\,\mathrm{MeV}/c^2$	–
K^+K^-	χ^2_{DOCA}	< 30	–
	p_T (K^+K^-)	$> 500\,\mathrm{MeV}/c^2$	–
	$m(K^+K^-)$	$\in [980, 1060]\,\mathrm{MeV}/c^2$	$\in [990, 1050]\,\mathrm{MeV}/c^2$
	$\chi^2_{\mathrm{vtx}}/\mathrm{nDoF}$	< 25	–
	$\chi^2_{\mathrm{track}}/\mathrm{nDoF}$ $(K^\pm)$	< 5	–
	$\Delta\ln\mathcal{L}_{K\pi}$ $(K^\pm)$	> 0	–
$B^0_s \to J/\psi K^+K^-$	$m(J/\psi K^+K^-)$	$\in [5150, 5550]\,\mathrm{MeV/c^2}$	$\in [5200, 5550]\,\mathrm{MeV/c^2}$
	$\chi^2_{\mathrm{vtx}}/\mathrm{nDoF}$	< 20	–
	t	> 0.2 ps	$\in [0.3, 15.0]$ ps
	σ_t	–	< 0.15 ps

Table 4.1 *Selection criteria for the stripping and preselection used to identify $B^0_s \to J/\psi K^+K^-$ candidates. The variables of the signal B^0_s meson in the preselection are calculated offline by the Decay Tree Fitter tool.*

in most of the LHCb analyses.

For all decay particles the fit of the common vertex is required to be of a certain quality ($\chi^2_{\mathrm{vtx}}/\mathrm{nDoF}$). A lower limit is set on the decay-time (t) of the signal B^0_s meson, to reject a large fraction of prompt *combinatorial* background. Combinatorial background is caused by random combinations of non-signal particles that build a signal candidate during the event reconstruction. The cut is optimised on discarding a large fraction of the background while keeping a high signal efficiency. The invariant mass $m(J/\psi K^+K^-)$ is chosen to be within a wide range of the B^0_s mass [24] to allow a proper background study in the analysis. The resulting $B^0_s \to J/\psi K^+K^-$ decay candidates are then associated to a PV in the event. The tracks corresponding to the signal decay are removed, and all PVs in the event are reconstructed. The χ^2_{IP} for the B^0_s signal candidate with respect to each of the PV is computed, and the signal meson is associated to the PV with the smallest value.

The next step of the selection is to impose a preselection, which is also specified in Table 4.1, with the goal of enhancing the purity of the signal sample. The decay-time cut in the stripping is applied to the result of an online kinematic fit. Offline, the decay-time is re-calculated by the Decay Tree Fitter tool (DTF) [43], which is provided by the `DaVinci` software mentioned in Section 3.7. The DTF also computes other variables, such as the decay-time uncertainty (σ_t) and the invariant masses. The DTF tool performs a fit to all four final

state tracks, while allowing additional constraints to increase mass, momentum and vertex *resolutions*. The $m(\mu^+\mu^-)$, J/ψ mass, is constrained to the world average value [24], which enhances the B_s^0 mass resolution. Additionally, the B_s^0 signal candidate is constrained to come from the associated primary vertex. This enhances the angular resolution, as the helicity angles in the analysis are computed by the particle momenta determined by the fit. The lower limit on the DTF decay-time is required to reduce the background from prompt combinatorial background and to remove any differences with the decay-time calculated in the stripping. The upper limit is set since only very few B_s^0 decay candidates are expected above it. The upper limit on the DTF decay-time uncertainty σ_t removes events with very poor decay-time determination.

By applying the trigger, stripping and preselection cuts a well-defined signal mass peak is observed when looking at the invariant mass. Figure 4.2 shows for visualisation the result for the larger 2016 dataset that is used for this thesis. The peak is visible around the B_s^0 mass [24], however a large background contribution is present under the peak over the full mass range, which mostly comes from combinatorial background. Section 4.4 will discuss the next step of the selection, which uses a multivariate strategy to eliminate most of the remaining background. The next section will discuss decision trees which are used by multivariate classification methods to reach a decision.

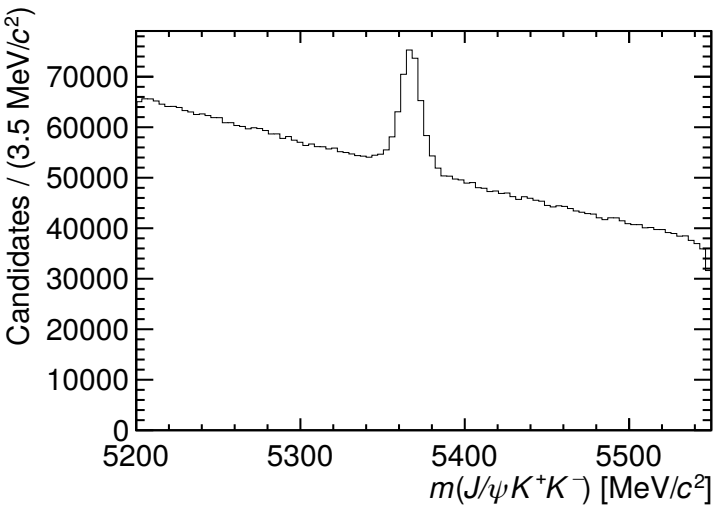

Figure 4.2 *Distribution of the $J/\psi K^+K^-$ invariant mass after the trigger, stripping and preselection in 2016.*

4.2 Decision Tree and Boosting

In this and next chapters multivariate analyses (MVAs) are employed, which are based on machine learning techniques. This section will therefore give a brief overview of the general functionality. The goal is to combine multiple variables into a single observable, the *classifier* variable, while analysing an ensemble of predictions, typically decision trees. A decision tree is a binary tree structure classifier and can be represented schematically as in Figure 4.3. The *root* node represents the full sample, and each *leaf* node at the bottom a class. Continuous yes/no decisions are taken on a single variable (x_i) each time, splitting the sample between two sub-nodes, until a final criterion is fulfilled, e.g. the number of candidates in each sub-node or the purity of the sub-sample.

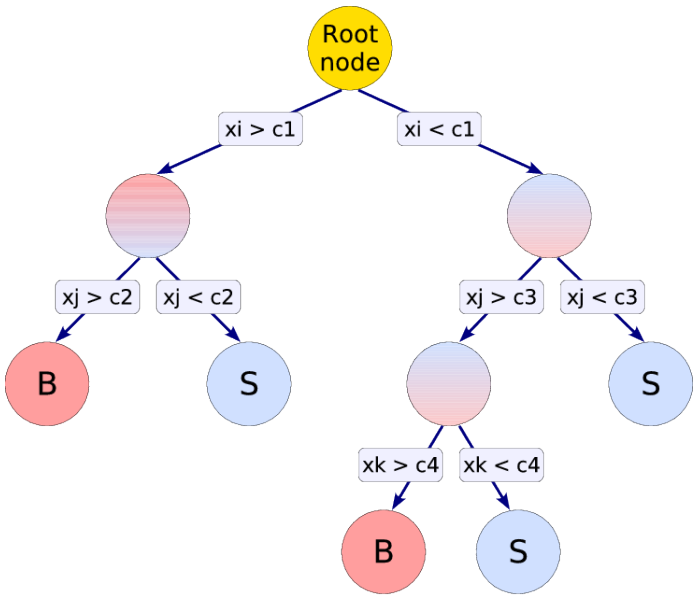

Figure 4.3 *Schematic view of a decision tree [57]. For each node the best cut on the most discriminating variable x is determined. The leaf nodes are classified either as signal (S) or background (B) depending on the majority of candidates.*

Decision trees are trained on pure samples of signal and background, hence can establish the best separation between the two by determining the optimal cut on the most discriminating variable. The same variable may be used several times, while others might not be used at all. At different sub-notes at the same level different variables can be chosen to evaluate, e.g. the variable x_j that is tested against c_2 and c_3. As the identity of the input events is known, the subset in the leaf nodes can directly be classified as signal or background related to that

subspace depending on the majority of events they contain. This type of decision tree is also referred to as a *classification* tree and is the most commonly used one. Another model is the *regression* tree, for which the leaf nodes take real numbers instead of discrete data classifications. Trees could be over-fitted, called *over-trained*, when too many sub-nodes have been used compared to the size of the input sample. The result is a tree that is trained on statistical variations in the samples, rather than to identify actual properties of signal and background. To prevent this from happening, tree parameters can be set that specify for example the maximum number of leaf nodes or variables or the minimum number of events per leaf node.

Decision trees can easily be affected by small fluctuations in the training sample, leading to a sub-optimal response actual data. To overcome the instability the *boosting* method is applied - an ensemble of weak trees is trained consecutively on the same training sample and their output is combined into a strong classifier. The trees are created iteratively and the outcome of each tree is given a weight relative to its accuracy, for which the results are compared to the truth information. Misclassified events are given a higher weight in the next iteration, and the next tree is re-trained based on the weight. After training, the sum of the individual weights is translated into a single boosted classifier - a Boosted Decision Tree (BDT) [58, 59]. The typical range of a BDT is between $+1$ and -1, where signal events are distributed towards $+1$ and background events towards -1. A special type is the *gradient*-boosted (GB) algorithm, which minimises a loss function - the deviation between the measured and true values. It is trained on an ensemble of weak regression trees which take as weight the gradient of the loss function.

4.3 Simulated Data Sample

Simulated data samples are used throughout this thesis, and are in particular used as input for the multivariate selection described in the next section. The production and corrections to simulation will therefore be discussed first. Simulated Monte Carlo (MC) samples are produced using the LHCb software framework described in Section 3.7. Two large simulation samples of $B_s^0 \to J/\psi K^+K^-$ are produced, for 2015 and 2016 separately, using the parameter values as in Table 4.2. The data-taking conditions specific to each year are applied, as well as relative contributions from *magnet up* and *magnet down*, since the LHCb magnet polarity is changed every two weeks during data-taking. The

simulation samples have the same trigger, stripping and selection applied as data.

Table 4.2 *Physics parameters used for the generation of simulated $B_s^0 \to J/\psi\, K^+K^-$ candidates.*

Parameter	Value
Δm_s	17.8 ps^{-1}
$\Delta\Gamma_s$	0.08543 ps^{-1}
Γ_s	0.6614 ps^{-1}
ϕ_s	-0.03 rad
$\lvert A_0(0)\rvert^2$	0.5242
$\lvert A_\parallel(0)\rvert^2$	0.2256
$\lvert A_\perp(0)\rvert^2$	0.2500
$\delta_\parallel - \delta_0$	3.26 rad
$\delta_\perp - \delta_0$	3.08 rad

In addition, simulated samples of $B^0 \to J/\psi K^*(892)^0$ and $\Lambda_b^0 \to J/\psi p^+K^-$ are generated, using physics parameter values specific for the decays, to study background events in the final data sample after selection. $B^0 \to J/\psi K^*(892)^0$ MC is additionally used in the decay time acceptance determination. Finally, a sample of $B_s^0 \to J/\psi K^+K^-$ candidates is generated with similar parameter values as in Table 4.2, except for the decay width difference $\Delta\Gamma_s = 0$ ps^{-1}, which is used to compute the decay-time and angular acceptances.

To be able to rely on simulation the samples have to match the distributions in data. However, a known difference is present for the distributions of the PID variables. Therefore, the distributions in simulation of the `ProbNN`x variables (introduced in Section 3.5.4) are corrected. A standard package commonly used by LHCb analyses, the `PIDCalib` package [60], is employed for this. The package has the possibility to take into account the correlations between different `ProbNN`x variables, as well as their dependence on the momentum (p) and transverse momentum (p_T) of the tracks, and the number of tracks in the event (N_{track}).

A further difference between simulation and data is observed for several key variables, such as the B_s^0 meson production kinematics and the track significance of the final state particles. By using gradient-boosted regression trees a weighting can be performed in multiple variables simultaneously [61]. This *GB reweighting* method gradually corrects a high dimensional distribution by applying an ensemble of weak weighting trees. GB reweighting is used in the following to perform a further matching of simulation to data, and in next steps of the

analysis as will be discussed in Chapter 5. The target sample is the data sample shown in Figure 4.2, but constrained to signal mass region $5320 < m(J/\psi K^+K^-) < 5420\,\mathrm{MeV/c^2}$, and the remaining background is subtracted using the *sPlot* technique, which will be discussed in Section 4.6. The variables below are used in the GB weighting procedure, because of known differences or because they will be used in the next selection step:

- $p_T\,(B_s^0)$ - the transverse momentum of the signal B_s^0
- $\eta\,(B_s^0)$ - pseudorapidity (see Equation 3.1) of the signal B_s^0
- $\chi^2_{\mathrm{track}}\,(\mu^\pm)$ - the significance of the track fit of the muons
- $\chi^2_{\mathrm{track}}\,(K^\pm)$ - the significance of the track fit of the kaons
- `nLongTracks` - the number of long tracks (as defined in Section 3.4.5)

The distributions for a selection of the variables mentioned in this section are presented for the 2016 simulation and data samples in Figure 4.4. A good agreement is observed after the weighting procedure.

4.4 Multivariate Based Selection

The Toolkit for Multivariate Analysis (TMVA) [57] has been exploited to further suppress the combinatorial background, visible under the signal mass peak in Figure 4.2. It provides a large variety of multivariate classification algorithms, each combining a set of observables into a single variable, considering correlations between input variables to provide the maximum discrimination power. Out of the numerous multivariate classification algorithms available, the gradient-boosted decision tree BDTG3 is found to provide the best background rejection and signal efficiency. This algorithm allows up to 3 more layers of sub-nodes in the BDT than the default number. A multivariate algorithm is trained on pure samples of signal and background. The $B_s^0 \to J/\psi K^+K^-$ simulation sample is confirmed in the previous section to give a good representation of the signal data after correction, hence the weighted simulation sample is used as the signal sample. To provide a background sample, events are selected in data in the mass region $5450 < m(J/\psi K^+K^-) < 5550\,\mathrm{MeV/c^2}$. This so-called *upper sideband* is assumed to contain only combinatorial background. In the BDT, variables that

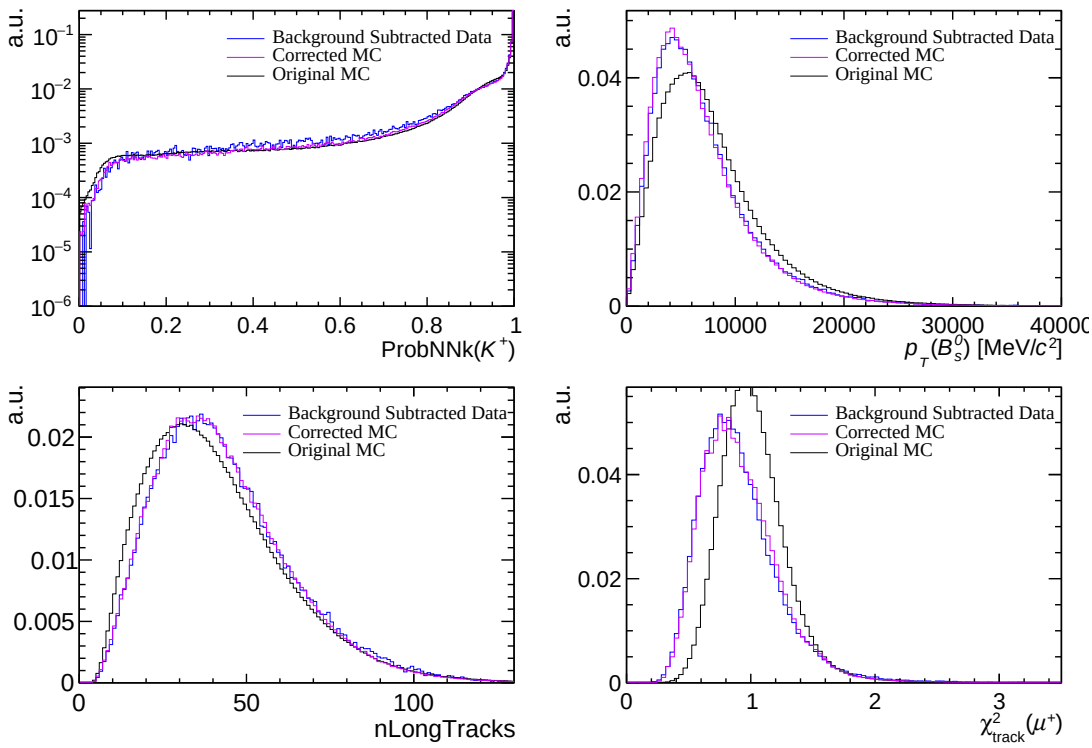

Figure 4.4 *A selection of PID re-sampled and GB reweighted variables for 2016 background subtracted data, and corrected and original simulated candidates:* `ProbNNk` (K^+), $p_T\,(B_s^0)$, `nLongTracks`, *and* $\chi^2_{\text{track}}\,(\mu^+)$.

would introduce angular biases or further decay-time acceptances are avoided, e.g. direction angle of the signal B_s^0 candidate or impact parameter χ^2 of final state particles. Ten variables are chosen based on their ability to discriminate between data and simulation:

- the maximum of the kaon tracks χ^2
- the maximum of the muon tracks χ^2
- the minimum of the logarithms of the two final state kaons `ProbNNk`
- the minimum of the logarithms of the two final state muons `ProbNNmu`
- the logarithm of the J/ψ decay vertex χ^2/nDoF
- the ϕ transverse momentum
- the B_s^0 transverse momentum
- the B_s^0 decay vertex χ^2/nDoF
- the logarithm of the B_s^0 impact parameter χ^2

- the logarithm of the B_s^0 DTF χ^2/nDoF

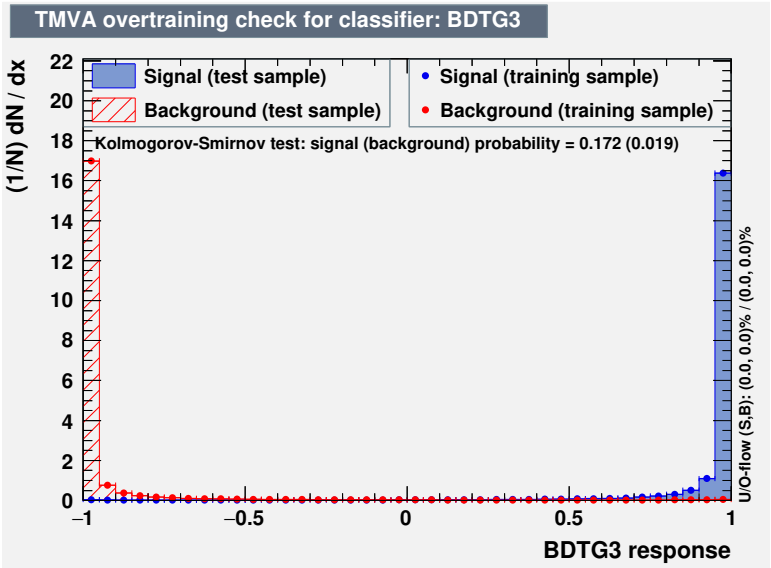

Figure 4.5 *BDT output for signal (blue) and background (red) events for training (points) and test (histogram) samples. Figure taken from Ref. [62].*

The final variable is computed by the DTF tool that performs the offline kinematic fit as mentioned in Section 4.1. The training is performed using 2016 data and simulation samples and the result can be found in Figure 4.5. A clear separation is visible between the signal (blue) and background (red) events. Figure A.1 shows the signal and background distributions for each variable separately. To check for over-training the signal and background samples are split in training and test samples. The training is done with 70% of the input samples, and afterwards applied to the test samples. A good agreement is observed between the distributions of the BDT response for the training (points) and test (histogram) samples, so no over-training is observed. The final step is to find the optimal cut on the BDT response, which is determined by maximising a figure of merit (FOM), usually a function depending on the number of signal events. The FOM criteria employed in this analysis is the effective signal sample size, which is determined using the sPlot method. Both will be explained in Section 4.6. A scan of the BDT cut value is performed, and for each value the FOM is computed. The optimal cut value is determined to be at > 0.58, which is indicated in the top plot in Figure 4.6 by the red vertical line. The 2016 data invariant mass after applying the cut is shown in the bottom plot. A clear signal peak is visible, however a small background contribution remains. The following sections will cover the final background subtractions. The trained BDT with its optimal cut

is applied to $B_s^0 \to J/\psi K^+K^-$ data and simulation of 2015 and 2016.

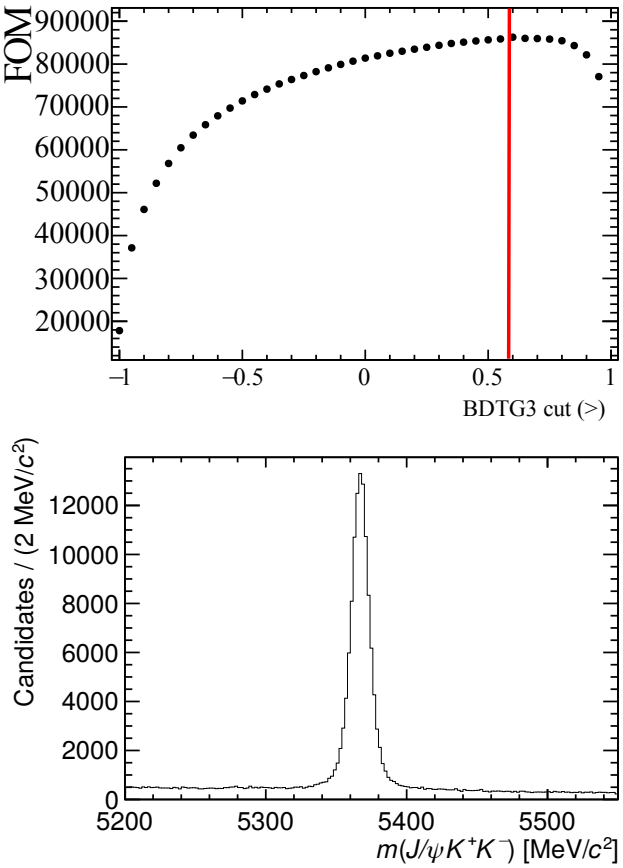

Figure 4.6 *Figure of merit evaluated over the BDT response with the optimal cut value indicated by the red vertical line (top), and the invariant mass in the 2016 data sample after applying the optimal BDT cut (bottom).*

4.5 Reflection Backgrounds

A small amount of background remains in the $m(J/\psi K^+K^-)$ distribution after applying the BDT cut. This is mainly combinatorial background which has a flat contribution, however another type of background is present as well. This type has a peaking structure, and comes from reflections: decays of other b-hadrons where one or more final state particles have been misidentified such that it has the same final state as the signal mode. As a result, the invariant mass of the B_s^0 candidate has been shifted with respect to B_s^0 candidates where all final state particles are correctly identified. The peaking background

distributions accumulate near the B_s^0 signal peak, hence should be removed before modelling the final signal distribution. The *lower* and upper sidebands - $[5200 < m(J/\psi K^+K^-) < 5347\,\mathrm{MeV/c^2}]$ and $[5387 < m(J/\psi K^+K^-) < 5550\,\mathrm{MeV/c^2}]$, respectively - of the broad B_s^0 mass spectrum are studied to identify the peaking backgrounds. Figure 4.7 shows the presence of misidentified simulated $\Lambda_b^0 \to J/\psi pK^-$ and $B^0 \to J/\psi K^+\pi^-$ signal events that survive the selection criteria for the invariant mass range considered in this analysis of $[5200 < m(J/\psi K^+K^-) < 5550\,\mathrm{MeV/c^2}]$. In the case of $\Lambda_b^0 \to J/\psi pK^-$, the proton has been misidentified as a kaon, leading to a lower final state invariant mass, and its distribution ends up at the lower mass range. For $B^0 \to J/\psi K^+\pi^-$ the opposite occurs due to a pion that has been misidentified as a kaon, resulting in a higher final state invariant mass.

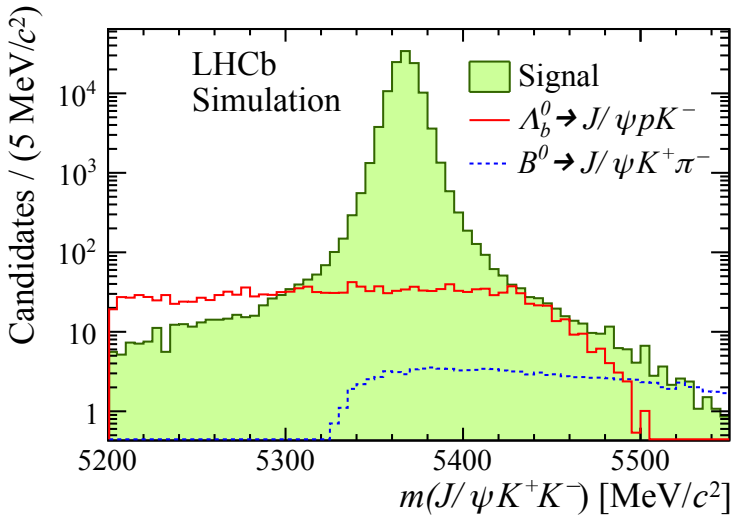

Figure 4.7 *Distribution of the invariant mass of $B_s^0 \to J/\psi K^+K^-$ signal MC (green filled area), and misidentified $\Lambda_b^0 \to J/\psi pK^-$ (solid red line) and $B^0 \to J/\psi K^+\pi^-$ (dotted blue line) MC. The distributions are weighted to correct for differences in the kinematics between data and simulation. Figure taken from Ref. [1].*

The veto for $B^0 \to J/\psi K^+\pi^-$ reflection events is optimised by studying events in the upper sideband which are interpreted as $J/\psi K^\pm\pi^\mp$. Table 4.3 shows the final applied veto which includes stringent pion identification requirements for the kaon that is most likely to be a pion, if the total invariant mass is within ± 15 MeV of the B^0 nominal mass. This veto is applied to the full B_s^0 mass range, and the number of expected remaining background events is calculated. The final contribution to the full dataset is negligible compared to the signal yield (see Section 4.6), hence the contribution can be ignored, for which a systematic is computed. All systematic uncertainties will be discussed in Chapter 7. A similar

procedure is followed to establish the $\Lambda_b^0 \to J/\psi p K^-$ veto. For this decay both lower and upper sidebands are considered. The identification condition is required for the kaon with larger `ProbNNp` and the invariant mass should be close to the Λ_b^0 nominal mass, as noted in Table 4.3. The expected remaining $\Lambda_b^0 \to J/\psi p K^-$

Table 4.3 *Vetoes applied on the reflection decays and the expected number of remaining background events in the full dataset after the vetoes.*

Background	Veto	Exp. rem. events
$B^0 \to J/\psi K^+\pi^-$	`ProbNNpi` > 0.7 or `ProbNNk` < 0.35 for most probable pion if $m(J/\psi K^\pm \pi^\mp) \pm 15$ MeV of $m(B^0)$ [24]	~ 120
$\Lambda_b^0 \to J/\psi p K^-$	`ProbNNp` > 0.7 for most probable proton if $m(J/\psi \overset{(-)}{p} K^\mp) \pm 15$ MeV of $m(\Lambda_b^0)$ [24]	1600 ± 160

background has a considerable contribution in the signal mass peak. To account for this, the simulated Λ_b^0 events are first reweighted to data for the angular, PID and kinematic distributions. Next, this corrected signal MC sample is injected in the data sample with negative weights such that they cancel out the contribution of the reflection background. The sum of the negative weights is fixed to the expected number of events of the reflection background. Uncertainties in the modelling of the peaking background lead to systematic uncertainties on the final parameter estimates.

4.6 Invariant Mass Distribution and sWeighting

After the elimination of reflection backgrounds in the invariant mass distribution shown in Figure 4.6, the remaining combinatorial background in the data sample can be subtracted using the sPlot technique [63]. This is a statistical tool which can be used to obtain distributions of variables for separate components within a data sample, e.g. signal and background. A discriminating variable for which the distributions are well understood is analysed to obtain separate signal and background distributions. From the separate distributions, the sPlot technique assigns a weight to each candidate: *sWeight* (w_i). The sWeights ensure that the weighted distribution represents the background-subtracted distribution. The sPlot method requires the discriminating variable for the sWeights to be uncorrelated (to *factorise*) with the variables that subsequently will be analysed.

In this analysis, the $J/\psi K^+K^-$ invariant mass is considered to calculate the

sWeights. A Probability Density Function (PDF) is constructed to fit to the mass, which models the signal by a single double-sided Crystal Ball (CB) [64], and the combinatorial background by an exponential function. A Crystal Ball function has a Gaussian core with mean μ, width σ and power law tail on one side, the threshold for which is controlled by the parameter α and the slope by n. The double-sided CB is able to properly describe the radiative tail (a charged final state particle radiates a photon) on the left and the tail caused by the J/ψ mass constraint (applied when building the B_s^0 candidate) on the right. The signal mass resolution, and therefore the invariant mass shape, is observed to be correlated to the helicity angle $\cos\theta_\mu$. To resolve this, the per-candidate mass uncertainty (σ_m) is considered as a conditional observable in the signal mass shape. A quadratic dependency on σ_m is incorporated in the width of the CB as $\sigma_{CB} = s_1 \times \sigma_m + s_2 \times \sigma_m^2$, where s_1 and s_2 (scale factors) are free parameters determined when fitting to data. The tail parameters are fixed to the values determined from a fit to corrected simulation signal events.

An additional background component that has to be considered in the PDF originates from suppressed $B^0 \to J/\psi K^+K^-$ decays. It has the same final state as the signal channel and is centred around the B^0 mass [24]. It is modelled in the nominal mass fit by a Gaussian function with its resolution, σ_{B^0}, fixed to the resolution determined by fitting the $B^0 \to J/\psi K^+\pi^-$ control channel, which will be discussed in Section 4.7. The difference between the mean of the Gaussian, μ_{B^0}, and of the CB, μ, is fixed to the mass difference between the B_s^0 and B^0 mesons taken from Ref. [24].

The full PDF can be described by the following formula:

$$\begin{aligned} \mathrm{PDF}(m|\sigma_m) = & f_{sig} CB(m; \mu, \alpha_1, n_1, \alpha_2, n_2, s_1, s_2|\sigma_m) \\ & + f_{bkg}((1 - f_{B^0})e^{-\gamma m} + f_{B^0} G(m; \mu_{B^0}, \sigma_{B^0})), \end{aligned} \tag{4.1}$$

where f_{sig} and f_{bkg} are the fractions of signal and background events in the dataset, γ is the coefficient in the exponential to describe the combinatorial background, and f_{B^0} the fraction of $B^0 \to J/\psi K^+K^-$ events in the total background.

When fitting the PDF to the $J/\psi K^+K^-$ invariant mass, an sWeight is determined for each candidate. The sWeights are typically larger than one in the centre of the signal peak, and gradually become smaller away from the peak to finally turn negative in the sidebands. Figure 4.8 shows as an example the sWeights

distribution for the $B_s^0 \to J/\psi K^+K^-$ signal events in the 2016 data sample, and the sWeights distribution versus the invariant mass. The analysis will be

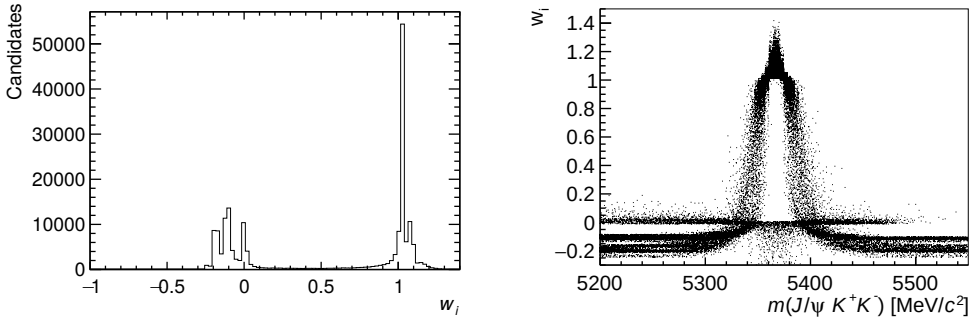

Figure 4.8 *(left) Distribution of sWeights for 2016 $B_s^0 \to J/\psi K^+K^-$ data. Positive values represent signal events, while negative values correspond to background events. The peak just above 0 corresponds mainly to events with an invariant mass below and above the B_s^0 mass [24]. (right) sWeights distributions versus the invariant mass for 2016 $B_s^0 \to J/\psi K^+K^-$ data.*

performed simultaneously in six $m(K^+K^-)$ bins, which will be explained in Section 6.5. For this reason, the sWeights are determined separately in the same six $m(K^+K^-)$ intervals which have boundaries at 990, 1008, 1016, 1020, 1024, 1032, and 1050 MeV/c^2. In the top plot of Figure 4.9 the six regions are indicated by dashed blue lines. The sample is further divided into the two years and the two trigger categories discussed in Section 4.1, biased and unbiased, leading to a total of 24 sub-samples, each with an independent signal and background fraction and different signal mass shapes. The yield for selected $B_s^0 \to J/\psi K^+K^-$ events in the full dataset is determined by cumulatively adding the sWeights for each event and is calculated to be $N_{sig} = 117694 \pm 364$. Figure 4.9 shows the result of the invariant mass fit to the full dataset in the bottom plot. The plot illustrates the signal, background and total fit, separately.

The FOM used in Section 4.4 to find the optimal BDT cut maximises the *effective signal sample* in data using the sWeights as follows [65]:

$$\text{FOM} = \frac{(\sum_i w_i)^2}{\sum_i w_i^2}. \tag{4.2}$$

The index i runs over all candidates in the sample and w_i are per-candidate weights determined from the invariant mass fit described previously. The denominator represents the total number of candidates. The numerator corresponds to a linear function of signal versus background events. When maximising the

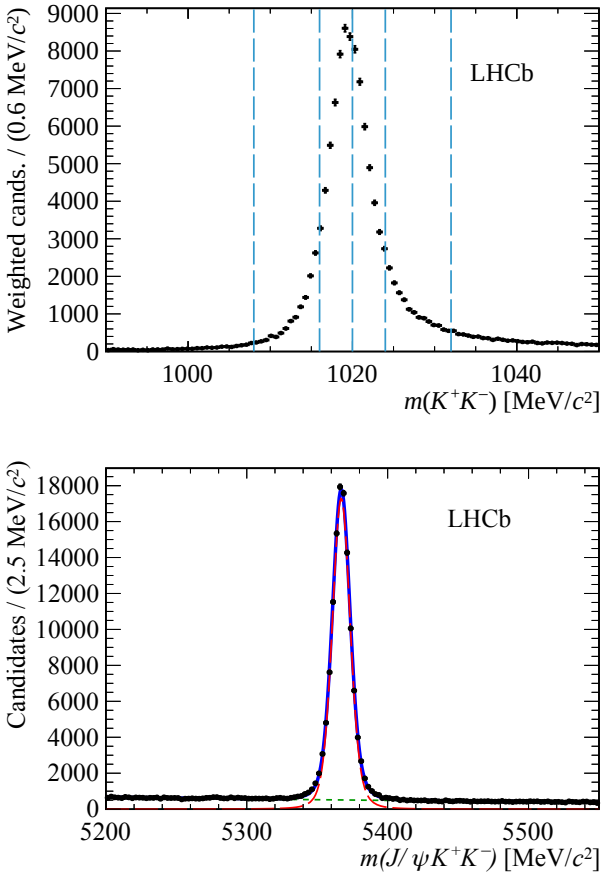

Figure 4.9 *Top: distribution of the K^+K^- invariant mass of selected candidates. The background is subtracted by the sPlot technique. The dashed blue lines indicate the boundaries of the six $m(K^+K^-)$ intervals that are used in the analysis. Bottom: distribution of the invariant mass of selected $B_s^0 \to J/\psi K^+K^-$ candidates in the full dataset. The signal contribution is indicated by the long-dashed red line, the background contribution by the dashed green line and the total fit function by the solid blue line. The $\Lambda_b^0 \to J/\psi p^+K^-$ background is statistically subtracted by injecting negative weights and the $B^0 \to J/\psi K^+K^-$ background is too small to be visible. Figures taken from Ref. [1].*

effective signal sample size by evaluating the FOM for each BDT cut, the optimal signal yield is found relative to the background contribution.

4.7 Control Channels

At various stages of the analysis, cross-checks are performed with *control channels* that are similar to the $B_s^0 \to J/\psi K^+K^-$ signal channel in final state particles and kinematics. The selection follows closely that of the signal decay and is described below in detail for $B^0 \to J/\psi K^+\pi^-$ and $B^+ \to J/\psi K^+$. Stripping lines written specifically for the decays are used to obtain the events, and individual physics parameter values are used to generate the simulation samples.

4.7.1 $B^0 \to J/\psi K^*(892)^0(\to K^+\pi^-)$

The $B^0 \to J/\psi K^+\pi^-$ channel, where the $K^+\pi^-$ predominantly originates from the resonant $K^*(892)^0$, has a similar final state signature. The K^{*0} is, analogous to the ϕ, a vector particle, hence the final state has the same P- and S-wave configuration, making it a good candidate for an angular efficiency cross-check, which will be discussed in Section 5.1. The final state is a direct probe of the flavour of the initial B^0 meson, of which the lifetime is precisely measured to be $\tau_{B^0} = 1.519 \pm 0.004\,\text{ps}$ [66]. The decay-time distribution can be described by one exponential due to a decay width difference between the two mass eigenstates in the B^0 system consistent with zero [24], and is therefore used for the decay-time efficiency determination in this analysis (Section 5.2).

To select the sample, the same trigger requirements as for the signal decay are applied and a stripping line written for the control channel is used. The following preselection is applied, which is similar to the $B_s^0 \to J/\psi K^+K^-$ selection:

- $5210 < m(J/\psi K^+\pi^-) < 5350\,\text{MeV/c}^2$
- $826 < m(K^+\pi^-) < 966\,\text{MeV/c}^2$
- $0.3 < t < 15.0$ ps
- $\sigma_t < 0.15$ ps
- $p_T(\pi^-) > 250\,\text{MeV/c}^2$

- $\Delta\ln\mathcal{L}_{K\pi}(\pi^-) < 0$ and $\Delta\ln\mathcal{L}_{K\pi}(\pi^-) \neq -1000$.

The decay-time t and uncertainty σ_t are computed offline by the DTF tool introduced in Section 4.1. The transverse momentum cut reduces the number of *multiple candidates*. Multiple candidates are signal candidates in an event which have a shared J/ψ and one or two different pions/kaons added and are consequently truly combinatorial in character.[1] The pion-identification upper bound reduces the probability of reconstructing two different B^0 candidates by swapping the kaon and pion mass hypotheses. The PID requirements furthermore remove most of the reflection background events. A study of the potential peaking backgrounds concludes their contribution to be negligible, except for a small presence of $B_s^0 \to J/\psi K^+\pi^-$, which is removed by selecting candidates with $m(J/\psi K^+\pi^-) < 5350\,\mathrm{MeV/c^2}$. The same BDT as is trained and optimised on the signal channel is used, applying the same selection requirement, except for the interchange of the K^- with the π^- and the ϕ with the K^{*0}. The simulation sample is matched to data in the same way as was performed for the $B_s^0 \to J/\psi K^+K^-$ simulation mentioned in Section 4.3.

The remaining background is statistically subtracted by the sPlot technique. The sWeights are determined separately for only 4 sub-samples, namely both years and trigger categories. The Hypatia function [67] is chosen to describe the signal distribution in the PDF, as it provides a better description of the signal peak for a higher number of events than the double-sided CB that was used for the signal channel. The Hypatia model requires for the core of the invariant mass distribution five shape parameters: ζ, β, λ, σ, and μ. The first two are set to zero since ζ is determined to be very small, whereas $\beta = 0$ means the core is symmetric left and right with respect to the mean. In the limit of $\zeta = 0$, λ does not depend on detector effects but solely on particle kinematics. The latter, mean and width are left floating in the fit to data. The tail parameters (α_1, α_2, n_1 and n_2) are fixed to values from a fit to the MC sample. Similar to the signal channel, the background is modelled by an exponential. A total of 552118 ± 948 selected $B^0 \to J/\psi K^+\pi^-$ events are found in the full dataset. The invariant mass fit is illustrated in Figure 4.10.

[1] The selection of $B_s^0 \to J/\psi K^+K^-$ does not consider multiple candidates, as the fraction in the signal sample is significantly small. A systematic is evaluated for this in Chapter 7.

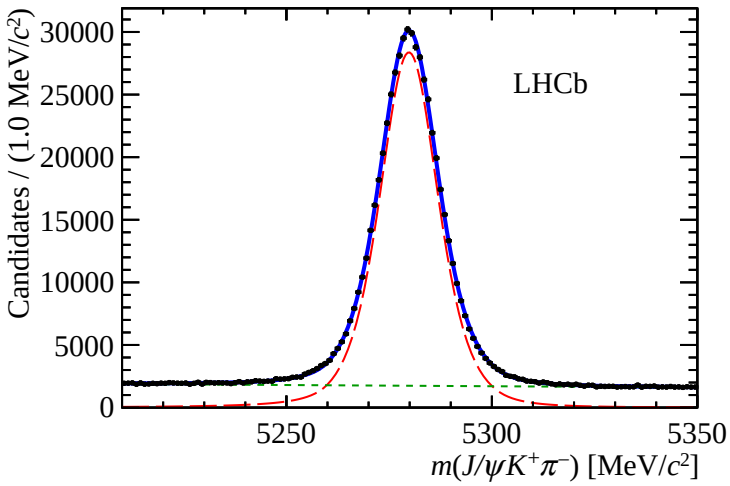

Figure 4.10 *Distribution of the invariant mass of selected $B^0 \to J/\psi K^+\pi^-$ events in the full dataset. The signal contribution - fitted with the Hypatia - is indicated by the long-dashed red line, the background contribution by the dashed green line and the total fit function by the solid blue line.*

4.7.2 $B^+ \to J/\psi K^+$

The $B^+ \to J/\psi K^+$ decay is similar to the signal decay, except for the absence of a second kaon among the decay products and the flavour specific final state. This channel has only one helicity angle, namely the muon helicity angle θ_μ, and proves to be a benchmark to test the angular efficiency determination from simulation, see Section 5.1. The channel is selected by the same trigger lines as the signal channel and by a stripping line explicitly written for the control channel. A similar preselection is applied to select the decay. Due to the absence of an intermediate state particle, the BDT has to be retrained. Nine variables are considered which are similar to the ones used for the signal channel:

- the kaon track χ^2
- the maximum of the muon tracks χ^2
- the logarithm of the kaon `ProbNNk`
- the minimum of the logarithm of the muons `ProbNNmu`
- the logarithm of the J/ψ decay vertex χ^2/nDoF
- the B^+ transverse momentum

- the B^+ decay vertex χ^2/nDoF
- the logarithm of the B^+ impact parameter χ^2
- the logarithm of the B^+ DTF χ^2/nDoF

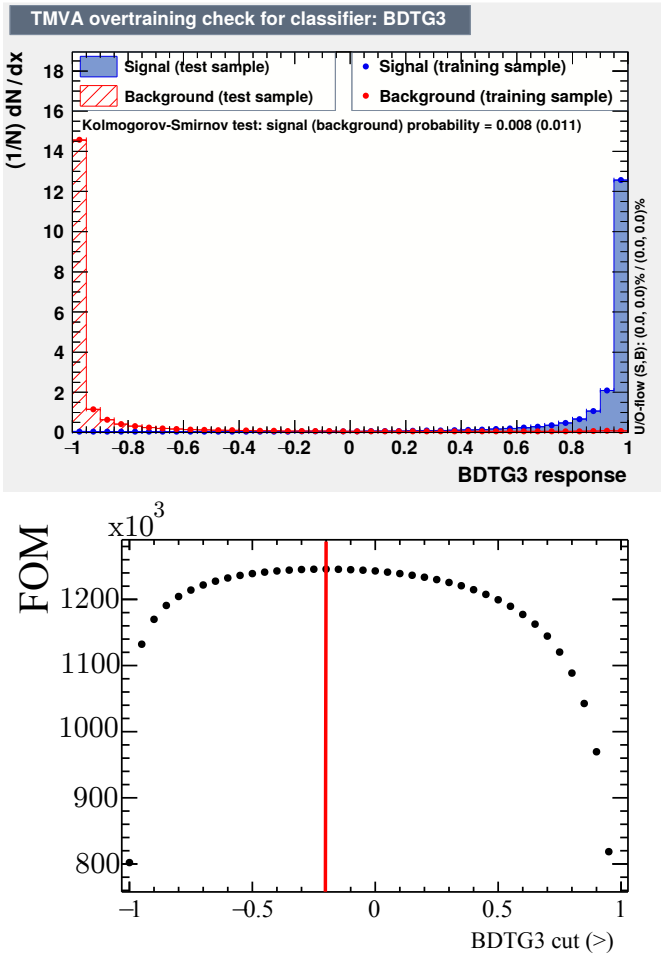

Figure 4.11 *Results for the $B^+ \to J/\psi K^+$ BDT training. Top: BDT output for signal (blue) and background (red). Bottom: FOM results evaluated over the BDT response with the optimal cut value indicated by the red vertical line.*

The final variable is computed by the DTF tool that performs the offline kinematic fit as mentioned in Section 4.1. Equivalent to the signal channel, the simulation sample is matched to data before the BDT training. The background sample is chosen from the upper sideband in the data sample, and the signal sample by restricting the mass range to be $5240 < m(J/\psi K^+) < 5320\,\mathrm{MeV/c^2}$ in the simulated sample. The top plot in Figure 4.11 illustrates the BDT response, which provides a good separation between signal and background, and matching distributions for the training and test samples. The same FOM as described in

Section 4.6 is used to find the optimal BDT cut value and concludes a value of > -0.2, indicated by the red vertical line in the bottom plot in Figure 4.11. Following the strategy as performed for $B^0 \to J/\psi K^+\pi^-$, the sample is then split in both years and trigger categories and the sPlot technique is applied by modelling the signal with a Hypatia function and the background with an exponential. The tail parameters of the Hypatia are fixed to values obtained by fitting to the simulation sample. A total of 1680775 ± 1520 selected $B^+ \to J/\psi K^+$ events are found in the full dataset. The invariant mass fit is illustrated in Figure 4.12.

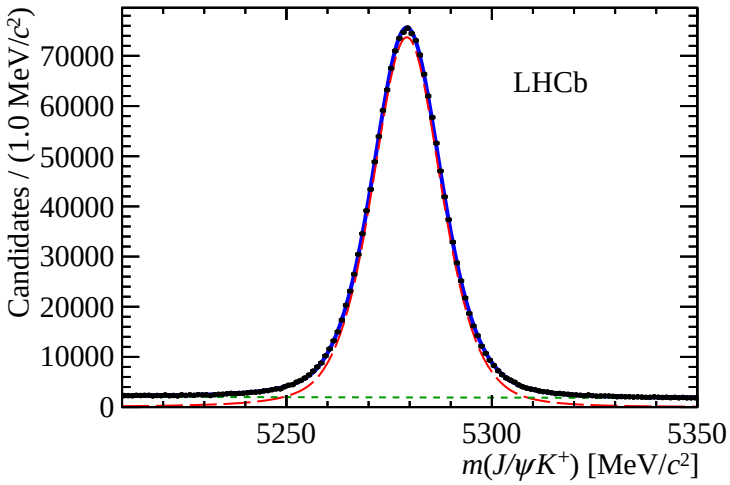

Figure 4.12 *Distribution of the invariant mass of selected $B^+ \to J/\psi K^+$ events in the full dataset. The signal contribution - fitted with the Hypatia - is indicated by the long-dashed red line, the background contribution by the dashed green line and the total fit function by the solid blue line.*

Chapter 5

Experimental Effects

The $B_s^0 \to J/\psi K^+K^-$ decay has a high yield and low background, making it an excellent channel to determine the *CP* violating phase ϕ_s. From Equation 2.26 it can be seen that the *CP* asymmetry shows an oscillatory behaviour versus time: $A_{CP} \propto -\Im(\lambda_f)\sin(\Delta m_s t)$, where $\Im(\lambda_f) \approx -\sin(\phi_s)$. Hence, the measurement of the amplitude is a direct probe of the phase ϕ_s. Figure 5.1 presents a simplified version of the $B_s^0 - \overline{B}_s^0$ mixing and its decay to the signal final state as a function of decay-time. Several assumptions are made to enhance the oscillation. The final state is considered to be only *CP*-even, and the *CP* violating parameters are set to $|\lambda_f| = 1$ and $\phi_s = 0.3$ rad (one order of magnitude larger than the prediction assuming the SM [23]). Furthermore, a perfect reconstruction of the decay and knowledge of the initial flavour of the B_s^0 meson are assumed. The values of Δm_s, Γ_s and $\Delta\Gamma_s$ are set to the current world averages [66].

Several experimental factors cause dilution of the observed sinusoid, and will be discussed in this chapter. They have to be taken into account to provide the correct estimates for ϕ_s and the other physics parameters that define the decay $B_s^0 \to J/\psi K^+K^-$. Chapter 6 will discuss the inclusion of the experimental effects in the maximum-likelihood fit to data, which uses the differential decay rate defined in Equation 2.31 as PDF. I have been involved in the determination of the angular and decay-time acceptance, and the optimisation of one of the flavour tagging algorithms.

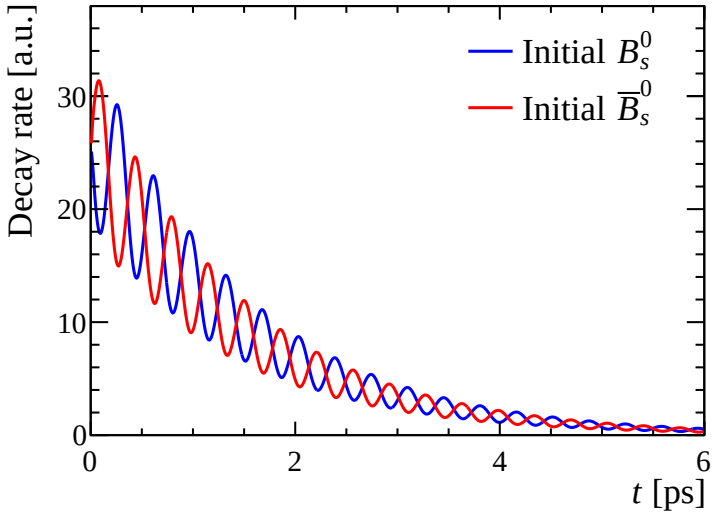

Figure 5.1 *Time-dependent decay distributions of the B_s^0 and $\overline{B}_s^0$ meson into $J/\psi K^+K^-$. The final state is assumed to be only CP-even. The mass and decay width variables of the B_s^0 system are set to the current world averages [66], $|\lambda_f| = 1$, $\phi_s = 0.3$ rad (one order of magnitude larger than the prediction assuming the SM [23]), and no experimental effects are taken into account. Figure taken from Ref. [68].*

5.1 Decay Angles

As mentioned in Section 2.6, the analysis has to be performed as a function of the helicity angles cos θ_K, cos θ_μ, and ϕ_h. The *angular resolution* - the precision of the measurement of the helicity angles - of the detector has previously been determined to be sufficiently good so that its effect can be ignored in the measurement [28, 56]. The LHCb detector geometry and selection requirements introduce an efficiency (*acceptance*) that varies as a function of the helicity angles, which needs to be explicitly accounted for. The angular acceptance is determined using simulated events, hence the angle and momenta distributions in simulation need to match that in data. The method to extract the acceptance and the iterative reweighting procedure used to make simulation identical to data are discussed next, followed by cross-checks using the B^0 and B^+ control channels.

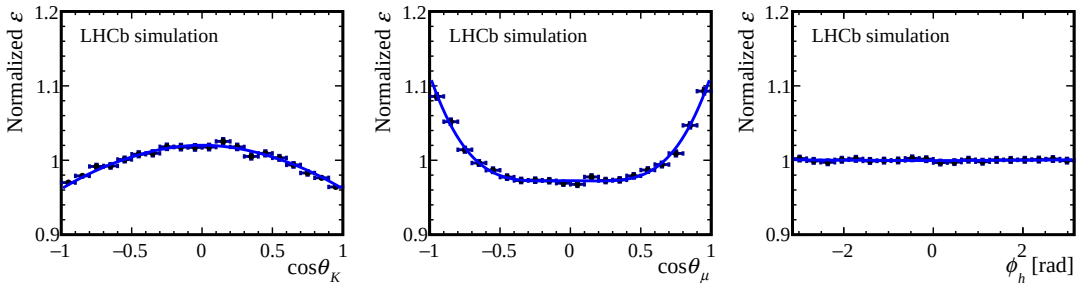

Figure 5.2 *Projections of the angular efficiency for each of the three helicity angles - $\cos\theta_K$ (left), $\cos\theta_\mu$ (centre) and ϕ_h (right)-, where in all cases the acceptance is integrated over the other two angles. The points are obtained by dividing the distribution of selected simulated $B_s^0 \to J/\psi K^+K^-$ decays by the distribution expected without any acceptance effect. The blue curve represents a fit of an even fourth-order polynomial to each of the one-dimensional efficiency histograms separately. Figures taken from Ref. [1].*

5.1.1 Acceptance

The three-dimensional angular efficiency is defined as the probability to reconstruct an event, given that it was generated with a certain set of decay angles. It is determined from simulated events. Figure 5.2 shows the efficiency distributions for each helicity angle separately - $\varepsilon(\cos\theta_K)$, $\varepsilon(\cos\theta_\mu)$, $\varepsilon(\phi_h)$ - for which the efficiency is integrated over the other two angles. The points are obtained by taking the ratio of the decay angle distribution for selected simulated $B_s^0 \to J/\psi K^+K^-$ signal events and the true angular distribution. The selected simulated sample has passed the detector simulation stage, and is weighted to match the kinematic distributions and physics parameters in data (following the procedure that will be discussed in Section 5.1.2). The true angular distribution is obtained from generated $B_s^0 \to J/\psi K^+K^-$ events that have physics parameters corresponding to the ones in Table 4.2. The blue curve is the result of a fourth-order polynomial fit the data points for each of the angles separately. The acceptance histograms for the different decay angles are only used for visualisation and are not used in the analysis. Instead, the angular acceptance, $\varepsilon(\vec{\Omega})$, is determined using the procedure described in detail in Ref. [69], which will be summarised in the following.

The PDF used to describe the distribution of $B_s^0 \to J/\psi K^+K^-$ signal events in data is constructed to be the differential decay rate represented in Equation 2.31, $\frac{\mathrm{d}\Gamma(t,\vec{\Omega})}{\mathrm{d}t\mathrm{d}\vec{\Omega}}$ - in the following referred to as $p(t,\vec{\Omega})$ -, divided by its normalisation. The acceptance is known to additionally vary as a function of decay-time, $\varepsilon(t,\vec{\Omega})$.

Including the decay-time and angular dependent efficiency in the PDF leads to the observed shape of the decays, $\mathrm{PDF}^{obs}(t, \vec{\Omega})$:

$$\mathrm{PDF}^{obs}(t, \vec{\Omega}) = \frac{\varepsilon(t, \vec{\Omega}) p(t, \vec{\Omega})}{\int\int \mathrm{d}t \mathrm{d}\vec{\Omega}\, \varepsilon(t, \vec{\Omega}) p(t, \vec{\Omega})}. \tag{5.1}$$

The efficiencies are assumed to factorise, for which a systematic will be assigned:

$$\varepsilon(t, \vec{\Omega}) = \varepsilon(t) \times \varepsilon(\vec{\Omega}). \tag{5.2}$$

The decay-time efficiency will be discussed in detail in Section 5.2.2, whereas this section will focus on the determination of the angular acceptance. Using this factorisation and the definition of the differential decay rate as a sum of ten separate time- and angular-dependent terms, as described in Equation 2.31, the PDF may be re-written as:

$$\mathrm{PDF}^{obs}(t, \vec{\Omega}) = \frac{\sum_{k=1}^{10} \varepsilon(t)\varepsilon(\vec{\Omega}) h_k(t) f_k(\vec{\Omega})}{\sum_{k=1}^{10} \int \mathrm{d}t \varepsilon(t) h_k(t) \int \mathrm{d}\vec{\Omega} \varepsilon(\vec{\Omega}) f_k(\vec{\Omega})}, \tag{5.3}$$

where f_k and h_k are defined in Table 2.1 and Equation 2.32, respectively. The efficiency terms in the numerator do not affect the measurement of any physics parameters, as will be explained in Chapter 6. In the denominator the time-dependent terms are dependent on the physics parameters, as will be discussed in the same chapter. The f_k, however, only depend on the decay angles - as can be seen from Table 2.1 -, which also holds for the angular efficiency. The second integral in the denominator can therefore be evaluated once and does not vary in any fitting process. The angular acceptance is described through ten *normalisation weights*, one for each term in the differential decay rate, which are defined as:

$$\xi_k \equiv \int \mathrm{d}\vec{\Omega} \varepsilon(\vec{\Omega}) f_k(\vec{\Omega}) \tag{5.4}$$

In Ref. [69] the integral over the full phase-space is approximated by a sum over all generated events. Furthermore, the efficiency is considered to be either zero or one, depending on if an event is accepted, leading to the sum over the accepted events after selection:

$$\xi_k = \frac{1}{N_{gen}} \sum_{i}^{accepted} \frac{f_k(\vec{\Omega_i})}{\mathrm{PDF}^{gen}(\vec{\Omega_i}|t_i)}, \tag{5.5}$$

where N_{gen} is the total number of generated events, and $\mathrm{PDF}^{gen}(\vec{\Omega_i}|t_i)$ the

true physical distribution at a given reconstructed decay-time t. The normalisation weights are thus determined by iterating over the selected simulated $B_s^0 \rightarrow J/\psi\, K^+K^-$ sample and summing the ratio of the relative angular function and the true physical distribution for the corresponding event. The normalisation weights avoid the need to determine a parametrisation of the angular efficiencies based on the histograms explicitly, hence they are model independent and are therefore not subject to any sort of systematic uncertainty due to the choice of the model. The acceptance terms are determined with respect to ξ_1. In case of a perfect angular acceptance, the weights reduce to $\xi_{1,2,3,7} = 1$ and $\xi_{4,5,6,8,9,10} = 0$. This is often referred to as a *flat* angular acceptance.

The normalisation weights are determined separately from the 2015 and 2016 simulation samples of selected $B_s^0 \rightarrow J/\psi K^+K^-$ signal events for the corresponding data sample. To decrease the statistical uncertainty on the normalisation weights the nominal simulation sample (with generation values defined in Table 4.2) is combined with an additional available set of simulated 2015 and 2016 samples, which have been produced with decay width difference $\Delta\Gamma_s = 0$ ps. A difference is observed in the acceptance for the decay-time biased and unbiased data samples (defined in Section 4.1 by the passed trigger lines), hence the weights are additionally evaluated separately for both trigger categories. An initial set that is determined from the combined simulated samples can be found in Table 5.1. A systematic is assigned for the limited size of the simulation data sample and for the assumption that the angular and decay-time acceptances factorise.

Table 5.1 *Initial angular acceptance weights determined from the combined MC samples.*

k		ξ_k/ξ_1			
		Unbiased 2015	Biased 2015	Unbiased 2016	Biased 2016
1	(00)	1 ± 0	1 ± 0	1 ± 0	1 ± 0
2	($\parallel\parallel$)	1.0270 ± 0.0019	1.0291 ± 0.0035	1.02497 ± 0.00065	1.0208 ± 0.0014
3	($\perp\perp$)	1.0270 ± 0.0018	1.0283 ± 0.0034	1.02469 ± 0.00064	1.0208 ± 0.0014
4	($\parallel\perp$)	-0.0019 ± 0.0015	-0.0096 ± 0.0029	-0.00063 ± 0.00052	0.0024 ± 0.0012
5	(0 $\parallel$)	0.00017 ± 0.00087	0.0039 ± 0.0017	0.00099 ± 0.00031	0.00321 ± 0.00067
6	(0 $\perp$)	0.00141 ± 0.00087	0.0020 ± 0.0017	0.00012 ± 0.00031	-0.00018 ± 0.00067
7	(SS)	1.0082 ± 0.0013	1.0137 ± 0.0024	1.00624 ± 0.00044	1.0113 ± 0.0010
8	(S$\parallel$)	-0.0007 ± 0.0011	-0.0033 ± 0.0022	0.00032 ± 0.00040	-0.00003 ± 0.00087
9	(S$\perp$)	0.0007 ± 0.0011	-0.0013 ± 0.0022	0.00024 ± 0.00041	-0.00003 ± 0.00088
10	(S0)	-0.0001 ± 0.0024	-0.0052 ± 0.0045	-0.00104 ± 0.00084	-0.0022 ± 0.0018

5.1.2 Iterative Reweighting

The acceptance determination from simulation is only valid if simulation accurately describes the distributions of the $B_s^0 \to J/\psi K^+K^-$ signal events in data. The kinematic distributions of the final state particles are directly correlated with the angular acceptance, as the helicity angles are functions of the momenta of the final state particles. Discrepancies are observed in the final state kinematics between data and simulation, hence Table 5.1 does not represent the acceptance in data correctly. These differences are primarily caused by an incorrect description of the signal B_s^0 momentum (see top right plot in Figure 4.4), and deviating $m(K^+K^-)$. Additionally, simulation could be generated with different underlying physical parameter values than those observed in data, leading to wrongly modelled angular distributions. For example, simulation does not include an S-wave component, which can cause differences in the observed kaon momentum spectrum. The simulation reweighting procedure discussed in Section 4.3 has been optimised for the use in the selection of the signal decay, and small differences remain in the final state kinematics. For the angular acceptance instead an iterative procedure is employed to match simulation to data. The procedure can be broken down into the following steps:

1. The combined simulation sample of $\Delta\Gamma_s \neq 0$ ps and $\Delta\Gamma_s = 0$ ps is GB reweighted (a technique introduced in Section 4.3) in the variables in $p(B_s^0)$, $p_T(B_s^0)$ and $m(K^+K^-)$ to match the distributions in data of the same year and trigger category. Additionally, the simulated events are corrected to have the same magnet polarity fraction as the data.

2. From this sample, an initial estimate of the normalisation weights is computed using Equation 5.5, while including the per-event weights determined in the previous step.

3. This initial estimate of the angular acceptance is included in a fit to the full data sample of $B_s^0 \to J/\psi K^+K^-$ signal events, making use of the maximum-likelihood fit that will be discussed in Chapter 6. The fit determines a first estimate of the physics parameters, however the angular acceptance does not properly model that in data yet.

4. The next step is to correct simulation for the difference in the underlying physics parameters, where the weights from the previous correction step are included as well. Each simulated event is additionally weighted by the

ratio between the PDF obtained from the fit to data in the previous step and the PDF using the generation values for simulation from Table 4.2, which does not include any acceptance and resolution effects. The aim is effectively to weight the simulated $B_s^0 \to J/\psi K^+K^-$ signal events to have been generated with the physical parameters in data.

5. This weighted simulated sample is furthermore GB reweighted in the final state kinematics $p(K^\pm)$ and $p_T(K^\pm)$ to data, to correct for any remaining differences.

6. A new set of normalisation weights is calculated using Equation 5.5, while including the per-event weights obtained in the previous step.

7. The fit to data is repeated using the normalisation weights from step 6, to obtain a new estimate of the physics parameters.

8. The procedure is repeated from step 4 until the observed change in the angular normalisation weights is negligible.

During the iterative procedure, the S-wave fraction in simulation gradually matches that in data. The result is in effect a simulated sample that is weighted to be a sample that is generated with the physics parameters observed in data. The final iteratively reweighted simulation sample can now safely be used to determine the angular acceptance for data. The final weights are presented in Table 5.2 and will be used in the final maximum-likelihood fit to data. Alternative iterative corrections are tested to evaluate a systematic.

Table 5.2 *Angular acceptance weights determined from the iteratively reweighted MC samples.*

k		ξ_k/ξ_1			
		Unbiased 2015	Biased 2015	Unbiased 2016	Biased 2016
1	(00)	1 ± 0	1 ± 0	1 ± 0	1 ± 0
2	($\parallel\parallel$)	1.0429 ± 0.0020	1.0392 ± 0.0038	1.03761 ± 0.00070	1.0327 ± 0.0015
3	($\perp\perp$)	1.0437 ± 0.0020	1.0374 ± 0.0038	1.03738 ± 0.00069	1.0327 ± 0.0015
4	($\parallel\perp$)	-0.0023 ± 0.0016	-0.0106 ± 0.0032	-0.00080 ± 0.00054	0.0029 ± 0.0012
5	(0 $\parallel$)	-0.00123 ± 0.00094	0.0037 ± 0.0018	0.00023 ± 0.00033	0.00309 ± 0.00073
6	(0 $\perp$)	0.00124 ± 0.00093	0.0023 ± 0.0018	0.00024 ± 0.00033	-0.00024 ± 0.00072
7	(SS)	1.0152 ± 0.0014	1.0213 ± 0.0027	1.01004 ± 0.00047	1.0190 ± 0.0011
8	(S$\parallel$)	-0.0012 ± 0.0012	-0.0044 ± 0.0024	0.00007 ± 0.00042	0.00012 ± 0.00093
9	(S$\perp$)	0.0006 ± 0.0012	-0.0008 ± 0.0024	0.00009 ± 0.00043	0.00010 ± 0.00094
10	(S0)	-0.0175 ± 0.0026	-0.0351 ± 0.0049	-0.00388 ± 0.00089	0.0054 ± 0.0019

5.1.3 Cross-checks

To validate the iterative reweighting procedure, the control channel $B^0 \to J/\psi K^+\pi^-$ is studied. This decay also has a P- and S-wave final state configuration, and is selected as described in Section 4.7. The simulation sample only contains $K^+\pi^-$ pairs that originate from the decay of a $K^*(892)^0$, and the final state is therefore purely described by the P-wave component. The proponents of Ref. [70] studied 2011 $B^0 \to J/\psi K^+\pi^-$ data, and observed a $\sim 6\%$ presence of S-wave, for which the simulation will be corrected. In addition, the physics parameters specific to the decay that are determined in Ref. [70] can provide a benchmark. The 2016 simulation sample is weighted to 2016 data using the same iterative reweighting procedure as performed for the signal channel, with the interchange of the B_s^0 with the B^0 and the K^- with the π^-. A set of normalisation weights are determined using Equation 5.5, while including the weights computed by the iterative reweighting procedure. The normalisation weights are used in a maximum-likelihood fit to $B^0 \to J/\psi K^+\pi^-$ data to obtain estimates for the physics parameters. The results are in agreement with Ref. [70] within 1σ.

To validate the strategy of determining the angular acceptance from simulation, the control channel $B^+ \to J/\psi K^+$ is used, selected as described in Section 4.7. Due to the single kaon in the final state, the decay has only one helicity angle, namely the helicity angle θ_μ between the two muons. Theory predicts that this angle follows a purely $\sin^2\theta_\mu$ distribution, making it an excellent candidate to test the validity of the simulation. The angular efficiency will be obtained directly from simulation and afterwards applied to data to verify the correction for the angular acceptance using simulation. The cross-check is performed with 2016 $B^+ \to J/\psi K^+$ data and simulation. The study is done as a function of $\eta(B^+)$, because of an performance issue of the simulation for charged tracks at low pseudorapidity. Nine regions are defined with boundaries at 2., 2.5, 3., 3.2, 3.5, 3.7, 4., 4.2, 4.5 and 5. First, in each $\eta(B^+)$ bin, the $\cos\theta_\mu$ distribution of simulated events is divided by the theoretically predicted $\sin^2\theta_\mu$ (or $1-\cos^2\theta_\mu$) distribution, to obtain acceptance histograms. Figure 5.3 shows the result in the first two bins of $\eta(B^+)$. Next, the $\cos\theta_\mu$ distribution of data events are per $\eta(B^+)$ region divided by the corresponding acceptance histogram. Finally, in each bin a fit is performed to the data points with the function $f(\cos\theta_\mu) = a(1 + b\cos^2\theta_\mu)$. In case of a perfect angular acceptance correction a value of $b = -1$ is expected. The data distributions in the first two bins can be found in Figure 5.4. A good

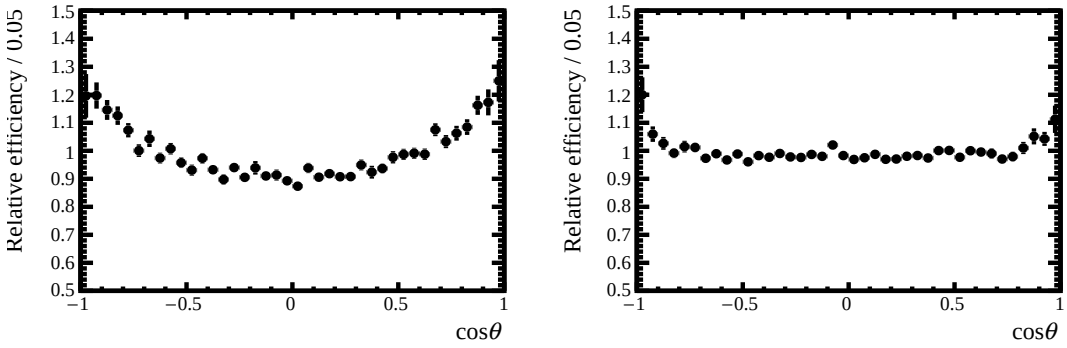

Figure 5.3 *Acceptance histograms of* $\cos\theta_\mu$ *distributions in 2016* $B^+ \to J/\psi K^+$ *simulation divided by the theoretical predicted distribution* $\sin^2\theta_\mu$ *in the first two* $\eta(B^+)$ *bins.*

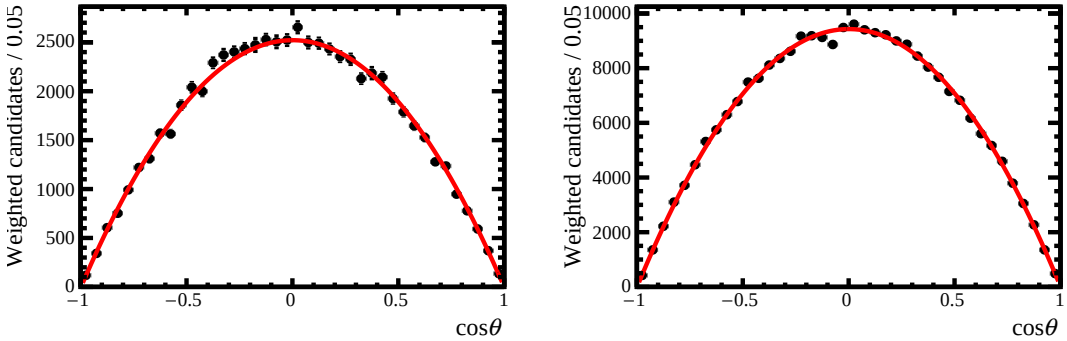

Figure 5.4 *Helicity angle distributions in 2016* $B^+ \to J/\psi K^+$ *data divided by the acceptance histograms of Figure 5.3. Only the first two* $\eta(B^+)$ *bins are shown together with the result of the fit of* $f(\cos\theta_\mu) = a(1 + b\cos^2\theta_\mu)$ *in red.*

agreement between the corrected data distribution and the fit is observed for all bins. The values of a and b are presented per bin in Figure 5.5 together with the result of performing a fit of a constant line. A value of $b = -1.0014 \pm 0.0011$ is determined, indicating that the simulation is able to correctly describe the angular acceptance as a function of $\eta(B^+)$ within 0.14%. As the data shows a drop-off at large $\eta(B^+)$, a consistency check is performed for using a flat line. The $\chi^2 = 8.8$ for the nine data points leads to a p-value of 0.36, which means it is sufficient to describe the data with a flat line.

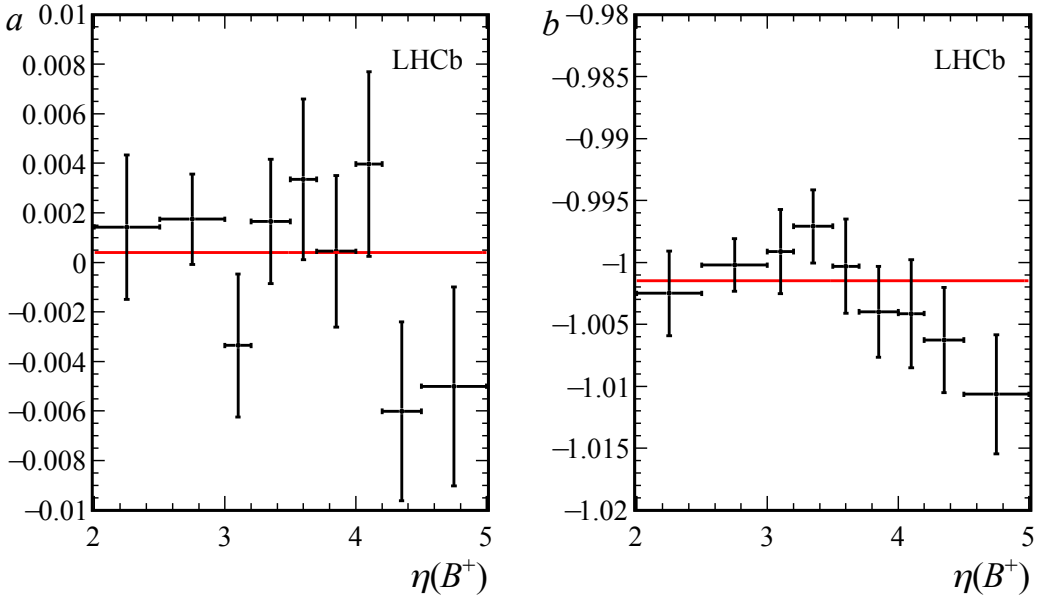

Figure 5.5 *Variation of the fit parameters a and b as a function of* $\eta(B^+)$*. The red line shows the results of a* χ^2 *fit to a constant line to the points.*

5.2 Decay-time

The decay rate of $B_s^0 \to J/\psi K^+K^-$ is determined as a function of decay-time. The detector has a finite precision on its measurement. A poor time resolution will smear out the observed oscillation, and decrease the relative precision on the ϕ_s measurement, hence the correct resolution determination is crucial. Furthermore, as mentioned in the previous section, a decay-time efficiency has to be considered in the analysis. The main inefficiencies are caused by the reconstruction efficiency of the detector at large decay-times, and by displacement requirements in the trigger and event selection at low times. The decay-time resolution and acceptance are determined in this section.

5.2.1 Resolution

The detector is able to locate the beam interaction point and decay vertex of B_s^0 mesons with high precision, as mentioned in Section 3.4.2, and therefore establish precise decay-time evaluation of each event. To properly observe the oscillation of the B_s^0 mixing, the decay-time resolution should be smaller than the fast B_s^0 oscillation period, $P = 2\pi/f = 2\pi/\Delta m_s \sim 350$ fs. The LHCb

detector resolution depends on the decay channel. In Run 2 the average *effective* decay-time resolution for a decay into 4 final state particles is of the order of $\sigma_{eff} \sim 45$ fs [38]. The main source of the finite detector resolution is the uncertainty of the decay length, i.e. how well primary and secondary vertices are fitted [42]. Figure 5.6 on the left shows the decay-time resolution using a simulated $B_s^0 \to J/\psi K^+K^-$ sample, by plotting the difference between measured and true decay-time. The resolution causes a damping on the observed $B_s^0 - \overline{B}_s^0$ oscillation amplitude by a factor, the *dilution* ($\mathcal{D}$) [71], which is given by:

$$\mathcal{D} = e^{-\sigma_{eff}^2 \frac{\Delta m_s^2}{2}}. \tag{5.6}$$

The width of the dilution is determined by the decay-time resolution, σ_{eff}.

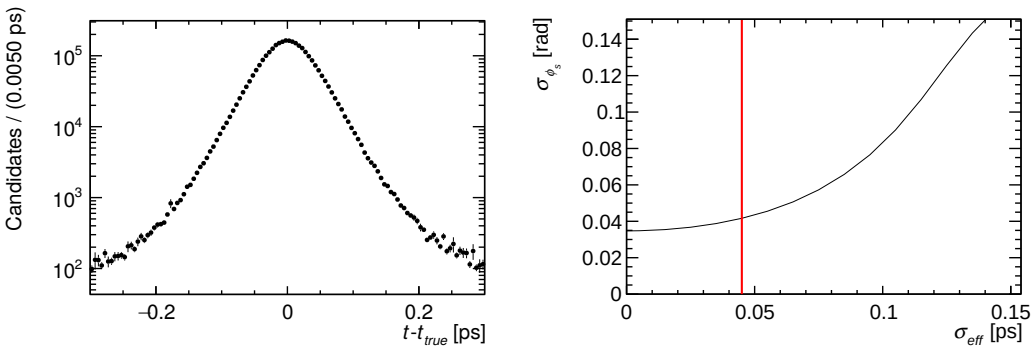

Figure 5.6 *Left: observed decay-time resolution for simulated 2016 $B_s^0 \to J/\psi K^+K^-$ signal events, which is obtained by plotting the difference between the observed and true decay-time. Right: the relative effect of the detector resolution on the ϕ_s uncertainty. The numbers are determined by a maximum-likelihood fit to data, where for each fit the resolution of all events is fixed to the same value. The red vertical line represents the detector resolution of $\sigma_{eff} \sim 45$ fs [38].*

Figure 5.6 on the right shows the effect of the decay-time resolution on the ϕ_s uncertainty. For this plot the maximum-likelihood fit is performed to the full dataset of $B_s^0 \to J/\psi K^+K^-$, signal events, where for each fit the resolution of all events is fixed to the same value. The detector resolution is indicated by the red vertical line, and shows the small influence on the ϕ_s uncertainty. However, the resolution has to be properly determined to avoid biasing its contribution to the observed oscillation amplitude. Instead of obtaining the resolution directly from simulation, information in data is used to obtain the proper resolution. As mentioned in Section 4.1, in the offline selection the decay-time uncertainty σ_t is calculated, which is different for each B_s^0 candidate. Figure 5.7 shows the distribution for $B_s^0 \to J/\psi K^+K^-$ signal events in data. A time resolution

model, dependent on the per-event decay-time uncertainty, is incorporated in the final maximum-likelihood fit to data to make optimal use of the available information. The measured distribution is calibrated, to eliminate any bias in the measurement. The calibration is performed in ten bins of σ_t to obtain the relation between the true and measured decay-time uncertainty.

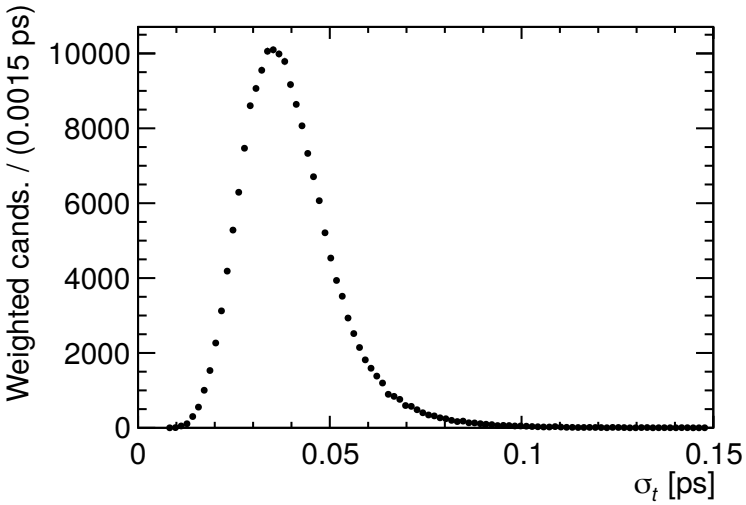

Figure 5.7 *Per-candidate decay-time uncertainty distribution for* $B_s^0 \to J/\psi\ K^+K^-$ *signal events in 2016 data.*

Prompt events are excellent candidates to calibrate the decay-time uncertainty, as they originate from the primary interaction directly, and not from a B_s^0 decay. Their decay-time is therefore expected to be zero, hence the detector resolution can be determined directly by studying the decay-time distribution. A data sample of prompt $J/\psi K^+K^-$ events is selected by a selection similar as described in Chapter 4 for the signal decay mode without any requirements on the decay-time, which would reject prompt events. In addition a *prescale* is applied, so that only a fraction of the flagged events are stored. This is often applied to channels with an expected high yield where it is not necessary or feasible to save all events. The result is a sample which is almost purely composed of events containing real-J/ψ candidates, without any background events. Figure 5.8 shows its decay-time distribution in the left plot, where negative decay-time values are non-physical, and therefore directly probe the detector resolution. The 2015 and 2016 data samples are combined for the calibration to reflect the mix of signal data. For this sample the decay-time resolution is determined in ten bins of its decay-time uncertainty, and the calibration is performed. This results in calibration parameters that will be used in the final maximum-likelihood fit of the signal

channel.

The resolution is determined for prompt $J/\psi K^+K^-$ events by fitting a PDF to the observed decay-time distribution. This PDF is build up by a delta function to represent the prompt decay distribution, $\delta(t)$, and a function of two exponentials to represent long-lived J/ψ mesons originating from b-hadron decays, $E(t)$, which are convolved with a resolution function, $\mathcal{R}(t)$. In addition, a shape is added for the small fraction of candidates that have a decay-time reconstructed with respect to a wrong PV, $W(t)$. The model of the PDF is then:

$$\text{PDF} = [f_{prompt}\delta(t) + (f_{ll})E(t)] \otimes \mathcal{R}(t) + f_{wpv}W(t), \tag{5.7}$$

where f_{prompt}, f_{ll} and f_{wpv} are the fractions in the sample of the corresponding category. Here ll stands for long-lived, and wpv for wrong primary vertex. The resolution function for the prompt sample is described by a sum of three Gaussian distributions:

$$\mathcal{R}(t) = \sum_{i=1}^{3} f_i \frac{1}{\sqrt{2\pi}\sigma_i} \exp\left[-\frac{(t-\mu)^2}{2\sigma_i^2}\right], \tag{5.8}$$

where σ_i are the individual widths for each of the Gaussian, μ is the common mean, and $\sum_i f_i = 1$. The mean is expected to be zero, and any deviation is assigned as a systematic. The left plot in Figure 5.8 shows a fit to the full prompt $J/\psi K^+K^-$ dataset for a region around the peak at 0 ps, where the different components are indicated.

The triple-Gaussian model can be translated into a single-Gaussian shape as in Equation 5.6 in two steps. First, the dilution of the amplitude of the $B_s^0 - \overline{B}_s^0$ oscillation for the triple-Gaussian model is computed as:

$$\mathcal{D} = \sum_{i=1}^{3} f_i e^{-\sigma_i^2 \frac{\Delta m_s^2}{2}}. \tag{5.9}$$

Then, the dilution is translated into an effective resolution by:

$$\sigma_{eff} = \sqrt{-\frac{2\ln\mathcal{D}}{\Delta m_s^2}}, \tag{5.10}$$

A single-Gaussian resolution with width σ_{eff} gives the same damping effect as the triple-Gaussian model, and allows an easier evaluation of systematic uncertainties.

The calibration sample is split into ten sub-samples according to the per-event

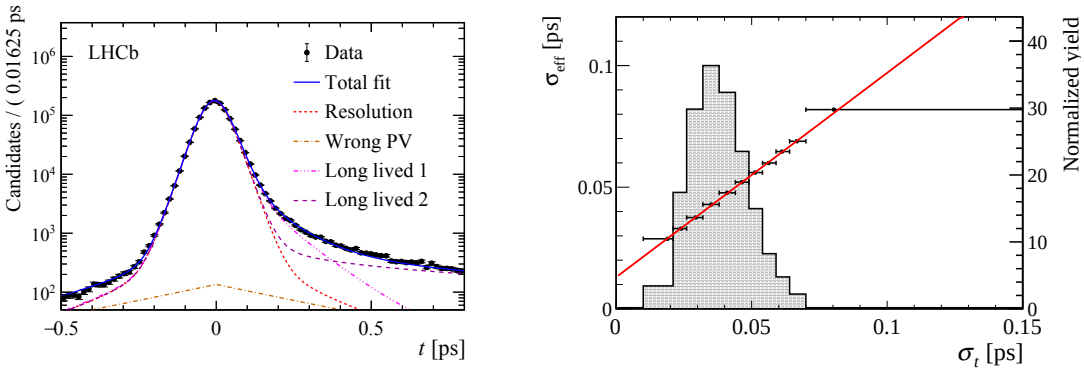

Figure 5.8 *Left: decay-time distribution of prompt $J/\psi K^+K^-$ signal events in the full dataset. The total fit result is presented by the blue solid line, the overall resolution by the dashed red line, and the wrong PV and the b-hadron J/ψ events components by the long-dashed-dotted brown, dashed-multiple-dotted pink and the long-dashed purple line, respectively. Right: variation of the effective decay-time resolution as a function of the bins in per-event decay-time uncertainty for prompt $J/\psi K^+K^-$ signal events, with a linear fit through the data points in red. The shaded histograms shows the distribution for $B_s^0 \to J/\psi K^+K^-$ signal events to which the right y axis applies. Figures taken from Ref. [1].*

decay-time uncertainty σ_t. In each bin the model of Equation 5.7 is fitted to the decay-time distribution in order to obtain the parameters that govern the decay-time resolution of Equation 5.8, and consequently compute σ_{eff}. Figure 5.8 shows the effective resolution, σ_{eff}, for each bin of the measured per-candidate decay-time uncertainty, σ_t, for prompt $J/\psi K^+K^-$ signal events. A linear dependence is observed on the per-candidate decay-time uncertainty and from a fit the calibration parameters are determined: $\sigma_{eff}(\sigma_t) = b_0 + b_1\sigma_t$, where $b_0 = 12.97 \pm 0.22$ fs and $b_1 = 0.846 \pm 0.006$. These numbers are included in the final maximum-likelihood fit to the full dataset to translate the per-event decay-time uncertainty of $B_s^0 \to J/\psi K^+K^-$ signal events into the true resolution. Figure 5.8 shows additionally the distribution of σ_t for the signal decay by the shaded histogram. An alternative function is fitted to compute a systematic uncertainty. By applying the calibration to $B_s^0 \to J/\psi K^+K^-$ signal events an effective decay-time resolution averaged over the ten bins of $\sigma_{eff} = 45.54 \pm 0.04 \pm 0.05$ fs is computed, where the first uncertainty is statistical, and the second contribution comes from the uncertainties on the calibration parameters. By using $\Delta m_s = 17.757 \pm 0.021$ ps^{-1} [66] and Equation 5.6, a dilution of $\mathcal{D} = 0.721 \pm 0.001$ is determined.

5.2.2 Acceptance

In order to correctly determine the lifetime-related parameters $\Delta\Gamma_s$ and Γ_s, we need to understand the decay-time acceptance. Section 4.1 classifies the HLT1 trigger lines used in the selection as decay-time biased and unbiased lines, hence a different distribution is expected for the events that pass the different trigger types. For visualisation, Figure 5.9 shows acceptance histograms for $B_s^0 \to J/\psi K^+K^-$ signal events in 2016 data separately for both trigger categories in the dataset. These are obtained using data by taking the ratio of the observed decay-time distribution and an exponential function, fixed to the world average value for Γ_s and convolved with a resolution model. In this analysis instead, the efficiency is determined by parametrising an efficiency function, $\varepsilon(t)$, which will be described in this section is and represented by the blue curve in Figure 5.9.

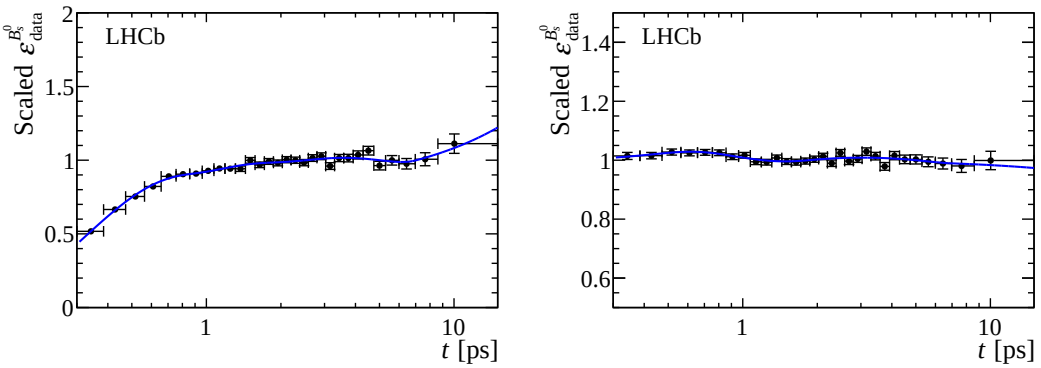

Figure 5.9 *Decay-time acceptance distributions for biased (left) and unbiased (right) $B_s^0 \to J/\psi K^+K^-$ signal events in 2016 data. The points are obtained by taking the ratio of the observed decay-time distribution and an exponential function convolved with a resolution model. The blue curve shows the efficiency parametrisation as described in the text. Figures taken from Ref. [1].*

The efficiency function is determined from a kinematically and topologically very similar decay. The control channel $B^0 \to J/\psi K^+\pi^-$ is chosen, because of its precisely measured lifetime and decay width difference $\Delta\Gamma_d \approx 0\,\text{ps}^{-1}$ [24] (as mentioned before in Section 4.7). The decay-time distribution is therefore described by only a single exponential, which allows a direct extraction of the decay-time acceptance by comparing the observed distribution with a single exponential. Small lifetime and kinematic differences between the signal and control decay cause small variations in the decay-time acceptances for the B_s^0 and B^0 signal events. These are taken into account by correcting with a ratio of

efficiencies of the simulated signal and control mode:

$$\varepsilon^{B_s^0}_{\text{data}}(t) = \varepsilon^{B^0}_{\text{data}}(t) \times \frac{\varepsilon^{B_s^0}_{\text{sim}}(t)}{\varepsilon^{B^0}_{\text{sim}}(t)}, \tag{5.11}$$

where $\varepsilon^{B_s^0}_{\text{data}}(t)$ and $\varepsilon^{B^0}_{\text{data}}(t)$ are the decay-time efficiencies of the B_s^0 signal and the B^0 control mode, respectively, and $\varepsilon^{B_s^0}_{\text{sim}}(t)/\varepsilon^{B^0}_{\text{sim}}(t)$ is the ratio of efficiencies of simulated signal and control decays after reconstruction and selection, determined by dividing both efficiency distributions as a function of time. The efficiency function parametrisation will be explained later.

Before extracting the B_s^0 decay-time acceptance, the B^0 simulated and data and B_s^0 simulated samples are GB weighted to match the B_s^0 data sample in various distributions. A less complex strategy than for the angular acceptance is employed, as differences between simulation and data are similar between the signal and control channel. The p and p_T distributions of the B^0 data signal events and the p_T of the B_s^0 and B^0 simulated signal events are corrected. As previously mentioned in this chapter, the simulation samples do not include an S-wave component. Furthermore, the fraction of S-wave is different between the $B_s^0 \to J/\psi K^+K^-$ and the $B^0 \to J/\psi K^+\pi^-$ decays. The simulation samples are therefore first reweighted to match the physics parameters in data. This is done by weighting the simulated events with the ratio between the PDF obtained from the final maximum-likelihood fit to data and the PDF using the generation values. Next, the simulated events are weighted to match the $m(K^+K^-)$ and $m(K^+\pi^-)$ distributions in data. The simulated events are furthermore corrected to have the same magnet polarity fraction as the data. A systematic is taken into account for the simulation corrections. To be able to use the simple model of only one exponential, the B_s^0 simulation sample used for this strategy is generated with decay width difference $\Delta\Gamma_s = 0$ ps, and a systematic is evaluated to account for this.

The following will describe the efficiency function parametrisation. A cubic spline [72] is chosen to model the decay-time efficiency distribution. This allows a direct implementation in the integral in the denominator of the final PDF (see Equation 5.3) which can then be calculated analytically. This discussed in more detail in Appendix B as well as in Ref. [73]. The cubic spline is defined by a set of interval boundaries, *knots*, and is described by a third order polynomial in each interval. At the knots it is required to be continuously differentiable, leading to a smooth function. In this analysis the spline, $s(t)$, is a linear combination of

"basis" cubic splines (*b-splines*), $b_i(t)$. For N number of intervals there are $N+1$ knots and $N+3$ b-splines, leading to the following:

$$s(t) = \sum_{i=0}^{N+2} c_i b_i(t), \tag{5.12}$$

where c_i is the coefficient of the respective b-spline. In each interval i there are four contributing b-splines, $b_i(t)$ for $i \in \{i, i+1, i+2, i+3\}$. In this analysis 7 knots are used to obtain a proper description of the acceptance function, leading to 9 coefficients. The first coefficient is fixed to unity. The choice of the knots is based on the exponential distribution of the decay-time: $[0.3, 0.58, 0.91, 1.35, 1.96, 3.01, 7.00]$ ps. After the last knot, the spline is extrapolated with a linear function. A systematic is calculated for the chosen knot positions. The spline avoids the use of acceptance histograms, which are more sensitive to statistical fluctuations as they represent the average acceptance over a given bin.

We want to obtain a single spline that parametrises the decay-time acceptance of the B_s^0 signal data, $\varepsilon_{\text{data}}^{B_s^0}(t)$ (left-hand side of Equation 5.11). First, the following three splines are defined:

- $s_{\text{sim}}^{B_s^0}(t)$ - the acceptance of the B_s^0 signal events in simulation
- $s_{\text{sim}}^{B^0/B_s^0}(t)$ - the ratio of acceptances of the B^0 and B_s^0 signal events in simulation
- $s_{\text{data}}^{B_s^0}(t)$ - the acceptance of the B_s^0 signal events in data

Each spline has nine free parameters that represent the spline coefficients. Then, to obtain each of the acceptances on the right-hand side of Equation 5.11, the decay-time distributions of each of the samples - $B^0 \to J/\psi K^+\pi^-$ data and simulation, and $B_s^0 \to J/\psi K^+K^-$ simulation - is described by a PDF composed of the product of a single exponential function convolved with a Gaussian resolution and an efficiency function which will be described below. Each efficiency will be determined in a fit, while the exponential distributions and resolution widths are fixed as explained later. The three decay-time efficiencies are parametrised in terms of the previously defined splines:

- $\varepsilon_{\text{sim}}^{B_s^0}(t) = s_{\text{sim}}^{B_s^0}(t)$

- $\varepsilon^{B^0}_{\text{sim}}(t) = s^{B^0/B^0_s}_{\text{sim}}(t) \times s^{B^0_s}_{\text{sim}}(t)$
- $\varepsilon^{B^0}_{\text{data}}(t) = s^{B^0_s}_{\text{data}}(t) \times s^{B^0/B^0_s}_{\text{sim}}(t)$.

Finally, a simultaneous fit is performed to each of the three decay-time distributions to determine the efficiencies, and as a result the nine coefficients of the three different splines. Due to the representation, the B^0_s data spline coefficients and their uncertainties are directly computed, which allows an easy control of the associated systematic uncertainty.

For the exponential distributions the decay width of the B^0 data sample is fixed to the current world average, $\Gamma_d = 0.6583 \pm 0.0017$ ps^{-1} [66], and the decay widths of the B^0 and B^0_s simulation samples to the values with which they are generated. The Gaussian resolution models are centred at zero. The Gaussian resolution widths are determined for the simulation samples following the method discussed in Section 5.2.1 and for the B^0 data sample by scaling the B^0_s resolution width by the ratio of widths observed in the two simulation samples. The resolution widths are $\sigma^{B^0_s}_{\text{sim}} = 42$ ps, $\sigma^{B^0}_{\text{sim}} = 42$ ps and $\sigma^{B^0}_{\text{data}} = 39$ fs. A systematic is evaluated for the resolution widths.

The decay-time acceptance coefficients are evaluated separately for both trigger categories and the two years of data-taking and can be found in Table 5.3. A systematic is determined for the statistical uncertainty on the coefficients due to the finite size of the simulation samples and B^0 data sample. The final acceptance splines for the $B^0_s \to J/\psi K^+K^-$ signal events in 2016 data are indicated in Figure 5.9 by the blue lines.

Table 5.3 *Coefficients of the cubic spline describing the decay-time acceptance for each data category.*

	Unbiased 2015	Biased 2015	Unbiased 2016	Biased 2016
c_0	1.0 ± 0.0	1.0 ± 0.0	1.0 ± 0.0	1.0 ± 0.0
c_1	1.053 ± 0.074	1.69 ± 0.27	1.007 ± 0.028	1.49 ± 0.11
c_2	1.096 ± 0.048	1.73 ± 0.2	1.03 ± 0.018	2.056 ± 0.095
c_3	0.97 ± 0.053	1.85 ± 0.24	1.0 ± 0.021	2.12 ± 0.12
c_4	1.052 ± 0.049	1.99 ± 0.23	0.982 ± 0.018	2.28 ± 0.11
c_5	1.051 ± 0.051	1.92 ± 0.23	0.998 ± 0.019	2.29 ± 0.12
c_6	1.027 ± 0.064	2.01 ± 0.27	1.004 ± 0.024	2.45 ± 0.14
c_7	1.09 ± 0.064	2.18 ± 0.28	0.983 ± 0.023	2.24 ± 0.13
c_8	1.047 ± 0.053	1.93 ± 0.24	0.981 ± 0.02	2.32 ± 0.12

5.2.3 Cross-checks

Validation studies have been performed of the methods employed to extract the decay-time resolution and acceptance. The decay-time resolution calibration is validated using simulation samples. The procedure described in Section 5.2.1 is first applied to a combined 2015 and 2016 sample of simulated prompt $J/\psi K^+K^-$ candidates, to obtain decay-time resolution calibration parameters. The decay-time distribution is fitted per σ_t bin, and an average effective resolution $\sigma_{eff} = 40.80 \pm 0.04 \pm 0.08$ fs is calculated. The first uncertainty comes from the size of the used samples, and the second from the uncertainties on the calibration parameters. Next, a similar procedure is applied to $B_s^0 \to J/\psi K^+K^-$ simulated events of the full dataset. Instead of fitting the decay-time distribution in bins of σ_t, the distribution $t - t_{true}$ as shown in Figure 5.6 is used to evaluate the resolution for each σ_t bin, from which an average effective resolution $\sigma_{eff} = 41.60 \pm 0.04 \pm 0.02$ fs is concluded. The difference between the simulation samples of 0.8 fs is considered as a systematic uncertainty on the $B_s^0 \to J/\psi K^+K^-$ data resolution for the translation of the prompt data resolution to the signal sample.

The control channels $B^0 \to J/\psi K^+\pi^-$ and $B^+ \to J/\psi K^+$ are studied to validate the decay-time acceptance method, in particular the correction factor that is considered for differences between the data samples. The procedure described in Section 5.2.2 is applied to 2016 data and simulation samples of the control modes that are selected as described in Section 4.7. First, the efficiency $\varepsilon^{B^+}_{\text{data}}(t)$ is computed by replacing the B_s^0 samples in Equation 5.11 by B^+ samples. In the simultaneous fit to the decay-time distributions of the B^0 simulation and data and B^+ simulation samples, the same resolution is assumed for all samples. The simulation decay widths are fixed to the generation values, and of the B^0 data to the current world average [24]. The same knot positions as when fitting the signal channel are used. The determined efficiency, $\varepsilon^{B^+}_{\text{data}}(t)$, is used in a maximum-likelihood fit to the B^+ signal data sample following the same procedure as this analysis, which will be described in Chapter 6, from which a decay width difference $\Gamma_u - \Gamma_d = -0.0478 \pm 0.0013$ ps^{-1} is computed. This is consistent with the current world average of $\Gamma_u - \Gamma_d = -0.0474 \pm 0.0023$ ps^{-1} [24] within a precision of 0.003 ps^{-1}. Next, a check is performed where the B^0 data and simulation samples are split according to several selection criteria, where one is used as the signal and the other as calibration in Equation 5.11. The obtained efficiency is used in a maximum-likelihood fit to the B^0 data sample that is categorised as the signal sample, and in all cases the obtained decay width

difference is consistent with zero within 0.003 ps^{-1}.

5.3 Flavour Tagging

To study the oscillation of B_s^0 mesons, it is important to determine the initial flavour of the b-quark at production. When decays have final states that are CP eigenstates, i.e. $f = \bar{f}$, it is experimentally not possible to precisely determine the signal meson flavour. One of the key qualities of the LHCb experiment is the ability to derive the flavour by employing particular pieces of information in the event, a technique that is called *flavour tagging*. The flavour is estimated for each decay, together with a probability that the estimate is wrong. Two independent classes of flavour tagging algorithms, the opposite-side (OS) taggers [74, 75] and the same-side (SS) taggers [76, 77], employ different features of the $b\bar{b}$ production in the pp collision. Each algorithm produces a tag decision per event $q = \{+1, -1, 0\}$ for B_s^0, $\overline{B}_s^0$, or untagged, respectively, and a mistag probability η defined in the range $0 \leq \eta \leq 0.5$, since $\eta > 0.5$ corresponds to the opposite decision with a mistag of $(1-\eta)$. For untagged candidates the flavour algorithms are unable to estimate the signal meson flavour, leading by definition to a mistag probability of 50% or $\eta = 0.5$. Imperfect knowledge of the initial flavour of the B_s^0 meson causes a dilution of the observed oscillation amplitude, hence directly affects the uncertainty on ϕ_s.

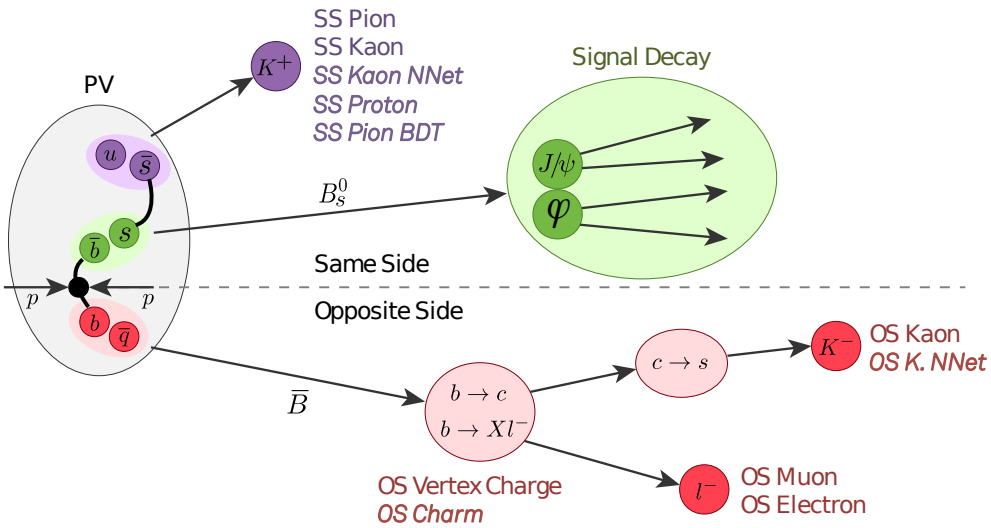

Figure 5.10 *Available flavour tagging algorithms for Run 2 analyses at LHCb [78].*

Figure 5.10 shows a schematic view of the $B_s^0 \to J/\psi K^+K^-$ decay and the

available flavour tagging algorithms. OS algorithms infer the signal meson flavour by studying charge information of the decay products coming from the decay of the b-hadron produced by the other b quark in the event. These include the charge of muons or electrons from semileptonic b decays, the overall charge of the secondary vertex, the charge of a reconstructed secondary charm hadron, and the charge of the kaon from opposite-side $b \to c \to s$ transitions. The information coming from all relevant algorithms are combined into a single OS tagging response. The SS tagger related to the signal decay is the same-side kaon (SSK) tagger, which exploits the additional kaon that tends to be produced in the hadronisation process of the signal B_s^0 ($\overline{B}_s^0$) meson by the partner of the s ($\bar{s}$) quark. The OS response can be combined with the SSK result to determine the final tagging performance.

5.3.1 Formalism

Each tagger takes as input both geometrical and kinematic information and provides, based on one or more multivariate classifiers, as output the tagging decision q and mistag probability η. The classifiers are optimised and calibrated on flavour specific channels, for which the final state is a direct probe of the flavour, such as the control channels $B^+ \to J/\psi K^+$ and $B_s^0 \to D_s^- \pi^+$. The control channels are chosen because of their large number of events and can be used as calibration channels as the true mistag rate can directly be compared. The algorithms are optimised to select on tracks related to the signal decay and to suppress contributions from low-energy hadronic (soft QCD) processes or other pp collisions (*underlying event*), which would reduce their performance. The tagging decisions are based on the charge of the track which is correlated to the signal b-meson flavour. Three important quantities are: the *mistag rate*, the *tagging efficiency* and the *tagging power*.

The fraction of events for which the algorithm is able to provide a tagging decision is defined as the tagging efficiency (ε_{tag}):

$$\varepsilon_{tag} = \frac{N_{tagged}}{N_{tagged} + N_{untagged}}, \tag{5.13}$$

where N_{tagged} is the number of events with a tag decision, and $N_{untagged}$ the number of events for which the flavour algorithm was unable to estimate the signal meson flavour. The tagged events are a collection of wrongly tagged events

(N_W) and correctly tagged events (N_R): $N_{tagged} = N_W + N_R$. The true mistag rate (ω) is thus:

$$\omega = \frac{N_W}{N_{tagged}}. \tag{5.14}$$

When the signal meson is charged, it is possible to directly compare the flavour of the reconstructed signal meson with the flavour tagging decision. Neutral mesons on the other hand are affected by neutral flavour oscillations, and the true mistag rate has to be extracted by a time-dependent fit on the flavour oscillations as a function of decay-time. In the case of non-flavour specific decays, such as $B_s^0 \to J/\psi K^+K^-$, the mistag rate can only be estimated and needs to be calibrated. The calibration is parametrised by a linear relationship between the true mistag from a flavour specific decay, ω, and estimated mistag from the tagging algorithm, η, providing the corrected mistag probability $\omega(\eta)$:

$$\begin{aligned} \omega(\eta) &= \left(p_0 + \frac{\Delta p_0}{2}\right) + \left(p_1 + \frac{\Delta p_1}{2}\right)(\eta - \langle\eta\rangle) \\ \overline{\omega}(\eta) &= \left(p_0 - \frac{\Delta p_0}{2}\right) + \left(p_1 - \frac{\Delta p_1}{2}\right)(\eta - \langle\eta\rangle)\,. \end{aligned} \tag{5.15}$$

Here $\omega(\eta)$ and $\overline{\omega}(\eta)$ are the calibrated mistag probabilities for B_s^0 and $\overline{B}_s^0$, respectively, and $\langle\eta\rangle$ is the average estimated mistag probability for the calibration channel. p_0 and p_1 are the main calibration parameters. The additional calibration parameters, Δp_0 and Δp_1, account for mistag differences for the initial B_s^0 and $\overline{B}_s^0$ mesons. The calibrations are performed separately for the OS and SSK algorithms. The calibration procedures that are applied in the following are standard techniques that are provided by the Flavour Tagging group of the LHCb experiment, but they were performed with a weighting specific for the signal decay $B_s^0 \to J/\psi K^+K^-$.

The mistag rate and tagging efficiency provide a determination of the sensitivity to the *CP* asymmetry, A_{CP}. The measured time-dependent *CP* asymmetry related to tagged events is distorted by the mistag rate with a dilution of:

$$\mathcal{D} = 1 - 2\omega. \tag{5.16}$$

The true *CP* asymmetry and its statistical error can be calculated as:

$$A_{CP} = \frac{A_{CP}^{meas}}{1 - 2\omega}, \qquad \sigma_{A_{CP}} \propto \frac{1}{\sqrt{\varepsilon_{tag} N}(1 - 2\omega)}. \tag{5.17}$$

From this, the effective tagging efficiency, i.e. tagging power, ε_{eff}, is defined which can be interpreted as the factor by which the effective sample size is reduced due to imperfect tagging:

$$\varepsilon_{eff} = \varepsilon_{tag}(1 - 2\omega)^2 = \varepsilon_{tag}\mathcal{D}^2. \tag{5.18}$$

The tagging power is a measure of the tagging performance.

5.3.2 Tagging Algorithm Optimisation

The tagging power quantifies the fraction of the sample equivalent to perfectly tagged events. This variable is therefore used as a figure of merit for the optimisation of the tagging algorithms. All tagging algorithms are developed following the same procedure and are trained and calibrated on either data or simulation. A detailed description of the optimisation performed by the Flavour Tagging group and the final obtained tagging powers after calibration can be found in Ref [79]. I have contributed to the optimisation of the SSK tagger.

The SSK tagging algorithm is optimised using a simulated $B_s^0 \to D_s^- \pi^+$ sample, because the fast B_s^0 oscillation would make it impossible to train on data. First, the algorithm is trained to select the best tagging track candidate(s). The variables used in the multivariate classifier are chosen because of various characteristics. The tracks should have a well defined PID to ensure it is the right particle. Furthermore, they should be associated with the signal PV, but should not originate from the signal decay. This is achieved by including geometrical conditions, e.g. on the pseudorapidity and the polar angle, and requiring a small momentum component pointing away from the beam axis. A higher number of primary vertices and track multiplicity have a negative result as it becomes harder to choose the right track candidate. A selection is developed, with the goal to maximise the tagging power and to enhance the purity of the tagging candidates. Next, the three best tagging track candidate(s) are chosen whose charge can be used to infer the flavour of the signal meson and to determine the predicted mistag rate. For the optimisation various multivariate algorithms are tested which use information related to the signal meson and the remaining tagging candidates. The result of the previous step is combined with the PID of the tagging candidate, and is used as input for the chosen classifier together with the p_T of the signal B_s^0 meson, and the number of tracks and PVs in the event.

The SSK tagging algorithm is trained with the aim to distinguish the B_s^0 and $\overline{B}_s^0$ mesons.

The OS tagging algorithms are optimised in a similar way as the SSK algorithm using either data or simulation samples of mainly $B^+ \to J/\psi K^+$ and $B^0 \to J/\psi K^+\pi^-$. The tagging track candidates do not come from the signal PV, but originate from the OS b-hadron decay. The selection is therefore different from the SSK track candidate selection by requiring a large momentum component pointing away from the beam axis and a large impact parameter significance with respect to the signal PV. Most algorithms also include the transverse momentum of the signal meson, and nPV and track multiplicity, as they have a large impact on the tagging power. Only the candidate with the highest transverse momentum is used for the next step. The OS taggers are then trained to achieve the best discrimination between tracks correctly and wrongly correlated to the signal meson flavour. This is done by training multivariate algorithms which use kinematic and geometrical information related to the signal meson and the remaining tagging candidate(s). The separate OS taggers are merged into a final combined OS tagger.

5.3.3 Same Side Tagger Calibration

To perform the SSK tagger calibration for $B_s^0 \to J/\psi K^+K^-$, the calibration decay $B_s^0 \to D_s^-\pi^+$ is chosen because of similar kinematic properties. A data sample is selected using requirements that are optimal for the decay channel as described in Ref. [80], and weighted to match the $B_s^0 \to J/\psi K^+K^-$ data signal events for variables on which the tagging performance depends: number of tracks and PVs in the event, B_s^0 pseudorapidity and B_s^0 transverse momentum. The neutral B_s^0 meson is subject to the $B_s^0 - \overline{B}_s^0$ mixing, hence oscillations have to be resolved. This is done by performing a maximum-likelihood fit to the decay-time distribution:

$$\mathrm{PDF}(t|q^{\mathrm{mix}}) = \epsilon(t)\left[\Gamma(t|q^{\mathrm{mix}}) \otimes \mathcal{R}(t - t_{true})\right], \tag{5.19}$$

where $\epsilon(t) = 1 - 1/(1 + (at)^n + b)$ is the decay-time acceptance function, which is determined directly in the fit, and $\mathcal{R}(t - t_{true})$ the decay-time resolution model, which is calibrated with a prompt $D_s^-\pi^+$ data sample following a similar

procedure as described in Section 5.2. The B_s^0 decay rate is described by:

$$\Gamma(t|q^{\text{mix}}) = \Gamma_s e^{-\Gamma_s t}\left[\cosh\frac{\Delta\Gamma_s t}{2} + q^{\text{mix}}(1-2\omega(\eta))\cos(\Delta m_s t)\right], \tag{5.20}$$

with q^{mix} equal to $+1$ (-1) if the B_s^0 meson has (has not) changed flavour between its production and decay, determined by comparing the flavour-tagging decision and charge of the pion. As can be seen from Equation 5.20 the amplitude of the oscillation is proportional to the dilution factor $(1-2\omega(\eta))$. The calibration parameters can therefore be determined by fitting the decay-time distribution of mixed and not-mixed B_s^0 mesons. Figure 5.11 on the left shows the result of fitting the PDF of Equation 5.19 to the $B_s^0 \to D_s^-\pi^+$ data sample, split by events that are tagged as being mixed or unmixed. The right plot shows the obtained relation between the true and estimated mistag probability for the SSK tagger to which the linear calibration of Equation 5.15 is fitted. In addition the η distribution for $B_s^0 \to J/\psi K^+K^-$ signal events is presented by the shaded histogram. The results

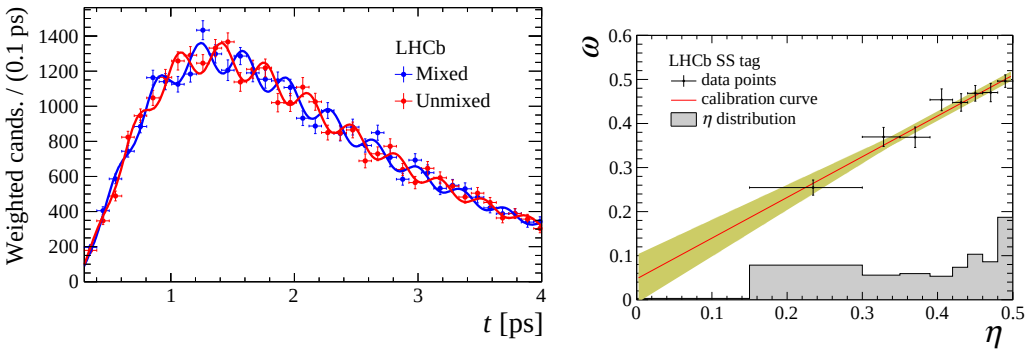

Figure 5.11 *Left: decay-time distribution of $B_s^0 \to D_s^-\pi^+$ signal events in data tagged as mixed or unmixed with the projections of the fit results. Right: calibration of the SSK tagger. The true mistag rate ω is represented by the black points in bins of estimated mistag rate η for the weighted $B_s^0 \to D_s^-\pi^+$ sample. The result of the calibration function is shown by the red line, with a yellow area representing the calibration uncertainty within one standard deviation. The shaded histogram shows the estimated mistag rate distribution for $B_s^0 \to J/\psi K^+K^-$ signal events. Figures taken from Ref. [1].*

for the calibration parameters can be found in Table 5.4. These values are used in the final maximum-likelihood fit to the full dataset. The systematic uncertainties on the parameters come from the decay-time resolution, calibration differences between the calibration and signal channel, and the modelling of combinatorial background in the $B_s^0 \to D_s^-\pi^+$ data sample. The mistag asymmetries Δp_0 and Δp_1 are set at zero, as the true initial flavour is not known. The uncertainties on

Table 5.4 *Tagging calibration parameters for the SSK and OS taggers for $B_s^0 \to J/\psi K^+K^-$ signal events in 2015 and 2016 data. Where given, the first uncertainty is statistical and the second is systematic. Numbers taken from Ref. [1].*

Tagger	SSK	OS
p_0	$0.4325 \pm 0.0108 \pm 0.0030$	$0.3890 \pm 0.0007 \pm 0.0028$
p_1	$0.92 \pm 0.13 \pm 0.02$	$0.849 \pm 0.006 \pm 0.027$
Δp_0	0.00 ± 0.03	0.0090 ± 0.0014
Δp_1	0.00 ± 0.03	0.014 ± 0.012
$\langle\eta\rangle$	0.417	0.360

these parameters are based on a study described in Ref. [77].

5.3.4 Opposite Side Tagger Calibration

For the OS tagger calibration, a data sample of $B^+ \to J/\psi K^+$ decays is used, which is also weighted to match the distributions of the $B_s^0 \to J/\psi K^+K^-$ data signal events in number of tracks and PVs in the event, B_s^0 pseudorapidity and B_s^0 transverse momentum. The calibration parameters can be determined by fitting a maximum-likelihood function directly to the estimated mistag rate:

$$\begin{aligned} \text{PDF}(a|\eta) &= (1-a)\omega(\eta) + a(1-\omega(\eta)) \\ \text{PDF}(a|\eta) &= (1-a)\overline{\omega}(\eta) + a(1-\overline{\omega}(\eta)), \end{aligned} \tag{5.21}$$

for an initial B^+ or B^- meson, respectively. The discrete variable a is one or zero for a correct or incorrect tagging decision, respectively, determined by comparing the flavour-tagging decision and charge of the kaon. Figure 5.12 shows the relation between the true and estimated mistag probability for the OS tagger and the calibration result. Additionally, the η distribution for $B_s^0 \to J/\psi K^+K^-$ signal events is presented by the shaded histogram. The calibration parameters can be found in Table 5.4. Sources for the systematic uncertainties come from the applicability of the calibration from the control channel to the signal decay and the combinatorial background model in the $B^+ \to J/\psi K^+$ data sample.

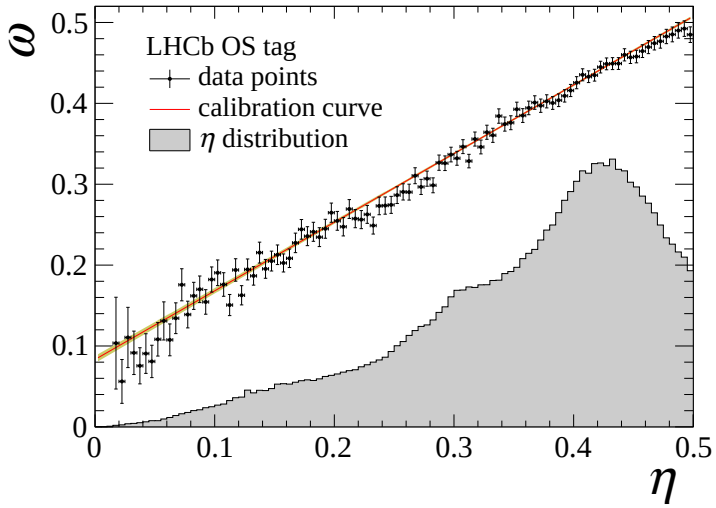

Figure 5.12 *Calibration of the OS tagger. The true mistag rate ω is represented by the black points in bins of estimated mistag rate η for the weighted $B^+ \to J/\psi K^+$ sample. The result of the calibration function is shown by the red line, with a yellow area representing the calibration uncertainty within one standard deviation. The shaded histogram shows the estimated mistag rate distribution for $B_s^0 \to J/\psi K^+K^-$ signal events. Figure taken from Ref. [1].*

5.3.5 Combination

The calibration parameters can now be used to correct the mistag probability determined in $B_s^0 \to J/\psi K^+K^-$ data, and to compute the tagging power. Equation 5.18 computes the tagging power for candidates that are exclusively tagged by either the OS or SSK tagger. In case both taggers give a decision for the event, their output has to be combined taking into account both decisions and their corresponding mistag probability. The following formula is derived for the tagging power, which uses all events in the sample, and furthermore includes the sWeights, w_i, determined as described in Section 4.6:

$$\varepsilon_{eff} = \frac{\sum_{\text{tagged}} w_i((A-B)^2/(A+B)^2)}{\sum_{\text{all}} w_i}, \tag{5.22}$$

where

$$\begin{aligned} A &= (1 + q^{OS}(1 - 2\omega^{OS}(\eta^{OS})))(1 + q^{SS}(1 - 2\omega^{SS}(\eta^{SS}))) \\ B &= (1 - q^{OS}(1 - 2\overline{\omega}^{OS}(\eta^{OS})))(1 - q^{SS}(1 - 2\overline{\omega}^{SS}(\eta^{SS}))). \end{aligned} \tag{5.23}$$

Here q^{OS} (q^{SSK}) is the tagging decision, η^{OS} (η^{SSK}) the uncalibrated mistag probability, and ω^{OS} (ω^{SSK}) and $\overline{\omega}^{OS}$ ($\overline{\omega}^{SSK}$) the calibrated mistag probability determined by the OS (SSK) tagger for B_s^0 and $\overline{B}_s^0$, respectively. Note that for

Table 5.5 *Flavour tagging results for $B_s^0 \to J/\psi K^+K^-$ signal events in the full dataset. For each tagging category the proportion in the dataset, the squared dilution and the tagging power is presented. The uncertainty on $\epsilon_{tag}\mathcal{D}^2$ is obtained by varying the tagging calibration parameters within their statistical and systematic uncertainties summed in quadrature. Numbers taken from Ref. [1].*

Category	$\epsilon_{tag}(\%)$	$\mathcal{D}^2$	$\varepsilon_{eff} = \epsilon_{tag}\mathcal{D}^2(\%)$
OS only	11.4	0.078	0.88 ± 0.04
SSK only	42.6	0.032	1.38 ± 0.30
OS & SSK	23.8	0.104	2.47 ± 0.15
Total	77.8	0.061	4.73 ± 0.34

events exclusively tagged by one of the taggers, for which $q^{OS} = 0$ (SS only) or $q^{SS} = 0$ (OS only), the squared dilution reduces to $\mathcal{D}^2 = (1-2\omega^{alg})^2$, where $alg = SS$ or OS, respectively. The final tagging results are summarised in Table 5.5. Per tagging category - OS only, SSK only, OS & SSK, and total - the percentage in the data sample, the squared dilution and the tagging power is shown. Approximately 78% of the signal candidates in the $B_s^0 \to J/\psi K^+K^-$ data sample are tagged and the final effective tagging power of $(4.73 \pm 0.34)\%$ is reached.

Chapter 6

Fitting and Results

The physics parameters that define the $B_s^0 \to J/\psi K^+K^-$ decay are determined by fitting the model of decay-time and decay angles, as discussed in Section 2.7, to the distribution of the selected signal events. The experimental effects covered in Chapter 5 are taken into account in the fit. This chapter will cover the explanation and construction of the final fit. The analysis is performed in multiple bins of the K^+K^- invariant mass range. The final physics parameter conventions are discussed as well as the `RAPIDFIT` framework. Finally, the results that I have obtained by performing the fit to the 2015 and 2016 dataset of $B_s^0 \to J/\psi K^+K^-$ signal events are presented.

6.1 Maximum Likelihood

The distribution of $B_s^0 \to J/\psi K^+K^-$ signal events follow a probability density function (PDF) describing all of the observable distributions. The PDF represents the probability per unit observable to be at a given point within the phase space. By definition, the normalised integral of the PDF is unity. The joint likelihood $\mathcal{L}$ of a set of parameters $\vec{\lambda}$ given a set of observables $\vec{x_i}$ that are distributed following a PDF is defined as the following:

$$\mathcal{L}(\vec{\lambda}) = \prod_{i=1}^{N} \mathrm{PDF}(\vec{x_i}; \vec{\lambda}), \tag{6.1}$$

which is the product of the PDF values for each event i in a dataset of N measurements. If we introduce the signal function, $p(\vec{x_i};\vec{\lambda})$, the PDF is expressed as follows:

$$\mathrm{PDF}(\vec{x_i};\vec{\lambda}) = \frac{p(\vec{x_i};\vec{\lambda})}{\int p(\vec{x_i};\vec{\lambda})\mathrm{d}\vec{x_i}}. \tag{6.2}$$

We want to find the best set of physics parameters, $\vec{\lambda}$, for which the joint probability of all the measurements is maximal. Instead of maximising Equation 6.1, the parameters are more commonly determined using a Negative Log Likelihood (NLL) function, which is represented by a sum over the dataset:

$$-\ln[\mathcal{L}(\vec{\lambda})] = -\sum_{i=1}^{N} \ln\left[\frac{p(\vec{x_i};\vec{\lambda})}{\int p(\vec{x_i};\vec{\lambda})\mathrm{d}\vec{x_i}}\right]. \tag{6.3}$$

The minimum of this function is equivalent to the maximum of Equation 6.1. The best fit is obtained by varying the set of parameters $\vec{\lambda}$ to find the global minima of the NLL, for which the following holds:

$$-\frac{\mathrm{d}\ln[\mathcal{L}(\vec{\lambda})]}{\mathrm{d}\vec{\lambda}} = -\frac{\mathrm{d}}{\mathrm{d}\vec{\lambda}}\sum_{i=1}^{N} \ln\left[\frac{p(\vec{x_i};\vec{\lambda})}{\int p(\vec{x_i};\vec{\lambda})\mathrm{d}\vec{x_i}}\right] = 0. \tag{6.4}$$

Efficiencies $\varepsilon(\vec{x_i})$ are incorporated as follows:

$$-\frac{\mathrm{d}}{\mathrm{d}\vec{\lambda}}\sum_{i=1}^{N} \ln\left[\frac{p(\vec{x_i};\vec{\lambda})\varepsilon(\vec{x_i})}{\int p(\vec{x_i};\vec{\lambda})\varepsilon(\vec{x_i})\mathrm{d}\vec{x_i}}\right] = 0. \tag{6.5}$$

As mentioned in Section 5.1, the efficiency in the numerator has no influence on the physics parameter estimates. This becomes clear when writing the efficiency as a separate term in the NLL:

$$-\frac{\mathrm{d}}{\mathrm{d}\vec{\lambda}}\sum_{i=1}^{N} \ln\left[\frac{p(\vec{x_i};\vec{\lambda})}{\int p(\vec{x_i};\vec{\lambda})\varepsilon(\vec{x_i})\mathrm{d}\vec{x_i}}\right] - \frac{\mathrm{d}}{\mathrm{d}\vec{\lambda}}\sum_{i=1}^{N} \ln[\varepsilon(\vec{x_i})] \tag{6.6}$$

As the efficiency does not depend on the physics parameters, it does not change in the minimisation. It only acts as an offset to the NLL, and can therefore be ignored in the minimisation. To find the best physics parameters for the dataset which minimise the NLL, the `MINUIT` package can be used, which employs a `MIGRAD` minimiser [81]. The computation of errors on the best fit values is explained in the next section.

6.2 Error Computation

During the minimisation also the uncertainties on the best set of physics parameters are calculated. The shape of the NLL function for a well behaved parameter is parabolic around the minimum. Since the first derivative is defined to be zero where the NLL reaches its minimum, the NLL shape for a given parameter μ can be described by the following:

$$\begin{aligned} -\ln[\mathcal{L}(\mu)] &= f(\mu) \\ &\approx f(\hat{\mu}) + \frac{\mathrm{d}f(\mu)}{\mathrm{d}\mu}\bigg|_{\hat{\mu}} (\mu - \hat{\mu}) + \frac{1}{2!}\frac{\mathrm{d}^2 f(\mu)}{\mathrm{d}\mu^2}\bigg|_{\hat{\mu}} (\mu - \hat{\mu})^2 \\ &\approx f(\hat{\mu}) + 0 + \frac{1}{2}\frac{\mathrm{d}^2 f(\mu)}{\mathrm{d}\mu^2}\bigg|_{\hat{\mu}} (\mu - \hat{\mu})^2 \\ &= f(\hat{\mu}) + \frac{1}{2\sigma_\mu^2}(\mu - \hat{\mu})^2. \end{aligned} \tag{6.7}$$

where $\hat{\mu}$ is the value of the parameter of interest in the minimum, and σ_μ determines the width of the parabola given by the second order derivative about the minima. The width σ_μ represents the statistical uncertainty on the parameter estimate. A broader parabola around the minimum means a larger value of σ_μ and therefore a larger uncertainty. More data on the other hand will reduce the statistical uncertainty on the parameter estimate, and lead to a narrower NLL shape. The parameter interval $\hat{\mu}\pm\sigma_\mu$ represents the range in which the probability that the true value lies is 68%. This is usually referred to as the 1σ *confidence interval*.

Equation 6.7 considers only a single parameter. When fitting for a set of physics parameters, $\vec{\lambda}$, a *profile likelihood* is build for each parameter by varying the values of parameter μ and minimising the full NLL function with respect to all other parameters for each value of μ. A Hessian matrix $\mathbf{H}$ is constructed, which includes the second-order partial derivatives for every combination of physics parameters. This matrix has dimension $n \times n$ for n parameters, and it includes correlations between the parameters. From this matrix the uncertainty on parameter i, λ_i, is determined by taking the inverse of the (i, i)-th element:

$$\sigma_{\lambda_i}(\lambda_i) = \sqrt{(\mathbf{H}^{-1})_{i,i}}. \tag{6.8}$$

In general, the statistical uncertainty σ_μ can be determined from the profile

likelihood by noting the value of μ where the NLL value rises by $\frac{1}{2}$. From Equation 6.7 it can be seen that this is where $\mu - \hat{\mu} = \sigma_\mu$. For a well behaved parameter, the range $\hat{\mu} \pm \sigma_\mu$ has the proper the 68% coverage. However, if the NLL has a non-parabolic shape, the value of σ_μ may not represent the proper error on the parameter estimate. An alternative approach constructs the 68% confidence interval by determining separately the parameter values above and below $\hat{\mu}$ for which the full NLL function re-minimised with respect to all other parameters increases by $\frac{1}{2}$. This method allows an asymmetric uncertainty. The possible packages for error computation are `HESSE` and `MINOS` for the parabolic and non-parabolic case, respectively [82], both provided by the `MINUIT` fitting framework. In the rest of this thesis the `HESSE` tool is used to determine the errors unless explicitly stated otherwise.

6.3 Including Weights and Constraints

Section 4.6 describes the method to obtain the signal distribution of $B_s^0 \to J/\psi K^+K^-$ events, namely by subtracting the background distribution from the data distribution. This is accomplished by computing per-event sWeights, w_i, which are positive for signal and negative for background candidates. The advantage of the sWeights is that they can easily be included in the NLL function to provide the signal distribution of the observables. There is no need to explicitly describe the background distributions. The sWeights, however, influence the shape of profile likelihoods of the NLL, and therefore bias the calculation of the parameter uncertainties. Ref. [83] discusses this in detail, and derives a correction factor α that accounts for the distortion. The sWeights and scale factor are included in the NLL function as follows:

$$-\ln[\mathcal{L}(\vec{\lambda})] = -\alpha \sum_{i=1}^{N} w_i \ln\left[\frac{p(\vec{x_i}|\vec{\lambda})}{\int p(\vec{x_i}|\vec{\lambda})\mathrm{d}\vec{x_i}}\right], \tag{6.9}$$

where the correction factor is defined as:

$$\alpha \equiv \frac{\sum_{i=1}^{N} w_i}{\sum_{i=1}^{N} w_i^2}. \tag{6.10}$$

When a dataset is unweighted, $w_i = 1$ and $\alpha = 1$, hence these terms vanish in the expression. The sWeights are determined in 6 bins of $m(K^+K^-)$, separately for each year and trigger category, leading to 24 datasets with independent weights.

For each set of weights, a different value of α is calculated.

Parameters can be constrained by external measurements, μ', when running the minimisation. These external constraints are added linearly to the NLL as extra terms:

$$-\ln[\mathcal{L}(\mu')] = -\frac{1}{2\sigma^2_{\mu'}}(\mu' - \hat{\mu}')^2. \tag{6.11}$$

Here $\sigma_{\mu'}$ is the error on given parameter μ', which has a central value of $\hat{\mu}'$. As a consequence, the uncertainties of externally determined parameters propagate into the statistical uncertainties of the parameters computed in the fit.

6.4 Signal PDF

The signal PDF is a sum of ten terms dependent on the helicity angles, each multiplied by a time dependent-function, $p(t, \vec{\Omega}; \vec{\lambda}) = \sum_{k=1}^{10} h_k(t; \vec{\lambda}) f_k(\vec{\Omega})$, where the physics parameters enter in the time-dependent functions (see Equation 2.32). Writing the observables $\vec{x_i} = \{t, \vec{\Omega}\}$ explicitly in Equation 6.2 gives:

$$\mathrm{PDF}(t, \vec{\Omega}; \vec{\lambda}) = \frac{p(t, \vec{\Omega}; \vec{\lambda})}{\int\int \mathrm{d}t \mathrm{d}\vec{\Omega}\, p(t, \vec{\Omega}; \vec{\lambda})}. \tag{6.12}$$

The PDF has a dependence on the flavour of the initial B_s^0 meson at production, which is included by the flavour tagging information discussed in Section 5.3. By combining $p(t, \vec{\Omega}; \vec{\lambda})$ for an initial B_s^0 meson and $\overline{p}(t, \vec{\Omega}; \vec{\lambda})$ for an initial $\overline{B}_s^0$ meson, a tagging dependent PDF can be constructed. Equation 5.23 is used to include the different calibrated mistag probabilities for both flavours. The tagging calibration parameters with their uncertainties shown in Table 5.4 are included in the PDF as external constraints. Representing the measured tagging variables as $\vec{T} = \{q^{OS}, q^{SS}, \eta^{OS}, \eta^{SS}\}$, the following expression is obtained:

$$\begin{aligned} p(t, \vec{\Omega}|\vec{T}; \vec{\lambda}) =& (1 + q^{OS}(1 - 2\omega^{OS}(\eta^{OS})))(1 + q^{SS}(1 - 2\omega^{SS}(\eta^{SS})))p(t, \vec{\Omega}; \vec{\lambda}) + \\ & (1 - q^{OS}(1 - 2\overline{\omega}^{OS}(\eta^{OS})))(1 - q^{SS}(1 - 2\overline{\omega}^{SS}(\eta^{SS})))\overline{p}(t, \vec{\Omega}; \vec{\lambda}). \end{aligned} \tag{6.13}$$

The calibrated mistag probabilities $\omega^{alg}(\eta^{alg})$ and $\overline{\omega}^{alg}(\eta^{alg})$, where $alg = OS$ or SS, are computed by Equation 5.15. The differential decay rate for the $\overline{B}_s^0$ meson, $\overline{p}(t, \vec{\Omega}; \vec{\lambda})$, is obtained by reversing the signs of c_k and d_k in the time-dependent functions $h_k(t; \vec{\lambda})$ defined in Equation 2.32.

Next, the detector effects have to be included. The decay-time resolution is modelled by a single Gaussian function with a width given by the effective resolution $\sigma_{eff}(\sigma_t)$, which depends on the per-candidate decay-time uncertainty σ_t and is calibrated in Section 5.2.1. The determined calibration parameters are fixed in the fit. The flavour tagged differential decay rate is convolved with the decay-time resolution, $G(t|\sigma_t)$. The decay-time and angular efficiencies, $\varepsilon(t,\vec{\Omega})$, are incorporated via multiplication:

$$\mathrm{PDF}(t,\vec{\Omega}|\vec{T},\sigma_t;\vec{\lambda}) = \frac{[p(t,\vec{\Omega}|\vec{T};\vec{\lambda})\otimes G(t|\sigma_t)]\times\varepsilon(t,\vec{\Omega})}{\int\int \mathrm{d}t\mathrm{d}\vec{\Omega}\sum_{k=1}^{10}[p(t,\vec{\Omega}|\vec{T};\vec{\lambda})\otimes G(t|\sigma_t)]\times\varepsilon(t,\vec{\Omega})}. \quad (6.14)$$

The efficiency terms in the numerator do not influence the parameter estimates as they do not depend on the physics parameters (see Equation 6.6), thus can be ignored in the minimisation. As the decay-time and angular acceptances are assumed to factorise (see Chapter 5), the denominator can be expressed as two different integrals:

$$\begin{aligned}&\int \mathrm{d}t\,[p(t|\vec{T};\vec{\lambda})\otimes G(t|\sigma_t)]\;\times\;\varepsilon(t)\int \mathrm{d}\vec{\Omega}\sum_{k=1}^{10} f_k(\vec{\Omega})\varepsilon(\vec{\Omega})\\ =&\int \mathrm{d}t\,[p(t|\vec{T};\vec{\lambda})\otimes G(t|\sigma_t)]\;\times\;s^{B_s^0}_{\mathrm{data}}(t)\sum_{k=1}^{10}\xi_k,\end{aligned} \quad (6.15)$$

with $p(t|\vec{T};\vec{\lambda})$ representing Equation 6.13 where the $\vec{\Omega}$ dependence has been factorised out. In the second line of Equation 6.15, the decay-time acceptance is replaced by the spline and the second integral by the normalisation weights, which are computed in Section 5.2.2 and 5.1, respectively. Ten normalisation weights are determined for the angular acceptance, one for each of the ten terms of the differential decay. As the weights do not depend on the physics parameters, they can be evaluated only once and do not vary in the minimisation. Separate acceptances are determined for the different years and trigger categories of the data.

6.5 C_{SP} factors

The final state of $B_s^0 \to J/\psi K^+K^-$ is a superposition of the resonant ϕ P-wave and K^+K^- S-wave, which show different behaviours across the $m(K^+K^-)$ range. The S-wave distribution is observed to be approximately uniformly distributed

over the full range, while the P-wave distribution features a peaking structure around the $\phi(1020)$ mass. The differential decay rate in Equation 2.31 does not include the $m(K^+K^-)$ dependence, and a correction factor is required for the integral of the interference terms over the $m(K^+K^-)$ range. First, we express the dependence for the P-wave and S-wave amplitudes by the lineshapes $p(m_{KK})$ and $s(m_{KK})$, respectively. These are normalised to unity over a given $m(K^+K^-)$ range $[m^L_{KK}, m^H_{KK}]$ as shown in Equation 6.16, where $i, j \in \{0, \parallel, \perp\}$. Then, when looking at the interference terms of the P-wave and S-wave, a correction factor arises, as $< p \times s^* > \neq < p > \times < s^* >$:

$$\begin{aligned}
\int_{m^L_{KK}}^{m^H_{KK}} A_i A_j^* \, p(m_{KK}) \, p^*(m_{KK}) \, \mathrm{d}m_{KK} &= |A_i A_j| \\
\int_{m^L_{KK}}^{m^H_{KK}} A_S A_S^* \, s(m_{KK}) \, s^*(m_{KK}) \, \mathrm{d}m_{KK} &= |A_S|^2 \\
\int_{m^L_{KK}}^{m^H_{KK}} A_i A_s^* \, p(m_{KK}) \, s^*(m_{KK}) \, \mathrm{d}m_{KK} &= |A_i A_S| C_{SP} e^{-i\theta_{SP}}.
\end{aligned} \tag{6.16}$$

While the phase θ_{SP} is absorbed in the measurement of δ_S, the correction factor C_{SP} must be included in the differential decay rate. The terms $1-7$ in Table 2.1 remain unaffected, whereas the terms $8-10$ are multiplied with the C_{SP} factor as $N_k \to C_{SP} N_k$.

To determine the C_{SP} factor, the procedure in Ref. [28] is followed. The data is split in six $m(K^+K^-)$ bins to keep the correction factors close to unity.[1] The ranges are given in Table 6.1 and correspond to the bins in the determination of the sWeights, as shown in the top plot of Figure 4.9. The choice of binning is centred around the ϕ mass [24]. In the centre the mass region is finest, and largest at the outer ranges. This is supported by the large number of events and small S-wave fraction, F_S, around the centre with respect to a small number of events and large F_S around the outer edges. For each bin i, a corresponding $C_{SP,i}$ factor is calculated by integrating the product of the normalised lineshapes over the relative m_{KK} range:

$$\frac{\int_{m^L_{KK}}^{m^H_{KK}} p(m_{KK}) \times s^*(m_{KK}) \, \mathrm{d}m_{KK}}{\sqrt{\int_{m^L_{KK}}^{m^H_{KK}} |p(m_{KK})|^2 \, \mathrm{d}m_{KK} \int_{m^L_{KK}}^{m^H_{KK}} |s(m_{KK})|^2 \, \mathrm{d}m_{KK}}} = C_{SP,i} e^{-i\theta_{SP,i}}. \tag{6.17}$$

[1] As a by-product the two-fold ambiguity of the differential decay rate in Equation 2.31 of $(\phi_s, \Delta\Gamma_s, \delta_\parallel, \delta_\perp, \delta_S, \delta_0) \to (\pi - \phi_s, -\Delta\Gamma_s, -\delta_\parallel, \pi - \delta_\perp, -\delta_S, -\delta_0)$ can be resolved by observing the trend of $\delta_S - \delta_\perp$. This has been validated in Ref. [84] and allows the direct determination of the sign of $\Delta\Gamma_s$.

For the calculation, the S-wave is assumed to be the $f_0(980)$ resonance, and is modelled by a Flatté amplitude [85] with parameters taken from Ref. [86]. The resonant P-wave is modelled by a relativistic Breit-Wigner distribution [87]. The mean and the width of the ϕ meson are taken from Ref. [24]. The lineshapes are constructed following the approach that is described in Ref. [88]. The S-wave is not well known, hence a systematic is determined by considering different variations of the S-wave model.

The bins are determined in terms of the measured mass, but the finite mass resolution of the detector will cause decay candidates to migrate between the bins. To account for this, an m_{KK} dependent efficiency is included in Equation 6.17, following the procedure described in Ref. [56]. The efficiency corrected C_{SP}

Table 6.1 *List of m_{KK} bin ranges and corresponding C_{SP} factors calculated as described in the text.*

bin	m_{KK} range [MeV/c^2]	C_{SP}
1	990-1008	0.8463
2	1008-1016	0.8756
3	1016-1020	0.8478
4	1020-1024	0.8833
5	1024-1032	0.9415
6	1032-1050	0.9756

factors for the different bins can be found in Table 6.1. The same factors are used for the two years of data-taking and both trigger categories. For the analysis, a simultaneous fit is performed to the six $m(K^+K^-)$ bins, where for each bin a corresponding pair of S-wave parameters - $F_{S,i}$ and $\delta_{S,i}$ - is determined, while the other free physics parameters are kept common between all bins.

6.6 Fitting Parameters

The NLL function using the model of decay-time and decay angles discussed in Section 2.7 is fitted to the selected 2015 and 2016 $B_s^0 \to J/\psi K^+K^-$ data sample. By minimising the NLL function, the set of physics parameters $\vec{\lambda}$ corresponding to the best description of the dataset is computed. The inclusion of the sWeights as discussed in Section 6.3 removes the need of a background description in the NLL. In addition, the tagging calibration parameters are included as a set of external constraints. As a result, the uncertainties on the tagging parameters are

propagated into the final fit, and directly affect the statistical uncertainties on the physics parameters.

The parameters that will be determined by the fit are firstly the *CP* violating parameters ϕ_s and λ, and the difference in decay width and mass between the two mass eigenstates of the $B_s^0 - \overline{B}_s^0$ system, $\Delta\Gamma_s$ and Δm_s. Instead of measuring the average decay width for the B_s^0 meson, Γ_s, we fit for the difference between the average decay width for the B_s^0 and B^0 system:

$$\Gamma_s - \Gamma_d. \tag{6.18}$$

This is because of the decay-time acceptance extraction described in Section 5.2.2, which depends on the decay-time acceptance of, among others, the data sample of the control channel $B^0 \to J/\psi K^+\pi^-$. The latter uses the current world average of Γ_d as an input. If this value gets updated, the B^0 data acceptance would change accordingly, and the same change would be observed in the decay-time acceptance of the signal, and consequently in the measured value for Γ_s. Instead of including a systematic for the uncertainty on the Γ_d world average, the difference between the decay widths is quoted, $\Gamma_s - \Gamma_d$. This parameter is independent of the exact value used for Γ_d in the acceptance computation, which is validated in Appendix C with a detail derivation. The parameter $\Gamma_s - \Gamma_d$ can be determined without an additional error due to the knowledge of Γ_d.

The sum of the squared *P*-wave amplitudes are defined to equal unity. Of the three amplitudes, two are fitted to, from which the third can be calculated:

$$|A_\parallel|^2 = 1 - |A_0|^2 - |A_\perp|^2. \tag{6.19}$$

Instead of fitting for the *S*-wave amplitude $|A_S|^2$, the fraction of the *S*-wave in the decay, F_S, is used, which is defined as:

$$F_s = \frac{|A_S|^2}{1 + |A_S|^2}. \tag{6.20}$$

It is only possible to measure differences between strong phases, and by convention the phase of the A_0 state is chosen to be zero, $\delta_0 = 0$. The fitting parameters of the *P*-wave therefore reduce to the differences $\delta_\parallel - \delta_0$ and $\delta_\perp - \delta_0$. For the *S*-wave phase, the difference to the perpendicular *P*-wave polarisation phase is used in the minimisation, $\delta_S - \delta_\perp$.

The NLL function is fitted simultaneously to the datasets corresponding to the years 2015 and 2016 and trigger categories biased and unbiased, which are subsequently divided in six $m(K^+K^-)$ bins. When performing the NLL to all data samples, only the S-wave parameters are independent for each $m(K^+K^-)$ bin, with all other free parameters taken to be common between all bins. This results in six different pairs of S-wave parameters measured in the full fit to data. As the angular and decay-time acceptances are computed separately for both years and trigger categories, the corresponding weights and coefficients are included when fitting the relative dataset.

The physics parameters that define the decay are the following:

$$\vec{\lambda} = \{\phi_s, |\lambda|, \Delta\Gamma_s, \Delta m_s, \Gamma_s - \Gamma_d, |A_\perp|^2, |A_0|^2, \delta_\parallel - \delta_0, \delta_\perp - \delta_0, F_S, \delta_S - \delta_\perp\}, \quad (6.21)$$

with six different S-wave fractions F_{Si} and phases $\delta_{Si} - \delta_\perp$ for the six $m(K^+K^-)$ bins, where $i \in \{1-6\}$. The parameters that are included as external constraints are the following:

$$\vec{\lambda}(constr) = \{p_0^{os}, \Delta p_0^{os}, p_1^{os}, \Delta p_1^{os}, p_0^{ss}, \Delta p_0^{ss}, p_1^{ss}, \Delta p_1^{ss}\} \quad (6.22)$$

The nominal fit assumes polarisation independence, however Section 2.7 mentions the possibility of NP models leading to differences in CP asymmetry between the different polarisation states [29]. As a test, the time-dependent functions in the differential decay rate can be expressed in the polarisation dependent CP violating parameters ϕ_p and $|\lambda_p|$, see Table 2.3. In the polarisation-dependent fit, the parameters ϕ_p and $|\lambda_p|$ are determined with respect to the longitudinal P-wave polarisation, to reduce correlation between fit parameters and to directly observe potential differences:

$$\vec{\lambda}(pol) = \{\phi_0, \phi_\parallel - \phi_0, \phi_\perp - \phi_0, \phi_S - \phi_0, |\lambda_0|, |\lambda_\parallel/\lambda_0|, |\lambda_\perp/\lambda_0|, |\lambda_S/\lambda_0|\} \quad (6.23)$$

6.7 RapidFit Framework

The physics parameter results for the $B_s^0 \to J/\psi K^+K^-$ full dataset presented in Section 6.8 are computed using the `RAPIDFIT` fitting framework, which is developed within Edinburgh University [89]. The published results in Ref. [1] originate from a different fitting program that has been used in the analysis. The

RAPIDFIT framework serves as an important cross-check, and both results have been tested extensively to agree. A comparison between the results in this thesis and the published results is presented in Appendix D, and shows consistency between the parameter values and uncertainties.

RAPIDFIT is a framework written in C++ and uses the MINUIT [81] fitting package and ROOT libraries [55] to perform NLL fits. It incorporates arbitrary PDFs and an XML configuration file, allowing for multiple complex analyses. The XML configuration file provides information that is used when performing the fit, such as the to be analysed dataset and phase space, signal PDF, requested set of observables and physics parameters, and external constraints. The RAPIDFIT framework has additional features, such as carrying out pseudo-experiment studies, producing pull and fit result plots, and calculating angular acceptance weights. During the analysis, I have been in charge of running the Edinburgh fitter and ensuring consistency with the one used for the publication. The analysis required additional features which I have implemented in the existing $B_s^0 \to J/\psi K^+K^-$ signal PDF and the framework itself:

- Polarisation dependency for the coefficients in the time-dependent functions in the differential decay rate as presented in Table 2.3
- External constraints of the tagging parameters
- Inclusion of splines for the decay-time acceptance
- Matching observable and physics parameters definitions as the other fitting frameworks

6.8 Results

Table 6.2 presents the results for the maximum-likelihood fit performed with the RapidFit framework including their statistical uncertainties. The statistical correlation matrix can be found in Table E.1. The first nine parameters are the key physics parameters and the parameters F_{Si} and $\delta_{Si} - \delta_\perp$ are the S-wave parameters. Figures E.1-E.3 present the profile likelihoods for each of the parameters, which are used to check that the fit found the global minima, and not a local one. The key parameters are common over the full K^+K^- mass range, while the S-wave parameters are different for each $m(K^+K^-)$ bin i defined in

Table 6.1. The results for the tagging parameters that are included in the fit as external constraints are shown in Table E.2 and their statistical correlation matrix in Table E.3. Their correlations with the key physics parameters and the six pairs of S-wave parameters are negligible. The background-subtracted data distributions with fit projections of the decay-time and helicity angles are shown in Figure 6.1.

Table 6.2 *Physics parameter estimates for $B_s^0 \to J/\psi K^+K^-$ signal events in the full dataset. Only statistical uncertainties are presented.*

Parameter	Fit result
ϕ_s [rad]	-0.080 ± 0.041
$\lvert\lambda\rvert$	1.014 ± 0.016
$\Gamma_s - \Gamma_d$ [ps^{-1}]	-0.0041 ± 0.0024
$\Delta\Gamma_s$ [ps^{-1}]	0.0764 ± 0.0077
Δm_s [ps^{-1}]	17.697 ± 0.059
$\lvert A_\perp\rvert^2$	0.2454 ± 0.0040
$\lvert A_0\rvert^2$	0.5189 ± 0.0029
$\delta_\perp - \delta_0$ [rad]	2.63 ± 0.13
$\delta_\parallel - \delta_0$ [rad]	3.062 ± 0.078
F_{S1}	0.493 ± 0.065
F_{S2}	0.0420 ± 0.0080
F_{S3}	0.0048 ± 0.0026
F_{S4}	0.0074 ± 0.0057
F_{S5}	0.075 ± 0.013
F_{S6}	0.152 ± 0.018
$\delta_{S1} - \delta_\perp$ [rad]	2.18 ± 0.19
$\delta_{S2} - \delta_\perp$ [rad]	1.55 ± 0.31
$\delta_{S3} - \delta_\perp$ [rad]	0.99 ± 0.39
$\delta_{S4} - \delta_\perp$ [rad]	-0.28 ± 0.18
$\delta_{S5} - \delta_\perp$ [rad]	-0.523 ± 0.094
$\delta_{S6} - \delta_\perp$ [rad]	-1.08 ± 0.14

To check for differences in *CP* asymmetry between the polarisation states, the coefficients of the time-dependent functions in the nominal fit are replaced by the time and polarisation-dependent coefficients shown in Table 2.3. The parameter estimates for the polarisation-dependent ϕ_p and $|\lambda_p|$ are presented in Table 6.3, and their statistical correlations in Table E.4. The results for the polarisation dependent fit are not significantly different from the nominal fit, hence no evidence of polarisation dependence is concluded.

The fit projections in Figure 6.1 show the sum of the B_s^0 and $\overline{B}_s^0$ decay-time

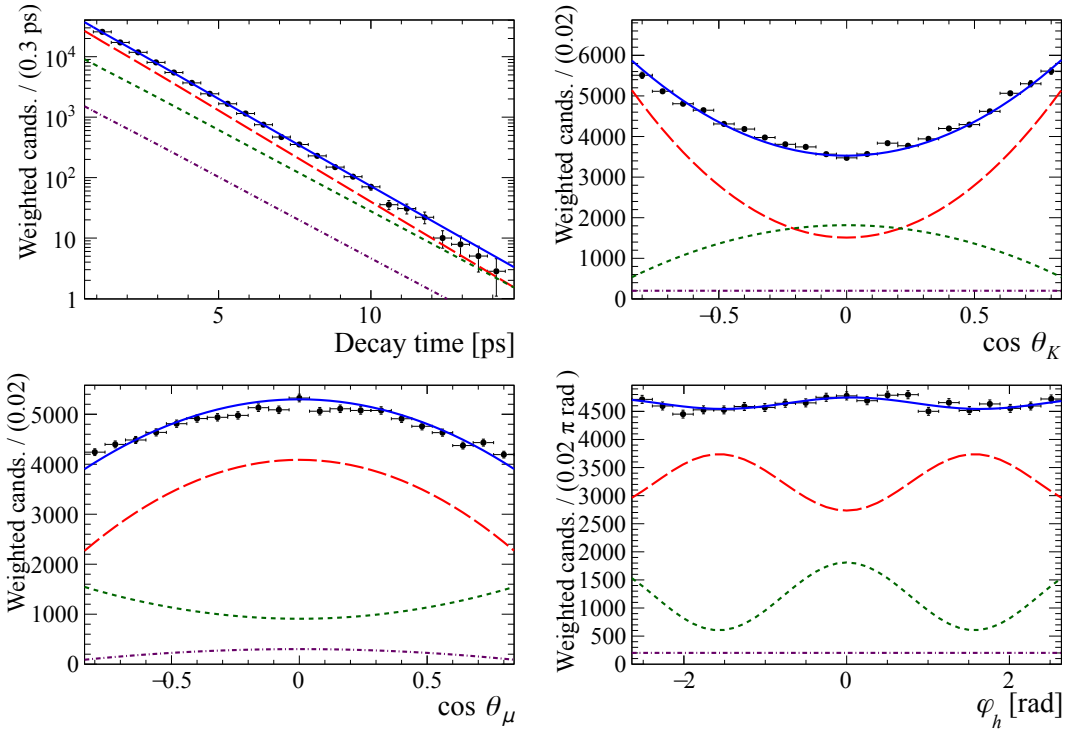

Figure 6.1 *Decay-time and helicity angle distributions for background subtracted $B_s^0 \to J/\psi K^+K^-$ decays (data points) with the one-dimensional projections of the PDF at the maximum-likelihood point. The solid blue line shows the total signal contribution, which contains (long-dashed red) CP-even, (short-dashed green), CP-odd and (dotted-dashed purple) S-wave contributions. Data and fit projections for the different samples considered (data-taking year, trigger and tagging categories, $m(K^+K^-)$ bins) are combined.*

Table 6.3 *Values for the polarisation-dependent ϕ_p and $|\lambda_p|$ for $B_s^0 \to J/\psi K^+K^-$ signal events in the full dataset. Only statistical uncertainties are presented.*

Parameter	Fit results
ϕ_0 [rad]	-0.078 ± 0.044
$\phi_\parallel - \phi_0$ [rad]	-0.048 ± 0.047
$\phi_\perp - \phi_0$ [rad]	-0.083 ± 0.060
$\phi_S - \phi_0$ [rad]	0.030 ± 0.043
$\lvert\lambda_0\rvert$	0.958 ± 0.045
$\lvert\lambda_\parallel/\lambda_0\rvert$	0.981 ± 0.080
$\lvert\lambda_\perp/\lambda_0\rvert$	1.24 ± 0.16
$\lvert\lambda_S/\lambda_0\rvert$	1.28 ± 0.16

distributions, for which any decay-time oscillation is diluted and not visible above the exponential. To obtain a visualisation of any oscillating difference between the decay rates of B_s^0 and $\overline{B}_s^0$ mesons, the asymmetry between tagged decays:

$$A_{tag}(t) = \frac{\#B_s^0 \,\text{tags}\,(t) - \#\overline{B}_s^0 \,\text{tags}\,(t)}{\#B_s^0 \,\text{tags}\,(t) + \#\overline{B}_s^0 \,\text{tags}\,(t)}, \tag{6.24}$$

is plotted in Figure 6.2. The black points represent the calculated tag asymmetries in data in intervals of decay-time. The red line is the result of fitting the signal PDF of Equation 6.14 integrated over the decay angles in small steps per decay-time interval. The fit is performed to pseudo-experiments taking as input the nominal fit results, while including detector efficiency and resolution effects and assuming perfect tagging. The asymmetry in Figure 6.2 is enhanced in various ways. First, the full decay-time range is mapped onto a single B_s^0 oscillation period following the procedure discussed in Ref. [90]. Next, each decay candidate in data is weighted by the product of its corresponding dilution factors from flavour tagging and the decay-time resolution. This gives a higher weight to events which have a smaller probability for a wrongly assigned tag or a better decay-time resolution. Finally, a per-event angular weight is considered to separate the contribution of the *CP*-even and *CP*-odd components:

$$w(\vec{\Omega}) = \frac{(f_1(\vec{\Omega}) \cdot N_1 + f_2(\vec{\Omega}) \cdot N_2) - (f_3(\vec{\Omega}) \cdot N_3 + f_7(\vec{\Omega}) \cdot N_7)}{(f_1(\vec{\Omega}) \cdot N_1 + f_2(\vec{\Omega}) \cdot N_2) + (f_3(\vec{\Omega}) \cdot N_3 + f_7(\vec{\Omega}) \cdot N_7)}, \tag{6.25}$$

where the individual terms are defined in Table 2.1. This avoids the cancellation that is induced by the dependence of the *CP* asymmetry on the *CP* eigenvalue η_f, as can be seen in Equation 2.26. This equation further states that in case of *CP* violation an oscillation in the asymmetry as a function of decay-time would be present, which is confirmed by Figure 6.2.

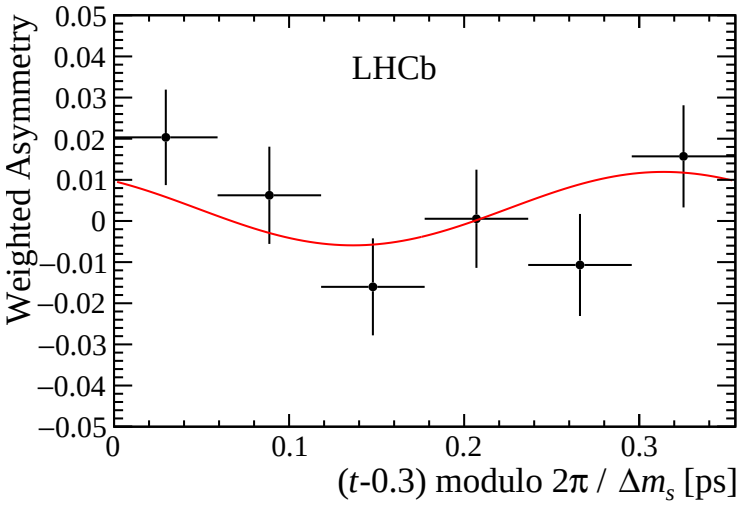

Figure 6.2 *Asymmetry in the number of decays with a B_s^0 and $\overline{B}_s^0$ flavour tag in data (black points) with the fit projection to pseudo-experiments that take the nominal fit results as input (red line) as a function of decay-time. The decay candidates are weighted as mentioned in the text to enhance the asymmetry and the full decay-time range is mapped onto one B_s^0 oscillation period. Figure taken from Ref. [1].*

Chapter 7

Systematic Uncertainties

Systematic uncertainties are calculated to express the effect of the choice of models or methods used in the analysis on the results. These are described in detail in Ref. [1] and summarised in the following. The final systematics for the main parameters are presented in Table 7.1 and for the S-wave fractions and phases in Appendix F.

7.1 $J/\psi K^+K^-$ Mass Model

Section 4.6 describes the model that is used to fit the invariant mass $m(J/\psi K^+K^-)$, for which several systematics are determined. Firstly, the quadratic dependence of the mass resolution on the per-candidate mass uncertainty is replaced by a linear function, $\sigma_{CB} = s_1 \times \sigma_m$. The whole analysis is repeated with this parametrisation and the difference in the physics parameters is assigned as a systematic.

Secondly, a systematic is determined for the statistical uncertainty of the signal weights. For this, the parameters of the invariant mass model are varied within their uncertainties and a new set of sWeights are calculated. No significant change is observed for the fit results, hence no systematic is assigned.

The sPlot technique requires the invariant mass to be uncorrelated with the variables that will be analysed. As mentioned before, the correlation with the helicity angle $\cos\theta_\mu$ has been taken into account by including the per-candidate mass uncertainty in the mass model. The signal mass shape is tested for a

dependence on the decay-time and the three decay angles by re-evaluating the sWeights in bins of these variables separately, and repeating the final fit to the full dataset. Only for the decay-time significant differences are observed for the physics parameters estimates, from which a systematic is obtained.

Finally, the modelling of the background components in the mass model is evaluated. The yield of the $\Lambda_b^0 \to J/\psi p K^-$ reflection background in the data sample is varied by $\pm 1\sigma$ of the expected number of events. Additionally, all $B^0 \to J/\psi K^+\pi^-$ events are removed from the data sample, by removing all events that are interpreted as $J/\psi K^\pm \pi^\pm$ for which the invariant mass is within ± 15 MeV of $m(B^0)$ [24]. A further check is performed for the suppressed $B^0 \to J/\psi K^+ K^-$ channel contribution, by leaving its resolution free in the mass fit used to calculate the sWeights. Lastly, a contribution of approximately 0.5% is expected from the channel $B_c^+ \to B_s^0 \pi^+$ [91, 92]. Pseudo-experiments are generated in which 0.5% of the candidates are replaced with B_s^0-from-B_c^+ decays that are randomly sampled from simulated $B_c^+ \to B_s^0 (\to J/\psi K^+ K^-)\pi^+$ events. All checks result in negligible differences on the final physics parameters.

7.2 Multiple Candidates

A small fraction of events is expected to have more than one B_s^0 candidate. For such an event the signal candidates have a shared J/ψ and one or two different pions/kaons added. Multiple candidates are mostly distributed like combinatorial background, however a part is found to peak under the signal mass peak. From the candidates that are likely to be clones in an event, one is randomly removed and the final fit is repeated. The variations in the fit results are assigned as a systematic.

7.3 Angular Acceptance

To evaluate the effect due to the limited size of the simulation sample the normalisation weights are shifted from the nominal by a random Gaussian variation using their covariance matrix as input for approximately one hundred times. The root mean square (RMS) of the resulting distributions for each of the parameter is assigned as a systematic.

Several variations are considered on the procedure of the angular acceptance determination described in Section 5.1. The iterative reweighting of simulation is performed using an alternative set of kinematic variables, firstly by including additionally the variables of step 1 - $p(B_s^0)$, $p_T(B_s^0)$ and $m(K^+K^-)$ - and secondly by including the transverse momentum of the two final state muons. As a further test, the GB reweighting is performed in approximately one hundred alternative configurations, by varying for example the depth of the trees. The fit is performed for each of these tests, and the maximum deviation for every parameter is considered as a systematic uncertainty.

As mentioned before, the angular and decay-time acceptances are assumed to factorise. In order to estimate the impact of this, the simulation samples that are produced with the generation values defined in Table 4.2 and the ones with decay width difference $\Delta\Gamma_s = 0$ ps are split into smaller samples of the same size of data. First, the nominal simulation samples are weighted to have $\Delta\Gamma_s = 0$ ps. Similarly, the $\Delta\Gamma_s = 0$ ps samples are weighted to have $\Delta\Gamma_s \neq 0$ ps. Fits are performed to the separate simulation samples and the differences between the fitted values and the generated values are taken as systematic uncertainties.

7.4 Decay-time Resolution

Various systematic effects on the decay-time resolution calibration are evaluated. The calibration parameters determined in Section 5.2.1 are varied within their statistical uncertainties and the effect on the physics parameters is found to be negligible. As mentioned in Section 5.2, the decay-time resolution calibration procedure is applied to simulated samples of prompt $J/\psi K^+K^-$ and $B_s^0 \to J/\psi K^+K^-$ candidates. The prompt data resolution is scaled by the ratio of the two simulation calibration curves, and a quadratic dependence is fit to the scaled resolution curve to determine an alternative calibration. A systematic is calculated from the difference in the final fit results. A third source for a systematic uncertainty is evaluated for the assumption of the mean μ in Equation 5.8 to be zero. It is found to vary in prompt data and a quadratic dependence of the mean on the decay-time uncertainty is included. Differences in the physics parameters using the alternatively determined resolution are assigned as a systematic. The fourth source of systematic uncertainty is the unknown fraction of pile-up, which is accounted for by fixing the fraction of wrongly assigned primary vertices to either 0 or 1.5% - three times the fraction that

is measured in the calibration sample - and repeating the fit. The effect is found to be small and a systematic for each parameter is determined by its maximum deviation.

7.5 Decay-time Acceptance

Section 5.2.2 describes the determination of the decay-time acceptance using splines. Several sources of systematic uncertainties are studied and found to be small. First, the effect due to the limited size of the data and simulated samples is evaluated by repeating the fit several times while varying the spline coefficients according to their covariance matrix. The RMS of the final parameter distributions are taken as systematic uncertainties. Then, the correction for the kinematics variables and the S-wave fraction in the B^0 simulation and data and B_s^0 simulation samples is omitted in the B_s^0 decay-time acceptance computation and the difference in the physics parameters is taken as a systematic. Next, the number of spline knots is doubled and found to have a negligible effect on the result. Finally, the nominal $\Delta\Gamma_s \neq 0$ ps simulation sample is used to determine the acceptance to evaluate a systematic for the use of the alternative $\Delta\Gamma_s = 0$ ps simulation sample. A final systematic contribution is tested by varying the used decay-time resolutions within 10% of their value and found to be negligible.

7.6 C_{SP} Factors

The P-wave model is known to be a ϕ resonance, which only has small model uncertainties. To evaluate a systematic for the knowledge of the C_{SP} factors, three variations of the model of the S-wave are therefore considered:

- The $f_0(980)$ mass and width parameters are varied within their statistical uncertainties as in Ref. [86]
- A second $f_0(980)$ solution reported in Ref. [86] with different parameters is considered
- A parametrisation with a cubic spline function determined from data is considered

New C_{SP} factors are determined for each alternative and used in the final maximum-likelihood fit to data. The maximum resulting variations of the fit values are taken as systematic, with the main contribution coming from the spline parametrisation.

7.7 Flavour Tagging

As mentioned in the previous chapter, the flavour tagging parameters are included as external constraints in the fit, hence their statistical and systematic uncertainties are propagated into the statistical uncertainties reported for the parameter results. By fixing and freeing the tagging parameters in the fit a final contribution of 0.015 rad on the ϕ_s statistical uncertainty is determined. The only additional systematic uncertainty for the flavour tagging is evaluated by considering a quadratic instead of a linear function for the calibration. The effect for all relevant parameters is found to be negligible, and no systematic is assigned.

7.8 Fit Bias

To study possible biases of the fitting procedure eight thousand pseudo-experiments are generated with the same size as data. The fit is performed to these samples and systematics are determined from the resulting pull distributions.

7.9 Length and Momentum Scale

The knowledge of the absolute value of the decay-time depends on the precision of the measured flight distance, momentum and mass. The LHCb length scale uncertainty is determined to be 0.022% in Ref. [93]. This translates directly into the same relative uncertainty on the parameters $\Gamma_s - \Gamma_d$, $\Delta\Gamma_s$ and Δm_s, and is only non-negligible for the latter. The other physics parameters are unaffected. The momentum scale uncertainty is found to be 0.03% in Ref. [42]. However, it affects both momentum and mass determination, hence cancels in the decay-time determination, leading to negligible uncertainties on all observables.

7.10 Further Checks

The measurement of the *CP* asymmetry that results from *CP* violation in the interference between $B_s^0 - \overline{B}_s^0$ mixing and decay could potentially be affected by time-independent effects, i.e. *CP* violation in mixing, direct *CP* violation in the decay, production asymmetry or tagging asymmetry. Several aspects of the analysis reduce the risk of these external factors affecting the measurement: the fit parameter $|\lambda|$ is measured, separate tagging calibrations for B_s^0 and $\overline{B}_s^0$ decisions are used, and separate normalisations of the PDF are determined for each tagging decision. Any residual asymmetry effects are negligible, which is verified by generating pseudo-experiments with a 3% $B_s^0 - \overline{B}_s^0$ production asymmetry. No significant residual biases are observed. Additionally, the analysis is repeated on subsets of the data, e.g. by splitting by magnet polarity, trigger conditions, and year of data-taking. The effect on the physics parameters is found to be negligible for all checks.

7.11 Summary

The final measurement of the main physics parameters in the nominal fit to $B_s^0 \to J/\psi K^+K^-$ is presented in Table 7.2, including the statistical and the total systematic uncertainties. The total systematic uncertainty per parameter is determined by the quadratic sum of all separate systematics, presented in Table 7.1 for the main parameters and in Appendix F for the S-wave fractions and phases. For all parameters except $\delta_{S1} - \delta_\perp$, the total systematic uncertainty is smaller than the statistical uncertainty. Especially the parameter of most interest, ϕ_s, is clearly statistically limited. Also the parameters $|\lambda|$, $\Delta\Gamma_s$ and Δm_s have a statistical uncertainty at least twice as large as the systematic uncertainty. They are mostly affected by the mass factorisation. The largest systematic uncertainty on the parameter $\Gamma_s - \Gamma_d$ originates from the sample size of the decay-time acceptance, in particular from the $B^0 \to J/\psi K^+\pi^-$ data sample. The largest systematic uncertainties on the polarisation amplitudes originate, as expected, from the angular acceptance.

The results of ϕ_s, $\Gamma_s - \Gamma_d$ and $\Delta\Gamma_s$ are the most precise single measurements to date. The value of ϕ_s is in agreement with the SM prediction [23] within 1.0σ, and consistent with no *CP* violation in the interference between direct decay and after

Table 7.1 *Summary of the statistical and systematic uncertainties for the main fit parameters.*

Source	ϕ_s [rad]	$\lvert\lambda\rvert$	$\Gamma_s - \Gamma_d$ [ps^{-1}]	$\Delta\Gamma_s$ [ps^{-1}]	Δm_s [ps^{-1}]	$\lvert A_\perp\rvert^2$	$\lvert A_0\rvert^2$	$\delta_\perp - \delta_0$ [rad]	$\delta_\parallel - \delta_0$ [rad]
Statistical uncertainty	0.041	0.016	0.0024	0.0077	0.059	0.0040	0.0029	0.13	0.078
Mass: σ_{CB} parametrisation	-	-	-	0.0002	0.001	0.0004	0.0006	-	0.003
Mass: factorisation	0.004	0.003	0.0007	0.0022	0.016	0.0005	0.0002	0.05	0.009
Multiple candidates	0.001	0.001	0.0003	0.0001	0.001	0.0001	0.0006	0.01	0.002
Angular acceptance: sample size	0.001	0.002	-	-	0.001	0.0004	0.0003	-	0.004
Angular acceptance: weighting	0.002	0.004	0.0001	0.0002	0.001	0.0011	0.0020	0.01	0.008
Angular acceptance: factorisation	0.001	0.001	0.0002	0.0010	0.003	0.0012	0.0008	0.03	0.006
Decay-time resolution: model applicability	-	-	-	-	0.001	-	-	-	0.001
Decay-time resolution: μ parametrisation	0.003	0.001	0.0002	0.0003	0.005	-	-	0.08	0.001
Decay-time resolution: wrong PV	-	-	-	-	0.001	-	-	-	0.001
Decay-time acceptance: sample size	-	-	0.0012	0.0008	-	0.0003	0.0002	-	-
Decay-time acceptance: kinematic weighting	-	-	0.0002	-	-	-	-	-	-
Decay-time acceptance: S-wave weighting	-	-	0.0001	0.0001	-	-	-	-	-
Decay-time acceptance: $\Delta\Gamma_s = 0$ simulation	-	-	0.0003	0.0005	-	0.0002	0.0001	-	-
$C_{\rm SP}$ factors	0.001	0.001	-	0.0001	0.002	0.0001	-	0.01	0.005
Fit bias	0.001	-	-	0.0003	0.001	0.0006	0.0001	0.02	0.033
Length and momentum scale	-	-	-	-	0.004	-	-	-	-
Quadratic sum of syst.	0.006	0.006	0.0015	0.0026	0.018	0.0019	0.0024	0.10	0.036

Table 7.2 *Final results for the key physics parameters for the full dataset of $B_s^0 \to J/\psi K^+K^-$ signal events. The central values and statistical uncertainties are the same as in Table 6.2.*

Parameter	Value $\pm$ stat $\pm$ syst
ϕ_s [rad]	$-0.080 \pm 0.041 \pm 0.006$
$\lvert\lambda\rvert$	$1.014 \pm 0.016 \pm 0.006$
$\Gamma_s - \Gamma_d$ [ps^{-1}]	$-0.0041 \pm 0.0024 \pm 0.0015$
$\Delta\Gamma_s$ [ps^{-1}]	$0.0764 \pm 0.0077 \pm 0.0026$
Δm_s [ps^{-1}]	$17.697 \pm 0.059 \pm 0.018$
$\lvert A_\perp\rvert^2$	$0.2454 \pm 0.0040 \pm 0.0019$
$\lvert A_0\rvert^2$	$0.5189 \pm 0.0029 \pm 0.0024$
$\delta_\perp - \delta_0$ [rad]	$2.63 \pm 0.13 \pm 0.10$
$\delta_\parallel - \delta_0$ [rad]	$3.062 \pm 0.078 \pm 0.036$

mixing with $\sigma = 1.9$. The experimental uncertainty on ϕ_s is significantly larger than the uncertainty on the predicted penguin contribution, which is discussed in Section 2.8 to be zero within 0.016 rad for the different polarisation states. This validates the direct comparison between the measurement and the SM prediction which ignores penguin contributions. Using the current world average $\Gamma_d = (0.6583 \pm 0.0017)$ ps^{-1} [66], a value of $\Gamma_s/\Gamma_d = 0.9931 \pm 0.0036_{stat} \pm 0.0023_{syst}$ is obtained. The uncertainty on Γ_d is negligible, and the uncertainty on the ratio is purely determined from the $\Gamma_s - \Gamma_d$ uncertainty. This value for Γ_s/Γ_d can be compared to the very precise theoretical prediction (see Equation 2.29). The results for the lifetime related parameters are in agreement with the SM predictions [26, 27] within 1.8σ. The $|\lambda|$ result indicates no direct *CP* violation within 0.8σ. The value of Δm_s is in good agreement with the current world average [24].

Chapter 8

Combination

The ϕ_s result presented in the previous chapter is in agreement with the SM prediction, however the experimental uncertainty is an order ten larger than the theoretical prediction. The experimental precision can be improved by analysing more data, but also by combining the result with previously published measurements of ϕ_s at LHCb, such as the analysis of Run 1 data of $B_s^0 \to J/\psi K^+K^-$ signal events published in Ref. [56]. I have worked on writing a framework to perform the combination. This chapter discusses the functionality of the framework and the combination of the ϕ_s result as published in Ref. [1] with other measurements performed at LHCb. The key feature of this framework is the ability to consider multiple measurements with any number of parameters, their statistical and systematic uncertainties and all possible correlations, including correlations between measurements.

8.1 Introduction

The combination framework has the possibility to fit the results of different measurements, *ResultSet*s, including statistical and systematic uncertainties, into a specified set of agreed combined output parameters, $\vec{P}^{fit}$. It is not required for the ResultSets to have the same parameters. Measured parameters can be linearly translated into the desired output parameters by defining the desired translations, e.g. $\{\Gamma_L, \Gamma_H\}$ into $\{\Gamma_s, \Delta\Gamma_s\}$. The user provides a JSON file with a *ResultList* of all ResultSets that will be combined. Each ResultSet contains per parameter the

name, value and statistical error. Furthermore, a statistical correlation matrix is included which has to follow the same order as the parameters of the relative ResultSet. Additionally, systematic uncertainties can be added with values in the same order as the parameter list and a correlation can be provided between parameters for the systematic in question. An example JSON file can be found in Appendix G.

The combination framework consists of two python files. One python file includes all the functions to do the calculations, and the other reads in the JSON file. In the latter the set of combined output parameters is defined, and additionally the necessary linear translations from input to desired output parameters. If required, Gaussian constraints from external measurements can be added with their value and error. The code then calls the function that determines the best values for the output parameters. This is done by minimisation using `MINUIT` of the χ^2 with respect to $\vec{P}^{fit}$, properly taking into account the correlations.

8.2 Functionality

This section describes the formalism of the code. Each experiment x measures a set of results, $\vec{v}_x^{meas}$, with their corresponding errors, $\vec{\sigma}_x$, and correlation matrix ρ_x. An overall vector, $\vec{v}_{all}^{meas}$, is created by adding all separate measurements:

$$\vec{v}_{all}^{meas} = \begin{bmatrix} \vec{v}_A^{meas} \\ \vec{v}_B^{meas} \\ \vec{v}_C^{meas} \\ \dots \end{bmatrix}. \tag{8.1}$$

Each experiment has a covariance matrix, E_x, determined from $\vec{\sigma}_x$ and ρ_x, from which an overall covariance matrix, E_{all}, is created. Where applicable correlations can be included between the experiments on the off-diagonal terms:

$$E_{all} = \begin{bmatrix} E_A & E_{AB} & 0 & \dots \\ 0 & E_B & 0 & \dots \\ E_{AC} & 0 & E_C & \dots \\ \dots & \dots & \dots & \dots \end{bmatrix}. \tag{8.2}$$

A desired set of output parameters, $\vec{P}^{fit}$, is defined, which is a complete set which either matches the parameters in the different $\vec{v}_x^{meas}$, or can be linearly transformed into parameters in $\vec{v}_x^{meas}$. The values of $\vec{P}^{fit}$ will be iterated by `MINUIT`.

The parameter values of the current iteration of $\vec{P}^{fit}$ are translated into fit values for the measured parameters $\vec{v}_{all}^{fit}$:

$$\begin{bmatrix} ... \\ \vec{v}_{all}^{fit} \\ ... \end{bmatrix} \longleftarrow \vec{P}^{fit}. \tag{8.3}$$

A difference vector, $\vec{\Delta}$, is defined as:

$$\vec{\Delta} = \vec{v}_{all}^{meas} - \vec{v}_{all}^{fit}. \tag{8.4}$$

The final χ^2 that will be minimised by `MINUIT` can then be described by:

$$\chi^2 = \vec{\Delta}^T E_{all}^{-1} \vec{\Delta}. \tag{8.5}$$

The χ^2 is minimised with respect to $\vec{P}^{fit}$ to get the best set of combined values of all parameters, taking into account all correlations.

8.3 Combination with Run 1 $B_s^0 \to J/\psi K^+K^-$

The results of the $B_s^0 \to J/\psi K^+K^-$ analysis using data recorded by the LHCb detector in the years 2015 and 2016 as published in Ref. [1] - in the following referred to as Run 2 - are combined with the results of the Run 1 analysis as presented in Ref. [56]. The following parameters are considered in the combination:

- Run 1 - ϕ_s, $|\lambda|$, Γ_s, $\Delta\Gamma_s$, Δm_s, $|A_\perp|^2$, $|A_0|^2$, $\delta_\perp - \delta_0$, $\delta_\parallel - \delta_0$
- Run 2 - ϕ_s, $|\lambda|$, $\Gamma_s - \Gamma_d$, $\Delta\Gamma_s$, Δm_s, $|A_\perp|^2$, $|A_0|^2$, $\delta_\perp - \delta_0$, $\delta_\parallel - \delta_0$, F_{S1}, F_{S2}, F_{S3}, F_{S4}, F_{S5}, F_{S6}, $\delta_{S1} - \delta_\perp$, $\delta_{S2} - \delta_\perp$, $\delta_{S3} - \delta_\perp$, $\delta_{S4} - \delta_\perp$, $\delta_{S5} - \delta_\perp$, $\delta_{S6} - \delta_\perp$

In Run 1 Γ_s was measured, while in Run 2 $\Gamma_s - \Gamma_d$ is measured. A linear transformation is included in the combination from $\Gamma_s - \Gamma_d$ to Γ_s, using the current world average of Γ_d [66]. By considering Γ_d as one of the fit parameters, its uncertainty can properly be taken into account as it will act as an external Gaussian constraint.

The analysis of Run 2 data is based on the Run 1 measurement, but some of the analysis methods or models have been updated or replaced. When using the same method, the final result will be affected in the same way, hence the systematic uncertainty will be correlated between Run periods. The following systematics appear in both analyses (see Table 7.1 for the systematic uncertainties for Run 2) and are evaluated as described below. For similar systematics, a full correlation is applied. The effect of correlated systematics on the combination is small, as will be shown in the following.

- Mass: factorisation - the analysis described in this thesis uses a signal mass model that resolves the correlation with the helicity angle $\cos\theta_\mu$ (Section 4.6), and the systematic only comes from a dependence on decay-time (Section 7.1). For the Run 1 analysis the origin is the $\cos\theta_\mu$ dependence. No correlation is therefore taken into account.

- C_{SP} factors - the same approach is used and the systematic is therefore considered to be fully correlated between the analyses.

- Decay-time resolution: model applicability - the analyses use a prompt $J/\psi K^+K^-$ data sample from different Runs, hence the systematic is considered uncorrelated between the analyses.

- Angular acceptance: sample size - different simulation samples are used to calculate the normalisation weights and the systematic is therefore considered to be uncorrelated between the analyses.

- Angular acceptance: weighting - both analyses use the iterative weighting procedure and the systematic is therefore considered to be fully correlated between the analyses.

- Decay-time acceptance related systematics - a new method has been developed in this analysis to obtain the decay time acceptance and all considered systematics are therefore uncorrelated.

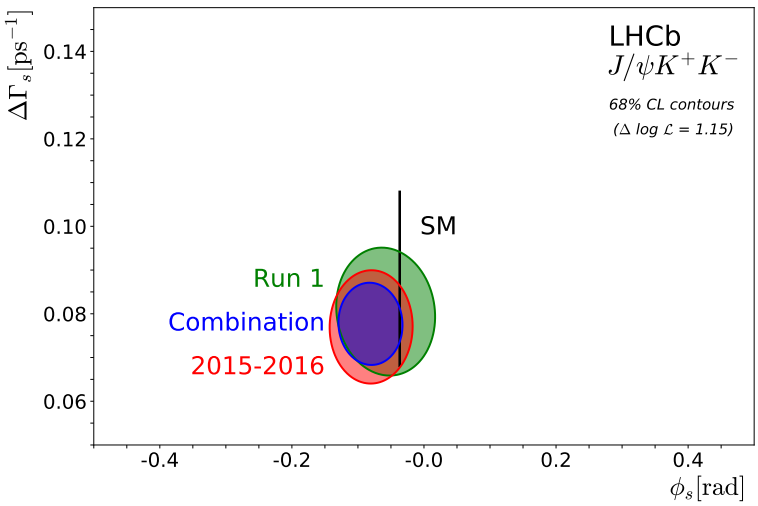

Figure 8.1 *Regions of 68% confidence level in the ϕ_s-$\Delta\Gamma_s$ plane for the Run 1 and 2015 and 2016 $B_s^0 \to J/\psi K^+K^-$ measurements and a combined contour. The ϕ_s and $\Delta\Gamma_s$ SM predictions are indicated by the thin black rectangle.*

- Length and momentum scales - the same detector is used and the systematic is therefore fully correlated.
- Fit bias - the same fit model is used by both analysis and the systematic is therefore fully correlated.

The JSON file as shown in Appendix G is used for the combination. The correlation matrices for the systematics are from private communication. The framework is not able to take into account asymmetric uncertainties, and in the few cases this arises then the largest uncertainty is used, of which the effect is negligible. Per Run a full covariance matrix is constructed by adding statistical and systematic uncertainties in quadrature at each element, including the statistical and any systematic correlations, where they exist, in off-diagonal terms. Correlations between similar systematic uncertainties between Runs are treated as mentioned before and are included as shown in Equation 8.2. Table H.1 shows the correlations for the Run 1 and the Run 2 main parameters that are input for the combination code. The χ^2 of Equation 8.5 is minimised with respect to the set of unique parameters between both Runs. The result of the combination including the total uncertainties is presented in Table 8.1, and the correlations in Table H.2. Figure 8.1 shows the 68% confidence level regions in the ϕ_s versus $\Delta\Gamma_s$ plane for the Run 1 analysis, Run 2 analysis, and their combination, and the SM prediction. The values agree with the SM expectations.

Table 8.1 *Physics parameter values determined for the combination of the Run 1 and Run 2 $B_s^0 \to J/\psi K^+K^-$ analyses as discussed in the text. The uncertainties quoted include the statistical and systematic uncertainties.*

Parameter	Combination value
ϕ_s [rad]	-0.081 ± 0.032
$\lvert\lambda\rvert$	0.995 ± 0.013
Γ_s [ps^{-1}]	0.6575 ± 0.0023
$\Delta\Gamma_s$ [ps^{-1}]	0.0776 ± 0.0062
Δm_s [ps^{-1}]	17.694 ± 0.042
$\lvert A_\perp\rvert^2$	0.2489 ± 0.0035
$\lvert A_0\rvert^2$	0.5196 ± 0.0034
$\delta_\perp - \delta_0$ [rad]	2.87 ± 0.11
$\delta_\parallel - \delta_0$ [rad]	3.155 ± 0.079
F_{S1}	0.487 ± 0.044
F_{S2}	0.0410 ± 0.0096
F_{S3}	0.0047 ± 0.0033
F_{S4}	0.0072 ± 0.0064
F_{S5}	0.074 ± 0.014
F_{S6}	0.152 ± 0.021
$\delta_{S1} - \delta_\perp$ [rad]	2.10 ± 0.28
$\delta_{S2} - \delta_\perp$ [rad]	1.55 ± 0.29
$\delta_{S3} - \delta_\perp$ [rad]	1.08 ± 0.48
$\delta_{S4} - \delta_\perp$ [rad]	-0.33 ± 0.28
$\delta_{S5} - \delta_\perp$ [rad]	-0.55 ± 0.10
$\delta_{S6} - \delta_\perp$ [rad]	-1.18 ± 0.19
Γ_d [ps^{-1}]	0.6594 ± 0.0016

To test the result, different steps of adding more information are compared. Figure 8.2 presents the result per parameter for the main nine parameters, with the value on the x-axis and the vertical error bar illustrating the total uncertainty. The comparison for Γ_d is not shown, since this is an external constraint. From bottom to top the points represent the following:

- y = 1.0: Result Run 1
- y = 2.0: Result Run 2
- y = 3.0: Simple average calculated
- y = 4.0: Fit with χ^2 minimisation to the parameters only including statistical errors and statistical correlation matrices
- y = 5.0: Fit with χ^2 minimisation to the parameters including statistical and systematic uncertainties and their correlations within the separate Runs, but not between them
- y = 6.0: Fit with χ^2 minimisation to the parameters including statistical and systematic uncertainties and their correlations within the separate Runs, but also including correlations between the Runs for the correlated systematics as described above

As can be seen from Figure 8.2, including the correlations between the ResultSets for similar systematics has a small effect on the combination values. This is expected as the total systematic uncertainty for each of the parameters is smaller than their individual statistical uncertainty, and the total systematic uncertainty includes various sources. The combination fit yields values that are mostly close to the simple average calculated, which does not include any correlations. For some of the parameters, the results are far from the simple average, or even fall outside of the range between the corresponding parameters from the two Runs, e.g. ϕ_s and Δm_s. This can be explained by looking at the correlations with other parameters in Table H.1. For the Run 1 ϕ_s result a correlation is present with $\delta_\perp - \delta_0$: $\rho_{\phi_s,\delta_\perp}(\text{Run 1}) = 0.15$, while for Run 2 the phase has a correlation with $|\lambda|$ instead: $\rho_{\phi_s,\lambda}(\text{Run 2}) = 0.17$, and these values change significantly between the run periods. Next, Δm_s is correlated for Run 1 with both $\delta_\perp - \delta_0$ and $|\lambda|$: $\rho_{\Delta m_s,\delta_\perp}(\text{Run 1}) = 0.64$ and $\rho_{\Delta m_s,\lambda}(\text{Run 1}) = -0.19$, while for Run 2 the mass difference is only correlated with $\delta_\perp - \delta_0$: $\rho_{\Delta m_s,\delta_\perp}(\text{Run 2}) = 0.61$.

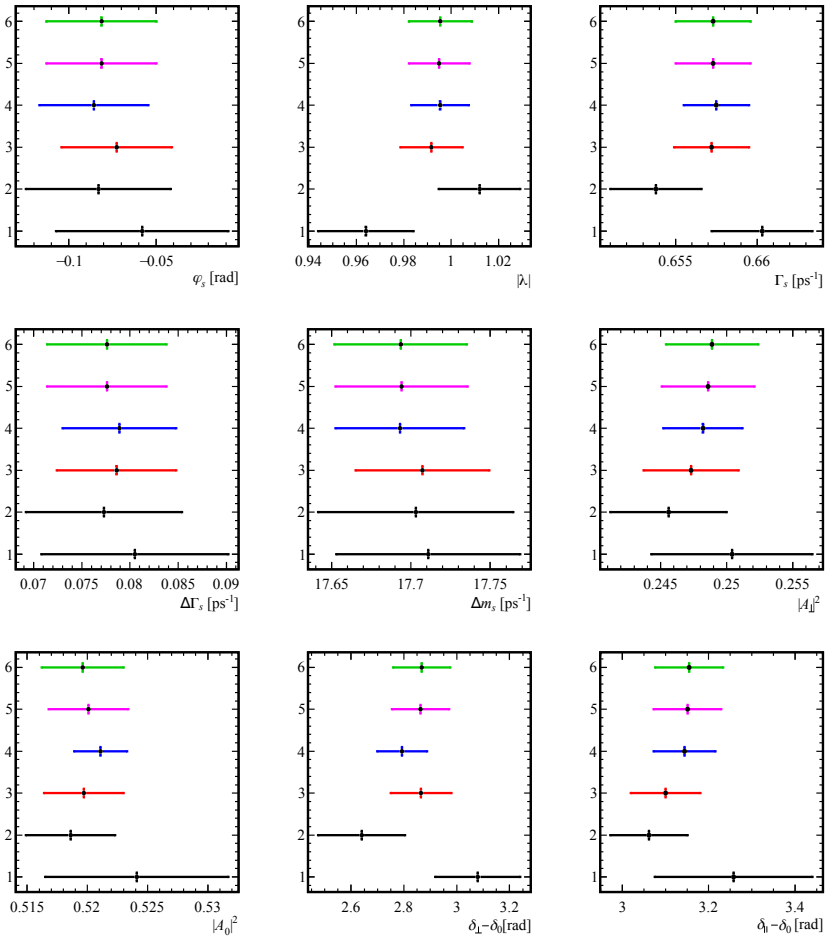

Figure 8.2 *Combination results as described in the text. The vertical error bar represents the combined statistical and systematic uncertainty on the parameter. Only the main parameters are shown.*

8.4 Combination with all LHCb ϕ_s Analyses

As mentioned before, the combination framework can combine any number of ResultSets. To improve the measurement of ϕ_s, the results of all analyses that measure ϕ_s via a $\bar{b} \to \bar{c}c\bar{s}$ transition using LHCb data are combined. The following ResultSets are considered:

1. Run 1 $B_s^0 \to J/\psi K^+K^-$ [56]
2. Run 2 $B_s^0 \to J/\psi K^+K^-$ [1]
3. Run 1 $B_s^0 \to J/\psi \pi^+\pi^-$ [94]
4. Run 2 $B_s^0 \to J/\psi \pi^+\pi^-$ [95]

5. $B_s^0 \to J/\psi K^+K^-$ in the $m(K^+K^-)$ region above the $\phi(1020)$ [96]

6. $B_s^0 \to \psi(2S)\phi$ [97]

7. $B_s^0 \to D_s^+ D_s^-$ [98]

Note that Run 2 means data of year 2015 and 2016. The JSON file as shown in Appendix G is used for the combination. The measured parameters are not all consistent between the analyses, which is taken into account in the combination:

- As previously mentioned, ResultSet 2 measures $\Gamma_s - \Gamma_d$, for which a linear translation to Γ_s is incorporated in the fit, using the current world average of Γ_d [66].
- ResultSet 4 measures $\Gamma_H - \Gamma_d$, where Γ_H is the average decay width of the heavy mass eigenstate of the $B_s^0 - \overline{B}_s^0$ system. The variable is parametrised as $\Gamma_s - \Gamma_d - \Delta\Gamma_s/2$ in the combination. Γ_d is treated as mentioned above.
- ResultSets 5 and 6 determine the decay-time acceptance with respect to $B^0 \to [c\bar{c}]K^+\pi^-$ control channels. The measurements therefore depend on the used value of Γ_d. Their result for Γ_s is translated into $\Gamma_s - \Gamma_d^{\text{input}}$, where Γ_d^{input} is the used value, and the systematic calculated for the value of Γ_d is removed. Then, Γ_d is treated as mentioned above.
- All ResultSets measure ϕ_s and $|\lambda|$, most also measure the lifetime related parameters. ResultSets 1, 2 and 6 additionally determine the polarisation amplitudes and phases. ResultSets 1, 2 and 5 furthermore determine Δm_s, and only ResultSet 2 and 6 measure S-wave amplitudes and phases.

This leads to a total of 28 parameters, where different polarisation parameters are considered for the $B_s^0 \to J/\psi K^+K^-$ and $B_s^0 \to \psi(2S)\phi$ analyses: $\{|A_\perp|^2, |A_0|^2, \delta_\perp - \delta_0, \delta_\parallel - \delta_0\, F_{Si}, \delta_{Si} - \delta_\perp\}$, with $i \in \{1-6\}$, and $\{|A_\perp^{\psi(2S)}|^2, |A_0^{\psi(2S)}|^2, \delta_\perp^{\psi(2S)}, \delta_\parallel^{\psi(2S)}, \left|A_S^{\psi(2S)}\right|^2, \delta_S^{\psi(2S)}\}$, respectively.

Some analyses fix or constrain certain parameters in the fit to values from other measurements, which could bias the results. The following variables are either fixed or constrained:

- ResultSet 3 and 4 fix the parameters Δm_s and Γ_L, the average decay width of the light mass eigenstate of the $B_s^0 - \overline{B}_s^0$ system fit. The effect of this

on the measurements has been checked with toy studies and found to be negligible.

- ResultSet 6 constrains the parameter Δm_s. The effect of this on the measurement has been determined to be negligible.

- ResultSet 7 constrains the parameters Δm_s, Γ_s and $\Delta\Gamma_s$. The effect of these constraints on the final measurement has been checked and found to be negligible.

For the combination the correlations between the systematics of ResultSet 1 and 2 that are mentioned in Section 8.3 are applied. Further correlations between all ResultSets are evaluated in a similar way and correlations are applied where relevant. Performing the average of the 7 ResultSets gives the result in Table 8.2, with the correlation matrix as shown in Table H.3. Figure 8.3 shows the 68% confidence level regions in the ϕ_s versus $\Delta\Gamma_s$ plane for all ResultSets, where 3 fb^{-1} means Run 1 data and 4.9 fb^{-1} the combination of Run 1 and 2015 and 2016 data. Note that the $B_s^0 \to J/\psi\pi^+\pi^-$ and $B_s^0 \to D_s^+ D_s^-$ analyses do not measure $\Delta\Gamma_s$, hence are represented by vertical bands. The result of the combination fit is illustrated as well as the SM predictions.

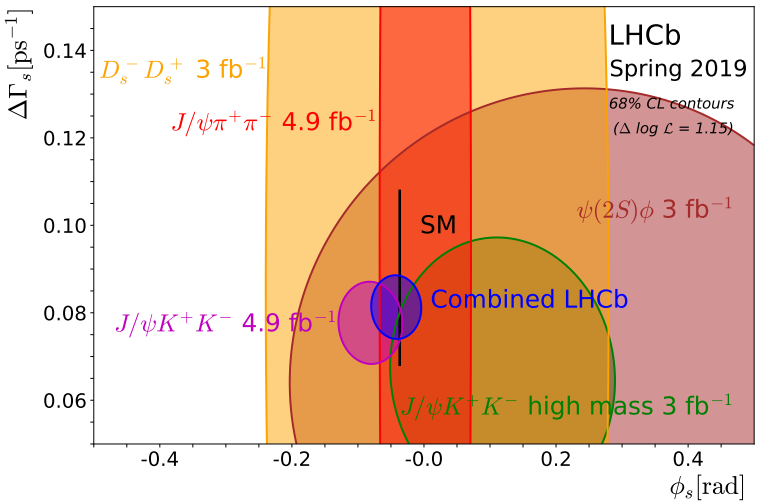

Figure 8.3 *68% confidence level regions in ϕ_s vs $\Delta\Gamma_s$ plain for the indiviual LHCb analyses and the combined contour. 3 fb^{-1} corresponds to the result using Run 1 data and 4.9 fb^{-1} using the combination of Run 1 and 2015 and 2016 data. The $B_s^0 \to J/\psi\pi^+\pi^-$ and $B_s^0 \to D_s^+ D_s^-$ analyses do not measure $\Delta\Gamma_s$, hence are represented by vertical bands. The ϕ_s and $\Delta\Gamma_s$ SM predictions are indicated by the thin black rectangle.*

Table 8.2 *Physics parameter values determined for the combination of all LHCb ϕ_s analyses as discussed in the text. The uncertainties quoted include the statistical and systematic uncertainties.*

Parameter	Combination value
ϕ_s [rad]	-0.042 ± 0.025
$\lvert\lambda\rvert$	0.993 ± 0.010
Γ_s [ps^{-1}]	0.6566 ± 0.0021
$\Delta\Gamma_s$ [ps^{-1}]	0.0811 ± 0.0048
Δm_s [ps^{-1}]	17.720 ± 0.041
$\lvert A_\perp\rvert^2$	0.2469 ± 0.0031
$\lvert A_0\rvert^2$	0.5212 ± 0.0028
$\delta_\perp - \delta_0$ [rad]	2.88 ± 0.11
$\delta_\parallel - \delta_0$ [rad]	3.153 ± 0.079
F_{S1}	0.486 ± 0.044
F_{S2}	0.0406 ± 0.0096
F_{S3}	0.0046 ± 0.0033
F_{S4}	0.0074 ± 0.0064
F_{S5}	0.073 ± 0.014
F_{S6}	0.150 ± 0.021
$\delta_{S1} - \delta_\perp$ [rad]	2.10 ± 0.28
$\delta_{S2} - \delta_\perp$ [rad]	1.54 ± 0.29
$\delta_{S3} - \delta_\perp$ [rad]	1.11 ± 0.48
$\delta_{S4} - \delta_\perp$ [rad]	-0.32 ± 0.28
$\delta_{S5} - \delta_\perp$ [rad]	-0.54 ± 0.10
$\delta_{S6} - \delta_\perp$ [rad]	-1.19 ± 0.19
Γ_d [ps^{-1}]	0.6596 ± 0.0016
$\left\lvert A_\perp^{\psi(2S)}\right\rvert^2$	0.255 ± 0.018
$\left\lvert A_0^{\psi(2S)}\right\rvert^2$	0.43 ± 0.012
$\delta_\parallel^{\psi(2S)}$ [rad]	3.67 ± 0.18
$\delta_\perp^{\psi(2S)}$ [rad]	3.13 ± 0.35
$\left\lvert A_S^{\psi(2S)}\right\rvert^2$	0.061 ± 0.026
$\delta_S^{\psi(2S)}$ [rad]	0.03 ± 0.14

The values of ϕ_s, $|\lambda|$, Γ_s and $\Delta\Gamma_s$ are the most precise to date. The value of ϕ_s is in agreement with the SM prediction [23] within 0.2σ, and with no *CP* violation in the interference between direct decay and after mixing within 1.7σ. The parameter $|\lambda|$ is consistent with unity within 0.7σ, implying no evidence for direct *CP* violation in the decay. The values of Γ_s and $\Delta\Gamma_s$ are consistent with the SM predictions [26, 27] within 1σ. The value of Δm_s is in good agreement with the current world average [24].

Chapter 9

Summary and Outlook

A time-dependent angular analysis has been performed of $B_s^0 \to J/\psi K^+K^-$ signal events in 1.9 fb^{-1} of data recorded by LHCb in the years 2015 and 2016. The following results are obtained:

$$\begin{aligned} \phi_s &= -0.080 \pm 0.041 \text{ (stat)} \pm 0.006 \text{ (syst) rad} \\ \Gamma_s - \Gamma_d &= -0.0041 \pm 0.0024 \text{ (stat)} \pm 0.0015 \text{ (syst) ps}^{-1} \\ \Delta\Gamma_s &= 0.0764 \pm 0.0077 \text{ (stat)} \pm 0.0026 \text{ (syst) ps}^{-1} \\ |\lambda| &= 1.014 \pm 0.016 \text{ (stat)} \pm 0.006 \text{ (syst)}. \end{aligned} \tag{9.1}$$

These are the most precise measurements of ϕ_s, $\Gamma_s - \Gamma_d$ and $\Delta\Gamma_s$ using a single decay channel. The results are statistically limited, hence adding more data will improve the precision. The published numbers are combined with the results from other ϕ_s analyses performed using LHCb data from Run 1 and the years 2015 and 2016, yielding the following numbers:

$$\begin{aligned} \phi_s &= -0.042 \pm 0.025 \text{ rad} \\ \Gamma_s &= 0.6566 \pm 0.0021 \text{ ps}^{-1} \\ \Delta\Gamma_s &= 0.0811 \pm 0.0048 \text{ ps}^{-1} \\ |\lambda| &= 0.993 \pm 0.010. \end{aligned} \tag{9.2}$$

The measurements are in agreement with the Standard Model predictions, and thus there is no evidence for New Physics.

9.1 Outlook

As can be seen from Figure 8.3, the Standard Model prediction of ϕ_s is more precise than the combination of the $B_s^0 \to J/\psi K^+K^-$ analyses and the combination of all ϕ_s analyses performed at LHCb. An analysis of the full Run 2 data - years 2015 to 2018 corresponding to 6 fb^{-1} of data - of $B_s^0 \to J/\psi K^+K^-$ is currently ongoing to improve the precision with an expected statistical uncertainty of 0.026 rad, estimated by scaling the event yield linearly with the recorded integrated luminosity. Adding all current data with future upgrades up until and including Run 5 would lead to a dataset of 300 fb^{-1}, from which a statistical uncertainty on ϕ_s of 4 mrad from $B_s^0 \to J/\psi K^+K^-$ only and 3 mrad from all LHCb ϕ_s analyses is expected [99], see Figure 9.1. This is compatible with the uncertainty on the value determined by the CKMfitter group of $^{+1.0}_{-0.7}$ mrad [23], hence will provide stringent constraints on New Physics.

Figure 9.1 shows the current and expected statistical uncertainty on ϕ_s per decay mode versus the amount of data collected by LHCb. The uncertainty for the combination of all decay modes and the Standard Model prediction are presented as well. The current results for ϕ_s are scaled by the expected running conditions, assuming current detector and flavour tagging performances. For this plot only tree diagrams are considered. Latest results show no sign of penguin contributions within a precision of 10 mrad [32]. It becomes imperative to update these measurements when the experimental precision on ϕ_s improves with future upgrades.

The Heavy Flavour Averaging Group (HFLAV) group [101] compares the LHCb combination results with analyses of $B_s^0 \to J/\psi K^+K^-$ performed by the CDF [102], DØ [103], ATLAS [104], CMS [105] experiments. Figure 9.2 shows the different measurements of ϕ_s and $\Delta\Gamma_s$ indicated by different colours as well as their combination computed by the HFLAV group and the Standard Model prediction. The ATLAS dataset corresponds to data taken in Run 1 (2012) and Run 2 ($2015 - 2017$), and the CMS dataset in Run 1 (2012). The results are in agreement with the Standard Model. As can be seen from the plot, LHCb provides the most precise measurement of ϕ_s. A combination of the ATLAS, CMS and LHCb results alone can provide a stringent constraint on New Physics, while considering the appropriate correlations. An accuracy of $\sigma_{\phi_s} \approx 20$ mrad is expected when combining the Run 1 and Run 2 results of ATLAS, CMS and LHCb. Future analyses performed by these experiments will follow similar

strategies to allow a straightforward combination.

Current observations confirm the amount of CP violation in the decay of $B_s^0 \to J/\psi K^+ K^-$ predicted by the SM, leaving the observed large matter-antimatter asymmetry in the Universe a mystery. With the scheduled improved precision in the next decades it might be possible to observe a deviation of the ϕ_s value, resulting in the need of non-SM contributions which might be able to explain the matter abundance in the Universe.

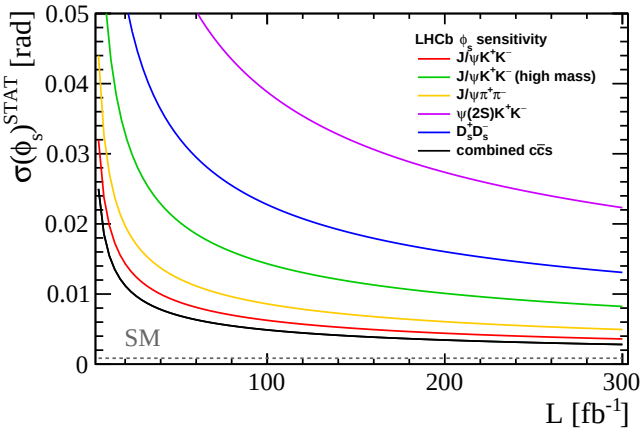

Figure 9.1 *Statistical uncertainty on ϕ_s versus amount of data collected by LHCb for different B_s^0 decay modes, represented by different coloured solid lines as shown in the legend. The Standard Model prediction is indicated by the dashed line. Run 1 and Run 2 combined corresponds to 9 fb^{-1} of data, and a total of 300 fb^{-1} is expected after Run 5. The current results are scaled using the expected running conditions and assuming current detector and flavour tagging performances. Figure taken from Ref. [100].*

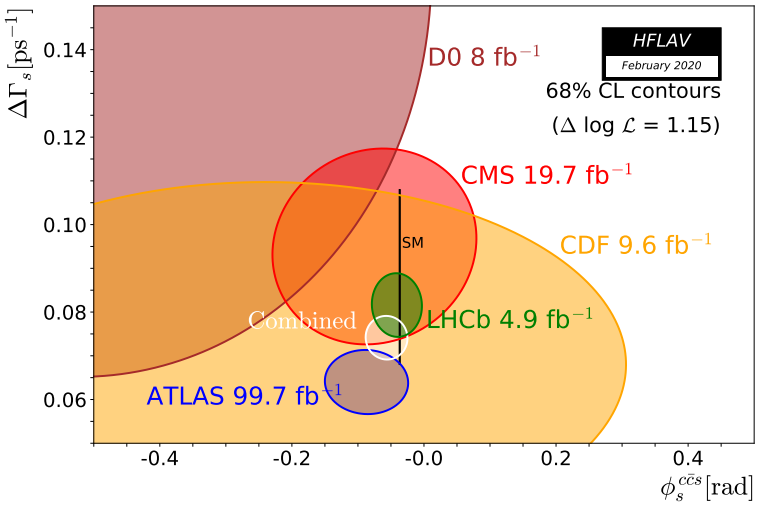

Figure 9.2 *68% confidence level regions in ϕ_s vs $\Delta\Gamma_s$ plain for the different experiments and the combined contour. The amount of collected data per experiment is indicated as well. The ϕ_s and $\Delta\Gamma_s$ Standard Model predictions are indicated by the thin black rectangle. Figure taken from Ref. [106].*

Appendix A

Variable Distributions

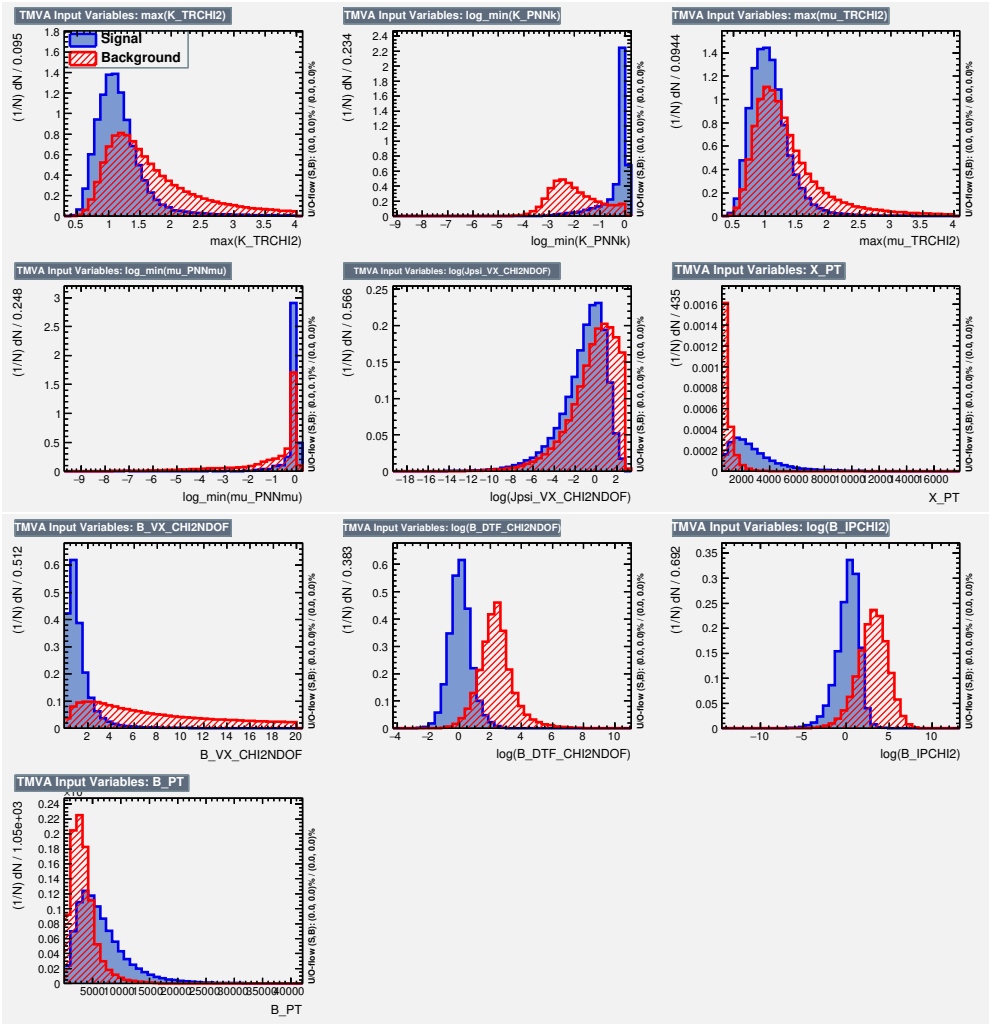

Figure A.1 *Distributions of the variables used for the BDT training for $B_s^0 \to J/\psi K^+K^-$ in the signal (blue filled) and background (red diagonally dashed) samples. Figure taken from Ref. [62].*

Appendix B

Decay-time Acceptance

This appendix describes the implementation of the spline that is used to describe the decay-time acceptance (Section 5.2.2) in the normalisation of the final PDF. The spline makes it possible to perform the normalisation of the PDF analytically. The derivation is performed in detail in Ref. [73].

B.1 Re-writing Time-dependent Differential Decay Rate

When performing a time-dependent analysis of neutral mesons, the differential decay rate includes mixing parameters:

$$\frac{\mathrm{d}\Gamma_{theo}(t)}{\mathrm{d}t} \sim e^{-\Gamma t}[A\cosh\frac{\Delta\Gamma t}{2} + B\sinh\frac{\Delta\Gamma t}{2} + C\cos(\Delta m t) + D\sin(\Delta m t)], \quad \text{(B.1)}$$

where $t > 0$, A, B, C and D are real coefficients, Γ is the average decay width of the two meson mass eigenstates, and $\Delta\Gamma$ and Δm the decay width and mass difference between the heavy and light mass eigenstates, respectively. This is equivalent to Equation 2.20. To obtain the experimentally observable decay rate, this is convolved with a Gaussian resolution model to include the finite decay-time resolution of the detector:

$$\frac{\mathrm{d}\Gamma_{exp}(t)}{\mathrm{d}t} = \int_{-\infty}^{+\infty} \mathrm{d}t'\theta(t')\frac{\mathrm{d}\Gamma_{theo}(t')}{\mathrm{d}t'}\mathcal{R}(t-t',\sigma,\mu), \quad \text{(B.2)}$$

with

$$\mathcal{R}(t-t',\sigma,\mu) = \frac{1}{\sqrt{2\pi\sigma^2}} e^{-\frac{(t-t'-\mu)^2}{2\sigma^2}}. \tag{B.3}$$

Here $\theta(t')$ is the Heavyside (step) function, σ represents the decay-time resolution and μ a possible bias in the reconstructed decay-time. Including the decay-time efficiency $a(t)$ is trivial:

$$\frac{\mathrm{d}\Gamma^{acc}_{exp}(t)}{\mathrm{d}t} = \frac{\mathrm{d}\Gamma_{exp}(t)}{\mathrm{d}t} a(t). \tag{B.4}$$

We want to find a function $a(t)$ that can describe the acceptance and for which the normalisation can be computed analytically:

$$\mathrm{PDF}(t) = \int \mathrm{d}t a(t) \frac{\mathrm{d}\Gamma_{exp}(t)}{\mathrm{d}t}. \tag{B.5}$$

Since $\sin(\Delta m t) = \Im(e^{i\Delta m t})$ and $\cos(\Delta m t) = \Re(e^{i\Delta m t})$ and the cosh and sinh terms can be written as the sum and difference of exponentials, the unnormalised PDF, p, can be described as the following without any acceptance:

$$\begin{aligned} p(t;\Gamma,\Delta m,\mu,\sigma) &= \frac{1}{\sqrt{2\pi\sigma^2}} \int_0^{+\infty} \mathrm{d}t' e^{-(\Gamma - i\Delta m)t'} e^{-\frac{(t-t'-\mu)^2}{2\sigma^2}} \\ &= \frac{1}{\pi} \int_0^{+\infty} \mathrm{d}y e^{-(x-y)^2 - 2zy} \\ &= \frac{1}{2} e^{-x^2} w(i(z-x)) = p(x;z). \end{aligned} \tag{B.6}$$

Where for the second line:

$$z = (\Gamma - i\Delta m)\sigma/2, \qquad x = \frac{t-\mu}{\sqrt{2}\sigma}, \qquad y = \frac{t'}{\sqrt{2}\sigma}, \tag{B.7}$$

and in the third line the *Faddeeva* function, $w(z)$, is implemented, which is related to the *complementary error function*:

$$w(z) = e^{-z^2} \mathrm{erfc}(-iz). \tag{B.8}$$

The normalisation of the PDF is now described by:

$$I_0(t_1,t_2;\Gamma,\Delta m,\mu,\sigma) = \int_{t_1}^{t_2} \mathrm{d}t p(t;\Gamma,\Delta m,\mu,\sigma) = \frac{\sigma}{\sqrt{2}} \hat{I}_0(x_1,x_2;z), \tag{B.9}$$

where

$$\hat{I}_0(x_1, x_2; z) \equiv \int_{x_1}^{x_2} \mathrm{d}x e^{-x^2} w(i(z-x)) = \frac{1}{2z}\Big[\mathrm{erf} - e^{-x^2} w(i(z-x))\Big]_{x1}^{x2}. \quad \text{(B.10)}$$

The simplest way of including an acceptance function for which the integral can be computed is by including a "piecewise constant" acceptance, as an histogram:

$$\begin{aligned}\int_{x_0}^{x_N} a(x) f(x; z) dx &= \sum_{i=0}^{N-1} \int_{x_i}^{x_{i+1}} a_i f(x; z) dx = \sum_{i=0}^{N-1} a_i \int_{x_i}^{x_{i+1}} f(x; z) dx \\ &= \sum_{i=0}^{N} a_i \hat{I}_0(x_i, x_{i+1}; z).\end{aligned} \quad \text{(B.11)}$$

A non-trivial decay-time acceptance can be approximated by piecewise constant or linear functions or by piecewise polynomials such as splines, which are explained in the next section. The acceptance function then becomes a sum of time functions as $a(t) = \sum_k a_k t^k$. Starting from Equation B.10, which is described in the coordinates x and z, the acceptance can be included by translating t^k into x^n using x defined in Equation B.7. Using $x^n = \frac{1}{2^n}\frac{d^n}{d\lambda^n}\Big|_{\lambda=0} e^{2\lambda x}$ the integral for n orders becomes:

$$\hat{I}_n(x_1, x_2; z) \equiv \int_{x_1}^{x_2} \mathrm{d}x x^n e^{-x^2} w(i(z-x)) = \frac{1}{2^n}\frac{d^n}{d\lambda^n}\Big|_{\lambda=0} \int_{x_1}^{x_2} \mathrm{d}x e^{2\lambda x} e^{-x^2} w(i(z-x)). \quad \text{(B.12)}$$

Considering a piecewise polynomial acceptance leads to:

$$\begin{aligned}\int_{x_0}^{x_N} a(x) f(x; z) dx &= \sum_{i=0}^{N-1} \int_{x_i}^{x_{i+1}} \Big(\sum_j a_{ij} x^j\Big) f(x; z) dx \\ &= \sum_{i=0}^{N-1} \sum_j a_{ij} \hat{I}_j(x_i, x_{i+1}; z).\end{aligned} \quad \text{(B.13)}$$

A single "piece", i.e. interval, is hereby described as follows:

$$N(x_i, x_{i+1}; z) = \int_{x_i}^{x_{i+1}} \sum_{j=0}^{3} a_{ij} x^j f(x; z) dx$$
$$= \begin{pmatrix} M_0(x_i, x_{i+1}; z) \\ M_1(x_i, x_{i+1}; z) \\ M_2(x_i, x_{i+1}; z) \\ M_3(x_i, x_{i+1}; z) \end{pmatrix} \begin{pmatrix} a_{i0} & \frac{a_{i1}}{2} & \frac{a_{i2}}{4} & \frac{a_{i3}}{8} \\ \frac{a_{i1}}{2} & \frac{a_{i2}}{2} & \frac{3a_{i3}}{8} & 0 \\ \frac{a_{i2}}{4} & \frac{3a_{i3}}{8} & 0 & 0 \\ \frac{a_{i3}}{8} & 0 & 0 & 0 \end{pmatrix} \begin{pmatrix} K_0(z) \\ K_1(z) \\ K_2(z) \\ K_3(z) \end{pmatrix}, \tag{B.14}$$

where $M_n(x_1, x_2; z) \equiv M_n(x_2; z) - M_n(x_1; z)$. The coefficients $M_n(x; z)$ and K_n are given in Table B.1. $M_n(x_i, x_{i+1}; z)$ depends on the intervals and parameters $\{\Gamma, \Delta m, \sigma, \mu\}$, a_{ij} on $a(t)$, and $K_n(z)$ on $\{\Gamma, \Delta m, \sigma\}$.

Table B.1 *The n^{th} order derivatives at $\lambda = 0$. These functions define the different orders of the third order polynomial.*

n	$K_n(z)$	$M_n(x; z)$
0	$\frac{1}{2z}$	$\mathrm{erf} - e^{-x^2} w(i(z-x))$
1	$\frac{1}{2z^2}$	$2e^{-x^2}\big[-\sqrt{\frac{1}{\pi}} - xw(i(z-x))\big]$
2	$\frac{1}{z}(1+\frac{1}{z^2})$	$2e^{-x^2}\big[-2x\sqrt{\frac{1}{\pi}} - (2x^2-1)w(i(z-x))$
3	$\frac{3}{z^2}(1+\frac{1}{z^2})$	$4e^{-x^2}\big[-(2x^2-1)\sqrt{\frac{1}{\pi}} - x(2x^2-3)w(i(z-x))\big]$

B.2 Spline

As mentioned in Section 5.2.2, the decay-time acceptance in this analysis is described by a cubic spline $s(t)$ [72] which is build up by cubic b-splines $b_i(t)$:

$$s(t) = \sum_{i=0}^{N+2} c_i b_i(t), \tag{B.15}$$

where c_i is the coefficient of the respective b-spline and $N+2$ represents the total number of b-splines. The normalisation of Equation B.14 then turns into the following:

$$N(x_i, x_{i+1}; z, \alpha_i, \beta_i, \gamma_i) = \int_{x_i}^{x_{i+1}} \sum_{j=0}^{3} \sum_{k=0}^{3-j} (M_j(x_{i+1}; z)) - (M_j(x_i; z)) b_{jk}(\alpha_i, \beta_i, \gamma_i) K_k(z), \tag{B.16}$$

where α_i, β_i, and γ_i are parameters that define the b-spline matrix b_{jk}.

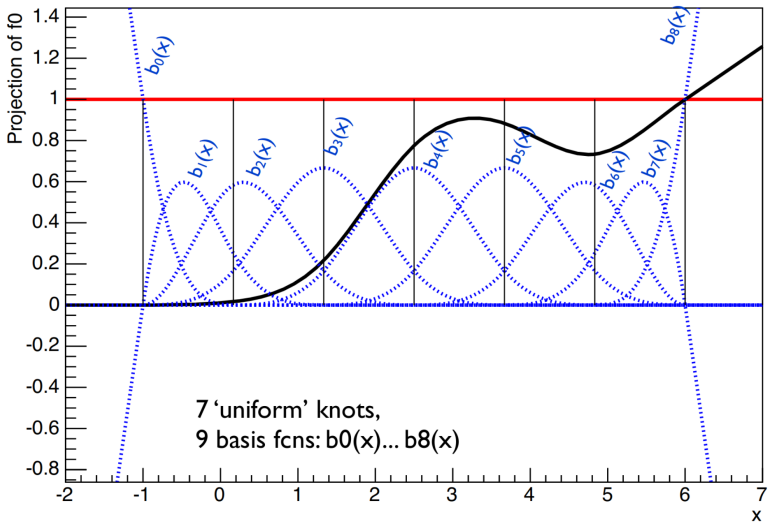

Figure B.1 *A representation of the 9 separate b-splines that make up the spline used to model the decay-time acceptance distribution. In each interval there are four contributing b-splines. Figure taken from Ref. [107].*

In this analysis 7 knots are defined, leading to 9 b-splines, see Figure B.1. For each interval i there are four contributing b-splines, $b_i(t)$ for $i \in \{i, i+1, i+2, i+3\}$:

$$s(t)|_i = c_i b_i(t) + c_{i+1} b_{i+1}(t) + c_{i+2} b_{i+2}(t) + c_{i+3} b_{i+3}(t). \tag{B.17}$$

This means that for each interval a linear combination of four matrices $b_{jk}(\alpha_i, \beta_i, \gamma_i)$ is computed, whose values depend on the defined knots.

Appendix C

The Fitting Parameter $\Gamma_s - \Gamma_d$

This appendix will explain the use of $\Gamma_s - \Gamma_d$ as a fitting parameter and show it is independent of the value used for Γ_d.

C.1 Decay-time Acceptance from B^0 Control Channel

As shown in Equation 5.11, the B_s^0 decay-time acceptance, $\varepsilon_{\rm data}^{B_s^0}(t)$, depends on the B^0 acceptance, $\varepsilon_{\rm data}^{B^0}(t)$. In order to determine $\varepsilon_{\rm data}^{B^0}(t)$, the decay-time of the control channel $B^0 \to J/\psi K^+\pi^-$ is fitted with an exponential set to its decay width, convolved with a resolution function, and multiplied with an acceptance function represented by splines. The free parameters are the coefficients for the acceptance, whereas the decay width is fixed to the current world average of $\Gamma_d^{wa} = (0.6583 \pm 0.0017)$ ps $^{-1}$ [66]. The B_s^0 decay-time acceptance is then derived from:

$$\varepsilon_{\rm data}^{B_s^0}(t) \propto \varepsilon_{\rm data}^{B^0}(t) = \frac{N^{B^0}(t)}{e^{-\Gamma_d t} \otimes \mathcal{R}^{B^0}(t)}, \tag{C.1}$$

where $N^{B^0}(t)$ represents the observed decay-time distribution of the B^0 control sample, and $\mathcal{R}^{B^0}(t)$ the decay-time resolution function of this decay. As can be seen, the decay-time acceptance of the signal channel depends on the chosen value of the B^0 decay width, Γ_d. In case the current world average will be updated,

this would result in a new value with a deviation $\delta\Gamma_d$:

$$\Gamma_d = \Gamma_d^{wa} + \delta\Gamma_d. \tag{C.2}$$

Then, the decay-time acceptance for the B_s^0 channel would change accordingly:

$$\begin{aligned}
\varepsilon_{\text{data}}^{B_s^0}(t|\Gamma_d) &\propto \frac{N^{B^0}(t)}{e^{-(\Gamma_d^{wa}+\delta\Gamma_d)t} \otimes \mathcal{R}^{B^0}(t)} \\
&\approx \frac{N^{B^0}(t)}{e^{-\Gamma_d^{wa}t} \otimes \mathcal{R}^{B^0}(t)} \times e^{\delta\Gamma_d t} \\
&= \varepsilon_{\text{data}}^{B_s^0}(t, \Gamma_d) \times e^{\delta\Gamma_d t}.
\end{aligned} \tag{C.3}$$

The approximation in the second step is valid, since the lower bound on the decay-time is significantly larger than the decay-time resolution, $0.3\ \text{ps}^{-1} \gg 0.045\ \text{ps}^{-1}$. As a result, the decay-time acceptance depends on an exponentially time-dependent factor of the variation in Γ_d. Hence, the same variation would be observed in the measured decay width of the B_s^0 system, Γ_s. By fitting with this parametrisation, a systematic uncertainty would arise on the parameter Γ_s due to the uncertainty on Γ_d^{wa}. Instead, the decay width difference $\Gamma_s - \Gamma_d$ is used as a fitting parameter, to be insensitive to the exact Γ_d value and to obtain a more precise measurement. The parameter $\Gamma_s - \Gamma_d$ is the actual quantity that is measured when taking the decay-time acceptance from a B^0 channel. The independence of the former on $\delta\Gamma_d$ can be justified by introducing the decay width difference $\Delta\Gamma_d^s \equiv \Gamma_s - \Gamma_d$, and including the variation in Γ_d:

$$\Gamma_s = \Gamma_d^{wa} + \delta\Gamma_d + \Delta\Gamma_d^s. \tag{C.4}$$

The relevant part of the PDF for the decay-time extraction can be represented by:

$$\begin{aligned}
p(t) &\approx \varepsilon_{\text{data}}^{B_s^0}(t, \Gamma_d) \times e^{\delta\Gamma_d t} \times \left[e^{-(\Gamma_d^{wa}+\delta\Gamma_d+\Delta\Gamma_d^s)t} \otimes \mathcal{R}(t|\sigma_{eff}(\sigma_t)) \right] \\
&\approx \varepsilon_{\text{data}}^{B_s^0}(t, \Gamma_d) \times e^{\delta\Gamma_d t} \times e^{-\delta\Gamma_d t} \left[e^{-(\Gamma_d^{wa}+\Delta\Gamma_d^s)t} \otimes \mathcal{R}(t|\sigma_{eff}(\sigma_t)) \right] \\
&= \varepsilon_{\text{data}}^{B_s^0}(t, \Gamma_d) \times \left[e^{-(\Gamma_d^{wa}+\Delta\Gamma_d^s)t} \otimes \mathcal{R}(t|\sigma_{eff}(\sigma_t)) \right].
\end{aligned} \tag{C.5}$$

Hence, the dependence of the decay-time acceptance on the variation in Γ_d vanishes.

Appendix D

Comparison to Official LHCb Result

This appendix contains the comparison between the fit results presented in this thesis and for the official LHCb publication in Ref. [1]. As described in Section 6.7 the results in this thesis have been computed by the `RAPIDFIT` fitting framework, and have been tested extensively to agree. Table D.1 compares the main parameters of the final fit and shows consistent results. The asymmetric error on the $\delta_{\parallel} - \delta_0$ published result is determined by the `MINOS` package.

Table D.1 *Comparison of the fit results for the $B_s^0 \to J/\psi K^+ K^-$ physics parameters presented in this thesis and in the LHCb publication in Ref. [1]. Only statistical uncertainties are presented.*

Parameter	This thesis	Published result
ϕ_s [rad]	-0.080 ± 0.041	-0.083 ± 0.041
$\lvert\lambda\rvert$	1.014 ± 0.016	1.012 ± 0.016
$\Gamma_s - \Gamma_d$ [ps^{-1}]	-0.0041 ± 0.0024	-0.0041 ± 0.0024
$\Delta\Gamma_s$ [ps^{-1}]	0.0764 ± 0.0077	0.0773 ± 0.0077
Δm_s [ps^{-1}]	17.697 ± 0.059	17.703 ± 0.059
$\lvert A_{\perp}\rvert^2$	0.2454 ± 0.0040	0.2456 ± 0.0040
$\lvert A_0\rvert^2$	0.5189 ± 0.0029	0.5186 ± 0.0029
$\delta_{\perp} - \delta_0$ [rad]	2.63 ± 0.13	2.64 ± 0.13
$\delta_{\parallel} - \delta_0$ [rad]	3.062 ± 0.078	$3.062^{+0.082}_{-0.074}$

Appendix E

`RapidFit` Results

Table E.1 presents the statistical correlations between the fit parameter estimates determined by the `RapidFit` framework for the nominal polarisation-independent fit to $B_s^0 \to J/\psi K^+K^-$ signal events in the full dataset. For this fit, the S-wave parameters are different for each of the $m(K^+K^-)$ bins as defined in Table 6.1, whereas the main nine parameters are shared between the bins. The nominal fit uses the differential decay rate of Equation 2.31. The parameter estimates for the tagging parameters that are included as external constraints can be found in Table E.2 with their correlations in Table E.3. Their correlations with the key physics parameters and the six pairs of S-wave parameters are negligible. The polarisation-dependent fit uses the coefficients shown in Table 2.3 for the time-dependent functions. The statistical correlation matrix for the polarisation dependent ϕ_p and $|\lambda_p|$ is shown in Table E.4.

Figures E.1-E.3 show the NLL profiles for the key physics parameters and S-wave fractions and phases. For these plots, the value of a chosen parameter is fixed and the NLL function is re-minimised with respect to all other parameters to determine the best minima. The 1σ confidence interval is between the parameter values above and below its value in the minimum, for which the NLL value is equal to $\frac{1}{2}$. The 3σ region corresponds to an NLL value of $4\frac{1}{2}$. The NLL scans for the key physics parameters follow a parabolic shape, while the S-wave parameters have less well behaved profiles. The likelihood scans are used to ensure that the fit has found the global minima, and not a local one.

	$\Gamma_s - \Gamma_d$	$\Delta\Gamma_s$	$\lvert A_\perp\rvert^2$	$\lvert A_0\rvert^2$	$\delta_\parallel - \delta_0$	$\delta_\perp - \delta_0$	F_{S1}	$\delta_{S1} - \delta_\perp$	Δm_s	ϕ_s	$\lvert\lambda\rvert$	F_{S2}	$\delta_{S2} - \delta_\perp$	F_{S3}	$\delta_{S3} - \delta_\perp$	F_{S4}	$\delta_{S4} - \delta_\perp$	F_{S5}	$\delta_{S5} - \delta_\perp$	F_{S6}	$\delta_{S6} - \delta_\perp$
$\Gamma_s - \Gamma_d$	1.00	-0.48	0.40	-0.32	0.03	-0.00	0.05	0.01	-0.01	-0.03	0.02	0.04	-0.00	0.03	-0.02	0.03	0.02	0.07	0.02	0.06	0.01
$\Delta\Gamma$		1.00	**-0.69**	**0.63**	-0.02	0.01	-0.07	-0.00	0.02	-0.00	-0.04	-0.05	0.01	-0.01	0.00	0.03	0.02	-0.06	0.00	-0.06	0.00
$\lvert A_\perp\rvert^2$			1.00	**-0.6**	0.15	0.01	0.04	0.02	-0.03	-0.03	0.02	-0.02	-0.01	-0.02	0.01	-0.05	-0.02	0.01	0.00	0.03	0.02
$\lvert A_0\rvert^2$				1.00	0.00	0.01	-0.05	-0.00	0.01	0.02	-0.02	-0.01	0.00	0.01	-0.02	0.05	0.03	-0.01	0.02	-0.03	0.01
$\delta_\parallel - \delta_0$					1.00	0.20	0.01	-0.02	-0.05	0.01	0.01	0.00	-0.04	0.04	-0.05	0.03	0.01	0.04	-0.00	0.01	-0.03
$\delta_\perp - \delta_0$						1.00	-0.01	-0.06	**0.74**	-0.02	0.04	0.01	-0.19	0.01	-0.01	0.05	-0.00	0.04	0.00	-0.07	-0.16
F_{S1}							1.00	0.08	-0.01	-0.00	0.01	0.00	-0.00	0.00	-0.00	-0.00	-0.00	0.00	-0.00	0.01	0.00
$\delta_{S1} - \delta_\perp$								1.00	-0.02	0.00	0.05	-0.00	0.01	0.00	0.00	-0.00	0.00	-0.00	0.00	0.01	0.02
Δm_s									1.00	-0.02	-0.02	0.00	-0.09	-0.06	0.09	0.12	0.07	0.07	0.07	-0.02	-0.04
ϕ_s										1.00	0.18	0.01	-0.05	0.04	-0.04	-0.03	-0.01	-0.02	-0.01	-0.02	-0.01
$\lvert\lambda\rvert$											1.00	0.04	-0.19	0.13	-0.14	-0.07	-0.06	-0.02	-0.04	0.01	0.02
F_{S2}												1.00	-0.05	0.01	-0.01	-0.00	-0.00	0.01	-0.00	0.01	-0.00
$\delta_{S2} - \delta_\perp$													1.00	-0.03	0.04	0.01	0.02	0.00	0.01	0.01	0.04
F_{S3}														1.00	**-0.73**	-0.01	-0.01	-0.00	-0.01	0.00	-0.01
$\delta_{S3} - \delta_\perp$															1.00	0.02	0.02	0.01	0.02	0.00	0.01
F_{S4}																1.00	**0.53**	0.02	0.02	0.01	0.01
$\delta_{S4} - \delta_\perp$																	1.00	0.01	0.01	0.01	0.01
F_{S5}																		1.00	0.46	0.01	0.00
$\delta_{S5} - \delta_\perp$																			1.00	0.00	0.01
F_{S6}																				1.00	0.43
$\delta_{S6} - \delta_\perp$																					1.00

Table E.1 *Statistical correlation matrix for the physics parameters in the nominal maximum-likelihood fit. The correlations larger than 0.50 are highlighted in bold.*

Table E.2 *Physics parameter estimates for the tagging parameters in the nominal maximum-likelihood fit to $B_s^0 \to J/\psi K^+K^-$ signal events in the full dataset. Only statistical uncertainties are presented.*

Tagging Parameter	Fit results
p_0^{os}	0.3892 ± 0.0028
Δp_0^{os}	0.0090 ± 0.0014
p_1^{os}	0.845 ± 0.027
Δp_1^{os}	0.015 ± 0.012
p_0^{ss}	0.4406 ± 0.0072
Δp_0^{ss}	0.002 ± 0.028
p_1^{ss}	0.617 ± 0.088
Δp_1^{ss}	-0.000 ± 0.030

	p_0^{os}	Δp_0^{os}	p_1^{os}	Δp_1^{os}	p_0^{ss}	Δp_0^{ss}	p_1^{ss}	Δp_1^{ss}
p_0^{os}	1.00	0.00	0.00	0.00	0.01	0.00	-0.01	0.00
Δp_0^{os}		1.00	0.00	0.00	0.00	0.00	0.00	0.00
p_1^{os}			1.00	0.00	-0.01	0.00	0.00	0.00
Δp_1^{os}				1.00	0.00	0.00	0.00	0.00
p_0^{ss}					1.00	0.01	-0.06	0.00
Δp_0^{ss}						1.00	0.01	0.01
p_1^{ss}							1.00	0.00
Δp_1^{ss}								1.00

Table E.3 *Statistical correlation matrix for the tagging parameters from the nominal maximum-likelihood fit.*

	ϕ_0	$\phi_\parallel - \phi_0$	$\phi_\perp - \phi_0$	$\phi_S - \phi_0$	$\lvert\lambda_0\rvert$	$\lvert\lambda_\parallel/\lambda_0\rvert$	$\lvert\lambda_\perp/\lambda_0\rvert$	$\lvert\lambda_S/\lambda_0\rvert$
ϕ_0	1.00	-0.19	0.01	0.15	0.03	-0.11	0.03	-0.02
$\phi_\parallel - \phi_0$		1.00	**0.59**	0.07	-0.17	**0.61**	-0.17	0.07
$\phi_\perp - \phi_0$			1.00	0.19	-0.14	0.29	-0.45	0.05
$\phi_S - \phi_0$				1.00	-0.12	-0.02	0.10	0.22
$\lvert\lambda_0\rvert$					1.00	-0.26	**-0.7**	**-0.76**
$\lvert\lambda_\parallel/\lambda_0\rvert$						1.00	-0.15	0.12
$\lvert\lambda_\perp/\lambda_0\rvert$							1.00	**0.55**
$\lvert\lambda_S/\lambda_0\rvert$								1.00

Table E.4 *Statistical correlation matrix for the ϕ_p and $|\lambda_p|$ parameters from the polarisation-dependent fit. The correlations larger than 0.50 are highlighted in bold.*

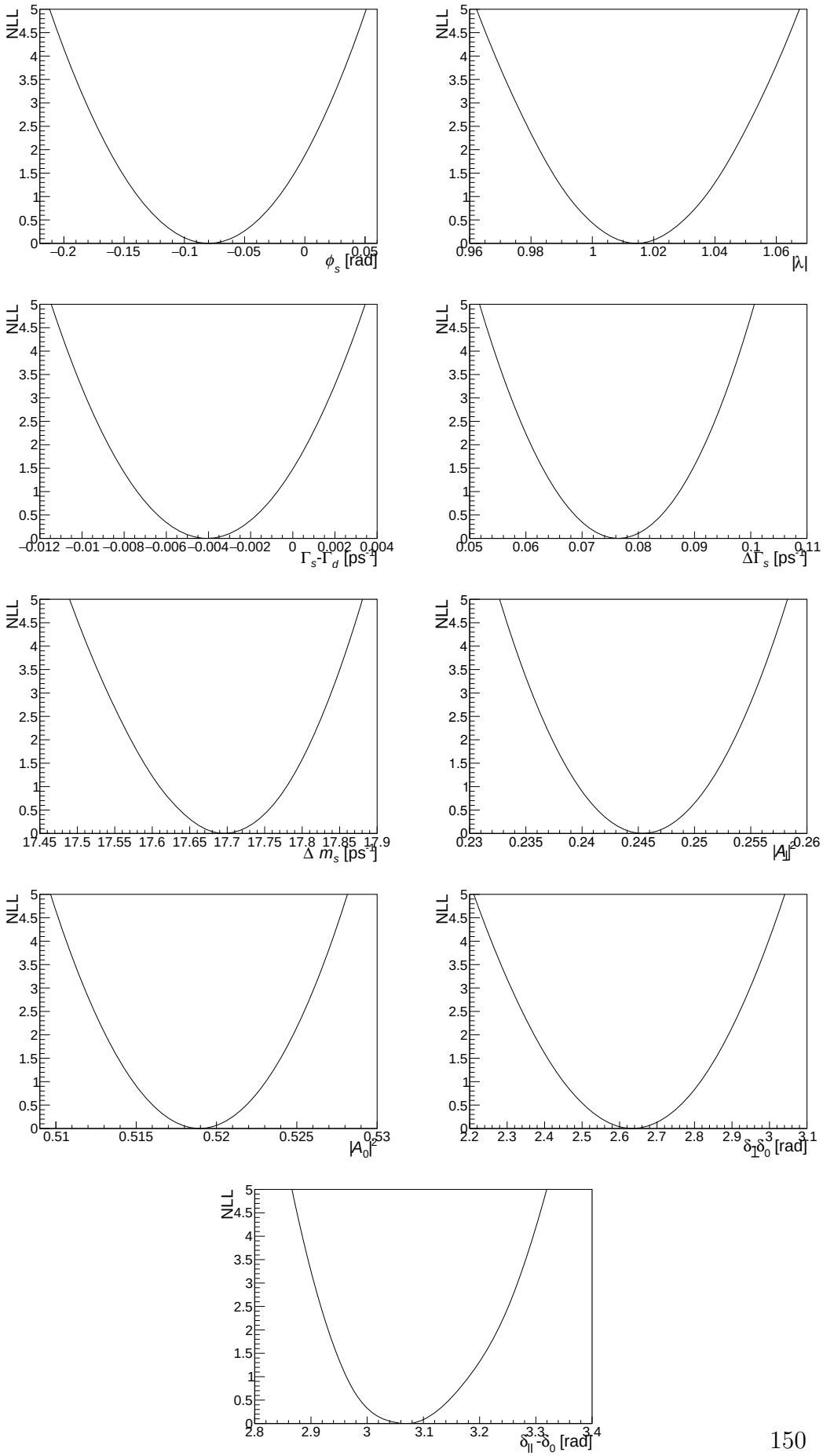

Figure E.1 *Likelihood scans for the key physics parameters that define the* $B_s^0 \to J/\psi K^+K^-$ *decay.*

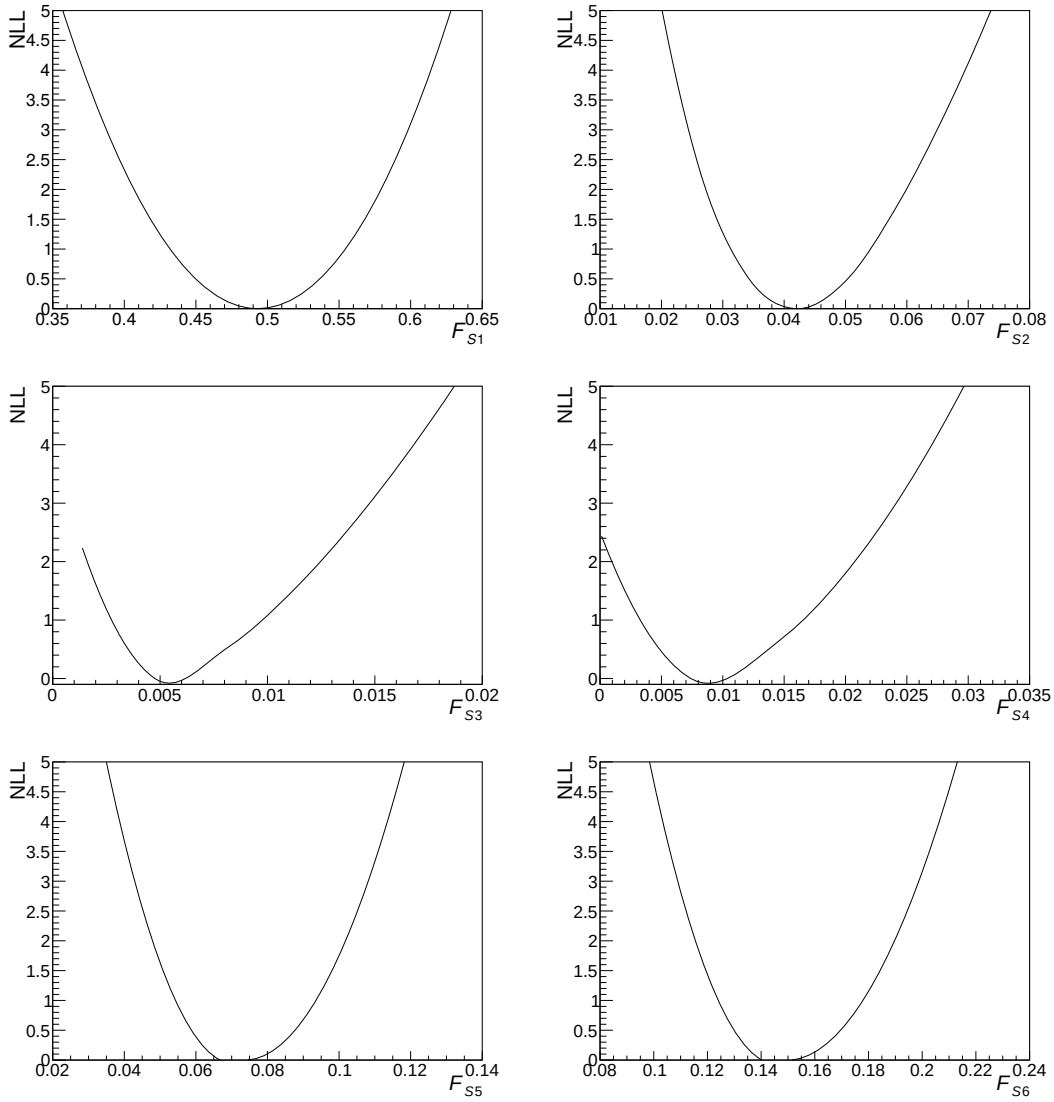

Figure E.2 *Likelihood scans for the S-wave fractions.*

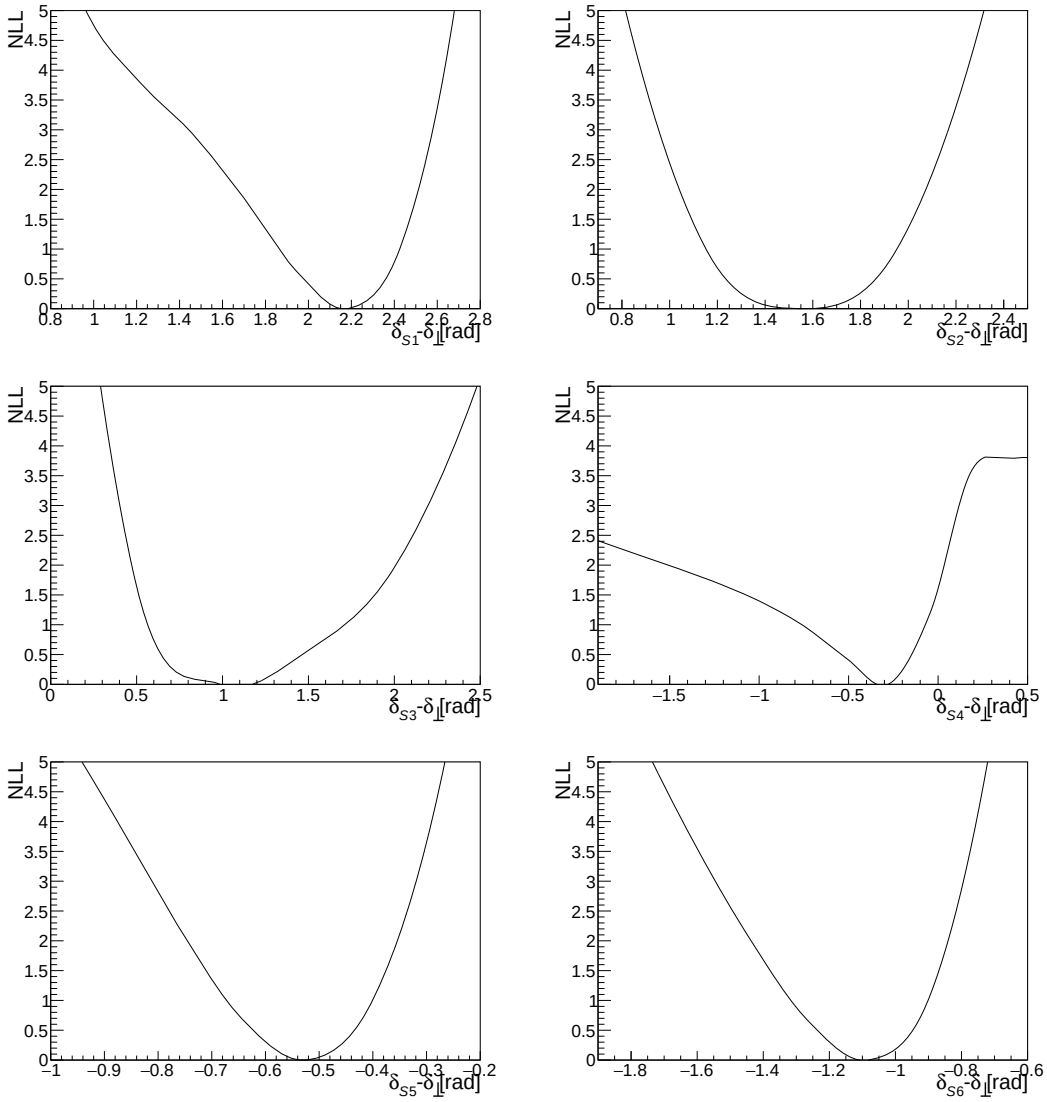

Figure E.3 *Likelihood scans for the S-wave phases.*

Appendix F

Systematic Uncertainties

Table F.1 and F.2 show the systematic uncertainties that were discussed in Chapter 7 for the S-wave fractions and phases, respectively. The statistical uncertainties determined by the `RapidFit` framework are shown as well for comparison.

Table F.1 *Summary of the systematic uncertainties for the S-wave fractions. The respective statistical uncertainty is given in the first row for comparison.*

Source	F_{S1}	F_{S2}	F_{S3}	F_{S4}	F_{S5}	F_{S6}
Statistical uncertainty	0.065	0.0080	0.0026	0.0057	0.013	0.018
Mass: σ_{CB} parametrisation	0.005	0.0006	-	0.0004	0.003	0.005
Mass: factorisation	0.006	0.0006	0.0001	0.0008	0.002	0.003
Multiple candidates	0.002	0.0012	0.0002	0.0007	0.001	0.001
Angular acceptance: sample size	0.001	0.0003	0.0001	0.0003	0.001	0.001
Angular acceptance: weighting	0.002	0.0003	0.0001	0.0006	0.001	0.001
Angular acceptance: factorisation	0.006	0.0007	0.0002	0.0001	0.001	0.002
Decay-time resolution: model applicability	-	0.0001		0.0001	-	-
Decay-time resolution: μ parametrisation	-	-	-	0.0001	-	-
Decay-time resolution: wrong PV	-	0.0001	-	0.0001	-	-
Decay-time acceptance: sample size	-	-	-	-	-	-
Decay-time acceptance: kinematic weighting	-	-	-	-	-	-
Decay-time acceptance: S-wave weighting	-	-	0.0001	-	-	-
Decay-time acceptance: $\Delta\Gamma_s = 0$ simulation	-	-	-	-	-	-
C_{SP} factors	0.001	0.0031	0.0004	0.0004	0.001	0.007
Fit bias	0.001	0.0042	0.0013	0.0007	-	0.001
Length and momentum scale	-	-	-	-	-	-
Quadratic sum of syst.	0.010	0.0055	0.0014	0.0016	0.004	0.009

Table F.2 *Summary of the systematic uncertainties for the S-wave phases. The respective statistical uncertainty is given in the first row for comparison.*

Source	$\delta_{S1} - \delta_\perp$ [rad]	$\delta_{S2} - \delta_\perp$ [rad]	$\delta_{S3} - \delta_\perp$ [rad]	$\delta_{S4} - \delta_\perp$ [rad]	$\delta_{S5} - \delta_\perp$ [rad]	$\delta_{S6} - \delta_\perp$ [rad]
Statistical uncertainty	0.19	0.31	0.39	0.18	0.094	0.14
Mass: σ_{CB} parametrisation	0.01	-	0.01	0.01	0.010	0.01
Mass: factorisation	0.08	0.03	0.02	0.01	0.008	0.03
Multiple candidates	0.01	-	0.02	0.01	0.004	0.01
Angular acceptance: sample size	-	0.01	0.01	0.01	0.004	-
Angular acceptance: weighting	0.01	0.02	0.03	0.01	0.005	-
Angular acceptance: factorisation	0.01	0.02	0.03	0.03	0.010	0.01
Decay-time resolution: model applicability	-	-	-	-	0.001	-
Decay-time resolution: μ parametrisation	-	-	-	-	0.006	-
Decay-time resolution: wrong PV	-	-	-	-	0.001	-
Decay-time acceptance: sample size	-	-	-	-	-	-
Decay-time acceptance: kinematic weighting	-	-	-	-	-	-
Decay-time acceptance: S-wave weighting	-	-	-	-	-	-
Decay-time acceptance: $\Delta\Gamma_s = 0$ simulation	-	-	-	-	-	-
C_{SP} factors	0.18	0.02	0.03	0.01	0.010	0.10
Fit bias	0.05	0.02	0.08	0.11	0.010	0.04
Length and momentum scale	-	-	-	-	-	-
Quadratic sum of syst.	0.20	0.05	0.10	0.12	0.024	0.11

Appendix G

Combination JSON files

The JSON that is used in the combination of the Run 1 [56] with the 2015-2016 [1] published result of $B_s^0 \to J/\psi K^+K^-$ is shown below.


```
{
        "ResultSet": [

{
      "ResultSetLabel": "2012-JPsiKK",
      "Description" : [
         "Contains the final 2012 3fb results for phis et. al. from JPsiKK",
         "The parameter values, stat and syst errors, and statistical correlation matrix
              taken",
         "from the paper LHCb-PAPER-2014-059",
         "The systematic error correlation matrices are from private communication"
      ],
      "Parameter": [
        {
          "Name": "gamma",
          "Value": 0.6603,
          "Error": 0.0027
        },
        {
          "Name": "deltaGammas",
          "Value": 0.0805,
          "Error": 0.0091
        },
        {
          "Name": "AperpSq",
          "Value": 0.2504,
          "Error": 0.0049
        },
        {
          "Name": "AzeroSq",
          "Value": 0.5241,
          "Error": 0.0034
        },
        {
          "Name": "para",
          "Value": 3.258,
          "Error": 0.17
        },
        {
          "Name": "perp",
          "Value": 3.08,
          "Error": 0.15
        },
        {
          "Name": "phis",
```

```
      "Value": -0.058,
      "Error": 0.049
    },
    {
      "Name": "lamb",
      "Value": 0.964,
      "Error": 0.019
    },
    {
      "Name": "dms",
      "Value": 17.711,
      "Error": 0.057
    }
  ],
  "StatisticalCorrelationMatrix": [
    [ 1.00  , -0.45 ,  0.39 , -0.31 , -0.07 , -0.02 ,  0.01 , -0.01,  0.01 ],
    [-0.45  ,  1.00 , -0.69 ,  0.65 ,  0.02 , -0.03 , -0.08 ,  0.02, -0.03 ],
    [ 0.39  , -0.69 ,  1.00 , -0.59 , -0.29 , -0.1  ,  0.04 , -0.03,  0.0  ],
    [-0.31  ,  0.65 , -0.59 ,  1.00 , -0.02 , -0.04 , -0.03 ,  0.02, -0.03 ],
    [-0.07  ,  0.02 , -0.29 , -0.02 ,  1.00 ,  0.42 ,  0.01 ,  0.05,  0.05 ],
    [-0.02  , -0.03 , -0.1  , -0.04 ,  0.42 ,  1.00 ,  0.14 , -0.17,  0.67 ],
    [ 0.01  , -0.08 ,  0.04 , -0.03 ,  0.01 ,  0.14 ,  1.00 , -0.02,  0.09 ],
    [-0.01  ,  0.02 , -0.03 ,  0.02 ,  0.05 , -0.17 , -0.02 ,  1.00, -0.21 ],
    [ 0.01  , -0.03 ,  0.0  , -0.03 ,  0.05 ,  0.67 ,  0.09 , -0.21,  1.00 ]
  ],
  "SystematicErrors": [
    {
      "Name": "MassFactorisation",
      "Values": [0.0, 0.0007, 0.0031, 0.0064, 0.05, 0.05, 0.002, 0.001, 0.004],
      "SystematicCorrelationMatrix": [
        [1.0, 1.0, -1.0, 1.0, -1.0, -1.0, -1.0, 1.0, -1.0],
        [1.0, 1.0, -1.0, 1.0, -1.0, -1.0, -1.0, 1.0, -1.0],
        [-1.0, -1.0, 1.0, -1.0, 1.0, 1.0, 1.0, -1.0, 1.0],
        [1.0, 1.0, -1.0, 1.0, -1.0, -1.0, -1.0, 1.0, -1.0],
        [-1.0, -1.0, 1.0, -1.0, 1.0, 1.0, 1.0, -1.0, 1.0],
        [-1.0, -1.0, 1.0, -1.0, 1.0, 1.0, 1.0, -1.0, 1.0],
        [-1.0, -1.0, 1.0, -1.0, 1.0, 1.0, 1.0, -1.0, 1.0],
        [1.0, 1.0, -1.0, 1.0, -1.0, -1.0, -1.0, 1.0, -1.0],
        [-1.0, -1.0, 1.0, -1.0, 1.0, 1.0, 1.0, -1.0, 1.0]
      ]
    },
    {
      "Name": "SignalWeights",
      "Values": [0.0001, 0.0008, 0.0, 0.0001, 0.002, 0.001, 0.0, 0.0, 0.0]
    },
    {
      "Name": "ResonantBackground",
      "Values": [0.0001, 0.0004, 0.0004, 0.0002, 0.02, 0.02, 0.002, 0.003, 0.001]
    },
    {
      "Name": "AngEfficiencyReweighting",
      "Values": [0.0001, 0.0, 0.0011, 0.002, 0.01, 0.0, 0.001, 0.005, 0.002],
      "SystematicCorrelationMatrix": [
        [  1.0,  0.81, 0.98, -0.97,  0.84, 0.82,  0.17,  0.38, 0.79],
        [ 0.81,   1.0, 0.90, -0.91,  0.74, 0.50, -0.24,-0.025, 0.62],
        [ 0.98,  0.90,  1.0,  -1.0,  0.84, 0.74,  0.04,  0.25, 0.75],
        [-0.97, -0.91, -1.0,   1.0, -0.83,-0.74,-0.038, -0.23,-0.77],
        [ 0.84,  0.74, 0.84, -0.83,   1.0, 0.68,-0.042,  0.33, 0.47],
        [ 0.82,  0.50, 0.74, -0.74,  0.68,  1.0,  0.65,  0.69, 0.86],
        [ 0.17, -0.24, 0.04,-0.038,-0.042, 0.65,   1.0,  0.78, 0.51],
        [ 0.38,-0.025, 0.25, -0.23,  0.33, 0.69,  0.78,   1.0, 0.35],
        [ 0.79,  0.62, 0.75, -0.77,  0.47, 0.86,  0.51,  0.35,  1.0]
      ]
    },
    {
      "Name": "AngEfficiencyStat",
      "Values": [0.0001, 0.0002, 0.0011, 0.0004, 0.02, 0.01, 0.004, 0.002, 0.001 ],
      "SystematicCorrelationMatrix": [
        [    1.0, 0.0,   0.89,  -0.22, -0.0071, -0.028,  0.027, -0.033,   0.14],
        [    0.0, 1.0,    0.0,    0.0,    0.0,    0.0,    0.0,    0.0,    0.0],
        [   0.89, 0.0,    1.0,  -0.36,  -0.027,  -0.12, -0.058,  0.025, -0.065],
        [  -0.22, 0.0,  -0.36,    1.0,   0.14,  0.054, 0.0054, -0.040, -0.097],
        [-0.0071, 0.0, -0.027,   0.14,    1.0,   0.60,  0.029, -0.013,  -0.19],
        [ -0.028, 0.0,  -0.12,  0.054,   0.60,    1.0,   0.72,  -0.48,   0.51],
        [  0.027, 0.0, -0.058, 0.0054,  0.029,   0.72,    1.0,  -0.58,   0.82],
        [ -0.033, 0.0,  0.025, -0.040, -0.013,  -0.48,  -0.58,    1.0,  -0.76],
        [   0.14, 0.0, -0.065, -0.097,  -0.19,   0.51,   0.82,  -0.76,    1.0]
```

```
        ]
      },
      {
        "Name": "DecayTimeResolutionPrompt",
        "Values": [0.0, 0.0, 0.0, 0.0, 0.0, 0.01, 0.002, 0.001, 0.005]
      },
      {
        "Name": "TriggerEfficiencyStat",
        "Values": [0.0011, 0.0009, 0.0, 0.0, 0.0, 0.0, 0.0, 0.0, 0.0]
      },
      {
        "Name": "TrackReconstructionSimul",
        "Values": [0.0007, 0.0029, 0.0005, 0.0006, 0.01, 0.001, 0.001, 0.001, 0.006],
        "SystematicCorrelationMatrix": [
          [1.0, 1.0, -1.0, 1.0, -1.0, -1.0, -1.0, 1.0, 1.0],
          [1.0, 1.0, -1.0, 1.0, -1.0, -1.0, -1.0, 1.0, 1.0],
          [-1.0, -1.0, 1.0, -1.0, 1.0, 1.0, 1.0, -1.0, -1.0],
          [1.0, 1.0, -1.0, 1.0, -1.0, -1.0, -1.0, 1.0, 1.0],
          [-1.0, -1.0, 1.0, -1.0, 1.0, 1.0, 1.0, -1.0, -1.0],
          [-1.0, -1.0, 1.0, -1.0, 1.0, 1.0, 1.0, -1.0, -1.0],
          [-1.0, -1.0, 1.0, -1.0, 1.0, 1.0, 1.0, -1.0, -1.0],
          [1.0, 1.0, -1.0, 1.0, -1.0, -1.0, -1.0, 1.0, 1.0],
          [1.0, 1.0, -1.0, 1.0, -1.0, -1.0, -1.0, 1.0, 1.0]
        ]
      },
      {
        "Name": "TrackReconstructionStat",
        "Values": [ 0.0005, 0.0002, 0.0, 0.0, 0.0, 0.0, 0.0, 0.0, 0.001 ]
      },
      {
        "Name": "LengthMomentumScales",
        "Values": [ 0.0002, 0.0, 0.0, 0.0, 0.0, 0.0, 0.0, 0.0, 0.005 ]
      },
      {
        "Name": "SPCouplingFactors",
        "Values": [ 0.0, 0.0, 0.0, 0.0, 0.01, 0.01, 0.0, 0.001, 0.002 ]
      },
      {
        "Name": "AngularResolution",
        "Values": [ 0.0, 0.0, 0.0006, 0.0001, 0.03, 0.01, 0.0, 0.0, 0.0 ]
      },
      {
        "Name": "BcBackground",
        "Values": [0.0005, 0.0, 0.0, 0.0, 0.0, 0.0, 0.0, 0.0, 0.0]
      },
      {
        "Name": "FitBias",
        "Values": [ 0.0, 0.0, 0.0005, 0.0, 0.0, 0.01, 0.0, 0.001, 0.0 ]
      }
    ]
}
,
{
    "ResultSetLabel": "2016-JPsiKK",
    "Description" : [
        "Contains the 2015-2016 2fb results for phis et. al. from polarisation independent nominal fit"
    ],
    "Parameter": [
      {
        "Name": "gsgd",
        "Value": -0.0041,
        "Error": 0.0024
      },
      {
        "Name": "deltaGammas",
        "Value": 0.0773,
        "Error": 0.0077
      },
      {
        "Name": "AperpSq",
        "Value": 0.2456,
        "Error": 0.0040
      },
      {
        "Name": "AzeroSq",
        "Value": 0.5186,
```

```
  "Error": 0.0029
},
{
  "Name": "para",
  "Value": 3.062,
  "Error": 0.082
},
{
  "Name": "perp",
  "Value": 2.64,
  "Error": 0.13
},
{
  "Name": "phis",
  "Value": -0.083,
  "Error": 0.041
},
{
  "Name": "lamb",
  "Value": 1.012,
  "Error": 0.016
},
{
  "Name": "dms",
  "Value": 17.703,
  "Error": 0.059
},
{
  "Name": "FS1",
  "Value": 0.492,
  "Error": 0.043
},
{
  "Name": "FS2",
  "Value": 0.041,
  "Error": 0.008
},
{
  "Name": "FS3",
  "Value": 0.0044,
  "Error": 0.0030
},
{
  "Name": "FS4",
  "Value": 0.0069,
  "Error": 0.0062
},
{
  "Name": "FS5",
  "Value": 0.073,
  "Error": 0.013
},
{
  "Name": "FS6",
  "Value": 0.152,
  "Error": 0.019
},
{
  "Name": "deltaS1",
  "Value": 2.21,
  "Error": 0.20
},
{
  "Name": "deltaS2",
  "Value": 1.56,
  "Error": 0.29
},
{
  "Name": "deltaS3",
  "Value": 1.09,
  "Error": 0.47
},
{
  "Name": "deltaS4",
  "Value": -0.28,
  "Error": 0.26
},
```

```
    {
      "Name": "deltaS5",
      "Value": -0.54,
      "Error": 0.10
    },
    {
      "Name": "deltaS6",
      "Value": -1.10,
      "Error": 0.16
    }
  ],
  "StatisticalCorrelationMatrix":
  [
  [1.0, -0.47, 0.39, -0.32, 0.03, -0.0, -0.03, 0.02, -0.01, 0.05, 0.04, 0.03, 0.03, 0.07,
       0.06, 0.01, -0.0, -0.02, 0.01, 0.02, 0.01],
  [-0.47, 1.0, -0.69, 0.63, -0.01, 0.01, -0.01, -0.04, 0.02, -0.07, -0.05, -0.02, 0.03,
       -0.06, -0.06, -0.0, 0.01, 0.01, 0.01, 0.0, 0.0],
  [0.39, -0.69, 1.0, -0.6, 0.12, 0.0, -0.02, 0.02, -0.03, 0.04, -0.02, -0.02, -0.05,
       0.01, 0.03, 0.02, -0.01, 0.01, -0.02, 0.0, 0.02],
  [-0.32, 0.63, -0.6, 1.0, 0.0, 0.01, 0.02, -0.02, 0.01, -0.05, -0.01, 0.01, 0.05, -0.01,
       -0.03, -0.0, 0.01, -0.01, 0.02, 0.01, 0.01],
  [0.03, -0.01, 0.12, 0.0, 1.0, 0.2, 0.01, -0.0, -0.04, 0.01, -0.01, 0.04, 0.02, 0.03,
       0.0, -0.02, -0.03, -0.04, 0.0, -0.01, -0.03],
  [-0.0, 0.01, 0.0, 0.01, 0.2, 1.0, 0.0, 0.07, 0.74, -0.01, -0.01, 0.01, 0.04, 0.03,
       -0.07, -0.06, -0.18, -0.01, -0.01, -0.0, -0.16],
  [-0.03, -0.01, -0.02, 0.02, 0.01, 0.0, 1.0, 0.19, 0.01, -0.0, 0.01, 0.04, -0.03, -0.01,
       -0.02, 0.0, -0.05, -0.04, -0.01, -0.0, -0.01],
  [0.02, -0.04, 0.02, -0.02, -0.0, 0.07, 0.19, 1.0, -0.0, 0.01, 0.02, 0.13, -0.09, -0.01,
       0.02, 0.05, -0.17, -0.14, -0.07, -0.03, 0.02],
  [-0.01, 0.02, -0.03, 0.01, -0.04, 0.74, 0.01, -0.0, 1.0, -0.01, -0.01, -0.07, 0.1,
       0.06, -0.03, -0.02, -0.08, 0.1, 0.05, 0.07, -0.05],
  [0.05, -0.07, 0.04, -0.05, 0.01, -0.01, -0.0, 0.01, -0.01, 1.0, 0.0, 0.0, -0.0, 0.0,
       0.01, 0.08, -0.0, -0.0, -0.0, -0.0, 0.0],
  [0.04, -0.05, -0.02, -0.01, -0.01, -0.01, 0.01, 0.02, -0.01, 0.0, 1.0, 0.01, 0.0, 0.01,
       0.01, -0.0, 0.08, -0.0, -0.0, -0.0, 0.0],
  [0.03, -0.02, -0.02, 0.01, 0.04, 0.01, 0.04, 0.13, -0.07, 0.0, 0.01, 1.0, -0.02, -0.0,
       0.0, 0.0, -0.03, -0.73, -0.02, -0.01, -0.01],
  [0.03, 0.03, -0.05, 0.05, 0.02, 0.04, -0.03, -0.09, 0.1, -0.0, 0.0, -0.02, 1.0, 0.02,
       0.0, -0.0, 0.01, 0.03, 0.46, 0.01, 0.0],
  [0.07, -0.06, 0.01, -0.01, 0.03, 0.03, -0.01, -0.01, 0.06, 0.0, 0.01, -0.0, 0.02, 1.0,
       0.01, -0.0, 0.0, 0.01, 0.01, 0.45, 0.0],
  [0.06, -0.06, 0.03, -0.03, 0.0, -0.07, -0.02, 0.02, -0.03, 0.01, 0.01, 0.0, 0.0, 0.01,
       1.0, 0.01, 0.01, 0.0, 0.01, 0.0, 0.43],
  [0.01, -0.0, 0.02, -0.0, -0.02, -0.06, 0.0, 0.05, -0.02, 0.08, -0.0, 0.0, -0.0, -0.0,
       0.01, 1.0, 0.01, 0.0, 0.0, 0.0, 0.02],
  [-0.0, 0.01, -0.01, 0.01, -0.03, -0.18, -0.05, -0.17, -0.08, -0.0, 0.08, -0.03, 0.01,
       0.0, 0.01, 0.01, 1.0, 0.03, 0.02, 0.01, 0.03],
  [-0.02, 0.01, 0.01, -0.01, -0.04, -0.01, -0.04, -0.14, 0.1, -0.0, -0.0, -0.73, 0.03,
       0.01, 0.0, 0.0, 0.03, 1.0, 0.02, 0.02, 0.02],
  [0.01, 0.01, -0.02, 0.02, 0.0, -0.01, -0.01, -0.07, 0.05, -0.0, -0.0, -0.02, 0.46,
       0.01, 0.01, 0.0, 0.02, 0.02, 1.0, 0.01, 0.01],
  [0.02, 0.0, 0.0, 0.01, -0.01, -0.0, -0.0, -0.03, 0.07, -0.0, -0.0, -0.01, 0.01, 0.45,
       0.0, 0.0, 0.01, 0.02, 0.01, 1.0, 0.01],
  [0.01, 0.0, 0.02, 0.01, -0.03, -0.16, -0.01, 0.02, -0.05, 0.0, 0.0, -0.01, 0.0, 0.0,
       0.43, 0.02, 0.03, 0.02, 0.01, 0.01, 1.0]]
,
  "SystematicErrors": [
    {
      "Name": "MassFactorisation",
      "Values": [0.0007, 0.0022, 0.0005, 0.0002, 0.0093, 0.0465, 0.004, 0.0037, 0.0156,
           0.0056, 0.0006, 0.0, 0.0004, 0.0018, 0.0025, 0.0803, 0.025, 0.0186, 0.009,
           0.0075, 0.0333],
      "SystematicCorrelationMatrix": [
      [1.0, -1.0, 1.0, 1.0, 1.0, 1.0, -1.0, 1.0, 1.0, -1.0, 1.0, 0.0, 1.0, 1.0, 1.0,
           -1.0, -1.0, -1.0, -1.0, -1.0, -1.0],
      [-1.0, 1.0, -1.0, -1.0, -1.0, -1.0, 1.0, -1.0, -1.0, 1.0, -1.0, 0.0, -1.0, -1.0,
           -1.0, 1.0, 1.0, 1.0, 1.0, 1.0, 1.0],
      [1.0, -1.0, 1.0, 1.0, 1.0, 1.0, -1.0, 1.0, 1.0, -1.0, 1.0, 0.0, 1.0, 1.0, 1.0,
           -1.0, -1.0, -1.0, -1.0, -1.0, -1.0],
      [1.0, -1.0, 1.0, 1.0, 1.0, 1.0, -1.0, 1.0, 1.0, -1.0, 1.0, 0.0, 1.0, 1.0, 1.0,
           -1.0, -1.0, -1.0, -1.0, -1.0, -1.0],
      [1.0, -1.0, 1.0, 1.0, 1.0, 1.0, -1.0, 1.0, 1.0, -1.0, 1.0, 0.0, 1.0, 1.0, 1.0,
           -1.0, -1.0, -1.0, -1.0, -1.0, -1.0],
      [1.0, -1.0, 1.0, 1.0, 1.0, 1.0, -1.0, 1.0, 1.0, -1.0, 1.0, 0.0, 1.0, 1.0, 1.0,
           -1.0, -1.0, -1.0, -1.0, -1.0, -1.0],
      [-1.0, 1.0, -1.0, -1.0, -1.0, -1.0, 1.0, -1.0, -1.0, 1.0, -1.0, 0.0, -1.0, -1.0,
           -1.0, 1.0, 1.0, 1.0, 1.0, 1.0, 1.0],
```

```
    [1.0, -1.0, 1.0, 1.0, 1.0, 1.0, -1.0, 1.0, 1.0, -1.0, 1.0, 0.0, 1.0, 1.0, 1.0,
        -1.0, -1.0, -1.0, -1.0, -1.0, -1.0],
    [1.0, -1.0, 1.0, 1.0, 1.0, 1.0, -1.0, 1.0, 1.0, -1.0, 1.0, 0.0, 1.0, 1.0, 1.0,
        -1.0, -1.0, -1.0, -1.0, -1.0, -1.0],
    [-1.0, 1.0, -1.0, -1.0, -1.0, -1.0, 1.0, -1.0, -1.0, 1.0, -1.0, 0.0, -1.0, -1.0,
        -1.0, 1.0, 1.0, 1.0, 1.0, 1.0, 1.0],
    [1.0, -1.0, 1.0, 1.0, 1.0, 1.0, -1.0, 1.0, 1.0, -1.0, 1.0, 0.0, 1.0, 1.0, 1.0,
        -1.0, -1.0, -1.0, -1.0, -1.0, -1.0],
    [0.0, 0.0, 0.0, 0.0, 0.0, 0.0, 0.0, 0.0, 0.0, 0.0, 0.0, 1.0, 0.0, 0.0, 0.0, 0.0,
        0.0, 0.0, 0.0, 0.0, 0.0],
    [1.0, -1.0, 1.0, 1.0, 1.0, 1.0, -1.0, 1.0, 1.0, -1.0, 1.0, 0.0, 1.0, 1.0, 1.0,
        -1.0, -1.0, -1.0, -1.0, -1.0, -1.0],
    [1.0, -1.0, 1.0, 1.0, 1.0, 1.0, -1.0, 1.0, 1.0, -1.0, 1.0, 0.0, 1.0, 1.0, 1.0,
        -1.0, -1.0, -1.0, -1.0, -1.0, -1.0],
    [1.0, -1.0, 1.0, 1.0, 1.0, 1.0, -1.0, 1.0, 1.0, -1.0, 1.0, 0.0, 1.0, 1.0, 1.0,
        -1.0, -1.0, -1.0, -1.0, -1.0, -1.0],
    [-1.0, 1.0, -1.0, -1.0, -1.0, -1.0, 1.0, -1.0, -1.0, 1.0, -1.0, 0.0, -1.0, -1.0,
        -1.0, 1.0, 1.0, 1.0, 1.0, 1.0, 1.0],
    [-1.0, 1.0, -1.0, -1.0, -1.0, -1.0, 1.0, -1.0, -1.0, 1.0, -1.0, 0.0, -1.0, -1.0,
        -1.0, 1.0, 1.0, 1.0, 1.0, 1.0, 1.0],
    [-1.0, 1.0, -1.0, -1.0, -1.0, -1.0, 1.0, -1.0, -1.0, 1.0, -1.0, 0.0, -1.0, -1.0,
        -1.0, 1.0, 1.0, 1.0, 1.0, 1.0, 1.0],
    [-1.0, 1.0, -1.0, -1.0, -1.0, -1.0, 1.0, -1.0, -1.0, 1.0, -1.0, 0.0, -1.0, -1.0,
        -1.0, 1.0, 1.0, 1.0, 1.0, 1.0, 1.0],
    [-1.0, 1.0, -1.0, -1.0, -1.0, -1.0, 1.0, -1.0, -1.0, 1.0, -1.0, 0.0, -1.0, -1.0,
        -1.0, 1.0, 1.0, 1.0, 1.0, 1.0, 1.0],
    [-1.0, 1.0, -1.0, -1.0, -1.0, -1.0, 1.0, -1.0, -1.0, 1.0, -1.0, 0.0, -1.0, -1.0,
        -1.0, 1.0, 1.0, 1.0, 1.0, 1.0, 1.0]
    ]
},
{
    "Name": "MassShape",
    "Values": [0.0, 0.0002, 0.0004, 0.0006, 0.0033, 0.0, 0.0, 0.0, 0.0012, 0.0049,
        0.0006, 0.0001, 0.0008, 0.0031, 0.005, 0.0054, 0.0014, 0.0141, 0.014, 0.0097,
        0.0117],

    "SystematicCorrelationMatrix": [
    [1.0, 0.0, 0.0, 0.0, 0.0, 0.0, 0.0, 0.0, 0.0, 0.0, 0.0, 0.0, 0.0, 0.0, 0.0, 0.0,
        0.0, 0.0, 0.0, 0.0, 0.0],
    [0.0, 1.0, -1.0, 1.0, 1.0, 1.0, 0.0, 0.0, 1.0, 1.0, 1.0, 1.0, 1.0, 1.0, 1.0, -1.0,
        1.0, -1.0, 1.0, 1.0, 1.0],
    [0.0, -1.0, 1.0, -1.0, -1.0, -1.0, 0.0, 0.0, -1.0, -1.0, -1.0, -1.0, -1.0, -1.0,
        -1.0, 1.0, -1.0, 1.0, -1.0, -1.0, -1.0],
    [0.0, 1.0, -1.0, 1.0, 1.0, 1.0, 0.0, 0.0, 1.0, 1.0, 1.0, 1.0, 1.0, 1.0, 1.0, -1.0,
        1.0, -1.0, 1.0, 1.0, 1.0],
    [0.0, 1.0, -1.0, 1.0, 1.0, 1.0, 0.0, 0.0, 1.0, 1.0, 1.0, 1.0, 1.0, 1.0, 1.0, -1.0,
        1.0, -1.0, 1.0, 1.0, 1.0],
    [0.0, 1.0, -1.0, 1.0, 1.0, 1.0, 0.0, 0.0, 1.0, 1.0, 1.0, 1.0, 1.0, 1.0, 1.0, -1.0,
        1.0, -1.0, 1.0, 1.0, 1.0],
    [0.0, 0.0, 0.0, 0.0, 0.0, 0.0, 1.0, 0.0, 0.0, 0.0, 0.0, 0.0, 0.0, 0.0, 0.0, 0.0,
        0.0, 0.0, 0.0, 0.0, 0.0],
    [0.0, 0.0, 0.0, 0.0, 0.0, 0.0, 0.0, 1.0, 0.0, 0.0, 0.0, 0.0, 0.0, 0.0, 0.0, 0.0,
        0.0, 0.0, 0.0, 0.0, 0.0],
    [0.0, 1.0, -1.0, 1.0, 1.0, 1.0, 0.0, 0.0, 1.0, 1.0, 1.0, 1.0, 1.0, 1.0, 1.0, -1.0,
        1.0, -1.0, 1.0, 1.0, 1.0],
    [0.0, 1.0, -1.0, 1.0, 1.0, 1.0, 0.0, 0.0, 1.0, 1.0, 1.0, 1.0, 1.0, 1.0, 1.0, -1.0,
        1.0, -1.0, 1.0, 1.0, 1.0],
    [0.0, 1.0, -1.0, 1.0, 1.0, 1.0, 0.0, 0.0, 1.0, 1.0, 1.0, 1.0, 1.0, 1.0, 1.0, -1.0,
        1.0, -1.0, 1.0, 1.0, 1.0],
    [0.0, 1.0, -1.0, 1.0, 1.0, 1.0, 0.0, 0.0, 1.0, 1.0, 1.0, 1.0, 1.0, 1.0, 1.0, -1.0,
        1.0, -1.0, 1.0, 1.0, 1.0],
    [0.0, 1.0, -1.0, 1.0, 1.0, 1.0, 0.0, 0.0, 1.0, 1.0, 1.0, 1.0, 1.0, 1.0, 1.0, -1.0,
        1.0, -1.0, 1.0, 1.0, 1.0],
    [0.0, 1.0, -1.0, 1.0, 1.0, 1.0, 0.0, 0.0, 1.0, 1.0, 1.0, 1.0, 1.0, 1.0, 1.0, -1.0,
        1.0, -1.0, 1.0, 1.0, 1.0],
    [0.0, 1.0, -1.0, 1.0, 1.0, 1.0, 0.0, 0.0, 1.0, 1.0, 1.0, 1.0, 1.0, 1.0, 1.0, -1.0,
        1.0, -1.0, 1.0, 1.0, 1.0],
    [0.0, -1.0, 1.0, -1.0, -1.0, -1.0, 0.0, 0.0, -1.0, -1.0, -1.0, -1.0, -1.0, -1.0,
        -1.0, 1.0, -1.0, 1.0, -1.0, -1.0, -1.0],
    [0.0, 1.0, -1.0, 1.0, 1.0, 1.0, 0.0, 0.0, 1.0, 1.0, 1.0, 1.0, 1.0, 1.0, 1.0, -1.0,
        1.0, -1.0, 1.0, 1.0, 1.0],
    [0.0, -1.0, 1.0, -1.0, -1.0, -1.0, 0.0, 0.0, -1.0, -1.0, -1.0, -1.0, -1.0, -1.0,
        -1.0, 1.0, -1.0, 1.0, -1.0, -1.0, -1.0],
    [0.0, 1.0, -1.0, 1.0, 1.0, 1.0, 0.0, 0.0, 1.0, 1.0, 1.0, 1.0, 1.0, 1.0, 1.0, -1.0,
        1.0, -1.0, 1.0, 1.0, 1.0],
    [0.0, 1.0, -1.0, 1.0, 1.0, 1.0, 0.0, 0.0, 1.0, 1.0, 1.0, 1.0, 1.0, 1.0, 1.0, -1.0,
        1.0, -1.0, 1.0, 1.0, 1.0],
```

```
    [0.0, 1.0, -1.0, 1.0, 1.0, 1.0, 0.0, 0.0, 1.0, 1.0, 1.0, 1.0, 1.0, 1.0, 1.0, -1.0,
        1.0, -1.0, 1.0, 1.0, 1.0]
  ]
 },
 {
   "Name": "SPCouplingFactors",
   "Values": [ 0.0, 0.0001, 0.0001, 0.0, 0.005, 0.013, 0.001, 0.001, 0.002, 0.001,
       0.0031, 0.0004, 0.0004, 0.001, 0.007, 0.18, 0.02, 0.03, 0.01, 0.01, 0.10],
   "SystematicCorrelationMatrix": [
     [1.0, 0.0, 0.0, 0.0, 0.0, 0.0, 0.0, 0.0, 0.0, 0.0, 0.0, 0.0, 0.0, 0.0, 0.0, 0.0,
         0.0, 0.0, 0.0, 0.0, 0.0],
     [0.0, 1.0, -1.0, 0.0, 0, 0, 0, 0, -1.0, 0, 1.0, 1.0, 1.0, 1.0, 0, 0, 1.0, 1.0,
         -1.0, -1.0, 0],
     [0.0, -1.0, 1.0, 0.0, 0, 0, 0, 0, 1.0, 0, -1.0, -1.0, -1.0, -1.0, 0, 0, -1.0,
         -1.0, 1.0, 1.0, 0],
     [0.0, 0.0, 0.0, 1.0, 0.0, 0.0, 0.0, 0.0, 0.0, 0.0, 0.0, 0.0, 0.0, 0.0, 0.0, 0.0,
         0.0, 0.0, 0.0, 0.0, 0.0],
     [0.0, 0, 0, 0.0, 1.0, 1.0, -1.0, -1.0, 0, 1.0, 0, 0, 0, 0, 1.0, -1.0, 0, 0, 0, 0,
         -1.0],
     [0.0, 0, 0, 0.0, 1.0, 1.0, -1.0, -1.0, 0, 1.0, 0, 0, 0, 0, 1.0, -1.0, 0, 0, 0, 0,
         -1.0],
     [0.0, 0, 0, 0.0, -1.0, -1.0, 1.0, 1.0, 0, -1.0, 0, 0, 0, 0, -1.0, 1.0, 0, 0, 0,
         0, 1.0],
     [0.0, 0, 0, 0.0, -1.0, -1.0, 1.0, 1.0, 0, -1.0, 0, 0, 0, 0, -1.0, 1.0, 0, 0, 0,
         0, 1.0],
     [0.0, -1.0, 1.0, 0.0, 0, 0, 0, 0, 1.0, 0, -1.0, -1.0, -1.0, -1.0, 0, 0, -1.0,
         -1.0, 1.0, 1.0, 0],
     [0.0, 0, 0, 0.0, 1.0, 1.0, -1.0, -1.0, 0, 1.0, 0, 0, 0, 0, 1.0, -1.0, 0, 0, 0, 0,
         -1.0],
     [0.0, 1.0, -1.0, 0.0, 0, 0, 0, 0, -1.0, 0, 1.0, 1.0, 1.0, 1.0, 0, 0, 1.0, 1.0,
         -1.0, -1.0, 0],
     [0.0, 1.0, -1.0, 0.0, 0, 0, 0, 0, -1.0, 0, 1.0, 1.0, 1.0, 1.0, 0, 0, 1.0, 1.0,
         -1.0, -1.0, 0],
     [0.0, 1.0, -1.0, 0.0, 0, 0, 0, 0, -1.0, 0, 1.0, 1.0, 1.0, 1.0, 0, 0, 1.0, 1.0,
         -1.0, -1.0, 0],
     [0.0, 1.0, -1.0, 0.0, 0, 0, 0, 0, -1.0, 0, 1.0, 1.0, 1.0, 1.0, 0, 0, 1.0, 1.0,
         -1.0, -1.0, 0],
     [0.0, 0, 0, 0.0, 1.0, 1.0, -1.0, -1.0, 0, 1.0, 0, 0, 0, 0, 1.0, -1.0, 0, 0, 0, 0,
         -1.0],
     [0.0, 0, 0, 0.0, -1.0, -1.0, 1.0, 1.0, 0, -1.0, 0, 0, 0, 0, -1.0, 1.0, 0, 0, 0,
         0, 1.0],
     [0.0, 1.0, -1.0, 0.0, 0, 0, 0, 0, -1.0, 0, 1.0, 1.0, 1.0, 1.0, 0, 0, 1.0, 1.0,
         -1.0, -1.0, 0],
     [0.0, 1.0, -1.0, 0.0, 0, 0, 0, 0, -1.0, 0, 1.0, 1.0, 1.0, 1.0, 0, 0, 1.0, 1.0,
         -1.0, -1.0, 0],
     [0.0, -1.0, 1.0, 0.0, 0, 0, 0, 0, 1.0, 0, -1.0, -1.0, -1.0, -1.0, 0, 0, -1.0,
         -1.0, 1.0, 1.0, 0],
     [0.0, -1.0, 1.0, 0.0, 0, 0, 0, 0, 1.0, 0, -1.0, -1.0, -1.0, -1.0, 0, 0, -1.0,
         -1.0, 1.0, 1.0, 0],
     [0.0, 0, 0, 0.0, -1.0, -1.0, 1.0, 1.0, 0, -1.0, 0, 0, 0, 0, -1.0, 1.0, 0, 0, 0,
         0, 1.0]
   ]
 },
 {
   "Name": "DecayTimeResolutionPrompt",
   "Values": [0.0, 0.0, 0.0, 0.0, 0.001, 0.001, 0.0, 0.0, 0.001, 0.0001, 0.0001, 0.0,
       0.0001, 0.0003, 0.0, 0.0, 0.0, 0.0, 0.002, 0.001, 0.001],
   "SystematicCorrelationMatrix": [
     [1.0, 0.0, 0.0, 0.0, 0.0, 0.0, 0.0, 0.0, 0.0, 0.0, 0.0, 0.0, 0.0, 0.0, 0.0, 0.0,
         0.0, 0.0, 0.0, 0.0, 0.0],
     [0.0, 1.0, 0.0, 0.0, 0.0, 0.0, 0.0, 0.0, 0.0, 0.0, 0.0, 0.0, 0.0, 0.0, 0.0, 0.0,
         0.0, 0.0, 0.0, 0.0, 0.0],
     [0.0, 0.0, 1.0, 0.0, 0.0, 0.0, 0.0, 0.0, 0.0, 0.0, 0.0, 0.0, 0.0, 0.0, 0.0, 0.0,
         0.0, 0.0, 0.0, 0.0, 0.0],
     [0.0, 0.0, 0.0, 1.0, 0.0, 0.0, 0.0, 0.0, 0.0, 0.0, 0.0, 0.0, 0.0, 0.0, 0.0, 0.0,
         0.0, 0.0, 0.0, 0.0, 0.0],
     [0.0, 0.0, 0.0, 0.0, 1.0, -1.0, 0.0, 0.0, -1.0, 1.0, 1.0, 0.0, 1.0, 1.0, 0.0,
         0.0, 0.0, 0.0, 1.0, 1.0, -1.0],
     [0.0, 0.0, 0.0, 0.0, -1.0, 1.0, 0.0, 0.0, 1.0, -1.0, -1.0, 0.0, -1.0, -1.0, 0.0,
         0.0, 0.0, 0.0, -1.0, -1.0, 1.0],
     [0.0, 0.0, 0.0, 0.0, 0.0, 0.0, 1.0, 0.0, 0.0, 0.0, 0.0, 0.0, 0.0, 0.0, 0.0, 0.0,
         0.0, 0.0, 0.0, 0.0, 0.0],
     [0.0, 0.0, 0.0, 0.0, 0.0, 0.0, 0.0, 1.0, 0.0, 0.0, 0.0, 0.0, 0.0, 0.0, 0.0, 0.0,
         0.0, 0.0, 0.0, 0.0, 0.0],
     [0.0, 0.0, 0.0, 0.0, -1.0, 1.0, 0.0, 0.0, 1.0, -1.0, -1.0, 0.0, -1.0, -1.0, 0.0,
         0.0, 0.0, 0.0, -1.0, -1.0, 1.0],
```

```
    [0.0, 0.0, 0.0, 0.0, 1.0, -1.0, 0.0, 0.0, -1.0, 1.0, 1.0, 0.0, 1.0, 1.0, 0.0,
        0.0, 0.0, 0.0, 1.0, 1.0, -1.0],
    [0.0, 0.0, 0.0, 0.0, 1.0, -1.0, 0.0, 0.0, -1.0, 1.0, 1.0, 0.0, 1.0, 1.0, 0.0,
        0.0, 0.0, 0.0, 1.0, 1.0, -1.0],
    [0.0, 0.0, 0.0, 0.0, 0.0, 0.0, 0.0, 0.0, 0.0, 0.0, 0.0, 1.0, 0.0, 0.0, 0.0, 0.0,
        0.0, 0.0, 0.0, 0.0, 0.0],
    [0.0, 0.0, 0.0, 0.0, 1.0, -1.0, 0.0, 0.0, -1.0, 1.0, 1.0, 0.0, 1.0, 1.0, 0.0,
        0.0, 0.0, 0.0, 1.0, 1.0, -1.0],
    [0.0, 0.0, 0.0, 0.0, 1.0, -1.0, 0.0, 0.0, -1.0, 1.0, 1.0, 0.0, 1.0, 1.0, 0.0,
        0.0, 0.0, 0.0, 1.0, 1.0, -1.0],
    [0.0, 0.0, 0.0, 0.0, 0.0, 0.0, 0.0, 0.0, 0.0, 0.0, 0.0, 0.0, 0.0, 0.0, 1.0, 0.0,
        0.0, 0.0, 0.0, 0.0, 0.0],
    [0.0, 0.0, 0.0, 0.0, 0.0, 0.0, 0.0, 0.0, 0.0, 0.0, 0.0, 0.0, 0.0, 0.0, 0.0, 1.0,
        0.0, 0.0, 0.0, 0.0, 0.0],
    [0.0, 0.0, 0.0, 0.0, 0.0, 0.0, 0.0, 0.0, 0.0, 0.0, 0.0, 0.0, 0.0, 0.0, 0.0, 0.0,
        1.0, 0.0, 0.0, 0.0, 0.0],
    [0.0, 0.0, 0.0, 0.0, 0.0, 0.0, 0.0, 0.0, 0.0, 0.0, 0.0, 0.0, 0.0, 0.0, 0.0, 0.0,
        0.0, 1.0, 0.0, 0.0, 0.0],
    [0.0, 0.0, 0.0, 0.0, 1.0, -1.0, 0.0, 0.0, -1.0, 1.0, 1.0, 0.0, 1.0, 1.0, 0.0,
        0.0, 0.0, 0.0, 1.0, 1.0, -1.0],
    [0.0, 0.0, 0.0, 0.0, 1.0, -1.0, 0.0, 0.0, -1.0, 1.0, 1.0, 0.0, 1.0, 1.0, 0.0,
        0.0, 0.0, 0.0, 1.0, 1.0, -1.0],
    [0.0, 0.0, 0.0, 0.0, -1.0, 1.0, 0.0, 0.0, 1.0, -1.0, -1.0, 0.0, -1.0, -1.0, 0.0,
        0.0, 0.0, 0.0, -1.0, -1.0, 1.0]
    ]
},
{
  "Name": "DecayTimeResolutionMean",
  "Values": [0.0002, 0.0003, 0.0, 0.0, 0.001, 0.080, 0.0032, 0.001, 0.005, 0.0001,
      0.0, 0.0, 0.0001, 0.0001, 0.0, 0.0, 0.003, 0.002, 0.003, 0.0056, 0.002],
  "SystematicCorrelationMatrix": [
  [1.0, 1.0, 0.0, 0.0, -1.0, -1.0, -1.0, -1.0, 1.0, -1.0, 0.0, 0.0, 1.0, 1.0, 0.0,
      0.0, 1.0, -1.0, 1.0, -1.0, -1.0],
  [1.0, 1.0, 0.0, 0.0, -1.0, -1.0, -1.0, -1.0, 1.0, -1.0, 0.0, 0.0, 1.0, 1.0, 0.0,
      0.0, 1.0, -1.0, 1.0, -1.0, -1.0],
  [0.0, 0.0, 1.0, 0.0, 0.0, 0.0, 0.0, 0.0, 0.0, 0.0, 0.0, 0.0, 0.0, 0.0, 0.0, 0.0,
      0.0, 0.0, 0.0, 0.0, 0.0],
  [0.0, 0.0, 0.0, 1.0, 0.0, 0.0, 0.0, 0.0, 0.0, 0.0, 0.0, 0.0, 0.0, 0.0, 0.0, 0.0,
      0.0, 0.0, 0.0, 0.0, 0.0],
  [-1.0, -1.0, 0.0, 0.0, 1.0, 1.0, 1.0, 1.0, -1.0, 1.0, 0.0, 0.0, -1.0, -1.0, 0.0,
      0.0, -1.0, 1.0, -1.0, 1.0, 1.0],
  [-1.0, -1.0, 0.0, 0.0, 1.0, 1.0, 1.0, 1.0, -1.0, 1.0, 0.0, 0.0, -1.0, -1.0, 0.0,
      0.0, -1.0, 1.0, -1.0, 1.0, 1.0],
  [-1.0, -1.0, 0.0, 0.0, 1.0, 1.0, 1.0, 1.0, -1.0, 1.0, 0.0, 0.0, -1.0, -1.0, 0.0,
      0.0, -1.0, 1.0, -1.0, 1.0, 1.0],
  [-1.0, -1.0, 0.0, 0.0, 1.0, 1.0, 1.0, 1.0, -1.0, 1.0, 0.0, 0.0, -1.0, -1.0, 0.0,
      0.0, -1.0, 1.0, -1.0, 1.0, 1.0],
  [1.0, 1.0, 0.0, 0.0, -1.0, -1.0, -1.0, -1.0, 1.0, -1.0, 0.0, 0.0, 1.0, 1.0, 0.0,
      0.0, 1.0, -1.0, 1.0, -1.0, -1.0],
  [-1.0, -1.0, 0.0, 0.0, 1.0, 1.0, 1.0, 1.0, -1.0, 1.0, 0.0, 0.0, -1.0, -1.0, 0.0,
      0.0, -1.0, 1.0, -1.0, 1.0, 1.0],
  [0.0, 0.0, 0.0, 0.0, 0.0, 0.0, 0.0, 0.0, 0.0, 0.0, 1.0, 0.0, 0.0, 0.0, 0.0, 0.0,
      0.0, 0.0, 0.0, 0.0, 0.0],
  [0.0, 0.0, 0.0, 0.0, 0.0, 0.0, 0.0, 0.0, 0.0, 0.0, 0.0, 1.0, 0.0, 0.0, 0.0, 0.0,
      0.0, 0.0, 0.0, 0.0, 0.0],
  [1.0, 1.0, 0.0, 0.0, -1.0, -1.0, -1.0, -1.0, 1.0, -1.0, 0.0, 0.0, 1.0, 1.0, 0.0,
      0.0, 1.0, -1.0, 1.0, -1.0, -1.0],
  [1.0, 1.0, 0.0, 0.0, -1.0, -1.0, -1.0, -1.0, 1.0, -1.0, 0.0, 0.0, 1.0, 1.0, 0.0,
      0.0, 1.0, -1.0, 1.0, -1.0, -1.0],
  [0.0, 0.0, 0.0, 0.0, 0.0, 0.0, 0.0, 0.0, 0.0, 0.0, 0.0, 0.0, 0.0, 0.0, 1.0, 0.0,
      0.0, 0.0, 0.0, 0.0, 0.0],
  [0.0, 0.0, 0.0, 0.0, 0.0, 0.0, 0.0, 0.0, 0.0, 0.0, 0.0, 0.0, 0.0, 0.0, 0.0, 1.0,
      0.0, 0.0, 0.0, 0.0, 0.0],
  [1.0, 1.0, 0.0, 0.0, -1.0, -1.0, -1.0, -1.0, 1.0, -1.0, 0.0, 0.0, 1.0, 1.0, 0.0,
      0.0, 1.0, -1.0, 1.0, -1.0, -1.0],
  [-1.0, -1.0, 0.0, 0.0, 1.0, 1.0, 1.0, 1.0, -1.0, 1.0, 0.0, 0.0, -1.0, -1.0, 0.0,
      0.0, -1.0, 1.0, -1.0, 1.0, 1.0],
  [1.0, 1.0, 0.0, 0.0, -1.0, -1.0, -1.0, -1.0, 1.0, -1.0, 0.0, 0.0, 1.0, 1.0, 0.0,
      0.0, 1.0, -1.0, 1.0, -1.0, -1.0],
  [-1.0, -1.0, 0.0, 0.0, 1.0, 1.0, 1.0, 1.0, -1.0, 1.0, 0.0, 0.0, -1.0, -1.0, 0.0,
      0.0, -1.0, 1.0, -1.0, 1.0, 1.0],
  [-1.0, -1.0, 0.0, 0.0, 1.0, 1.0, 1.0, 1.0, -1.0, 1.0, 0.0, 0.0, -1.0, -1.0, 0.0,
      0.0, -1.0, 1.0, -1.0, 1.0, 1.0]
  ]
},
{
  "Name": "DecayTimeResolutionWrongPVComponent",
```

```
  "Values": [0.0, 0.0, 0.0, 0.0, 0.001, 0.001, 0.0, 0.0, 0.001, 0.0001, 0.0001, 0.0,
       0.0001, 0.0002, 0.0, 0.0, 0.001, 0.001, 0.001, 0.001, 0.001],
  "SystematicCorrelationMatrix": [
  [1.0, 0.0, 0.0, 0.0, 0.0, 0.0, 0.0, 0.0, 0.0, 0.0, 0.0, 0.0, 0.0, 0.0, 0.0, 0.0,
       0.0, 0.0, 0.0, 0.0, 0.0],
  [0.0, 1.0, 0.0, 0.0, 0.0, 0.0, 0.0, 0.0, 0.0, 0.0, 0.0, 0.0, 0.0, 0.0, 0.0, 0.0,
       0.0, 0.0, 0.0, 0.0, 0.0],
  [0.0, 0.0, 1.0, 0.0, 0.0, 0.0, 0.0, 0.0, 0.0, 0.0, 0.0, 0.0, 0.0, 0.0, 0.0, 0.0,
       0.0, 0.0, 0.0, 0.0, 0.0],
  [0.0, 0.0, 0.0, 1.0, 0.0, 0.0, 0.0, 0.0, 0.0, 0.0, 0.0, 0.0, 0.0, 0.0, 0.0, 0.0,
       0.0, 0.0, 0.0, 0.0, 0.0],
  [0.0, 0.0, 0.0, 0.0, 1.0, 0, 0.0, 0.0, 0, -1.0, 0, 0.0, 0, 1.0, 0.0, 0.0, 1.0, 0,
       0, 0, 0],
  [0.0, 0.0, 0.0, 0.0, 0, 1.0, 0.0, 0.0, 1.0, 0, -1.0, 0.0, -1.0, 0, 0.0, 0.0, 0,
       1.0, -1.0, -1.0, 1.0],
  [0.0, 0.0, 0.0, 0.0, 0.0, 0.0, 1.0, 0.0, 0.0, 0.0, 0.0, 0.0, 0.0, 0.0, 0.0, 0.0,
       0.0, 0.0, 0.0, 0.0, 0.0],
  [0.0, 0.0, 0.0, 0.0, 0.0, 0.0, 0.0, 1.0, 0.0, 0.0, 0.0, 0.0, 0.0, 0.0, 0.0, 0.0,
       0.0, 0.0, 0.0, 0.0, 0.0],
  [0.0, 0.0, 0.0, 0.0, 0, 1.0, 0.0, 0.0, 1.0, 0, -1.0, 0.0, -1.0, 0, 0.0, 0.0, 0,
       1.0, -1.0, -1.0, 1.0],
  [0.0, 0.0, 0.0, 0.0, -1.0, 0, 0.0, 0.0, 0, 1.0, 0, 0.0, 0, -1.0, 0.0, 0.0, -1.0, 0,
        0, 0, 0],
  [0.0, 0.0, 0.0, 0.0, 0, -1.0, 0.0, 0.0, -1.0, 0, 1.0, 0.0, 1.0, 0, 0.0, 0.0, 0,
       -1.0, 1.0, 1.0, -1.0],
  [0.0, 0.0, 0.0, 0.0, 0.0, 0.0, 0.0, 0.0, 0.0, 0.0, 0.0, 1.0, 0.0, 0.0, 0.0, 0.0,
       0.0, 0.0, 0.0, 0.0, 0.0],
  [0.0, 0.0, 0.0, 0.0, 0, -1.0, 0.0, 0.0, -1.0, 0, 1.0, 0.0, 1.0, 0, 0.0, 0.0, 0,
       -1.0, 1.0, 1.0, -1.0],
  [0.0, 0.0, 0.0, 0.0, 1.0, 0, 0.0, 0.0, 0, -1.0, 0, 0.0, 0, 1.0, 0.0, 0.0, 1.0, 0,
       0, 0, 0],
  [0.0, 0.0, 0.0, 0.0, 0.0, 0.0, 0.0, 0.0, 0.0, 0.0, 0.0, 0.0, 0.0, 0.0, 1.0, 0.0,
       0.0, 0.0, 0.0, 0.0, 0.0],
  [0.0, 0.0, 0.0, 0.0, 0.0, 0.0, 0.0, 0.0, 0.0, 0.0, 0.0, 0.0, 0.0, 0.0, 0.0, 1.0,
       0.0, 0.0, 0.0, 0.0, 0.0],
  [0.0, 0.0, 0.0, 0.0, 1.0, 0, 0.0, 0.0, 0, -1.0, 0, 0.0, 0, 1.0, 0.0, 0.0, 1.0, 0,
       0, 0, 0],
  [0.0, 0.0, 0.0, 0.0, 0, 1.0, 0.0, 0.0, 1.0, 0, -1.0, 0.0, -1.0, 0, 0.0, 0.0, 0,
       1.0, -1.0, -1.0, 1.0],
  [0.0, 0.0, 0.0, 0.0, 0, -1.0, 0.0, 0.0, -1.0, 0, 1.0, 0.0, 1.0, 0, 0.0, 0.0, 0,
       -1.0, 1.0, 1.0, -1.0],
  [0.0, 0.0, 0.0, 0.0, 0, -1.0, 0.0, 0.0, -1.0, 0, 1.0, 0.0, 1.0, 0, 0.0, 0.0, 0,
       -1.0, 1.0, 1.0, -1.0],
  [0.0, 0.0, 0.0, 0.0, 0, 1.0, 0.0, 0.0, 1.0, 0, -1.0, 0.0, -1.0, 0, 0.0, 0.0, 0,
       1.0, -1.0, -1.0, 1.0]
  ]
},
{
  "Name": "AngEfficiencyStat",
  "Values": [0.00003, 0.0, 0.00036, 0.0003, 0.0044, 0.0025, 0.0011, 0.0018, 0.0011,
       0.0007, 0.00032, 0.00011, 0.00026, 0.0006, 0.0006, 0.003, 0.006, 0.013, 0.012,
       0.0044, 0.004],
  "SystematicCorrelationMatrix": [
  [1.0, 0.0, 0.89, -0.22, -0.0071, -0.028, 0.027, -0.033, 0.14, 0.43, 0.13, 0.18,
       0.35, 0.37, 0.36, 0.16, 0.029, -0.12, 0.21, 0.31, 0.42],
  [0.0, 1.0, 0.0, 0.0, 0.0, 0.0, 0.0, 0.0, 0.0, 0.0, 0.0, 0.0, 0.0, 0.0, 0.0, 0.0,
       0.0, 0.0, 0.0, 0.0, 0.0],
  [0.89, 0.0, 1.0, -0.36, -0.027, -0.12, -0.058, 0.025, -0.065, 0.12, -0.13, -0.048,
       -0.012, 0.0036, 0.044, 0.22, -0.0094, -0.012, 0.0098, 0.082, 0.23],
  [-0.22, 0.0, -0.36, 1.0, 0.14, 0.054, 0.0054, -0.04, -0.097, -0.28, -0.12, -0.12,
       -0.11, -0.13, -0.17, -0.015, 0.021, 0.036, -0.1, -0.13, -0.17],
  [-0.0071, 0.0, -0.027, 0.14, 1.0, 0.6, 0.029, -0.013, -0.19, -0.15, -0.11, -0.073,
       -0.11, -0.11, -0.14, -0.049, -0.095, -0.021, -0.092, -0.12, -0.2],
  [-0.028, 0.0, -0.12, 0.054, 0.6, 1.0, 0.72, -0.48, 0.51, -0.03, -0.2, -0.26, 0.16,
       0.061, -0.04, -0.15, 0.24, 0.015, -0.12, -0.16, -0.4],
  [0.027, 0.0, -0.058, 0.0054, 0.029, 0.72, 1.0, -0.58, 0.82, -0.14, 0.075, -0.005,
       0.065, -0.044, -0.2, -0.49, 0.4, 0.36, 0.23, 0.17, -0.074],
  [-0.033, 0.0, 0.025, -0.04, -0.013, -0.48, -0.58, 1.0, -0.76, 0.07, 0.008, 0.23,
       -0.19, -0.043, 0.13, 0.52, -0.96, -0.57, -0.21, -0.15, 0.15],
  [0.14, 0.0, -0.065, -0.097, -0.19, 0.51, 0.82, -0.76, 1.0, 0.23, 0.39, 0.22, 0.45,
       0.34, 0.15, -0.6, 0.67, 0.4, 0.51, 0.49, 0.22],
  [0.43, 0.0, 0.12, -0.28, -0.15, -0.03, -0.14, 0.07, 0.23, 1.0, 0.4, 0.36, 0.95,
       0.98, 0.99, 0.28, -0.079, -0.58, 0.22, 0.33, 0.39],
  [0.13, 0.0, -0.13, -0.12, -0.11, -0.2, 0.075, 0.008, 0.39, 0.4, 1.0, 0.97, 0.4,
       0.46, 0.32, -0.64, 0.1, 0.29, 0.95, 0.96, 0.91],
  [0.18, 0.0, -0.048, -0.12, -0.073, -0.26, -0.005, 0.23, 0.22, 0.36, 0.97, 1.0, 0.3,
        0.38, 0.28, -0.53, -0.12, 0.2, 0.89, 0.92, 0.94],
```

```
    [0.35, 0.0, -0.012, -0.11, -0.11, 0.16, 0.065, -0.19, 0.45, 0.95, 0.4, 0.3, 1.0,
        0.99, 0.94, 0.13, 0.14, -0.45, 0.27, 0.35, 0.32],
    [0.37, 0.0, 0.0036, -0.13, -0.11, 0.061, -0.044, -0.043, 0.34, 0.98, 0.46, 0.38,
        0.99, 1.0, 0.97, 0.17, 0.021, -0.5, 0.29, 0.39, 0.39],
    [0.36, 0.0, 0.044, -0.17, -0.14, -0.04, -0.2, 0.13, 0.15, 0.99, 0.32, 0.28, 0.94,
        0.97, 1.0, 0.38, -0.15, -0.67, 0.11, 0.22, 0.3],
    [0.16, 0.0, 0.22, -0.015, -0.049, -0.15, -0.49, 0.52, -0.6, 0.28, -0.64, -0.53,
        0.13, 0.17, 0.38, 1.0, -0.58, -0.88, -0.8, -0.71, -0.48],
    [0.029, 0.0, -0.0094, 0.021, -0.095, 0.24, 0.4, -0.96, 0.67, -0.079, 0.1, -0.12,
        0.14, 0.021, -0.15, -0.58, 1.0, 0.67, 0.31, 0.26, -0.012],
    [-0.12, 0.0, -0.012, 0.036, -0.021, 0.015, 0.36, -0.57, 0.4, -0.58, 0.29, 0.2,
        -0.45, -0.5, -0.67, -0.88, 0.67, 1.0, 0.54, 0.44, 0.24],
    [0.21, 0.0, 0.0098, -0.1, -0.092, -0.12, 0.23, -0.21, 0.51, 0.22, 0.95, 0.89, 0.27,
        0.29, 0.11, -0.8, 0.31, 0.54, 1.0, 0.99, 0.89],
    [0.31, 0.0, 0.082, -0.13, -0.12, -0.16, 0.17, -0.15, 0.49, 0.33, 0.96, 0.92, 0.35,
        0.39, 0.22, -0.71, 0.26, 0.44, 0.99, 1.0, 0.94],
    [0.42, 0.0, 0.23, -0.17, -0.2, -0.4, -0.074, 0.15, 0.22, 0.39, 0.91, 0.94, 0.32,
        0.39, 0.3, -0.48, -0.012, 0.24, 0.89, 0.94, 1.0]
    ]
},
{
    "Name": "AngEfficiencyReweighting",
    "Values": [0.00006, 0.00021, 0.00112, 0.00200, 0.0077, 0.0057, 0.0022, 0.0043,
        0.0012, 0.0023, 0.00026, 0.00006, 0.00059, 0.0012, 0.0014, 0.005, 0.016, 0.031,
        0.011, 0.0046, 0.004],
    "SystematicCorrelationMatrix": [
    [1.0, 0.81, 0.98, -0.97, 0.84, 0.82, 0.17, 0.38, 0.79,
    0.97, 0.92, 0.0, 0.94, 0.95, 0.96, 0.91, -0.41, -0.9, 0.86, 0.92, 0.96],
    [0.81, 1.0, 0.9, -0.91, 0.74, 0.5, -0.24, -0.025, 0.62,
    0.91, 0.86, 0.0, 0.91, 0.9, 0.9, 0.69, 0.017, -0.66, 0.88, 0.9, 0.88],
    [0.98, 0.9, 1.0, -1.0, 0.84, 0.74, 0.04, 0.25, 0.75,
    0.98, 0.92, 0.0, 0.95, 0.96, 0.97, 0.87, -0.27, -0.84, 0.89, 0.94, 0.96],
    [-0.97, -0.91, -1.0, 1.0, -0.83, -0.74, -0.038, -0.23, -0.77,
    -0.99, -0.94, 0.0, -0.96, -0.97, -0.98, -0.85, 0.25, 0.84, -0.91, -0.95, -0.96],
    [0.84, 0.74, 0.84, -0.83, 1.0, 0.68, -0.042, 0.33, 0.47,
    0.83, 0.79, 0.0, 0.8, 0.82, 0.83, 0.79, -0.32, -0.76, 0.72, 0.78, 0.81],
    [0.82, 0.5, 0.74, -0.74, 0.68, 1.0, 0.65, 0.69, 0.86,
    0.77, 0.78, 0.0, 0.76, 0.78, 0.78, 0.86, -0.76, -0.94, 0.65, 0.71, 0.78],
    [0.17, -0.24, 0.04, -0.038, -0.042, 0.65, 1.0, 0.78, 0.51,
    0.069, 0.14, 0.0, 0.068, 0.087, 0.085, 0.33, -0.85, -0.46, 0.0027, 0.043, 0.13],
    [0.38, -0.025, 0.25, -0.23, 0.33, 0.69, 0.78, 1.0, 0.35,
    0.25, 0.32, 0.0, 0.21, 0.26, 0.27, 0.61, -0.99, -0.66, 0.13, 0.2, 0.36],
    [0.79, 0.62, 0.75, -0.77, 0.47, 0.86, 0.51, 0.35, 1.0,
    0.8, 0.82, 0.0, 0.83, 0.82, 0.81, 0.71, -0.45, -0.82, 0.78, 0.8, 0.79],
    [0.97, 0.91, 0.98, -0.99, 0.83, 0.77, 0.069, 0.25, 0.8,
    1.0, 0.96, 0.0, 0.99, 0.99, 1.0, 0.87, -0.28, -0.88, 0.92, 0.97, 0.98],
    [0.92, 0.86, 0.92, -0.94, 0.79, 0.78, 0.14, 0.32, 0.82,
    0.96, 1.0, 0.0, 0.96, 0.97, 0.96, 0.8, -0.35, -0.87, 0.97, 0.99, 0.99],
    [0.0, 0.0, 0.0, 0.0, 0.0, 0.0, 0.0, 0.0, 0.0,
    0.0, 0.0, 1.0, 0.0, 0.0, 0.0, 0.0, 0.0, 0.0, 0.0, 0.0, 0.0],
    [0.94, 0.91, 0.95, -0.96, 0.8, 0.76, 0.068, 0.21, 0.83,
    0.99, 0.96, 0.0, 1.0, 1.0, 1.0, 0.84, -0.25, -0.87, 0.93, 0.97, 0.96],
    [0.95, 0.9, 0.96, -0.97, 0.82, 0.78, 0.087, 0.26, 0.82,
    0.99, 0.97, 0.0, 1.0, 1.0, 1.0, 0.86, -0.29, -0.88, 0.93, 0.97, 0.97],
    [0.96, 0.9, 0.97, -0.98, 0.83, 0.78, 0.085, 0.27, 0.81,
    1.0, 0.96, 0.0, 1.0, 1.0, 1.0, 0.88, -0.3, -0.89, 0.92, 0.97, 0.97],
    [0.91, 0.69, 0.87, -0.85, 0.79, 0.86, 0.33, 0.61, 0.71,
    0.87, 0.8, 0.0, 0.84, 0.86, 0.88, 1.0, -0.62, -0.96, 0.66, 0.77, 0.86],
    [-0.41, 0.017, -0.27, 0.25, -0.32, -0.76, -0.85, -0.99, -0.45,
    -0.28, -0.35, 0.0, -0.25, -0.29, -0.3, -0.62, 1.0, 0.69, -0.15, -0.23, -0.37],
    [-0.9, -0.66, -0.84, 0.84, -0.76, -0.94, -0.46, -0.66, -0.82,
    -0.88, -0.87, 0.0, -0.87, -0.88, -0.89, -0.96, 0.69, 1.0, -0.73, -0.81, -0.89],
    [0.86, 0.88, 0.89, -0.91, 0.72, 0.65, 0.0027, 0.13, 0.78,
    0.92, 0.97, 0.0, 0.93, 0.93, 0.92, 0.66, -0.15, -0.73, 1.0, 0.99, 0.95],
    [0.92, 0.9, 0.94, -0.95, 0.78, 0.71, 0.043, 0.2, 0.8,
    0.97, 0.99, 0.0, 0.97, 0.97, 0.97, 0.77, -0.23, -0.81, 0.99, 1.0, 0.98],
    [0.96, 0.88, 0.96, -0.96, 0.81, 0.78, 0.13, 0.36, 0.79,
    0.98, 0.99, 0.0, 0.96, 0.97, 0.97, 0.86, -0.37, -0.89, 0.95, 0.98, 1.0]
    ]
},
{
    "Name": "AngEfficiencyDependence",
    "Values": [0.00021, 0.00095, 0.0012, 0.00084, 0.0055, 0.029, 0.0012, 0.0007,
        0.0028, 0.0063, 0.00069, 0.00024, 0.00015, 0.0010, 0.0016, 0.013, 0.022, 0.027,
        0.032, 0.010, 0.010],
    "SystematicCorrelationMatrix": [
```

```
    [1.0, -1.0, 1.0, -1.0, 1.0, 1.0, 1.0, -1.0, 1.0, -1.0, -1.0, 1.0, 1.0, 1.0, -1.0,
        -1.0, 1.0, -1.0, -1.0, -1.0, -1.0],
    [-1.0, 1.0, -1.0, 1.0, -1.0, -1.0, -1.0, 1.0, -1.0, 1.0, 1.0, -1.0, -1.0, -1.0,
        1.0, 1.0, -1.0, 1.0, 1.0, 1.0, 1.0],
    [1.0, -1.0, 1.0, -1.0, 1.0, 1.0, 1.0, -1.0, 1.0, -1.0, -1.0, 1.0, 1.0, 1.0, -1.0,
        -1.0, 1.0, -1.0, -1.0, -1.0, -1.0],
    [-1.0, 1.0, -1.0, 1.0, -1.0, -1.0, -1.0, 1.0, -1.0, 1.0, 1.0, -1.0, -1.0, -1.0,
        1.0, 1.0, -1.0, 1.0, 1.0, 1.0, 1.0],
    [1.0, -1.0, 1.0, -1.0, 1.0, 1.0, 1.0, -1.0, 1.0, -1.0, -1.0, 1.0, 1.0, 1.0, -1.0,
        -1.0, 1.0, -1.0, -1.0, -1.0, -1.0],
    [1.0, -1.0, 1.0, -1.0, 1.0, 1.0, 1.0, -1.0, 1.0, -1.0, -1.0, 1.0, 1.0, 1.0, -1.0,
        -1.0, 1.0, -1.0, -1.0, -1.0, -1.0],
    [1.0, -1.0, 1.0, -1.0, 1.0, 1.0, 1.0, -1.0, 1.0, -1.0, -1.0, 1.0, 1.0, 1.0, -1.0,
        -1.0, 1.0, -1.0, -1.0, -1.0, -1.0],
    [-1.0, 1.0, -1.0, 1.0, -1.0, -1.0, -1.0, 1.0, -1.0, 1.0, 1.0, -1.0, -1.0, -1.0,
        1.0, 1.0, -1.0, 1.0, 1.0, 1.0, 1.0],
    [1.0, -1.0, 1.0, -1.0, 1.0, 1.0, 1.0, -1.0, 1.0, -1.0, -1.0, 1.0, 1.0, 1.0, -1.0,
        -1.0, 1.0, -1.0, -1.0, -1.0, -1.0],
    [-1.0, 1.0, -1.0, 1.0, -1.0, -1.0, -1.0, 1.0, -1.0, 1.0, 1.0, -1.0, -1.0, -1.0,
        1.0, 1.0, -1.0, 1.0, 1.0, 1.0, 1.0],
    [-1.0, 1.0, -1.0, 1.0, -1.0, -1.0, -1.0, 1.0, -1.0, 1.0, 1.0, -1.0, -1.0, -1.0,
        1.0, 1.0, -1.0, 1.0, 1.0, 1.0, 1.0],
    [1.0, -1.0, 1.0, -1.0, 1.0, 1.0, 1.0, -1.0, 1.0, -1.0, -1.0, 1.0, 1.0, 1.0, -1.0,
        -1.0, 1.0, -1.0, -1.0, -1.0, -1.0],
    [1.0, -1.0, 1.0, -1.0, 1.0, 1.0, 1.0, -1.0, 1.0, -1.0, -1.0, 1.0, 1.0, 1.0, -1.0,
        -1.0, 1.0, -1.0, -1.0, -1.0, -1.0],
    [1.0, -1.0, 1.0, -1.0, 1.0, 1.0, 1.0, -1.0, 1.0, -1.0, -1.0, 1.0, 1.0, 1.0, -1.0,
        -1.0, 1.0, -1.0, -1.0, -1.0, -1.0],
    [-1.0, 1.0, -1.0, 1.0, -1.0, -1.0, -1.0, 1.0, -1.0, 1.0, 1.0, -1.0, -1.0, -1.0,
        1.0, 1.0, -1.0, 1.0, 1.0, 1.0, 1.0],
    [-1.0, 1.0, -1.0, 1.0, -1.0, -1.0, -1.0, 1.0, -1.0, 1.0, 1.0, -1.0, -1.0, -1.0,
        1.0, 1.0, -1.0, 1.0, 1.0, 1.0, 1.0],
    [1.0, -1.0, 1.0, -1.0, 1.0, 1.0, 1.0, -1.0, 1.0, -1.0, -1.0, 1.0, 1.0, 1.0, -1.0,
        -1.0, 1.0, -1.0, -1.0, -1.0, -1.0],
    [-1.0, 1.0, -1.0, 1.0, -1.0, -1.0, -1.0, 1.0, -1.0, 1.0, 1.0, -1.0, -1.0, -1.0,
        1.0, 1.0, -1.0, 1.0, 1.0, 1.0, 1.0],
    [-1.0, 1.0, -1.0, 1.0, -1.0, -1.0, -1.0, 1.0, -1.0, 1.0, 1.0, -1.0, -1.0, -1.0,
        1.0, 1.0, -1.0, 1.0, 1.0, 1.0, 1.0],
    [-1.0, 1.0, -1.0, 1.0, -1.0, -1.0, -1.0, 1.0, -1.0, 1.0, 1.0, -1.0, -1.0, -1.0,
        1.0, 1.0, -1.0, 1.0, 1.0, 1.0, 1.0]
  ]
},
{
  "Name": "DecayTimeEfficiencyKnotPos",
  "Values": [0.00019, 0.0, 0.0, 0.0, 0.0, 0.0, 0.0, 0.0, 0.0]
},
{
  "Name": "DecayTimeEfficiencyPDFReweighting",
  "Values": [0.00009, 0.00007, 0.0, 0.0, 0.0, 0.0, 0.0, 0.0, 0.0],
  "SystematicCorrelationMatrix": [
    [1.0, 1.0, 0.0, 0.0, 0.0, 0.0, 0.0, 0.0, 0.0],
    [1.0, 1.0, 0.0, 0.0, 0.0, 0.0, 0.0, 0.0, 0.0],
    [0.0, 0.0, 1.0, 0.0, 0.0, 0.0, 0.0, 0.0, 0.0],
    [0.0, 0.0, 0.0, 1.0, 0.0, 0.0, 0.0, 0.0, 0.0],
    [0.0, 0.0, 0.0, 0.0, 1.0, 0.0, 0.0, 0.0, 0.0],
    [0.0, 0.0, 0.0, 0.0, 0.0, 1.0, 0.0, 0.0, 0.0],
    [0.0, 0.0, 0.0, 0.0, 0.0, 0.0, 1.0, 0.0, 0.0],
    [0.0, 0.0, 0.0, 0.0, 0.0, 0.0, 0.0, 1.0, 0.0],
    [0.0, 0.0, 0.0, 0.0, 0.0, 0.0, 0.0, 0.0, 1.0]
  ]
},
{
  "Name": "DecayTimeEfficiencyKinReweighting",
  "Values": [0.00021, 0.0, 0.0, 0.0, 0.0, 0.0, 0.0, 0.0, 0.0]
},
{
  "Name": "DecayTimeEfficiencyStat",
  "Values": [0.0012, 0.00083, 0.0003, 0.0002, 0.0, 0.0, 0.0, 0.0, 0.0],
  "SystematicCorrelationMatrix": [
    [1.0, -0.077, 0.060, -0.058, 0.0, 0.0, 0.0, 0.0, 0.0],
    [-0.077, 1.0, -0.99, 0.99, 0.0, 0.0, 0.0, 0.0, 0.0],
    [0.060, -0.99, 1.0, -1.0, 0.0, 0.0, 0.0, 0.0, 0.0],
    [-0.058, 0.99, -1.0, 1.0, 0.0, 0.0, 0.0, 0.0, 0.0],
    [0.0, 0.0, 0.0, 0.0, 1.0, 0.0, 0.0, 0.0, 0.0],
    [0.0, 0.0, 0.0, 0.0, 0.0, 1.0, 0.0, 0.0, 0.0],
```

```
    [0.0, 0.0, 0.0, 0.0, 0.0, 0.0, 1.0, 0.0, 0.0],
    [0.0, 0.0, 0.0, 0.0, 0.0, 0.0, 0.0, 1.0, 0.0],
    [0.0, 0.0, 0.0, 0.0, 0.0, 0.0, 0.0, 0.0, 1.0]
  ]
},
{
  "Name": "DecayTimeEfficiencyOtherMC",
  "Values": [0.00031, 0.0005, 0.00018, 0.00012, 0.0, 0.0, 0.0, 0.0, 0.0],
  "SystematicCorrelationMatrix": [
    [ 1.0, -1.0, 1.0,-1.0, 0.0, 0.0, 0.0, 0.0, 0.0],
    [-1.0,  1.0,-1.0, 1.0, 0.0, 0.0, 0.0, 0.0, 0.0],
    [ 1.0, -1.0, 1.0,-1.0, 0.0, 0.0, 0.0, 0.0, 0.0],
    [-1.0,  1.0,-1.0, 1.0, 0.0, 0.0, 0.0, 0.0, 0.0],
    [ 0.0,  0.0, 0.0, 0.0, 1.0, 0.0, 0.0, 0.0, 0.0],
    [ 0.0,  0.0, 0.0, 0.0, 0.0, 1.0, 0.0, 0.0, 0.0],
    [ 0.0,  0.0, 0.0, 0.0, 0.0, 0.0, 1.0, 0.0, 0.0],
    [ 0.0,  0.0, 0.0, 0.0, 0.0, 0.0, 0.0, 1.0, 0.0],
    [ 0.0,  0.0, 0.0, 0.0, 0.0, 0.0, 0.0, 0.0, 1.0]
  ]
},
{
  "Name": "LengthMomentumScales",
  "Values": [ 0.0, 0.0, 0.0, 0.0, 0.0, 0.0, 0.0, 0.0, 0.004 ]
},
{
  "Name": "BKGCAT60",
  "Values": [0.00020, 0.00012, 0.00013, 0.00019, 0.0017, 0.0, 0.0005, 0.0014, 0.0,
       0.0, 0.00022, 0.00009, 0.0002, 0.00056, 0.00052, 0.0, 0.0, 0.0, 0.0041, 0.0018,
        0.0019],
  "SystematicCorrelationMatrix": [
  [1.0, -1.0, 0.0, 1.0, 0.0, 0.0, 1.0, 0.0, 0.0, 0.0, 0.0, 0.0, 0.0, 0.0, 0.0, 0.0,
       0.0, 0.0, 0.0, 0.0, 0.0],
  [-1.0, 1.0, 0.0, -1.0, 0.0, 0.0, -1.0, 0.0, 0.0, 0.0, 0.0, 0.0, 0.0, 0.0, 0.0, 0.0,
        0.0, 0.0, 0.0, 0.0, 0.0],
  [0.0, 0.0, 1.0, 0.0, -1.0, 0.0, 0.0, -1.0, 0.0, 0.0, -1.0, -1.0, -1.0, -1.0, -1.0,
       0.0, 0.0, 0.0, -1.0, -1.0, -1.0],
  [1.0, -1.0, 0.0, 1.0, 0.0, 0.0, 1.0, 0.0, 0.0, 0.0, 0.0, 0.0, 0.0, 0.0, 0.0, 0.0,
       0.0, 0.0, 0.0, 0.0, 0.0],
  [0.0, 0.0, -1.0, 0.0, 1.0, 0.0, 0.0, 1.0, 0.0, 0.0, 1.0, 1.0, 1.0, 1.0, 1.0, 0.0,
       0.0, 0.0, 1.0, 1.0, 1.0],
  [0.0, 0.0, 0.0, 0.0, 0.0, 1.0, 0.0, 0.0, 0.0, 0.0, 0.0, 0.0, 0.0, 0.0, 0.0, 0.0,
       0.0, 0.0, 0.0, 0.0, 0.0],
  [1.0, -1.0, 0.0, 1.0, 0.0, 0.0, 1.0, 0.0, 0.0, 0.0, 0.0, 0.0, 0.0, 0.0, 0.0, 0.0,
       0.0, 0.0, 0.0, 0.0, 0.0],
  [0.0, 0.0, -1.0, 0.0, 1.0, 0.0, 0.0, 1.0, 0.0, 0.0, 1.0, 1.0, 1.0, 1.0, 1.0, 0.0,
       0.0, 0.0, 1.0, 1.0, 1.0],
  [0.0, 0.0, 0.0, 0.0, 0.0, 0.0, 0.0, 1.0, 0.0, 0.0, 0.0, 0.0, 0.0, 0.0, 0.0, 0.0,
       0.0, 0.0, 0.0, 0.0, 0.0],
  [0.0, 0.0, 0.0, 0.0, 0.0, 0.0, 0.0, 0.0, 0.0, 1.0, 0.0, 0.0, 0.0, 0.0, 0.0, 0.0,
       0.0, 0.0, 0.0, 0.0, 0.0],
  [0.0, 0.0, -1.0, 0.0, 1.0, 0.0, 0.0, 1.0, 0.0, 0.0, 1.0, 1.0, 1.0, 1.0, 1.0, 0.0,
       0.0, 0.0, 1.0, 1.0, 1.0],
  [0.0, 0.0, -1.0, 0.0, 1.0, 0.0, 0.0, 1.0, 0.0, 0.0, 1.0, 1.0, 1.0, 1.0, 1.0, 0.0,
       0.0, 0.0, 1.0, 1.0, 1.0],
  [0.0, 0.0, -1.0, 0.0, 1.0, 0.0, 0.0, 1.0, 0.0, 0.0, 1.0, 1.0, 1.0, 1.0, 1.0, 0.0,
       0.0, 0.0, 1.0, 1.0, 1.0],
  [0.0, 0.0, -1.0, 0.0, 1.0, 0.0, 0.0, 1.0, 0.0, 0.0, 1.0, 1.0, 1.0, 1.0, 1.0, 0.0,
       0.0, 0.0, 1.0, 1.0, 1.0],
  [0.0, 0.0, -1.0, 0.0, 1.0, 0.0, 0.0, 1.0, 0.0, 0.0, 1.0, 1.0, 1.0, 1.0, 1.0, 0.0,
       0.0, 0.0, 1.0, 1.0, 1.0],
  [0.0, 0.0, -1.0, 0.0, 1.0, 0.0, 0.0, 1.0, 0.0, 0.0, 1.0, 1.0, 1.0, 1.0, 1.0, 0.0,
       0.0, 0.0, 1.0, 1.0, 1.0],
  [0.0, 0.0, 0.0, 0.0, 0.0, 0.0, 0.0, 0.0, 0.0, 0.0, 0.0, 0.0, 0.0, 0.0, 0.0, 1.0,
       0.0, 0.0, 0.0, 0.0, 0.0],
  [0.0, 0.0, 0.0, 0.0, 0.0, 0.0, 0.0, 0.0, 0.0, 0.0, 0.0, 0.0, 0.0, 0.0, 0.0, 0.0,
       1.0, 0.0, 0.0, 0.0, 0.0],
  [0.0, 0.0, 0.0, 0.0, 0.0, 0.0, 0.0, 0.0, 0.0, 0.0, 0.0, 0.0, 0.0, 0.0, 0.0, 0.0,
       0.0, 1.0, 0.0, 0.0, 0.0],
  [0.0, 0.0, -1.0, 0.0, 1.0, 0.0, 0.0, 1.0, 0.0, 0.0, 1.0, 1.0, 1.0, 1.0, 1.0, 0.0,
       0.0, 0.0, 1.0, 1.0, 1.0],
  [0.0, 0.0, -1.0, 0.0, 1.0, 0.0, 0.0, 1.0, 0.0, 0.0, 1.0, 1.0, 1.0, 1.0, 1.0, 0.0,
       0.0, 0.0, 1.0, 1.0, 1.0],
  [0.0, 0.0, -1.0, 0.0, 1.0, 0.0, 0.0, 1.0, 0.0, 0.0, 1.0, 1.0, 1.0, 1.0, 1.0, 0.0,
       0.0, 0.0, 1.0, 1.0, 1.0]
  ]
},
{
  "Name": "FitBias",
```

```
  "Values": [0.0, 0.0003, 0.0006, 0.0001, 0.033, 0.022, 0.001, 0.0, 0.001, 0.0008,
      0.0042, 0.0013, 0.0007, 0.0002, 0.0007, 0.05, 0.02, 0.08, 0.11, 0.01, 0.04],
  "SystematicCorrelationMatrix": [
    [1.0, -1.0, 1.0, -1.0, -1.0, -1.0, 1.0, -1.0, -1.0, -1.0, -1.0, -1.0, 1.0, 1.0,
        -1.0, 1.0, 1.0, -1.0, 1.0, 1.0, 1.0],
    [-1.0, 1.0, -1.0, 1.0, 1.0, 1.0, -1.0, 1.0, 1.0, 1.0, 1.0, 1.0, -1.0, -1.0, 1.0,
        -1.0, -1.0, 1.0, -1.0, -1.0, -1.0],
    [1.0, -1.0, 1.0, -1.0, -1.0, -1.0, 1.0, -1.0, -1.0, -1.0, -1.0, -1.0, 1.0, 1.0,
        -1.0, 1.0, 1.0, -1.0, 1.0, 1.0, 1.0],
    [-1.0, 1.0, -1.0, 1.0, 1.0, 1.0, -1.0, 1.0, 1.0, 1.0, 1.0, 1.0, -1.0, -1.0, 1.0,
        -1.0, -1.0, 1.0, -1.0, -1.0, -1.0],
    [-1.0, 1.0, -1.0, 1.0, 1.0, 1.0, -1.0, 1.0, 1.0, 1.0, 1.0, 1.0, -1.0, -1.0, 1.0,
        -1.0, -1.0, 1.0, -1.0, -1.0, -1.0],
    [-1.0, 1.0, -1.0, 1.0, 1.0, 1.0, -1.0, 1.0, 1.0, 1.0, 1.0, 1.0, -1.0, -1.0, 1.0,
        -1.0, -1.0, 1.0, -1.0, -1.0, -1.0],
    [1.0, -1.0, 1.0, -1.0, -1.0, -1.0, 1.0, -1.0, -1.0, -1.0, -1.0, -1.0, 1.0, 1.0,
        -1.0, 1.0, 1.0, -1.0, 1.0, 1.0, 1.0],
    [-1.0, 1.0, -1.0, 1.0, 1.0, 1.0, -1.0, 1.0, 1.0, 1.0, 1.0, 1.0, -1.0, -1.0, 1.0,
        -1.0, -1.0, 1.0, -1.0, -1.0, -1.0],
    [-1.0, 1.0, -1.0, 1.0, 1.0, 1.0, -1.0, 1.0, 1.0, 1.0, 1.0, 1.0, -1.0, -1.0, 1.0,
        -1.0, -1.0, 1.0, -1.0, -1.0, -1.0],
    [-1.0, 1.0, -1.0, 1.0, 1.0, 1.0, -1.0, 1.0, 1.0, 1.0, 1.0, 1.0, -1.0, -1.0, 1.0,
        -1.0, -1.0, 1.0, -1.0, -1.0, -1.0],
    [-1.0, 1.0, -1.0, 1.0, 1.0, 1.0, -1.0, 1.0, 1.0, 1.0, 1.0, 1.0, -1.0, -1.0, 1.0,
        -1.0, -1.0, 1.0, -1.0, -1.0, -1.0],
    [-1.0, 1.0, -1.0, 1.0, 1.0, 1.0, -1.0, 1.0, 1.0, 1.0, 1.0, 1.0, -1.0, -1.0, 1.0,
        -1.0, -1.0, 1.0, -1.0, -1.0, -1.0],
    [1.0, -1.0, 1.0, -1.0, -1.0, -1.0, 1.0, -1.0, -1.0, -1.0, -1.0, -1.0, 1.0, 1.0,
        -1.0, 1.0, 1.0, -1.0, 1.0, 1.0, 1.0],
    [1.0, -1.0, 1.0, -1.0, -1.0, -1.0, 1.0, -1.0, -1.0, -1.0, -1.0, -1.0, 1.0, 1.0,
        -1.0, 1.0, 1.0, -1.0, 1.0, 1.0, 1.0],
    [-1.0, 1.0, -1.0, 1.0, 1.0, 1.0, -1.0, 1.0, 1.0, 1.0, 1.0, 1.0, -1.0, -1.0, 1.0,
        -1.0, -1.0, 1.0, -1.0, -1.0, -1.0],
    [1.0, -1.0, 1.0, -1.0, -1.0, -1.0, 1.0, -1.0, -1.0, -1.0, -1.0, -1.0, 1.0, 1.0,
        -1.0, 1.0, 1.0, -1.0, 1.0, 1.0, 1.0],
    [1.0, -1.0, 1.0, -1.0, -1.0, -1.0, 1.0, -1.0, -1.0, -1.0, -1.0, -1.0, 1.0, 1.0,
        -1.0, 1.0, 1.0, -1.0, 1.0, 1.0, 1.0],
    [-1.0, 1.0, -1.0, 1.0, 1.0, 1.0, -1.0, 1.0, 1.0, 1.0, 1.0, 1.0, -1.0, -1.0, 1.0,
        -1.0, -1.0, 1.0, -1.0, -1.0, -1.0],
    [1.0, -1.0, 1.0, -1.0, -1.0, -1.0, 1.0, -1.0, -1.0, -1.0, -1.0, -1.0, 1.0, 1.0,
        -1.0, 1.0, 1.0, -1.0, 1.0, 1.0, 1.0],
    [1.0, -1.0, 1.0, -1.0, -1.0, -1.0, 1.0, -1.0, -1.0, -1.0, -1.0, -1.0, 1.0, 1.0,
        -1.0, 1.0, 1.0, -1.0, 1.0, 1.0, 1.0],
    [1.0, -1.0, 1.0, -1.0, -1.0, -1.0, 1.0, -1.0, -1.0, -1.0, -1.0, -1.0, 1.0, 1.0,
        -1.0, 1.0, 1.0, -1.0, 1.0, 1.0, 1.0]
  ]
},
{
  "Name": "MultipleCandidates",
  "Values": [0.00033, 0.00011, 0.00012, 0.0001, 0.0021, 0.0073, 0.0011, 0.0011,
      0.0014, 0.0017, 0.0012, 0.00015, 0.00067, 0.0014, 0.00059, 0.011, 0.0, 0.024,
      0.0068, 0.0041, 0.0072],
  "SystematicCorrelationMatrix": [
    [1.0, -1.0, 1.0, -1.0, -1.0, -1.0, 1.0, -1.0, -1.0, 1.0, -1.0, -1.0, -1.0, -1.0,
        1.0, -1.0, 0.0, 1.0, -1.0, -1.0, -1.0],
    [-1.0, 1.0, -1.0, 1.0, 1.0, 1.0, -1.0, 1.0, 1.0, -1.0, 1.0, 1.0, 1.0, 1.0, -1.0,
        1.0, 0.0, -1.0, 1.0, 1.0, 1.0],
    [1.0, -1.0, 1.0, -1.0, -1.0, -1.0, 1.0, -1.0, -1.0, 1.0, -1.0, -1.0, -1.0, -1.0,
        1.0, -1.0, 0.0, 1.0, -1.0, -1.0, -1.0],
    [-1.0, 1.0, -1.0, 1.0, 1.0, 1.0, -1.0, 1.0, 1.0, -1.0, 1.0, 1.0, 1.0, 1.0, -1.0,
        1.0, 0.0, -1.0, 1.0, 1.0, 1.0],
    [-1.0, 1.0, -1.0, 1.0, 1.0, 1.0, -1.0, 1.0, 1.0, -1.0, 1.0, 1.0, 1.0, 1.0, -1.0,
        1.0, 0.0, -1.0, 1.0, 1.0, 1.0],
    [-1.0, 1.0, -1.0, 1.0, 1.0, 1.0, -1.0, 1.0, 1.0, -1.0, 1.0, 1.0, 1.0, 1.0, -1.0,
        1.0, 0.0, -1.0, 1.0, 1.0, 1.0],
    [1.0, -1.0, 1.0, -1.0, -1.0, -1.0, 1.0, -1.0, -1.0, 1.0, -1.0, -1.0, -1.0, -1.0,
        1.0, -1.0, 0.0, 1.0, -1.0, -1.0, -1.0],
    [-1.0, 1.0, -1.0, 1.0, 1.0, 1.0, -1.0, 1.0, 1.0, -1.0, 1.0, 1.0, 1.0, 1.0, -1.0,
        1.0, 0.0, -1.0, 1.0, 1.0, 1.0],
    [-1.0, 1.0, -1.0, 1.0, 1.0, 1.0, -1.0, 1.0, 1.0, -1.0, 1.0, 1.0, 1.0, 1.0, -1.0,
        1.0, 0.0, -1.0, 1.0, 1.0, 1.0],
    [1.0, -1.0, 1.0, -1.0, -1.0, -1.0, 1.0, -1.0, -1.0, 1.0, -1.0, -1.0, -1.0, -1.0,
        1.0, -1.0, 0.0, 1.0, -1.0, -1.0, -1.0],
    [-1.0, 1.0, -1.0, 1.0, 1.0, 1.0, -1.0, 1.0, 1.0, -1.0, 1.0, 1.0, 1.0, 1.0, -1.0,
        1.0, 0.0, -1.0, 1.0, 1.0, 1.0],
    [-1.0, 1.0, -1.0, 1.0, 1.0, 1.0, -1.0, 1.0, 1.0, -1.0, 1.0, 1.0, 1.0, 1.0, -1.0,
        1.0, 0.0, -1.0, 1.0, 1.0, 1.0],
    [1.0, -1.0, 1.0, -1.0, -1.0, -1.0, 1.0, -1.0, -1.0, 1.0, -1.0, -1.0, -1.0, -1.0,
        1.0, -1.0, 0.0, 1.0, -1.0, -1.0, -1.0],
    [-1.0, 1.0, -1.0, 1.0, 1.0, 1.0, -1.0, 1.0, 1.0, -1.0, 1.0, 1.0, 1.0, 1.0, -1.0,
        1.0, 0.0, -1.0, 1.0, 1.0, 1.0],
    [-1.0, 1.0, -1.0, 1.0, 1.0, 1.0, -1.0, 1.0, 1.0, -1.0, 1.0, 1.0, 1.0, 1.0, -1.0,
        1.0, 0.0, -1.0, 1.0, 1.0, 1.0],
    [1.0, -1.0, 1.0, -1.0, -1.0, -1.0, 1.0, -1.0, -1.0, 1.0, -1.0, -1.0, -1.0, -1.0,
        1.0, -1.0, 0.0, 1.0, -1.0, -1.0, -1.0],
    [-1.0, 1.0, -1.0, 1.0, 1.0, 1.0, -1.0, 1.0, 1.0, -1.0, 1.0, 1.0, 1.0, 1.0, -1.0,
        1.0, 0.0, -1.0, 1.0, 1.0, 1.0],
    [-1.0, 1.0, -1.0, 1.0, 1.0, 1.0, -1.0, 1.0, 1.0, -1.0, 1.0, 1.0, 1.0, 1.0, -1.0,
        1.0, 0.0, -1.0, 1.0, 1.0, 1.0],
```

```
            [-1.0, 1.0, -1.0, 1.0, 1.0, 1.0, -1.0, 1.0, 1.0, -1.0, 1.0, 1.0, 1.0, 1.0, -1.0,
                1.0, 0.0, -1.0, 1.0, 1.0, 1.0],
            [-1.0, 1.0, -1.0, 1.0, 1.0, 1.0, -1.0, 1.0, 1.0, -1.0, 1.0, 1.0, 1.0, 1.0, -1.0,
                1.0, 0.0, -1.0, 1.0, 1.0, 1.0],
            [1.0, -1.0, 1.0, -1.0, -1.0, -1.0, 1.0, -1.0, -1.0, 1.0, -1.0, -1.0, -1.0, -1.0,
                1.0, -1.0, 0.0, 1.0, -1.0, -1.0, -1.0],
            [-1.0, 1.0, -1.0, 1.0, 1.0, 1.0, -1.0, 1.0, 1.0, -1.0, 1.0, 1.0, 1.0, 1.0, -1.0,
                1.0, 0.0, -1.0, 1.0, 1.0, 1.0],
            [0.0, 0.0, 0.0, 0.0, 0.0, 0.0, 0.0, 0.0, 0.0, 0.0, 0.0, 0.0, 0.0, 0.0, 0.0, 0.0,
                1.0, 0.0, 0.0, 0.0, 0.0],
            [1.0, -1.0, 1.0, -1.0, -1.0, -1.0, 1.0, -1.0, -1.0, 1.0, -1.0, -1.0, -1.0, -1.0,
                1.0, -1.0, 0.0, 1.0, -1.0, -1.0, -1.0],
            [-1.0, 1.0, -1.0, 1.0, 1.0, 1.0, -1.0, 1.0, 1.0, -1.0, 1.0, 1.0, 1.0, 1.0, -1.0,
                1.0, 0.0, -1.0, 1.0, 1.0, 1.0],
            [-1.0, 1.0, -1.0, 1.0, 1.0, 1.0, -1.0, 1.0, 1.0, -1.0, 1.0, 1.0, 1.0, 1.0, -1.0,
                1.0, 0.0, -1.0, 1.0, 1.0, 1.0],
            [-1.0, 1.0, -1.0, 1.0, 1.0, 1.0, -1.0, 1.0, 1.0, -1.0, 1.0, 1.0, 1.0, 1.0, -1.0,
                1.0, 0.0, -1.0, 1.0, 1.0, 1.0]
          ]
          },
        {
          "Name": "QuadOSTagging",
          "Values": [0.0, 0.0, 0.0, 0.0, 0.0, 0.0, 0.0, 0.0, 0.0, 0.0, 0.0, 0.0, 0.0002, 0.0,
              0.0, 0.0, 0.003, 0.001, 0.001, 0.0, 0.001],
          "SystematicCorrelationMatrix": [
            [1.0, 0.0, 0.0, 0.0, 0.0, 0.0, 0.0, 0.0, 0.0, 0.0, 0.0, 0.0, 0.0, 0.0, 0.0, 0.0,
                0.0, 0.0, 0.0, 0.0, 0.0],
            [0.0, 1.0, 0.0, 0.0, 0.0, 0.0, 0.0, 0.0, 0.0, 0.0, 0.0, 0.0, 0.0, 0.0, 0.0, 0.0,
                0.0, 0.0, 0.0, 0.0, 0.0],
            [0.0, 0.0, 1.0, 0.0, 0.0, 0.0, 0.0, 0.0, 0.0, 0.0, 0.0, 0.0, 0.0, 0.0, 0.0, 0.0,
                0.0, 0.0, 0.0, 0.0, 0.0],
            [0.0, 0.0, 0.0, 1.0, 0.0, 0.0, 0.0, 0.0, 0.0, 0.0, 0.0, 0.0, 0.0, 0.0, 0.0, 0.0,
                0.0, 0.0, 0.0, 0.0, 0.0],
            [0.0, 0.0, 0.0, 0.0, 1.0, 0.0, 0.0, 0.0, 0.0, 0.0, 0.0, 0.0, 0.0, 0.0, 0.0, 0.0,
                0.0, 0.0, 0.0, 0.0, 0.0],
            [0.0, 0.0, 0.0, 0.0, 0.0, 1.0, 0.0, 0.0, 0.0, 0.0, 0.0, 0.0, 0.0, 0.0, 0.0, 0.0,
                0.0, 0.0, 0.0, 0.0, 0.0],
            [0.0, 0.0, 0.0, 0.0, 0.0, 0.0, 1.0, 0.0, 0.0, 0.0, 0.0, 0.0, 0.0, 0.0, 0.0, 0.0,
                0.0, 0.0, 0.0, 0.0, 0.0],
            [0.0, 0.0, 0.0, 0.0, 0.0, 0.0, 0.0, 1.0, 0.0, 0.0, 0.0, 0.0, 0.0, 0.0, 0.0, 0.0,
                0.0, 0.0, 0.0, 0.0, 0.0],
            [0.0, 0.0, 0.0, 0.0, 0.0, 0.0, 0.0, 0.0, 1.0, 0.0, 0.0, 0.0, 0.0, 0.0, 0.0, 0.0,
                0.0, 0.0, 0.0, 0.0, 0.0],
            [0.0, 0.0, 0.0, 0.0, 0.0, 0.0, 0.0, 0.0, 0.0, 1.0, 0.0, 0.0, 0.0, 0.0, 0.0, 0.0,
                0.0, 0.0, 0.0, 0.0, 0.0],
            [0.0, 0.0, 0.0, 0.0, 0.0, 0.0, 0.0, 0.0, 0.0, 0.0, 1.0, 0.0, 0.0, 0.0, 0.0, 0.0,
                0.0, 0.0, 0.0, 0.0, 0.0],
            [0.0, 0.0, 0.0, 0.0, 0.0, 0.0, 0.0, 0.0, 0.0, 0.0, 0.0, 1.0, 0.0, 0.0, 0.0, 0.0,
                0.0, 0.0, 0.0, 0.0, 0.0],
            [0.0, 0.0, 0.0, 0.0, 0.0, 0.0, 0.0, 0.0, 0.0, 0.0, 0.0, 0.0, 1.0, 0.0, 0.0, 0.0,
                1.0, 1.0, 1.0, 0.0, 1.0],
            [0.0, 0.0, 0.0, 0.0, 0.0, 0.0, 0.0, 0.0, 0.0, 0.0, 0.0, 0.0, 0.0, 1.0, 0.0, 0.0,
                0.0, 0.0, 0.0, 0.0, 0.0],
            [0.0, 0.0, 0.0, 0.0, 0.0, 0.0, 0.0, 0.0, 0.0, 0.0, 0.0, 0.0, 0.0, 0.0, 1.0, 0.0,
                0.0, 0.0, 0.0, 0.0, 0.0],
            [0.0, 0.0, 0.0, 0.0, 0.0, 0.0, 0.0, 0.0, 0.0, 0.0, 0.0, 0.0, 0.0, 0.0, 0.0, 1.0,
                0.0, 0.0, 0.0, 0.0, 0.0],
            [0.0, 0.0, 0.0, 0.0, 0.0, 0.0, 0.0, 0.0, 0.0, 0.0, 0.0, 0.0, 1.0, 0.0, 0.0, 0.0,
                1.0, 1.0, 1.0, 0.0, 1.0],
            [0.0, 0.0, 0.0, 0.0, 0.0, 0.0, 0.0, 0.0, 0.0, 0.0, 0.0, 0.0, 1.0, 0.0, 0.0, 0.0,
                1.0, 1.0, 1.0, 0.0, 1.0],
            [0.0, 0.0, 0.0, 0.0, 0.0, 0.0, 0.0, 0.0, 0.0, 0.0, 0.0, 0.0, 1.0, 0.0, 0.0, 0.0,
                1.0, 1.0, 1.0, 0.0, 1.0],
            [0.0, 0.0, 0.0, 0.0, 0.0, 0.0, 0.0, 0.0, 0.0, 0.0, 0.0, 0.0, 0.0, 0.0, 0.0, 0.0,
                0.0, 0.0, 0.0, 1.0, 0.0],
            [0.0, 0.0, 0.0, 0.0, 0.0, 0.0, 0.0, 0.0, 0.0, 0.0, 0.0, 0.0, 1.0, 0.0, 0.0, 0.0,
                1.0, 1.0, 1.0, 0.0, 1.0]
          ]
        }
      ]
}
,
{
  "ResultSetLabel": "GammaD",
  "Description" : ["GammaD"],
  "Parameter": [
    {
```

```
            "Name": "gammaD",
            "Value": 0.65833,
            "Error": 0.00173
        }
    ]
}
```


The JSON that is used in the combination of all LHCb $\phi_s^{\bar{c}c\bar{s}}$ analyses [1, 56, 94–98] is shown below.


```
{
        "ResultSet": [
{
    "ResultSetLabel": "2012-JPsiKK",
    "Description" : [
        "Contains the final 2012 3fb results for phis et. al. from JPsiKK",
        "The parameter values, stat and syst errors, and statistical correlation matrix
            taken",
        "from the paper LHCb-PAPER-2014-059",
        "The systematic error correlation matrices are from private communication"
    ],
    "Parameter": [
      {
        "Name": "gamma",
        "Value": 0.6603,
        "Error": 0.0027
      },
      {
        "Name": "deltaGammas",
        "Value": 0.0805,
        "Error": 0.0091
      },
      {
        "Name": "AperpSq",
        "Value": 0.2504,
        "Error": 0.0049
      },
      {
        "Name": "AzeroSq",
        "Value": 0.5241,
        "Error": 0.0034
      },
      {
        "Name": "para",
        "Value": 3.258,
        "Error": 0.17
      },
      {
        "Name": "perp",
        "Value": 3.08,
        "Error": 0.15
      },
      {
        "Name": "phis",
        "Value": -0.058,
        "Error": 0.049
      },
      {
        "Name": "lamb",
        "Value": 0.964,
        "Error": 0.019
      },
      {
        "Name": "dms",
        "Value": 17.711,
        "Error": 0.057
      }
    ],
    "StatisticalCorrelationMatrix": [
      [ 1.00  , -0.45 ,  0.39 , -0.31 , -0.07 , -0.02 ,  0.01 , -0.01,  0.01 ],
      [-0.45  ,  1.00 , -0.69 ,  0.65 ,  0.02 , -0.03 , -0.08 ,  0.02, -0.03 ],
      [ 0.39  , -0.69 ,  1.00 , -0.59 , -0.29 , -0.1  ,  0.04 , -0.03,  0.0  ],
      [-0.31  ,  0.65 , -0.59 ,  1.00 , -0.02 , -0.04 , -0.03 ,  0.02, -0.03 ],
      [-0.07  ,  0.02 , -0.29 , -0.02 ,  1.00 ,  0.42 ,  0.01 ,  0.05,  0.05 ],
      [-0.02  , -0.03 , -0.1  , -0.04 ,  0.42 ,  1.00 ,  0.14 , -0.17,  0.67 ],
```

```
    [ 0.01  , -0.08 ,  0.04 , -0.03 ,  0.01 ,  0.14 ,  1.00 , -0.02,  0.09 ],
    [-0.01  ,  0.02 , -0.03 ,  0.02 ,  0.05 , -0.17 , -0.02 ,  1.00, -0.21 ],
    [ 0.01  , -0.03 ,  0.0  , -0.03 ,  0.05 ,  0.67 ,  0.09 , -0.21,  1.00 ]
  ],
  "SystematicErrors": [
    {
      "Name": "MassFactorisationCosThMu",
      "Values": [0.0, 0.0007, 0.0031, 0.0064, 0.05, 0.05, 0.002, 0.001, 0.004],
      "SystematicCorrelationMatrix": [
        [1.0, 1.0, -1.0, 1.0, -1.0, -1.0, -1.0, 1.0, -1.0],
        [1.0, 1.0, -1.0, 1.0, -1.0, -1.0, -1.0, 1.0, -1.0],
        [-1.0, -1.0, 1.0, -1.0, 1.0, 1.0, 1.0, -1.0, 1.0],
        [1.0, 1.0, -1.0, 1.0, -1.0, -1.0, -1.0, 1.0, -1.0],
        [-1.0, -1.0, 1.0, -1.0, 1.0, 1.0, 1.0, -1.0, 1.0],
        [-1.0, -1.0, 1.0, -1.0, 1.0, 1.0, 1.0, -1.0, 1.0],
        [-1.0, -1.0, 1.0, -1.0, 1.0, 1.0, 1.0, -1.0, 1.0],
        [1.0, 1.0, -1.0, 1.0, -1.0, -1.0, -1.0, 1.0, -1.0],
        [-1.0, -1.0, 1.0, -1.0, 1.0, 1.0, 1.0, -1.0, 1.0]
      ]
    },
    {
      "Name": "SignalWeights",
      "Values": [0.0001, 0.0008, 0.0, 0.0001, 0.002, 0.001, 0.0, 0.0, 0.0]
    },
    {
      "Name": "ResonantBackground",
      "Values": [0.0001, 0.0004, 0.0004, 0.0002, 0.02, 0.02, 0.002, 0.003, 0.001]
    },
    {
      "Name": "AngEfficiencyReweighting",
      "Values": [0.0001, 0.0, 0.0011, 0.002, 0.01, 0.0, 0.001, 0.005, 0.002],
      "SystematicCorrelationMatrix": [
        [  1.0,  0.81, 0.98, -0.97,  0.84, 0.82,  0.17,  0.38, 0.79],
        [ 0.81,   1.0, 0.90, -0.91,  0.74, 0.50, -0.24,-0.025, 0.62],
        [ 0.98,  0.90,  1.0,  -1.0,  0.84, 0.74,  0.04,  0.25, 0.75],
        [-0.97, -0.91, -1.0,   1.0, -0.83,-0.74,-0.038, -0.23,-0.77],
        [ 0.84,  0.74, 0.84, -0.83,   1.0, 0.68,-0.042,  0.33, 0.47],
        [ 0.82,  0.50, 0.74, -0.74,  0.68,  1.0,  0.65,  0.69, 0.86],
        [ 0.17, -0.24, 0.04,-0.038,-0.042, 0.65,   1.0,  0.78, 0.51],
        [ 0.38,-0.025, 0.25, -0.23,  0.33, 0.69,  0.78,   1.0, 0.35],
        [ 0.79,  0.62, 0.75, -0.77,  0.47, 0.86,  0.51,  0.35,  1.0]
      ]
    },
    {
      "Name": "AngEfficiencyStat",
      "Values": [0.0001, 0.0002, 0.0011, 0.0004, 0.02, 0.01, 0.004, 0.002, 0.001 ],
      "SystematicCorrelationMatrix": [
        [    1.0, 0.0,   0.89,  -0.22, -0.0071, -0.028,  0.027, -0.033,   0.14],
        [    0.0, 1.0,    0.0,    0.0,    0.0,    0.0,    0.0,    0.0,    0.0],
        [   0.89, 0.0,    1.0,  -0.36,  -0.027,  -0.12, -0.058,  0.025, -0.065],
        [  -0.22, 0.0,  -0.36,    1.0,   0.14,  0.054, 0.0054, -0.040, -0.097],
        [-0.0071, 0.0, -0.027,   0.14,    1.0,   0.60,  0.029, -0.013,  -0.19],
        [ -0.028, 0.0,  -0.12,  0.054,   0.60,    1.0,   0.72,  -0.48,   0.51],
        [  0.027, 0.0, -0.058, 0.0054,  0.029,   0.72,    1.0,  -0.58,   0.82],
        [ -0.033, 0.0,  0.025, -0.040,  -0.013,  -0.48,  -0.58,    1.0,  -0.76],
        [   0.14, 0.0, -0.065, -0.097,   -0.19,   0.51,   0.82,  -0.76,    1.0]
      ]
    },
    {
      "Name": "DecayTimeResolutionPromptKKRun1",
      "Values": [0.0, 0.0, 0.0, 0.0, 0.0, 0.01, 0.002, 0.001, 0.005]
    },
    {
      "Name": "TriggerEfficiencyStat",
      "Values": [0.0011, 0.0009, 0.0, 0.0, 0.0, 0.0, 0.0, 0.0, 0.0]
    },
    {
      "Name": "TrackReconstructionSimul",
      "Values": [0.0007, 0.0029, 0.0005, 0.0006, 0.01, 0.001, 0.001, 0.001, 0.006],
      "SystematicCorrelationMatrix": [
        [1.0, 1.0, -1.0, 1.0, -1.0, -1.0, -1.0, 1.0, 1.0],
        [1.0, 1.0, -1.0, 1.0, -1.0, -1.0, -1.0, 1.0, 1.0],
        [-1.0, -1.0, 1.0, -1.0, 1.0, 1.0, 1.0, -1.0, -1.0],
        [1.0, 1.0, -1.0, 1.0, -1.0, -1.0, -1.0, 1.0, 1.0],
        [-1.0, -1.0, 1.0, -1.0, 1.0, 1.0, 1.0, -1.0, -1.0],
        [-1.0, -1.0, 1.0, -1.0, 1.0, 1.0, 1.0, -1.0, -1.0],
        [-1.0, -1.0, 1.0, -1.0, 1.0, 1.0, 1.0, -1.0, -1.0],
```

```
            [1.0, 1.0, -1.0, 1.0, -1.0, -1.0, -1.0, 1.0, 1.0],
            [1.0, 1.0, -1.0, 1.0, -1.0, -1.0, -1.0, 1.0, 1.0]
          ]
        },
        {
          "Name": "TrackReconstructionStat",
          "Values": [ 0.0005, 0.0002, 0.0, 0.0, 0.0, 0.0, 0.0, 0.0, 0.001 ]
        },
        {
          "Name": "LengthMomentumScales",
          "Values": [ 0.0002, 0.0, 0.0, 0.0, 0.0, 0.0, 0.0, 0.0, 0.005 ]
        },
        {
          "Name": "SPCouplingFactors",
          "Values": [ 0.0, 0.0, 0.0, 0.0, 0.01, 0.01, 0.0, 0.001, 0.002 ]
        },
        {
          "Name": "AngularResolution",
          "Values": [ 0.0, 0.0, 0.0006, 0.0001, 0.03, 0.01, 0.0, 0.0, 0.0 ]
        },
        {
          "Name": "Bc",
          "Values": [0.0005, 0.0, 0.0, 0.0, 0.0, 0.0, 0.0, 0.0, 0.0]
        },
        {
          "Name": "FitBias",
          "Values": [ 0.0, 0.0, 0.0005, 0.0, 0.0, 0.01, 0.0, 0.001, 0.0 ],
          "SystematicCorrelationMatrix": [
          [1.0, 0.0, 0.0, 0.0, 0.0, 0.0, 0.0, 0.0, 0.0],
          [0.0, 1.0, 0.0, 0.0, 0.0, 0.0, 0.0, 0.0, 0.0],
          [0.0, 0.0, 1.0, 0.0, 0.0, 1.0, 0.0, 1.0, 0.0],
          [0.0, 0.0, 0.0, 1.0, 0.0, 0.0, 0.0, 0.0, 0.0],
          [0.0, 0.0, 0.0, 0.0, 1.0, 0.0, 0.0, 0.0, 0.0],
          [0.0, 0.0, 1.0, 0.0, 0.0, 1.0, 0.0, 1.0, 0.0],
          [0.0, 0.0, 0.0, 0.0, 0.0, 0.0, 1.0, 0.0, 0.0],
          [0.0, 0.0, 1.0, 0.0, 0.0, 1.0, 0.0, 1.0, 0.0],
          [0.0, 0.0, 0.0, 0.0, 0.0, 0.0, 0.0, 0.0, 1.0]
          ]
        }
      ]
}
,
{
      "ResultSetLabel": "2016-JPsiKK",
      "Description" : [
         "Contains the 2015-2016 2fb results for phis et. al. from polarisation independent
             nominal fit"
      ],
      "Parameter": [
        {
          "Name": "gsgd",
          "Value": -0.0041,
          "Error": 0.0024
        },
        {
          "Name": "deltaGammas",
          "Value": 0.0773,
          "Error": 0.0077
        },
        {
          "Name": "AperpSq",
          "Value": 0.2456,
          "Error": 0.0040
        },
        {
          "Name": "AzeroSq",
          "Value": 0.5186,
          "Error": 0.0029
        },
        {
          "Name": "para",
          "Value": 3.062,
          "Error": 0.082
        },
        {
          "Name": "perp",
          "Value": 2.64,
```

```
  "Error": 0.13
},
{
  "Name": "phis",
  "Value": -0.083,
  "Error": 0.041
},
{
  "Name": "lamb",
  "Value": 1.012,
  "Error": 0.016
},
{
  "Name": "dms",
  "Value": 17.703,
  "Error": 0.059
},
{
  "Name": "FS1",
  "Value": 0.492,
  "Error": 0.043
},
{
  "Name": "FS2",
  "Value": 0.041,
  "Error": 0.008
},
{
  "Name": "FS3",
  "Value": 0.0044,
  "Error": 0.0030
},
{
  "Name": "FS4",
  "Value": 0.0069,
  "Error": 0.0062
},
{
  "Name": "FS5",
  "Value": 0.073,
  "Error": 0.013
},
{
  "Name": "FS6",
  "Value": 0.152,
  "Error": 0.019
},
{
  "Name": "deltaS1",
  "Value": 2.21,
  "Error": 0.20
},
{
  "Name": "deltaS2",
  "Value": 1.56,
  "Error": 0.29
},
{
  "Name": "deltaS3",
  "Value": 1.09,
  "Error": 0.47
},
{
  "Name": "deltaS4",
  "Value": -0.28,
  "Error": 0.26
},
{
  "Name": "deltaS5",
  "Value": -0.54,
  "Error": 0.10
},
{
  "Name": "deltaS6",
  "Value": -1.10,
  "Error": 0.16
}
```

```
],
"StatisticalCorrelationMatrix":
[
[1.0, -0.47, 0.39, -0.32, 0.03, -0.0, -0.03, 0.02, -0.01, 0.05, 0.04, 0.03, 0.03, 0.07,
  0.06, 0.01, -0.0, -0.02, 0.01, 0.02, 0.01],
[-0.47, 1.0, -0.69, 0.63, -0.01, 0.01, -0.01, -0.04, 0.02, -0.07, -0.05, -0.02, 0.03,
  -0.06, -0.06, -0.0, 0.01, 0.01, 0.01, 0.0, 0.0],
[0.39, -0.69, 1.0, -0.6, 0.12, 0.0, -0.02, 0.02, -0.03, 0.04, -0.02, -0.02, -0.05,
  0.01, 0.03, 0.02, -0.01, 0.01, -0.02, 0.0, 0.02],
[-0.32, 0.63, -0.6, 1.0, 0.0, 0.01, 0.02, -0.02, 0.01, -0.05, -0.01, 0.01, 0.05, -0.01,
  -0.03, -0.0, 0.01, -0.01, 0.02, 0.01, 0.01],
[0.03, -0.01, 0.12, 0.0, 1.0, 0.2, 0.01, -0.0, -0.04, 0.01, -0.01, 0.04, 0.02, 0.03,
  0.0, -0.02, -0.03, -0.04, 0.0, -0.01, -0.03],
[-0.0, 0.01, 0.0, 0.01, 0.2, 1.0, 0.0, 0.07, 0.74, -0.01, -0.01, 0.01, 0.04, 0.03,
  -0.07, -0.06, -0.18, -0.01, -0.01, -0.0, -0.16],
[-0.03, -0.01, -0.02, 0.02, 0.01, 0.0, 1.0, 0.19, 0.01, -0.0, 0.01, 0.04, -0.03, -0.01,
  -0.02, 0.0, -0.05, -0.04, -0.01, -0.0, -0.01],
[0.02, -0.04, 0.02, -0.02, -0.0, 0.07, 0.19, 1.0, -0.0, 0.01, 0.02, 0.13, -0.09, -0.01,
  0.02, 0.05, -0.17, -0.14, -0.07, -0.03, 0.02],
[-0.01, 0.02, -0.03, 0.01, -0.04, 0.74, 0.01, -0.0, 1.0, -0.01, -0.01, -0.07, 0.1,
  0.06, -0.03, -0.02, -0.08, 0.1, 0.05, 0.07, -0.05],
[0.05, -0.07, 0.04, -0.05, 0.01, -0.01, -0.0, 0.01, -0.01, 1.0, 0.0, 0.0, -0.0, 0.0,
  0.01, 0.08, -0.0, -0.0, -0.0, -0.0, 0.0],
[0.04, -0.05, -0.02, -0.01, -0.01, -0.01, 0.01, 0.02, -0.01, 0.0, 1.0, 0.01, 0.0, 0.01,
  0.01, -0.0, 0.08, -0.0, -0.0, -0.0, 0.0],
[0.03, -0.02, -0.02, 0.01, 0.04, 0.01, 0.04, 0.13, -0.07, 0.0, 0.01, 1.0, -0.02, -0.0,
  0.0, 0.0, -0.03, -0.73, -0.02, -0.01, -0.01],
[0.03, 0.03, -0.05, 0.05, 0.02, 0.04, -0.03, -0.09, 0.1, -0.0, 0.0, -0.02, 1.0, 0.02,
  0.0, -0.0, 0.01, 0.03, 0.46, 0.01, 0.0],
[0.07, -0.06, 0.01, -0.01, 0.03, 0.03, -0.01, -0.01, 0.06, 0.0, 0.01, -0.0, 0.02, 1.0,
  0.01, -0.0, 0.0, 0.01, 0.01, 0.45, 0.0],
[0.06, -0.06, 0.03, -0.03, 0.0, -0.07, -0.02, 0.02, -0.03, 0.01, 0.01, 0.0, 0.0, 0.01,
  1.0, 0.01, 0.01, 0.0, 0.01, 0.0, 0.43],
[0.01, -0.0, 0.02, -0.0, -0.02, -0.06, 0.0, 0.05, -0.02, 0.08, -0.0, 0.0, -0.0, -0.0,
  0.01, 1.0, 0.01, 0.0, 0.0, 0.0, 0.02],
[-0.0, 0.01, -0.01, 0.01, -0.03, -0.18, -0.05, -0.17, -0.08, -0.0, 0.08, -0.03, 0.01,
  0.0, 0.01, 0.01, 1.0, 0.03, 0.02, 0.01, 0.03],
[-0.02, 0.01, 0.01, -0.01, -0.04, -0.01, -0.04, -0.14, 0.1, -0.0, -0.0, -0.73, 0.03,
  0.01, 0.0, 0.0, 0.03, 1.0, 0.02, 0.02, 0.02],
[0.01, 0.01, -0.02, 0.02, 0.0, -0.01, -0.01, -0.07, 0.05, -0.0, -0.0, -0.02, 0.46,
  0.01, 0.01, 0.0, 0.02, 0.02, 1.0, 0.01, 0.01],
[0.02, 0.0, 0.0, 0.01, -0.01, -0.0, -0.0, -0.03, 0.07, -0.0, -0.0, -0.01, 0.01, 0.45,
  0.0, 0.0, 0.01, 0.02, 0.01, 1.0, 0.01],
[0.01, 0.0, 0.02, 0.01, -0.03, -0.16, -0.01, 0.02, -0.05, 0.0, 0.0, -0.01, 0.0, 0.0,
  0.43, 0.02, 0.03, 0.02, 0.01, 0.01, 1.0]]
,
"SystematicErrors": [
  {
    "Name": "MassFactorisationTime",
    "Values": [0.0007, 0.0022, 0.0005, 0.0002, 0.0093, 0.0465, 0.004, 0.0037, 0.0156,
        0.0056, 0.0006, 0.0, 0.0004, 0.0018, 0.0025, 0.0803, 0.025, 0.0186, 0.009,
        0.0075, 0.0333],
    "SystematicCorrelationMatrix": [
    [1.0, -1.0, 1.0, 1.0, 1.0, 1.0, -1.0, 1.0, 1.0, -1.0, 1.0, 0.0, 1.0, 1.0, 1.0,
        -1.0, -1.0, -1.0, -1.0, -1.0, -1.0],
    [-1.0, 1.0, -1.0, -1.0, -1.0, -1.0, 1.0, -1.0, -1.0, 1.0, -1.0, 0.0, -1.0, -1.0,
        -1.0, 1.0, 1.0, 1.0, 1.0, 1.0, 1.0],
    [1.0, -1.0, 1.0, 1.0, 1.0, 1.0, -1.0, 1.0, 1.0, -1.0, 1.0, 0.0, 1.0, 1.0, 1.0,
        -1.0, -1.0, -1.0, -1.0, -1.0, -1.0],
    [1.0, -1.0, 1.0, 1.0, 1.0, 1.0, -1.0, 1.0, 1.0, -1.0, 1.0, 0.0, 1.0, 1.0, 1.0,
        -1.0, -1.0, -1.0, -1.0, -1.0, -1.0],
    [1.0, -1.0, 1.0, 1.0, 1.0, 1.0, -1.0, 1.0, 1.0, -1.0, 1.0, 0.0, 1.0, 1.0, 1.0,
        -1.0, -1.0, -1.0, -1.0, -1.0, -1.0],
    [1.0, -1.0, 1.0, 1.0, 1.0, 1.0, -1.0, 1.0, 1.0, -1.0, 1.0, 0.0, 1.0, 1.0, 1.0,
        -1.0, -1.0, -1.0, -1.0, -1.0, -1.0],
    [-1.0, 1.0, -1.0, -1.0, -1.0, -1.0, 1.0, -1.0, -1.0, 1.0, -1.0, 0.0, -1.0, -1.0,
        -1.0, 1.0, 1.0, 1.0, 1.0, 1.0, 1.0],
    [1.0, -1.0, 1.0, 1.0, 1.0, 1.0, -1.0, 1.0, 1.0, -1.0, 1.0, 0.0, 1.0, 1.0, 1.0,
        -1.0, -1.0, -1.0, -1.0, -1.0, -1.0],
    [1.0, -1.0, 1.0, 1.0, 1.0, 1.0, -1.0, 1.0, 1.0, -1.0, 1.0, 0.0, 1.0, 1.0, 1.0,
        -1.0, -1.0, -1.0, -1.0, -1.0, -1.0],
    [-1.0, 1.0, -1.0, -1.0, -1.0, -1.0, 1.0, -1.0, -1.0, 1.0, -1.0, 0.0, -1.0, -1.0,
        -1.0, 1.0, 1.0, 1.0, 1.0, 1.0, 1.0],
    [1.0, -1.0, 1.0, 1.0, 1.0, 1.0, -1.0, 1.0, 1.0, -1.0, 1.0, 0.0, 1.0, 1.0, 1.0,
        -1.0, -1.0, -1.0, -1.0, -1.0, -1.0],
    [0.0, 0.0, 0.0, 0.0, 0.0, 0.0, 0.0, 0.0, 0.0, 0.0, 1.0, 0.0, 0.0, 0.0, 0.0,
        0.0, 0.0, 0.0, 0.0, 0.0],
```

```
  [1.0, -1.0, 1.0, 1.0, 1.0, 1.0, -1.0, 1.0, 1.0, -1.0, 1.0, 0.0, 1.0, 1.0, 1.0,
       -1.0, -1.0, -1.0, -1.0, -1.0, -1.0],
  [1.0, -1.0, 1.0, 1.0, 1.0, 1.0, -1.0, 1.0, 1.0, -1.0, 1.0, 0.0, 1.0, 1.0, 1.0,
       -1.0, -1.0, -1.0, -1.0, -1.0, -1.0],
  [1.0, -1.0, 1.0, 1.0, 1.0, 1.0, -1.0, 1.0, 1.0, -1.0, 1.0, 0.0, 1.0, 1.0, 1.0,
       -1.0, -1.0, -1.0, -1.0, -1.0, -1.0],
  [-1.0, 1.0, -1.0, -1.0, -1.0, -1.0, 1.0, -1.0, -1.0, 1.0, -1.0, 0.0, -1.0, -1.0,
       -1.0, 1.0, 1.0, 1.0, 1.0, 1.0, 1.0],
  [-1.0, 1.0, -1.0, -1.0, -1.0, -1.0, 1.0, -1.0, -1.0, 1.0, -1.0, 0.0, -1.0, -1.0,
       -1.0, 1.0, 1.0, 1.0, 1.0, 1.0, 1.0],
  [-1.0, 1.0, -1.0, -1.0, -1.0, -1.0, 1.0, -1.0, -1.0, 1.0, -1.0, 0.0, -1.0, -1.0,
       -1.0, 1.0, 1.0, 1.0, 1.0, 1.0, 1.0],
  [-1.0, 1.0, -1.0, -1.0, -1.0, -1.0, 1.0, -1.0, -1.0, 1.0, -1.0, 0.0, -1.0, -1.0,
       -1.0, 1.0, 1.0, 1.0, 1.0, 1.0, 1.0],
  [-1.0, 1.0, -1.0, -1.0, -1.0, -1.0, 1.0, -1.0, -1.0, 1.0, -1.0, 0.0, -1.0, -1.0,
       -1.0, 1.0, 1.0, 1.0, 1.0, 1.0, 1.0],
  [-1.0, 1.0, -1.0, -1.0, -1.0, -1.0, 1.0, -1.0, -1.0, 1.0, -1.0, 0.0, -1.0, -1.0,
       -1.0, 1.0, 1.0, 1.0, 1.0, 1.0, 1.0]
  ]
},
{
  "Name": "MassShape",
  "Values": [0.0, 0.0002, 0.0004, 0.0006, 0.0033, 0.0, 0.0, 0.0, 0.0012, 0.0049,
       0.0006, 0.0001, 0.0008, 0.0031, 0.005, 0.0054, 0.0014, 0.0141, 0.014, 0.0097,
       0.0117],
  "SystematicCorrelationMatrix": [
  [1.0, 0.0, 0.0, 0.0, 0.0, 0.0, 0.0, 0.0, 0.0, 0.0, 0.0, 0.0, 0.0, 0.0, 0.0, 0.0,
       0.0, 0.0, 0.0, 0.0, 0.0],
  [0.0, 1.0, -1.0, 1.0, 1.0, 1.0, 0.0, 0.0, 1.0, 1.0, 1.0, 1.0, 1.0, 1.0, 1.0, -1.0,
       1.0, -1.0, 1.0, 1.0, 1.0],
  [0.0, -1.0, 1.0, -1.0, -1.0, -1.0, 0.0, 0.0, -1.0, -1.0, -1.0, -1.0, -1.0, -1.0,
       -1.0, 1.0, -1.0, 1.0, -1.0, -1.0, -1.0],
  [0.0, 1.0, -1.0, 1.0, 1.0, 1.0, 0.0, 0.0, 1.0, 1.0, 1.0, 1.0, 1.0, 1.0, 1.0, -1.0,
       1.0, -1.0, 1.0, 1.0, 1.0],
  [0.0, 1.0, -1.0, 1.0, 1.0, 1.0, 0.0, 0.0, 1.0, 1.0, 1.0, 1.0, 1.0, 1.0, 1.0, -1.0,
       1.0, -1.0, 1.0, 1.0, 1.0],
  [0.0, 1.0, -1.0, 1.0, 1.0, 1.0, 0.0, 0.0, 1.0, 1.0, 1.0, 1.0, 1.0, 1.0, 1.0, -1.0,
       1.0, -1.0, 1.0, 1.0, 1.0],
  [0.0, 0.0, 0.0, 0.0, 0.0, 0.0, 1.0, 0.0, 0.0, 0.0, 0.0, 0.0, 0.0, 0.0, 0.0, 0.0,
       0.0, 0.0, 0.0, 0.0, 0.0],
  [0.0, 0.0, 0.0, 0.0, 0.0, 0.0, 0.0, 1.0, 0.0, 0.0, 0.0, 0.0, 0.0, 0.0, 0.0, 0.0,
       0.0, 0.0, 0.0, 0.0, 0.0],
  [0.0, 1.0, -1.0, 1.0, 1.0, 1.0, 0.0, 0.0, 1.0, 1.0, 1.0, 1.0, 1.0, 1.0, 1.0, -1.0,
       1.0, -1.0, 1.0, 1.0, 1.0],
  [0.0, 1.0, -1.0, 1.0, 1.0, 1.0, 0.0, 0.0, 1.0, 1.0, 1.0, 1.0, 1.0, 1.0, 1.0, -1.0,
       1.0, -1.0, 1.0, 1.0, 1.0],
  [0.0, 1.0, -1.0, 1.0, 1.0, 1.0, 0.0, 0.0, 1.0, 1.0, 1.0, 1.0, 1.0, 1.0, 1.0, -1.0,
       1.0, -1.0, 1.0, 1.0, 1.0],
  [0.0, 1.0, -1.0, 1.0, 1.0, 1.0, 0.0, 0.0, 1.0, 1.0, 1.0, 1.0, 1.0, 1.0, 1.0, -1.0,
       1.0, -1.0, 1.0, 1.0, 1.0],
  [0.0, 1.0, -1.0, 1.0, 1.0, 1.0, 0.0, 0.0, 1.0, 1.0, 1.0, 1.0, 1.0, 1.0, 1.0, -1.0,
       1.0, -1.0, 1.0, 1.0, 1.0],
  [0.0, 1.0, -1.0, 1.0, 1.0, 1.0, 0.0, 0.0, 1.0, 1.0, 1.0, 1.0, 1.0, 1.0, 1.0, -1.0,
       1.0, -1.0, 1.0, 1.0, 1.0],
  [0.0, -1.0, 1.0, -1.0, -1.0, -1.0, 0.0, 0.0, -1.0, -1.0, -1.0, -1.0, -1.0, -1.0,
       -1.0, 1.0, -1.0, 1.0, -1.0, -1.0, -1.0],
  [0.0, 1.0, -1.0, 1.0, 1.0, 1.0, 0.0, 0.0, 1.0, 1.0, 1.0, 1.0, 1.0, 1.0, 1.0, -1.0,
       1.0, -1.0, 1.0, 1.0, 1.0],
  [0.0, -1.0, 1.0, -1.0, -1.0, -1.0, 0.0, 0.0, -1.0, -1.0, -1.0, -1.0, -1.0, -1.0,
       -1.0, 1.0, -1.0, 1.0, -1.0, -1.0, -1.0],
  [0.0, 1.0, -1.0, 1.0, 1.0, 1.0, 0.0, 0.0, 1.0, 1.0, 1.0, 1.0, 1.0, 1.0, 1.0, -1.0,
       1.0, -1.0, 1.0, 1.0, 1.0],
  [0.0, 1.0, -1.0, 1.0, 1.0, 1.0, 0.0, 0.0, 1.0, 1.0, 1.0, 1.0, 1.0, 1.0, 1.0, -1.0,
       1.0, -1.0, 1.0, 1.0, 1.0],
  [0.0, 1.0, -1.0, 1.0, 1.0, 1.0, 0.0, 0.0, 1.0, 1.0, 1.0, 1.0, 1.0, 1.0, 1.0, -1.0,
       1.0, -1.0, 1.0, 1.0, 1.0]
 ]
},
{
  "Name": "SPCouplingFactors",
  "Values": [ 0.0, 0.0001, 0.0001, 0.0, 0.005, 0.013, 0.001, 0.001, 0.002, 0.001,
       0.0031, 0.0004, 0.0004, 0.001, 0.007, 0.18, 0.02, 0.03, 0.01, 0.01, 0.10],
  "SystematicCorrelationMatrix": [
    [1.0, 0.0, 0.0, 0.0, 0.0, 0.0, 0.0, 0.0, 0.0, 0.0, 0.0, 0.0, 0.0, 0.0, 0.0, 0.0,
         0.0, 0.0, 0.0, 0.0, 0.0],
```

```
    [0.0, 1.0, -1.0, 0.0, 0, 0, 0, 0, -1.0, 0, 1.0, 1.0, 1.0, 1.0, 0, 0, 1.0, 1.0,
        -1.0, -1.0, 0],
    [0.0, -1.0, 1.0, 0.0, 0, 0, 0, 0, 1.0, 0, -1.0, -1.0, -1.0, -1.0, 0, 0, -1.0,
        -1.0, 1.0, 1.0, 0],
    [0.0, 0.0, 0.0, 1.0, 0.0, 0.0, 0.0, 0.0, 0.0, 0.0, 0.0, 0.0, 0.0, 0.0, 0.0, 0.0,
        0.0, 0.0, 0.0, 0.0, 0.0],
    [0.0, 0, 0, 0.0, 1.0, 1.0, -1.0, -1.0, 0, 1.0, 0, 0, 0, 0, 1.0, -1.0, 0, 0, 0, 0,
        -1.0],
    [0.0, 0, 0, 0.0, 1.0, 1.0, -1.0, -1.0, 0, 1.0, 0, 0, 0, 0, 1.0, -1.0, 0, 0, 0, 0,
        -1.0],
    [0.0, 0, 0, 0.0, -1.0, -1.0, 1.0, 1.0, 0, -1.0, 0, 0, 0, 0, -1.0, 1.0, 0, 0, 0,
        0, 1.0],
    [0.0, 0, 0, 0.0, -1.0, -1.0, 1.0, 1.0, 0, -1.0, 0, 0, 0, 0, -1.0, 1.0, 0, 0, 0,
        0, 1.0],
    [0.0, -1.0, 1.0, 0.0, 0, 0, 0, 0, 1.0, 0, -1.0, -1.0, -1.0, -1.0, 0, 0, -1.0,
        -1.0, 1.0, 1.0, 0],
    [0.0, 0, 0, 0.0, 1.0, 1.0, -1.0, -1.0, 0, 1.0, 0, 0, 0, 0, 1.0, -1.0, 0, 0, 0, 0,
        -1.0],
    [0.0, 1.0, -1.0, 0.0, 0, 0, 0, 0, -1.0, 0, 1.0, 1.0, 1.0, 1.0, 0, 0, 1.0, 1.0,
        -1.0, -1.0, 0],
    [0.0, 1.0, -1.0, 0.0, 0, 0, 0, 0, -1.0, 0, 1.0, 1.0, 1.0, 1.0, 0, 0, 1.0, 1.0,
        -1.0, -1.0, 0],
    [0.0, 1.0, -1.0, 0.0, 0, 0, 0, 0, -1.0, 0, 1.0, 1.0, 1.0, 1.0, 0, 0, 1.0, 1.0,
        -1.0, -1.0, 0],
    [0.0, 1.0, -1.0, 0.0, 0, 0, 0, 0, -1.0, 0, 1.0, 1.0, 1.0, 1.0, 0, 0, 1.0, 1.0,
        -1.0, -1.0, 0],
    [0.0, 0, 0, 0.0, 1.0, 1.0, -1.0, -1.0, 0, 1.0, 0, 0, 0, 0, 1.0, -1.0, 0, 0, 0, 0,
        -1.0],
    [0.0, 0, 0, 0.0, -1.0, -1.0, 1.0, 1.0, 0, -1.0, 0, 0, 0, 0, -1.0, 1.0, 0, 0, 0,
        0, 1.0],
    [0.0, 1.0, -1.0, 0.0, 0, 0, 0, 0, -1.0, 0, 1.0, 1.0, 1.0, 1.0, 0, 0, 1.0, 1.0,
        -1.0, -1.0, 0],
    [0.0, 1.0, -1.0, 0.0, 0, 0, 0, 0, -1.0, 0, 1.0, 1.0, 1.0, 1.0, 0, 0, 1.0, 1.0,
        -1.0, -1.0, 0],
    [0.0, -1.0, 1.0, 0.0, 0, 0, 0, 0, 1.0, 0, -1.0, -1.0, -1.0, -1.0, 0, 0, -1.0,
        -1.0, 1.0, 1.0, 0],
    [0.0, -1.0, 1.0, 0.0, 0, 0, 0, 0, 1.0, 0, -1.0, -1.0, -1.0, -1.0, 0, 0, -1.0,
        -1.0, 1.0, 1.0, 0],
    [0.0, 0, 0, 0.0, -1.0, -1.0, 1.0, 1.0, 0, -1.0, 0, 0, 0, 0, -1.0, 1.0, 0, 0, 0,
        0, 1.0]
  ]
},
{
  "Name": "DecayTimeResolutionPromptKKRun2",
  "Values": [0.0, 0.0, 0.0, 0.0, 0.001, 0.001, 0.0, 0.0, 0.001, 0.0001, 0.0001, 0.0,
      0.0001, 0.0003, 0.0, 0.0, 0.0, 0.0, 0.002, 0.001, 0.001],
  "SystematicCorrelationMatrix": [
    [1.0, 0.0, 0.0, 0.0, 0.0, 0.0, 0.0, 0.0, 0.0, 0.0, 0.0, 0.0, 0.0, 0.0, 0.0, 0.0,
        0.0, 0.0, 0.0, 0.0, 0.0],
    [0.0, 1.0, 0.0, 0.0, 0.0, 0.0, 0.0, 0.0, 0.0, 0.0, 0.0, 0.0, 0.0, 0.0, 0.0, 0.0,
        0.0, 0.0, 0.0, 0.0, 0.0],
    [0.0, 0.0, 1.0, 0.0, 0.0, 0.0, 0.0, 0.0, 0.0, 0.0, 0.0, 0.0, 0.0, 0.0, 0.0, 0.0,
        0.0, 0.0, 0.0, 0.0, 0.0],
    [0.0, 0.0, 0.0, 1.0, 0.0, 0.0, 0.0, 0.0, 0.0, 0.0, 0.0, 0.0, 0.0, 0.0, 0.0, 0.0,
        0.0, 0.0, 0.0, 0.0, 0.0],
    [0.0, 0.0, 0.0, 0.0, 1.0, -1.0, 0.0, 0.0, -1.0, 1.0, 1.0, 0.0, 1.0, 1.0, 0.0,
        0.0, 0.0, 0.0, 1.0, 1.0, -1.0],
    [0.0, 0.0, 0.0, 0.0, -1.0, 1.0, 0.0, 0.0, 1.0, -1.0, -1.0, 0.0, -1.0, -1.0, 0.0,
        0.0, 0.0, 0.0, -1.0, -1.0, 1.0],
    [0.0, 0.0, 0.0, 0.0, 0.0, 0.0, 1.0, 0.0, 0.0, 0.0, 0.0, 0.0, 0.0, 0.0, 0.0, 0.0,
        0.0, 0.0, 0.0, 0.0, 0.0],
    [0.0, 0.0, 0.0, 0.0, 0.0, 0.0, 0.0, 1.0, 0.0, 0.0, 0.0, 0.0, 0.0, 0.0, 0.0, 0.0,
        0.0, 0.0, 0.0, 0.0, 0.0],
    [0.0, 0.0, 0.0, 0.0, -1.0, 1.0, 0.0, 0.0, 1.0, -1.0, -1.0, 0.0, -1.0, -1.0, 0.0,
        0.0, 0.0, 0.0, -1.0, -1.0, 1.0],
    [0.0, 0.0, 0.0, 0.0, 1.0, -1.0, 0.0, 0.0, -1.0, 1.0, 1.0, 0.0, 1.0, 1.0, 0.0,
        0.0, 0.0, 0.0, 1.0, 1.0, -1.0],
    [0.0, 0.0, 0.0, 0.0, 1.0, -1.0, 0.0, 0.0, -1.0, 1.0, 1.0, 0.0, 1.0, 1.0, 0.0,
        0.0, 0.0, 0.0, 1.0, 1.0, -1.0],
    [0.0, 0.0, 0.0, 0.0, 0.0, 0.0, 0.0, 0.0, 0.0, 0.0, 0.0, 1.0, 0.0, 0.0, 0.0, 0.0,
        0.0, 0.0, 0.0, 0.0, 0.0],
    [0.0, 0.0, 0.0, 0.0, 1.0, -1.0, 0.0, 0.0, -1.0, 1.0, 1.0, 0.0, 1.0, 1.0, 0.0,
        0.0, 0.0, 0.0, 1.0, 1.0, -1.0],
    [0.0, 0.0, 0.0, 0.0, 1.0, -1.0, 0.0, 0.0, -1.0, 1.0, 1.0, 0.0, 1.0, 1.0, 0.0,
        0.0, 0.0, 0.0, 1.0, 1.0, -1.0],
    [0.0, 0.0, 0.0, 0.0, 0.0, 0.0, 0.0, 0.0, 0.0, 0.0, 0.0, 0.0, 0.0, 0.0, 1.0, 0.0,
        0.0, 0.0, 0.0, 0.0, 0.0],
```

```
    [0.0, 0.0, 0.0, 0.0, 0.0, 0.0, 0.0, 0.0, 0.0, 0.0, 0.0, 0.0, 0.0, 0.0, 0.0, 1.0,
        0.0, 0.0, 0.0, 0.0, 0.0],
    [0.0, 0.0, 0.0, 0.0, 0.0, 0.0, 0.0, 0.0, 0.0, 0.0, 0.0, 0.0, 0.0, 0.0, 0.0, 0.0,
        1.0, 0.0, 0.0, 0.0, 0.0],
    [0.0, 0.0, 0.0, 0.0, 0.0, 0.0, 0.0, 0.0, 0.0, 0.0, 0.0, 0.0, 0.0, 0.0, 0.0, 0.0,
        0.0, 1.0, 0.0, 0.0, 0.0],
    [0.0, 0.0, 0.0, 0.0, 1.0, -1.0, 0.0, 0.0, -1.0, 1.0, 1.0, 0.0, 1.0, 1.0, 0.0,
        0.0, 0.0, 0.0, 1.0, 1.0, -1.0],
    [0.0, 0.0, 0.0, 0.0, 1.0, -1.0, 0.0, 0.0, -1.0, 1.0, 1.0, 0.0, 1.0, 1.0, 0.0,
        0.0, 0.0, 0.0, 1.0, 1.0, -1.0],
    [0.0, 0.0, 0.0, 0.0, -1.0, 1.0, 0.0, 0.0, 1.0, -1.0, -1.0, 0.0, -1.0, -1.0, 0.0,
        0.0, 0.0, 0.0, -1.0, -1.0, 1.0]
    ]
},
{
  "Name": "DecayTimeResolutionMean",
  "Values": [0.0002, 0.0003, 0.0, 0.0, 0.001, 0.080, 0.0032, 0.001, 0.005, 0.0001,
      0.0, 0.0, 0.0001, 0.0001, 0.0, 0.0, 0.003, 0.002, 0.003, 0.0056, 0.002],
  "SystematicCorrelationMatrix": [
  [1.0, 1.0, 0.0, 0.0, -1.0, -1.0, -1.0, -1.0, 1.0, -1.0, 0.0, 0.0, 1.0, 1.0, 0.0,
      0.0, 1.0, -1.0, 1.0, -1.0, -1.0],
  [1.0, 1.0, 0.0, 0.0, -1.0, -1.0, -1.0, -1.0, 1.0, -1.0, 0.0, 0.0, 1.0, 1.0, 0.0,
      0.0, 1.0, -1.0, 1.0, -1.0, -1.0],
  [0.0, 0.0, 1.0, 0.0, 0.0, 0.0, 0.0, 0.0, 0.0, 0.0, 0.0, 0.0, 0.0, 0.0, 0.0, 0.0,
      0.0, 0.0, 0.0, 0.0, 0.0],
  [0.0, 0.0, 0.0, 1.0, 0.0, 0.0, 0.0, 0.0, 0.0, 0.0, 0.0, 0.0, 0.0, 0.0, 0.0, 0.0,
      0.0, 0.0, 0.0, 0.0, 0.0],
  [-1.0, -1.0, 0.0, 0.0, 1.0, 1.0, 1.0, 1.0, -1.0, 1.0, 0.0, 0.0, -1.0, -1.0, 0.0,
      0.0, -1.0, 1.0, -1.0, 1.0, 1.0],
  [-1.0, -1.0, 0.0, 0.0, 1.0, 1.0, 1.0, 1.0, -1.0, 1.0, 0.0, 0.0, -1.0, -1.0, 0.0,
      0.0, -1.0, 1.0, -1.0, 1.0, 1.0],
  [-1.0, -1.0, 0.0, 0.0, 1.0, 1.0, 1.0, 1.0, -1.0, 1.0, 0.0, 0.0, -1.0, -1.0, 0.0,
      0.0, -1.0, 1.0, -1.0, 1.0, 1.0],
  [-1.0, -1.0, 0.0, 0.0, 1.0, 1.0, 1.0, 1.0, -1.0, 1.0, 0.0, 0.0, -1.0, -1.0, 0.0,
      0.0, -1.0, 1.0, -1.0, 1.0, 1.0],
  [1.0, 1.0, 0.0, 0.0, -1.0, -1.0, -1.0, -1.0, 1.0, -1.0, 0.0, 0.0, 1.0, 1.0, 0.0,
      0.0, 1.0, -1.0, 1.0, -1.0, -1.0],
  [-1.0, -1.0, 0.0, 0.0, 1.0, 1.0, 1.0, 1.0, -1.0, 1.0, 0.0, 0.0, -1.0, -1.0, 0.0,
      0.0, -1.0, 1.0, -1.0, 1.0, 1.0],
  [0.0, 0.0, 0.0, 0.0, 0.0, 0.0, 0.0, 0.0, 0.0, 0.0, 1.0, 0.0, 0.0, 0.0, 0.0, 0.0,
      0.0, 0.0, 0.0, 0.0, 0.0],
  [0.0, 0.0, 0.0, 0.0, 0.0, 0.0, 0.0, 0.0, 0.0, 0.0, 0.0, 1.0, 0.0, 0.0, 0.0, 0.0,
      0.0, 0.0, 0.0, 0.0, 0.0],
  [1.0, 1.0, 0.0, 0.0, -1.0, -1.0, -1.0, -1.0, 1.0, -1.0, 0.0, 0.0, 1.0, 1.0, 0.0,
      0.0, 1.0, -1.0, 1.0, -1.0, -1.0],
  [1.0, 1.0, 0.0, 0.0, -1.0, -1.0, -1.0, -1.0, 1.0, -1.0, 0.0, 0.0, 1.0, 1.0, 0.0,
      0.0, 1.0, -1.0, 1.0, -1.0, -1.0],
  [0.0, 0.0, 0.0, 0.0, 0.0, 0.0, 0.0, 0.0, 0.0, 0.0, 0.0, 0.0, 0.0, 0.0, 1.0, 0.0,
      0.0, 0.0, 0.0, 0.0, 0.0],
  [0.0, 0.0, 0.0, 0.0, 0.0, 0.0, 0.0, 0.0, 0.0, 0.0, 0.0, 0.0, 0.0, 0.0, 0.0, 1.0,
      0.0, 0.0, 0.0, 0.0, 0.0],
  [1.0, 1.0, 0.0, 0.0, -1.0, -1.0, -1.0, -1.0, 1.0, -1.0, 0.0, 0.0, 1.0, 1.0, 0.0,
      0.0, 1.0, -1.0, 1.0, -1.0, -1.0],
  [-1.0, -1.0, 0.0, 0.0, 1.0, 1.0, 1.0, 1.0, -1.0, 1.0, 0.0, 0.0, -1.0, -1.0, 0.0,
      0.0, -1.0, 1.0, -1.0, 1.0, 1.0],
  [1.0, 1.0, 0.0, 0.0, -1.0, -1.0, -1.0, -1.0, 1.0, -1.0, 0.0, 0.0, 1.0, 1.0, 0.0,
      0.0, 1.0, -1.0, 1.0, -1.0, -1.0],
  [-1.0, -1.0, 0.0, 0.0, 1.0, 1.0, 1.0, 1.0, -1.0, 1.0, 0.0, 0.0, -1.0, -1.0, 0.0,
      0.0, -1.0, 1.0, -1.0, 1.0, 1.0],
  [-1.0, -1.0, 0.0, 0.0, 1.0, 1.0, 1.0, 1.0, -1.0, 1.0, 0.0, 0.0, -1.0, -1.0, 0.0,
      0.0, -1.0, 1.0, -1.0, 1.0, 1.0]
  ]
},
{
  "Name": "DecayTimeResolutionWrongPVComponent",
  "Values": [0.0, 0.0, 0.0, 0.0, 0.001, 0.001, 0.0, 0.0, 0.001, 0.0001, 0.0001, 0.0,
      0.0001, 0.0002, 0.0, 0.0, 0.001, 0.001, 0.001, 0.001, 0.001],
  "SystematicCorrelationMatrix": [
  [1.0, 0.0, 0.0, 0.0, 0.0, 0.0, 0.0, 0.0, 0.0, 0.0, 0.0, 0.0, 0.0, 0.0, 0.0, 0.0,
      0.0, 0.0, 0.0, 0.0, 0.0],
  [0.0, 1.0, 0.0, 0.0, 0.0, 0.0, 0.0, 0.0, 0.0, 0.0, 0.0, 0.0, 0.0, 0.0, 0.0, 0.0,
      0.0, 0.0, 0.0, 0.0, 0.0],
  [0.0, 0.0, 1.0, 0.0, 0.0, 0.0, 0.0, 0.0, 0.0, 0.0, 0.0, 0.0, 0.0, 0.0, 0.0, 0.0,
      0.0, 0.0, 0.0, 0.0, 0.0],
  [0.0, 0.0, 0.0, 1.0, 0.0, 0.0, 0.0, 0.0, 0.0, 0.0, 0.0, 0.0, 0.0, 0.0, 0.0, 0.0,
      0.0, 0.0, 0.0, 0.0, 0.0],
  [0.0, 0.0, 0.0, 0.0, 1.0, 0, 0.0, 0.0, 0, -1.0, 0, 0.0, 0, 1.0, 0.0, 0.0, 1.0, 0,
```

```
      0, 0, 0],
    [0.0, 0.0, 0.0, 0, 1.0, 0.0, 0.0, 1.0, 0, -1.0, 0.0, -1.0, 0, 0.0, 0.0, 0,
      1.0, -1.0, -1.0, 1.0],
    [0.0, 0.0, 0.0, 0.0, 0.0, 0.0, 1.0, 0.0, 0.0, 0.0, 0.0, 0.0, 0.0, 0.0, 0.0, 0.0,
      0.0, 0.0, 0.0, 0.0, 0.0],
    [0.0, 0.0, 0.0, 0.0, 0.0, 0.0, 0.0, 1.0, 0.0, 0.0, 0.0, 0.0, 0.0, 0.0, 0.0, 0.0,
      0.0, 0.0, 0.0, 0.0, 0.0],
    [0.0, 0.0, 0.0, 0.0, 0, 1.0, 0.0, 0.0, 1.0, 0, -1.0, 0.0, -1.0, 0, 0.0, 0.0, 0,
      1.0, -1.0, -1.0, 1.0],
    [0.0, 0.0, 0.0, 0.0, -1.0, 0, 0.0, 0.0, 0, 1.0, 0, 0.0, 0, -1.0, 0.0, 0.0, -1.0, 0,
       0, 0, 0],
    [0.0, 0.0, 0.0, 0.0, 0, -1.0, 0.0, 0.0, -1.0, 0, 1.0, 0.0, 1.0, 0, 0.0, 0.0, 0,
      -1.0, 1.0, 1.0, -1.0],
    [0.0, 0.0, 0.0, 0.0, 0.0, 0.0, 0.0, 0.0, 0.0, 0.0, 0.0, 1.0, 0.0, 0.0, 0.0, 0.0,
      0.0, 0.0, 0.0, 0.0, 0.0],
    [0.0, 0.0, 0.0, 0.0, 0, -1.0, 0.0, 0.0, -1.0, 0, 1.0, 0.0, 1.0, 0, 0.0, 0.0, 0,
      -1.0, 1.0, 1.0, -1.0],
    [0.0, 0.0, 0.0, 0.0, 1.0, 0, 0.0, 0.0, 0, -1.0, 0, 0.0, 0, 1.0, 0.0, 0.0, 1.0, 0,
      0, 0, 0],
    [0.0, 0.0, 0.0, 0.0, 0.0, 0.0, 0.0, 0.0, 0.0, 0.0, 0.0, 0.0, 0.0, 0.0, 1.0, 0.0,
      0.0, 0.0, 0.0, 0.0, 0.0],
    [0.0, 0.0, 0.0, 0.0, 0.0, 0.0, 0.0, 0.0, 0.0, 0.0, 0.0, 0.0, 0.0, 0.0, 0.0, 1.0,
      0.0, 0.0, 0.0, 0.0, 0.0],
    [0.0, 0.0, 0.0, 0.0, 1.0, 0, 0.0, 0.0, 0, -1.0, 0, 0.0, 0, 1.0, 0.0, 0.0, 1.0, 0,
      0, 0, 0],
    [0.0, 0.0, 0.0, 0.0, 0, 1.0, 0.0, 0.0, 1.0, 0, -1.0, 0.0, -1.0, 0, 0.0, 0.0, 0,
      1.0, -1.0, -1.0, 1.0],
    [0.0, 0.0, 0.0, 0.0, 0, -1.0, 0.0, 0.0, -1.0, 0, 1.0, 0.0, 1.0, 0, 0.0, 0.0, 0,
      -1.0, 1.0, 1.0, -1.0],
    [0.0, 0.0, 0.0, 0.0, 0, -1.0, 0.0, 0.0, -1.0, 0, 1.0, 0.0, 1.0, 0, 0.0, 0.0, 0,
      -1.0, 1.0, 1.0, -1.0],
    [0.0, 0.0, 0.0, 0.0, 0, 1.0, 0.0, 0.0, 1.0, 0, -1.0, 0.0, -1.0, 0, 0.0, 0.0, 0,
      1.0, -1.0, -1.0, 1.0]
    ]
  },
  {
    "Name": "AngEfficiencyStat",
    "Values": [0.00003, 0.0, 0.00036, 0.0003, 0.0044, 0.0025, 0.0011, 0.0018, 0.0011,
      0.0007, 0.00032, 0.00011, 0.00026, 0.0006, 0.0006, 0.003, 0.006, 0.013, 0.012,
      0.0044, 0.004],
    "SystematicCorrelationMatrix": [
    [1.0, 0.0, 0.89, -0.22, -0.0071, -0.028, 0.027, -0.033, 0.14, 0.43, 0.13, 0.18,
      0.35, 0.37, 0.36, 0.16, 0.029, -0.12, 0.21, 0.31, 0.42],
    [0.0, 1.0, 0.0, 0.0, 0.0, 0.0, 0.0, 0.0, 0.0, 0.0, 0.0, 0.0, 0.0, 0.0, 0.0, 0.0,
      0.0, 0.0, 0.0, 0.0, 0.0],
    [0.89, 0.0, 1.0, -0.36, -0.027, -0.12, -0.058, 0.025, -0.065, 0.12, -0.13, -0.048,
      -0.012, 0.0036, 0.044, 0.22, -0.0094, -0.012, 0.0098, 0.082, 0.23],
    [-0.22, 0.0, -0.36, 1.0, 0.14, 0.054, 0.0054, -0.04, -0.097, -0.28, -0.12, -0.12,
      -0.11, -0.13, -0.17, -0.015, 0.021, 0.036, -0.1, -0.13, -0.17],
    [-0.0071, 0.0, -0.027, 0.14, 1.0, 0.6, 0.029, -0.013, -0.19, -0.15, -0.11, -0.073,
      -0.11, -0.11, -0.14, -0.049, -0.095, -0.021, -0.092, -0.12, -0.2],
    [-0.028, 0.0, -0.12, 0.054, 0.6, 1.0, 0.72, -0.48, 0.51, -0.03, -0.2, -0.26, 0.16,
      0.061, -0.04, -0.15, 0.24, 0.015, -0.12, -0.16, -0.4],
    [0.027, 0.0, -0.058, 0.0054, 0.029, 0.72, 1.0, -0.58, 0.82, -0.14, 0.075, -0.005,
      0.065, -0.044, -0.2, -0.49, 0.4, 0.36, 0.23, 0.17, -0.074],
    [-0.033, 0.0, 0.025, -0.04, -0.013, -0.48, -0.58, 1.0, -0.76, 0.07, 0.008, 0.23,
      -0.19, -0.043, 0.13, 0.52, -0.96, -0.57, -0.21, -0.15, 0.15],
    [0.14, 0.0, -0.065, -0.097, -0.19, 0.51, 0.82, -0.76, 1.0, 0.23, 0.39, 0.22, 0.45,
      0.34, 0.15, -0.6, 0.67, 0.4, 0.51, 0.49, 0.22],
    [0.43, 0.0, 0.12, -0.28, -0.15, -0.03, -0.14, 0.07, 0.23, 1.0, 0.4, 0.36, 0.95,
      0.98, 0.99, 0.28, -0.079, -0.58, 0.22, 0.33, 0.39],
    [0.13, 0.0, -0.13, -0.12, -0.11, -0.2, 0.075, 0.008, 0.39, 0.4, 1.0, 0.97, 0.4,
      0.46, 0.32, -0.64, 0.1, 0.29, 0.95, 0.96, 0.91],
    [0.18, 0.0, -0.048, -0.12, -0.073, -0.26, -0.005, 0.23, 0.22, 0.36, 0.97, 1.0, 0.3,
       0.38, 0.28, -0.53, -0.12, 0.2, 0.89, 0.92, 0.94],
    [0.35, 0.0, -0.012, -0.11, -0.11, 0.16, 0.065, -0.19, 0.45, 0.95, 0.4, 0.3, 1.0,
      0.99, 0.94, 0.13, 0.14, -0.45, 0.27, 0.35, 0.32],
    [0.37, 0.0, 0.0036, -0.13, -0.11, 0.061, -0.044, -0.043, 0.34, 0.98, 0.46, 0.38,
      0.99, 1.0, 0.97, 0.17, 0.021, -0.5, 0.29, 0.39, 0.39],
    [0.36, 0.0, 0.044, -0.17, -0.14, -0.04, -0.2, 0.13, 0.15, 0.99, 0.32, 0.28, 0.94,
      0.97, 1.0, 0.38, -0.15, -0.67, 0.11, 0.22, 0.3],
    [0.16, 0.0, 0.22, -0.015, -0.049, -0.15, -0.49, 0.52, -0.6, 0.28, -0.64, -0.53,
      0.13, 0.17, 0.38, 1.0, -0.58, -0.88, -0.8, -0.71, -0.48],
    [0.029, 0.0, -0.0094, 0.021, -0.095, 0.24, 0.4, -0.96, 0.67, -0.079, 0.1, -0.12,
      0.14, 0.021, -0.15, -0.58, 1.0, 0.67, 0.31, 0.26, -0.012],
    [-0.12, 0.0, -0.012, 0.036, -0.021, 0.015, 0.36, -0.57, 0.4, -0.58, 0.29, 0.2,
      -0.45, -0.5, -0.67, -0.88, 0.67, 1.0, 0.54, 0.44, 0.24],
```

```
    [0.21, 0.0, 0.0098, −0.1, −0.092, −0.12, 0.23, −0.21, 0.51, 0.22, 0.95, 0.89, 0.27,
        0.29, 0.11, −0.8, 0.31, 0.54, 1.0, 0.99, 0.89],
    [0.31, 0.0, 0.082, −0.13, −0.12, −0.16, 0.17, −0.15, 0.49, 0.33, 0.96, 0.92, 0.35,
        0.39, 0.22, −0.71, 0.26, 0.44, 0.99, 1.0, 0.94],
    [0.42, 0.0, 0.23, −0.17, −0.2, −0.4, −0.074, 0.15, 0.22, 0.39, 0.91, 0.94, 0.32,
        0.39, 0.3, −0.48, −0.012, 0.24, 0.89, 0.94, 1.0]
    ]
  },
  {
    "Name": "AngEfficiencyReweighting",
    "Values": [0.00006, 0.00021, 0.00112, 0.00200, 0.0077, 0.0057, 0.0022, 0.0043,
        0.0012, 0.0023, 0.00026, 0.00006, 0.00059, 0.0012, 0.0014, 0.005, 0.016, 0.031,
        0.011, 0.0046, 0.004],
    "SystematicCorrelationMatrix": [
    [1.0, 0.81, 0.98, −0.97, 0.84, 0.82, 0.17, 0.38, 0.79, 0.97, 0.92, 0.0, 0.94, 0.95,
        0.96, 0.91, −0.41, −0.9, 0.86, 0.92, 0.96],
    [0.81, 1.0, 0.9, −0.91, 0.74, 0.5, −0.24, −0.025, 0.62, 0.91, 0.86, 0.0, 0.91, 0.9,
        0.9, 0.69, 0.017, −0.66, 0.88, 0.9, 0.88],
    [0.98, 0.9, 1.0, −1.0, 0.84, 0.74, 0.04, 0.25, 0.75, 0.98, 0.92, 0.0, 0.95, 0.96,
        0.97, 0.87, −0.27, −0.84, 0.89, 0.94, 0.96],
    [−0.97, −0.91, −1.0, 1.0, −0.83, −0.74, −0.038, −0.23, −0.77, −0.99, −0.94, 0.0,
        −0.96, −0.97, −0.98, −0.85, 0.25, 0.84, −0.91, −0.95, −0.96],
    [0.84, 0.74, 0.84, −0.83, 1.0, 0.68, −0.042, 0.33, 0.47, 0.83, 0.79, 0.0, 0.8,
        0.82, 0.83, 0.79, −0.32, −0.76, 0.72, 0.78, 0.81],
    [0.82, 0.5, 0.74, −0.74, 0.68, 1.0, 0.65, 0.69, 0.86, 0.77, 0.78, 0.0, 0.76, 0.78,
        0.78, 0.86, −0.76, −0.94, 0.65, 0.71, 0.78],
    [0.17, −0.24, 0.04, −0.038, −0.042, 0.65, 1.0, 0.78, 0.51, 0.069, 0.14, 0.0, 0.068,
        0.087, 0.085, 0.33, −0.85, −0.46, 0.0027, 0.043, 0.13],
    [0.38, −0.025, 0.25, −0.23, 0.33, 0.69, 0.78, 1.0, 0.35, 0.25, 0.32, 0.0, 0.21,
        0.26, 0.27, 0.61, −0.99, −0.66, 0.13, 0.2, 0.36],
    [0.79, 0.62, 0.75, −0.77, 0.47, 0.86, 0.51, 0.35, 1.0, 0.8, 0.82, 0.0, 0.83, 0.82,
        0.81, 0.71, −0.45, −0.82, 0.78, 0.8, 0.79],
    [0.97, 0.91, 0.98, −0.99, 0.83, 0.77, 0.069, 0.25, 0.8, 1.0, 0.96, 0.0, 0.99, 0.99,
        1.0, 0.87, −0.28, −0.88, 0.92, 0.97, 0.98],
    [0.92, 0.86, 0.92, −0.94, 0.79, 0.78, 0.14, 0.32, 0.82, 0.96, 1.0, 0.0, 0.96, 0.97,
        0.96, 0.8, −0.35, −0.87, 0.97, 0.99, 0.99],
    [0.0, 0.0, 0.0, 0.0, 0.0, 0.0, 0.0, 0.0, 0.0, 0.0, 0.0, 1.0, 0.0, 0.0, 0.0, 0.0,
        0.0, 0.0, 0.0, 0.0, 0.0],
    [0.94, 0.91, 0.95, −0.96, 0.8, 0.76, 0.068, 0.21, 0.83, 0.99, 0.96, 0.0, 1.0, 1.0,
        1.0, 0.84, −0.25, −0.87, 0.93, 0.97, 0.96],
    [0.95, 0.9, 0.96, −0.97, 0.82, 0.78, 0.087, 0.26, 0.82, 0.99, 0.97, 0.0, 1.0, 1.0,
        1.0, 0.86, −0.29, −0.88, 0.93, 0.97, 0.97],
    [0.96, 0.9, 0.97, −0.98, 0.83, 0.78, 0.085, 0.27, 0.81, 1.0, 0.96, 0.0, 1.0, 1.0,
        1.0, 0.88, −0.3, −0.89, 0.92, 0.97, 0.97],
    [0.91, 0.69, 0.87, −0.85, 0.79, 0.86, 0.33, 0.61, 0.71, 0.87, 0.8, 0.0, 0.84, 0.86,
        0.88, 1.0, −0.62, −0.96, 0.66, 0.77, 0.86],
    [−0.41, 0.017, −0.27, 0.25, −0.32, −0.76, −0.85, −0.99, −0.45, −0.28, −0.35, 0.0,
        −0.25, −0.29, −0.3, −0.62, 1.0, 0.69, −0.15, −0.23, −0.37],
    [−0.9, −0.66, −0.84, 0.84, −0.76, −0.94, −0.46, −0.66, −0.82, −0.88, −0.87, 0.0,
        −0.87, −0.88, −0.89, −0.96, 0.69, 1.0, −0.73, −0.81, −0.89],
    [0.86, 0.88, 0.89, −0.91, 0.72, 0.65, 0.0027, 0.13, 0.78, 0.92, 0.97, 0.0, 0.93,
        0.93, 0.92, 0.66, −0.15, −0.73, 1.0, 0.99, 0.95],
    [0.92, 0.9, 0.94, −0.95, 0.78, 0.71, 0.043, 0.2, 0.8, 0.97, 0.99, 0.0, 0.97, 0.97,
        0.97, 0.77, −0.23, −0.81, 0.99, 1.0, 0.98],
    [0.96, 0.88, 0.96, −0.96, 0.81, 0.78, 0.13, 0.36, 0.79, 0.98, 0.99, 0.0, 0.96,
        0.97, 0.97, 0.86, −0.37, −0.89, 0.95, 0.98, 1.0]
    ]
  },
  {
    "Name": "AngEfficiencyDependence",
    "Values": [0.00021, 0.00095, 0.0012, 0.00084, 0.0055, 0.029, 0.0012, 0.0007,
        0.0028, 0.0063, 0.00069, 0.00024, 0.00015, 0.0010, 0.0016, 0.013, 0.022, 0.027,
        0.032, 0.010, 0.010],
    "SystematicCorrelationMatrix": [
    [1.0, −1.0, 1.0, −1.0, 1.0, 1.0, 1.0, −1.0, 1.0, −1.0, −1.0, 1.0, 1.0, 1.0, −1.0,
        −1.0, 1.0, −1.0, −1.0, −1.0, −1.0],
    [−1.0, 1.0, −1.0, 1.0, −1.0, −1.0, −1.0, 1.0, −1.0, 1.0, 1.0, −1.0, −1.0, −1.0,
        1.0, 1.0, −1.0, 1.0, 1.0, 1.0, 1.0],
    [1.0, −1.0, 1.0, −1.0, 1.0, 1.0, 1.0, −1.0, 1.0, −1.0, −1.0, 1.0, 1.0, 1.0, −1.0,
        −1.0, 1.0, −1.0, −1.0, −1.0, −1.0],
    [−1.0, 1.0, −1.0, 1.0, −1.0, −1.0, −1.0, 1.0, −1.0, 1.0, 1.0, −1.0, −1.0, −1.0,
        1.0, 1.0, −1.0, 1.0, 1.0, 1.0, 1.0],
    [1.0, −1.0, 1.0, −1.0, 1.0, 1.0, 1.0, −1.0, 1.0, −1.0, −1.0, 1.0, 1.0, 1.0, −1.0,
        −1.0, 1.0, −1.0, −1.0, −1.0, −1.0],
    [1.0, −1.0, 1.0, −1.0, 1.0, 1.0, 1.0, −1.0, 1.0, −1.0, −1.0, 1.0, 1.0, 1.0, −1.0,
        −1.0, 1.0, −1.0, −1.0, −1.0, −1.0],
    [1.0, −1.0, 1.0, −1.0, 1.0, 1.0, 1.0, −1.0, 1.0, −1.0, −1.0, 1.0, 1.0, 1.0, −1.0,
```

```
      -1.0, 1.0, -1.0, -1.0, -1.0, -1.0],
    [-1.0, 1.0, -1.0, 1.0, -1.0, -1.0, -1.0, 1.0, -1.0, 1.0, 1.0, -1.0, -1.0, -1.0,
      1.0, 1.0, -1.0, 1.0, 1.0, 1.0, 1.0],
    [1.0, -1.0, 1.0, -1.0, 1.0, 1.0, 1.0, -1.0, 1.0, -1.0, -1.0, 1.0, 1.0, 1.0, -1.0,
      -1.0, 1.0, -1.0, -1.0, -1.0, -1.0],
    [-1.0, 1.0, -1.0, 1.0, -1.0, -1.0, -1.0, 1.0, -1.0, 1.0, 1.0, -1.0, -1.0, -1.0,
      1.0, 1.0, -1.0, 1.0, 1.0, 1.0, 1.0],
    [-1.0, 1.0, -1.0, 1.0, -1.0, -1.0, -1.0, 1.0, -1.0, 1.0, 1.0, -1.0, -1.0, -1.0,
      1.0, 1.0, -1.0, 1.0, 1.0, 1.0, 1.0],
    [1.0, -1.0, 1.0, -1.0, 1.0, 1.0, 1.0, -1.0, 1.0, -1.0, -1.0, 1.0, 1.0, 1.0, -1.0,
      -1.0, 1.0, -1.0, -1.0, -1.0, -1.0],
    [1.0, -1.0, 1.0, -1.0, 1.0, 1.0, 1.0, -1.0, 1.0, -1.0, -1.0, 1.0, 1.0, 1.0, -1.0,
      -1.0, 1.0, -1.0, -1.0, -1.0, -1.0],
    [1.0, -1.0, 1.0, -1.0, 1.0, 1.0, 1.0, -1.0, 1.0, -1.0, -1.0, 1.0, 1.0, 1.0, -1.0,
      -1.0, 1.0, -1.0, -1.0, -1.0, -1.0],
    [-1.0, 1.0, -1.0, 1.0, -1.0, -1.0, -1.0, 1.0, -1.0, 1.0, 1.0, -1.0, -1.0, -1.0,
      1.0, 1.0, -1.0, 1.0, 1.0, 1.0, 1.0],
    [-1.0, 1.0, -1.0, 1.0, -1.0, -1.0, -1.0, 1.0, -1.0, 1.0, 1.0, -1.0, -1.0, -1.0,
      1.0, 1.0, -1.0, 1.0, 1.0, 1.0, 1.0],
    [1.0, -1.0, 1.0, -1.0, 1.0, 1.0, 1.0, -1.0, 1.0, -1.0, -1.0, 1.0, 1.0, 1.0, -1.0,
      -1.0, 1.0, -1.0, -1.0, -1.0, -1.0],
    [-1.0, 1.0, -1.0, 1.0, -1.0, -1.0, -1.0, 1.0, -1.0, 1.0, 1.0, -1.0, -1.0, -1.0,
      1.0, 1.0, -1.0, 1.0, 1.0, 1.0, 1.0],
    [-1.0, 1.0, -1.0, 1.0, -1.0, -1.0, -1.0, 1.0, -1.0, 1.0, 1.0, -1.0, -1.0, -1.0,
      1.0, 1.0, -1.0, 1.0, 1.0, 1.0, 1.0],
    [-1.0, 1.0, -1.0, 1.0, -1.0, -1.0, -1.0, 1.0, -1.0, 1.0, 1.0, -1.0, -1.0, -1.0,
      1.0, 1.0, -1.0, 1.0, 1.0, 1.0, 1.0]
  ]
},
{
  "Name": "DecayTimeEfficiencyKnotPos",
  "Values": [0.00019, 0.0, 0.0, 0.0, 0.0, 0.0, 0.0, 0.0, 0.0, 0.0, 0.0, 0.0, 0.0,
      0.0, 0.0, 0.0, 0.0, 0.0, 0.0, 0.0, 0.0]
},
{
  "Name": "DecayTimeEfficiencyPDFReweighting",
  "Values": [0.00009, 0.00007, 0.0, 0.0, 0.0, 0.0, 0.0, 0.0, 0.0, 0.0, 0.0, 0.0, 0.0,
      0.0, 0.0, 0.0, 0.0, 0.0, 0.0, 0.0, 0.0],
  "SystematicCorrelationMatrix": [
    [1.0, 1.0, 0.0, 0.0, 0.0, 0.0, 0.0, 0.0, 0.0, 0.0, 0.0, 0.0, 0.0, 0.0, 0.0, 0.0,
      0.0, 0.0, 0.0, 0.0, 0.0],
    [1.0, 1.0, 0.0, 0.0, 0.0, 0.0, 0.0, 0.0, 0.0, 0.0, 0.0, 0.0, 0.0, 0.0, 0.0, 0.0,
      0.0, 0.0, 0.0, 0.0, 0.0],
    [0.0, 0.0, 1.0, 0.0, 0.0, 0.0, 0.0, 0.0, 0.0, 0.0, 0.0, 0.0, 0.0, 0.0, 0.0, 0.0,
      0.0, 0.0, 0.0, 0.0, 0.0],
    [0.0, 0.0, 0.0, 1.0, 0.0, 0.0, 0.0, 0.0, 0.0, 0.0, 0.0, 0.0, 0.0, 0.0, 0.0, 0.0,
      0.0, 0.0, 0.0, 0.0, 0.0],
    [0.0, 0.0, 0.0, 0.0, 1.0, 0.0, 0.0, 0.0, 0.0, 0.0, 0.0, 0.0, 0.0, 0.0, 0.0, 0.0,
      0.0, 0.0, 0.0, 0.0, 0.0],
    [0.0, 0.0, 0.0, 0.0, 0.0, 1.0, 0.0, 0.0, 0.0, 0.0, 0.0, 0.0, 0.0, 0.0, 0.0, 0.0,
      0.0, 0.0, 0.0, 0.0, 0.0],
    [0.0, 0.0, 0.0, 0.0, 0.0, 0.0, 1.0, 0.0, 0.0, 0.0, 0.0, 0.0, 0.0, 0.0, 0.0, 0.0,
      0.0, 0.0, 0.0, 0.0, 0.0],
    [0.0, 0.0, 0.0, 0.0, 0.0, 0.0, 0.0, 1.0, 0.0, 0.0, 0.0, 0.0, 0.0, 0.0, 0.0, 0.0,
      0.0, 0.0, 0.0, 0.0, 0.0],
    [0.0, 0.0, 0.0, 0.0, 0.0, 0.0, 0.0, 0.0, 1.0, 0.0, 0.0, 0.0, 0.0, 0.0, 0.0, 0.0,
      0.0, 0.0, 0.0, 0.0, 0.0],
    [ 0.0,  0.0, 0.0, 0.0, 0.0, 0.0, 0.0, 0.0, 0.0, 1.0, 0.0, 0.0, 0.0, 0.0, 0.0, 0.0,
      0.0, 0.0, 0.0, 0.0, 0.0],
    [ 0.0,  0.0, 0.0, 0.0, 0.0, 0.0, 0.0, 0.0, 0.0, 0.0, 1.0, 0.0, 0.0, 0.0, 0.0, 0.0,
      0.0, 0.0, 0.0, 0.0, 0.0],
    [ 0.0,  0.0, 0.0, 0.0, 0.0, 0.0, 0.0, 0.0, 0.0, 0.0, 0.0, 1.0, 0.0, 0.0, 0.0, 0.0,
      0.0, 0.0, 0.0, 0.0, 0.0],
    [ 0.0,  0.0, 0.0, 0.0, 0.0, 0.0, 0.0, 0.0, 0.0, 0.0, 0.0, 0.0, 1.0, 0.0, 0.0, 0.0,
      0.0, 0.0, 0.0, 0.0, 0.0],
    [ 0.0,  0.0, 0.0, 0.0, 0.0, 0.0, 0.0, 0.0, 0.0, 0.0, 0.0, 0.0, 0.0, 1.0, 0.0, 0.0,
      0.0, 0.0, 0.0, 0.0, 0.0],
    [ 0.0,  0.0, 0.0, 0.0, 0.0, 0.0, 0.0, 0.0, 0.0, 0.0, 0.0, 0.0, 0.0, 0.0, 1.0, 0.0,
      0.0, 0.0, 0.0, 0.0, 0.0],
    [ 0.0,  0.0, 0.0, 0.0, 0.0, 0.0, 0.0, 0.0, 0.0, 0.0, 0.0, 0.0, 0.0, 0.0, 0.0, 1.0,
      0.0, 0.0, 0.0, 0.0, 0.0],
    [ 0.0,  0.0, 0.0, 0.0, 0.0, 0.0, 0.0, 0.0, 0.0, 0.0, 0.0, 0.0, 0.0, 0.0, 0.0, 0.0,
      1.0, 0.0, 0.0, 0.0, 0.0],
    [ 0.0,  0.0, 0.0, 0.0, 0.0, 0.0, 0.0, 0.0, 0.0, 0.0, 0.0, 0.0, 0.0, 0.0, 0.0, 0.0,
      0.0, 1.0, 0.0, 0.0, 0.0],
```

```
    [ 0.0,  0.0, 0.0, 0.0, 0.0, 0.0, 0.0, 0.0, 0.0, 0.0, 0.0, 0.0, 0.0, 0.0, 0.0, 0.0,
      0.0, 0.0, 1.0, 0.0, 0.0],
    [ 0.0,  0.0, 0.0, 0.0, 0.0, 0.0, 0.0, 0.0, 0.0, 0.0, 0.0, 0.0, 0.0, 0.0, 0.0, 0.0,
      0.0, 0.0, 0.0, 1.0, 0.0],
    [ 0.0,  0.0, 0.0, 0.0, 0.0, 0.0, 0.0, 0.0, 0.0, 0.0, 0.0, 0.0, 0.0, 0.0, 0.0, 0.0,
      0.0, 0.0, 0.0, 0.0, 1.0]
    ]
  },
  {
    "Name": "DecayTimeEfficiencyKinReweighting",
    "Values": [0.00021, 0.0, 0.0, 0.0, 0.0, 0.0, 0.0, 0.0, 0.0, 0.0, 0.0, 0.0, 0.0,
      0.0, 0.0, 0.0, 0.0, 0.0, 0.0, 0.0, 0.0]
  },
  {
    "Name": "DecayTimeEfficiencyStatRun2",
    "Values": [0.0012, 0.00083, 0.0003, 0.0002, 0.0, 0.0, 0.0, 0.0, 0.0, 0.0, 0.0, 0.0,
      0.0, 0.0, 0.0, 0.0, 0.0, 0.0, 0.0, 0.0, 0.0],
    "SystematicCorrelationMatrix": [
      [1.0, -0.077, 0.060, -0.058, 0.0, 0.0, 0.0, 0.0, 0.0, 0.0, 0.0, 0.0, 0.0, 0.0,
        0.0, 0.0, 0.0, 0.0, 0.0, 0.0, 0.0],
      [-0.077, 1.0, -0.99, 0.99, 0.0, 0.0, 0.0, 0.0, 0.0, 0.0, 0.0, 0.0, 0.0, 0.0,
        0.0, 0.0, 0.0, 0.0, 0.0, 0.0, 0.0],
      [0.060, -0.99, 1.0, -1.0, 0.0, 0.0, 0.0, 0.0, 0.0, 0.0, 0.0, 0.0, 0.0, 0.0,
        0.0, 0.0, 0.0, 0.0, 0.0, 0.0, 0.0],
      [-0.058, 0.99, -1.0, 1.0, 0.0, 0.0, 0.0, 0.0, 0.0, 0.0, 0.0, 0.0, 0.0, 0.0,
        0.0, 0.0, 0.0, 0.0, 0.0, 0.0, 0.0],
      [0.0, 0.0, 0.0, 0.0, 1.0, 0.0, 0.0, 0.0, 0.0, 0.0, 0.0, 0.0, 0.0, 0.0, 0.0,
        0.0, 0.0, 0.0, 0.0, 0.0, 0.0],
      [0.0, 0.0, 0.0, 0.0, 0.0, 1.0, 0.0, 0.0, 0.0, 0.0, 0.0, 0.0, 0.0, 0.0, 0.0,
        0.0, 0.0, 0.0, 0.0, 0.0, 0.0],
      [0.0, 0.0, 0.0, 0.0, 0.0, 0.0, 1.0, 0.0, 0.0, 0.0, 0.0, 0.0, 0.0, 0.0, 0.0,
        0.0, 0.0, 0.0, 0.0, 0.0, 0.0],
      [0.0, 0.0, 0.0, 0.0, 0.0, 0.0, 0.0, 1.0, 0.0, 0.0, 0.0, 0.0, 0.0, 0.0, 0.0,
        0.0, 0.0, 0.0, 0.0, 0.0, 0.0],
      [0.0, 0.0, 0.0, 0.0, 0.0, 0.0, 0.0, 0.0, 1.0, 0.0, 0.0, 0.0, 0.0, 0.0, 0.0,
        0.0, 0.0, 0.0, 0.0, 0.0, 0.0],
      [0.0, 0.0, 0.0, 0.0, 0.0, 0.0, 0.0, 0.0, 0.0, 1.0, 0.0, 0.0, 0.0, 0.0, 0.0,
        0.0, 0.0, 0.0, 0.0, 0.0, 0.0],
    [ 0.0,  0.0, 0.0, 0.0, 0.0, 0.0, 0.0, 0.0, 0.0, 0.0, 1.0, 0.0, 0.0, 0.0, 0.0,
      0.0, 0.0, 0.0, 0.0, 0.0, 0.0],
    [ 0.0,  0.0, 0.0, 0.0, 0.0, 0.0, 0.0, 0.0, 0.0, 0.0, 0.0, 1.0, 0.0, 0.0, 0.0,
      0.0, 0.0, 0.0, 0.0, 0.0, 0.0],
    [ 0.0,  0.0, 0.0, 0.0, 0.0, 0.0, 0.0, 0.0, 0.0, 0.0, 0.0, 0.0, 1.0, 0.0, 0.0,
      0.0, 0.0, 0.0, 0.0, 0.0, 0.0],
    [ 0.0,  0.0, 0.0, 0.0, 0.0, 0.0, 0.0, 0.0, 0.0, 0.0, 0.0, 0.0, 0.0, 1.0, 0.0,
      0.0, 0.0, 0.0, 0.0, 0.0, 0.0],
    [ 0.0,  0.0, 0.0, 0.0, 0.0, 0.0, 0.0, 0.0, 0.0, 0.0, 0.0, 0.0, 0.0, 0.0, 1.0,
      0.0, 0.0, 0.0, 0.0, 0.0, 0.0],
    [ 0.0,  0.0, 0.0, 0.0, 0.0, 0.0, 0.0, 0.0, 0.0, 0.0, 0.0, 0.0, 0.0, 0.0, 0.0,
      1.0, 0.0, 0.0, 0.0, 0.0, 0.0],
    [ 0.0,  0.0, 0.0, 0.0, 0.0, 0.0, 0.0, 0.0, 0.0, 0.0, 0.0, 0.0, 0.0, 0.0, 0.0,
      0.0, 1.0, 0.0, 0.0, 0.0, 0.0],
    [ 0.0,  0.0, 0.0, 0.0, 0.0, 0.0, 0.0, 0.0, 0.0, 0.0, 0.0, 0.0, 0.0, 0.0, 0.0,
      0.0, 0.0, 1.0, 0.0, 0.0, 0.0],
    [ 0.0,  0.0, 0.0, 0.0, 0.0, 0.0, 0.0, 0.0, 0.0, 0.0, 0.0, 0.0, 0.0, 0.0, 0.0,
      0.0, 0.0, 0.0, 1.0, 0.0, 0.0],
    [ 0.0,  0.0, 0.0, 0.0, 0.0, 0.0, 0.0, 0.0, 0.0, 0.0, 0.0, 0.0, 0.0, 0.0, 0.0,
      0.0, 0.0, 0.0, 0.0, 1.0, 0.0],
    [ 0.0,  0.0, 0.0, 0.0, 0.0, 0.0, 0.0, 0.0, 0.0, 0.0, 0.0, 0.0, 0.0, 0.0, 0.0,
      0.0, 0.0, 0.0, 0.0, 0.0, 1.0]
    ]
  },
  {
    "Name": "DecayTimeEfficiencyOtherMC",
    "Values": [0.00031, 0.0005, 0.00018, 0.00012, 0.0, 0.0, 0.0, 0.0, 0.0, 0.0, 0.0,
      0.0, 0.0, 0.0, 0.0, 0.0, 0.0, 0.0, 0.0, 0.0, 0.0],
    "SystematicCorrelationMatrix": [
    [ 1.0, -1.0, 1.0,-1.0, 0.0, 0.0, 0.0, 0.0, 0.0, 0.0, 0.0, 0.0, 0.0, 0.0, 0.0, 0.0,
      0.0, 0.0, 0.0, 0.0, 0.0],
    [-1.0,  1.0,-1.0, 1.0, 0.0, 0.0, 0.0, 0.0, 0.0, 0.0, 0.0, 0.0, 0.0, 0.0, 0.0, 0.0,
      0.0, 0.0, 0.0, 0.0, 0.0],
    [ 1.0, -1.0, 1.0,-1.0, 0.0, 0.0, 0.0, 0.0, 0.0, 0.0, 0.0, 0.0, 0.0, 0.0, 0.0, 0.0,
      0.0, 0.0, 0.0, 0.0, 0.0],
    [-1.0,  1.0,-1.0, 1.0, 0.0, 0.0, 0.0, 0.0, 0.0, 0.0, 0.0, 0.0, 0.0, 0.0, 0.0, 0.0,
      0.0, 0.0, 0.0, 0.0, 0.0],
    [ 0.0,  0.0, 0.0, 0.0, 1.0, 0.0, 0.0, 0.0, 0.0, 0.0, 0.0, 0.0, 0.0, 0.0, 0.0, 0.0,
      0.0, 0.0, 0.0, 0.0, 0.0],
```

```
    [ 0.0,  0.0, 0.0, 0.0, 0.0, 1.0, 0.0, 0.0, 0.0, 0.0, 0.0, 0.0, 0.0, 0.0, 0.0, 0.0,
      0.0, 0.0, 0.0, 0.0, 0.0],
    [ 0.0,  0.0, 0.0, 0.0, 0.0, 0.0, 1.0, 0.0, 0.0, 0.0, 0.0, 0.0, 0.0, 0.0, 0.0, 0.0,
      0.0, 0.0, 0.0, 0.0, 0.0],
    [ 0.0,  0.0, 0.0, 0.0, 0.0, 0.0, 0.0, 1.0, 0.0, 0.0, 0.0, 0.0, 0.0, 0.0, 0.0, 0.0,
      0.0, 0.0, 0.0, 0.0, 0.0],
    [ 0.0,  0.0, 0.0, 0.0, 0.0, 0.0, 0.0, 0.0, 1.0, 0.0, 0.0, 0.0, 0.0, 0.0, 0.0, 0.0,
      0.0, 0.0, 0.0, 0.0, 0.0],
    [ 0.0,  0.0, 0.0, 0.0, 0.0, 0.0, 0.0, 0.0, 0.0, 1.0, 0.0, 0.0, 0.0, 0.0, 0.0, 0.0,
      0.0, 0.0, 0.0, 0.0, 0.0],
    [ 0.0,  0.0, 0.0, 0.0, 0.0, 0.0, 0.0, 0.0, 0.0, 0.0, 1.0, 0.0, 0.0, 0.0, 0.0, 0.0,
      0.0, 0.0, 0.0, 0.0, 0.0],
    [ 0.0,  0.0, 0.0, 0.0, 0.0, 0.0, 0.0, 0.0, 0.0, 0.0, 0.0, 1.0, 0.0, 0.0, 0.0, 0.0,
      0.0, 0.0, 0.0, 0.0, 0.0],
    [ 0.0,  0.0, 0.0, 0.0, 0.0, 0.0, 0.0, 0.0, 0.0, 0.0, 0.0, 0.0, 1.0, 0.0, 0.0, 0.0,
      0.0, 0.0, 0.0, 0.0, 0.0],
    [ 0.0,  0.0, 0.0, 0.0, 0.0, 0.0, 0.0, 0.0, 0.0, 0.0, 0.0, 0.0, 0.0, 1.0, 0.0, 0.0,
      0.0, 0.0, 0.0, 0.0, 0.0],
    [ 0.0,  0.0, 0.0, 0.0, 0.0, 0.0, 0.0, 0.0, 0.0, 0.0, 0.0, 0.0, 0.0, 0.0, 1.0, 0.0,
      0.0, 0.0, 0.0, 0.0, 0.0],
    [ 0.0,  0.0, 0.0, 0.0, 0.0, 0.0, 0.0, 0.0, 0.0, 0.0, 0.0, 0.0, 0.0, 0.0, 0.0, 1.0,
      0.0, 0.0, 0.0, 0.0, 0.0],
    [ 0.0,  0.0, 0.0, 0.0, 0.0, 0.0, 0.0, 0.0, 0.0, 0.0, 0.0, 0.0, 0.0, 0.0, 0.0, 0.0,
      1.0, 0.0, 0.0, 0.0, 0.0],
    [ 0.0,  0.0, 0.0, 0.0, 0.0, 0.0, 0.0, 0.0, 0.0, 0.0, 0.0, 0.0, 0.0, 0.0, 0.0, 0.0,
      0.0, 1.0, 0.0, 0.0, 0.0],
    [ 0.0,  0.0, 0.0, 0.0, 0.0, 0.0, 0.0, 0.0, 0.0, 0.0, 0.0, 0.0, 0.0, 0.0, 0.0, 0.0,
      0.0, 0.0, 1.0, 0.0, 0.0],
    [ 0.0,  0.0, 0.0, 0.0, 0.0, 0.0, 0.0, 0.0, 0.0, 0.0, 0.0, 0.0, 0.0, 0.0, 0.0, 0.0,
      0.0, 0.0, 0.0, 1.0, 0.0],
    [ 0.0,  0.0, 0.0, 0.0, 0.0, 0.0, 0.0, 0.0, 0.0, 0.0, 0.0, 0.0, 0.0, 0.0, 0.0, 0.0,
      0.0, 0.0, 0.0, 0.0, 1.0]
    ]
  },
  {
    "Name": "LengthMomentumScales",
    "Values": [ 0.0, 0.0, 0.0, 0.0, 0.0, 0.0, 0.0, 0.0, 0.004, 0.0, 0.0, 0.0, 0.0, 0.0,
        0.0, 0.0, 0.0, 0.0, 0.0, 0.0, 0.0]
  },
  {
    "Name": "BKGCAT60",
    "Values": [0.00020, 0.00012, 0.00013, 0.00019, 0.0017, 0.0, 0.0005, 0.0014, 0.0,
      0.0, 0.00022, 0.00009, 0.0002, 0.00056, 0.00052, 0.0, 0.0, 0.0, 0.0041, 0.0018,
       0.0019],
    "SystematicCorrelationMatrix": [
    [1.0, -1.0, 0.0, 1.0, 0.0, 0.0, 1.0, 0.0, 0.0, 0.0, 0.0, 0.0, 0.0, 0.0, 0.0, 0.0,
      0.0, 0.0, 0.0, 0.0, 0.0],
    [-1.0, 1.0, 0.0, -1.0, 0.0, 0.0, -1.0, 0.0, 0.0, 0.0, 0.0, 0.0, 0.0, 0.0, 0.0, 0.0,
       0.0, 0.0, 0.0, 0.0, 0.0],
    [0.0, 0.0, 1.0, 0.0, -1.0, 0.0, 0.0, -1.0, 0.0, 0.0, -1.0, -1.0, -1.0, -1.0, -1.0,
      0.0, 0.0, 0.0, -1.0, -1.0, -1.0],
    [1.0, -1.0, 0.0, 1.0, 0.0, 0.0, 1.0, 0.0, 0.0, 0.0, 0.0, 0.0, 0.0, 0.0, 0.0, 0.0,
      0.0, 0.0, 0.0, 0.0, 0.0],
    [0.0, 0.0, -1.0, 0.0, 1.0, 0.0, 0.0, 1.0, 0.0, 0.0, 1.0, 1.0, 1.0, 1.0, 1.0, 0.0,
      0.0, 0.0, 1.0, 1.0, 1.0],
    [0.0, 0.0, 0.0, 0.0, 0.0, 1.0, 0.0, 0.0, 0.0, 0.0, 0.0, 0.0, 0.0, 0.0, 0.0, 0.0,
      0.0, 0.0, 0.0, 0.0, 0.0],
    [1.0, -1.0, 0.0, 1.0, 0.0, 0.0, 1.0, 0.0, 0.0, 0.0, 0.0, 0.0, 0.0, 0.0, 0.0, 0.0,
      0.0, 0.0, 0.0, 0.0, 0.0],
    [0.0, 0.0, -1.0, 0.0, 1.0, 0.0, 0.0, 1.0, 0.0, 0.0, 1.0, 1.0, 1.0, 1.0, 1.0, 0.0,
      0.0, 0.0, 1.0, 1.0, 1.0],
    [0.0, 0.0, 0.0, 0.0, 0.0, 0.0, 0.0, 0.0, 1.0, 0.0, 0.0, 0.0, 0.0, 0.0, 0.0, 0.0,
      0.0, 0.0, 0.0, 0.0, 0.0],
    [0.0, 0.0, 0.0, 0.0, 0.0, 0.0, 0.0, 0.0, 0.0, 1.0, 0.0, 0.0, 0.0, 0.0, 0.0, 0.0,
      0.0, 0.0, 0.0, 0.0, 0.0],
    [0.0, 0.0, -1.0, 0.0, 1.0, 0.0, 0.0, 1.0, 0.0, 0.0, 1.0, 1.0, 1.0, 1.0, 1.0, 0.0,
      0.0, 0.0, 1.0, 1.0, 1.0],
    [0.0, 0.0, -1.0, 0.0, 1.0, 0.0, 0.0, 1.0, 0.0, 0.0, 1.0, 1.0, 1.0, 1.0, 1.0, 0.0,
      0.0, 0.0, 1.0, 1.0, 1.0],
    [0.0, 0.0, -1.0, 0.0, 1.0, 0.0, 0.0, 1.0, 0.0, 0.0, 1.0, 1.0, 1.0, 1.0, 1.0, 0.0,
      0.0, 0.0, 1.0, 1.0, 1.0],
    [0.0, 0.0, -1.0, 0.0, 1.0, 0.0, 0.0, 1.0, 0.0, 0.0, 1.0, 1.0, 1.0, 1.0, 1.0, 0.0,
      0.0, 0.0, 1.0, 1.0, 1.0],
    [0.0, 0.0, -1.0, 0.0, 1.0, 0.0, 0.0, 1.0, 0.0, 0.0, 1.0, 1.0, 1.0, 1.0, 1.0, 0.0,
      0.0, 0.0, 1.0, 1.0, 1.0],
    [0.0, 0.0, 0.0, 0.0, 0.0, 0.0, 0.0, 0.0, 0.0, 0.0, 0.0, 0.0, 0.0, 0.0, 0.0, 1.0,
      0.0, 0.0, 0.0, 0.0, 0.0],
```

```
    [0.0, 0.0, 0.0, 0.0, 0.0, 0.0, 0.0, 0.0, 0.0, 0.0, 0.0, 0.0, 0.0, 0.0, 0.0, 0.0,
        1.0, 0.0, 0.0, 0.0, 0.0],
    [0.0, 0.0, 0.0, 0.0, 0.0, 0.0, 0.0, 0.0, 0.0, 0.0, 0.0, 0.0, 0.0, 0.0, 0.0, 0.0,
        0.0, 1.0, 0.0, 0.0, 0.0],
    [0.0, 0.0, -1.0, 0.0, 1.0, 0.0, 0.0, 1.0, 0.0, 0.0, 1.0, 1.0, 1.0, 1.0, 1.0, 0.0,
        0.0, 0.0, 1.0, 1.0, 1.0],
    [0.0, 0.0, -1.0, 0.0, 1.0, 0.0, 0.0, 1.0, 0.0, 0.0, 1.0, 1.0, 1.0, 1.0, 1.0, 0.0,
        0.0, 0.0, 1.0, 1.0, 1.0],
    [0.0, 0.0, -1.0, 0.0, 1.0, 0.0, 0.0, 1.0, 0.0, 0.0, 1.0, 1.0, 1.0, 1.0, 1.0, 0.0,
        0.0, 0.0, 1.0, 1.0, 1.0]
    ]
  },
  {
    "Name": "FitBias",
    "Values": [0.0, 0.0003, 0.0006, 0.0001, 0.033, 0.022, 0.001, 0.0, 0.001, 0.0008,
        0.0042, 0.0013, 0.0007, 0.0002, 0.0007, 0.05, 0.02, 0.08, 0.11, 0.01, 0.04],
    "SystematicCorrelationMatrix": [
      [ 1.0, -1.0,  1.0, -1.0, -1.0, -1.0,  1.0, -1.0, -1.0, -1.0, -1.0, -1.0,  1.0,
          1.0, -1.0,  1.0,  1.0, -1.0,  1.0,  1.0, 1.0],
      [-1.0,  1.0, -1.0,  1.0,  1.0,  1.0, -1.0,  1.0,  1.0,  1.0,  1.0,  1.0, -1.0,
         -1.0,  1.0, -1.0, -1.0,  1.0, -1.0, -1.0, -1.0],
      [ 1.0, -1.0,  1.0, -1.0, -1.0, -1.0,  1.0, -1.0, -1.0, -1.0, -1.0, -1.0,  1.0,
          1.0, -1.0,  1.0,  1.0, -1.0,  1.0,  1.0,  1.0],
      [-1.0,  1.0, -1.0,  1.0,  1.0,  1.0, -1.0,  1.0,  1.0,  1.0,  1.0,  1.0, -1.0,
         -1.0,  1.0, -1.0, -1.0,  1.0, -1.0, -1.0, -1.0],
      [-1.0,  1.0, -1.0,  1.0,  1.0,  1.0, -1.0,  1.0,  1.0,  1.0,  1.0,  1.0, -1.0,
         -1.0,  1.0, -1.0, -1.0,  1.0, -1.0, -1.0, -1.0],
      [-1.0,  1.0, -1.0,  1.0,  1.0,  1.0, -1.0,  1.0,  1.0,  1.0,  1.0,  1.0, -1.0,
         -1.0,  1.0, -1.0, -1.0,  1.0, -1.0, -1.0, -1.0],
      [ 1.0, -1.0,  1.0, -1.0, -1.0, -1.0,  1.0, -1.0, -1.0, -1.0, -1.0, -1.0,  1.0,
          1.0, -1.0,  1.0,  1.0, -1.0,  1.0,  1.0,  1.0],
      [-1.0,  1.0, -1.0,  1.0,  1.0,  1.0, -1.0,  1.0,  1.0,  1.0,  1.0,  1.0, -1.0,
         -1.0,  1.0, -1.0, -1.0,  1.0, -1.0, -1.0, -1.0],
      [-1.0,  1.0, -1.0,  1.0,  1.0,  1.0, -1.0,  1.0,  1.0,  1.0,  1.0,  1.0, -1.0,
         -1.0,  1.0, -1.0, -1.0,  1.0, -1.0, -1.0, -1.0],
      [-1.0,  1.0, -1.0,  1.0,  1.0,  1.0, -1.0,  1.0,  1.0,  1.0,  1.0,  1.0, -1.0,
         -1.0,  1.0, -1.0, -1.0,  1.0, -1.0, -1.0, -1.0],
      [-1.0,  1.0, -1.0,  1.0,  1.0,  1.0, -1.0,  1.0,  1.0,  1.0,  1.0,  1.0, -1.0,
         -1.0,  1.0, -1.0, -1.0,  1.0, -1.0, -1.0, -1.0],
      [-1.0,  1.0, -1.0,  1.0,  1.0,  1.0, -1.0,  1.0,  1.0,  1.0,  1.0,  1.0, -1.0,
         -1.0,  1.0, -1.0, -1.0,  1.0, -1.0, -1.0, -1.0],
      [ 1.0, -1.0,  1.0, -1.0, -1.0, -1.0,  1.0, -1.0, -1.0, -1.0, -1.0, -1.0,  1.0,
          1.0, -1.0,  1.0,  1.0, -1.0,  1.0,  1.0,  1.0],
      [ 1.0, -1.0,  1.0, -1.0, -1.0, -1.0,  1.0, -1.0, -1.0, -1.0, -1.0, -1.0,  1.0,
          1.0, -1.0,  1.0,  1.0, -1.0,  1.0,  1.0,  1.0],
      [-1.0,  1.0, -1.0,  1.0,  1.0,  1.0, -1.0,  1.0,  1.0,  1.0,  1.0,  1.0, -1.0,
         -1.0,  1.0, -1.0, -1.0,  1.0, -1.0, -1.0, -1.0],
      [ 1.0, -1.0,  1.0, -1.0, -1.0, -1.0,  1.0, -1.0, -1.0, -1.0, -1.0, -1.0,  1.0,
          1.0, -1.0,  1.0,  1.0, -1.0,  1.0,  1.0,  1.0],
      [ 1.0, -1.0,  1.0, -1.0, -1.0, -1.0,  1.0, -1.0, -1.0, -1.0, -1.0, -1.0,  1.0,
          1.0, -1.0,  1.0,  1.0, -1.0,  1.0,  1.0,  1.0],
      [-1.0,  1.0, -1.0,  1.0,  1.0,  1.0, -1.0,  1.0,  1.0,  1.0,  1.0,  1.0, -1.0,
         -1.0,  1.0, -1.0, -1.0,  1.0, -1.0, -1.0, -1.0],
      [ 1.0, -1.0,  1.0, -1.0, -1.0, -1.0,  1.0, -1.0, -1.0, -1.0, -1.0, -1.0,  1.0,
          1.0, -1.0,  1.0,  1.0, -1.0,  1.0,  1.0,  1.0],
      [ 1.0, -1.0,  1.0, -1.0, -1.0, -1.0,  1.0, -1.0, -1.0, -1.0, -1.0, -1.0,  1.0,
          1.0, -1.0,  1.0,  1.0, -1.0,  1.0,  1.0,  1.0],
      [ 1.0, -1.0,  1.0, -1.0, -1.0, -1.0,  1.0, -1.0, -1.0, -1.0, -1.0, -1.0,  1.0,
          1.0, -1.0,  1.0,  1.0, -1.0,  1.0,  1.0,  1.0]
    ]
  },
  {
    "Name": "MultipleCandidates",
    "Values": [0.00033, 0.00011, 0.00012, 0.0001, 0.0021, 0.0073, 0.0011, 0.0011,
        0.0014, 0.0017, 0.0012, 0.00015, 0.00067, 0.0014, 0.00059, 0.011, 0.0, 0.024,
        0.0068, 0.0041, 0.0072],
    "SystematicCorrelationMatrix": [
      [1.0, -1.0, 1.0, -1.0, -1.0, -1.0, 1.0, -1.0, -1.0, 1.0, -1.0, -1.0, -1.0, -1.0,
          1.0, -1.0, 0.0, 1.0, -1.0, -1.0, -1.0],
      [-1.0, 1.0, -1.0, 1.0, 1.0, 1.0, -1.0, 1.0, 1.0, -1.0, 1.0, 1.0, 1.0, 1.0, -1.0,
          1.0, 0.0, -1.0, 1.0, 1.0, 1.0],
      [1.0, -1.0, 1.0, -1.0, -1.0, -1.0, 1.0, -1.0, -1.0, 1.0, -1.0, -1.0, -1.0, -1.0,
          1.0, -1.0, 0.0, 1.0, -1.0, -1.0, -1.0],
      [-1.0, 1.0, -1.0, 1.0, 1.0, 1.0, -1.0, 1.0, 1.0, -1.0, 1.0, 1.0, 1.0, 1.0, -1.0,
          1.0, 0.0, -1.0, 1.0, 1.0, 1.0],
      [-1.0, 1.0, -1.0, 1.0, 1.0, 1.0, -1.0, 1.0, 1.0, -1.0, 1.0, 1.0, 1.0, 1.0, -1.0,
          1.0, 0.0, -1.0, 1.0, 1.0, 1.0],
```

```
    [-1.0, 1.0, -1.0, 1.0, 1.0, 1.0, -1.0, 1.0, 1.0, -1.0, 1.0, 1.0, 1.0, 1.0, -1.0,
        1.0, 0.0, -1.0, 1.0, 1.0, 1.0],
    [1.0, -1.0, 1.0, -1.0, -1.0, -1.0, 1.0, -1.0, -1.0, 1.0, -1.0, -1.0, -1.0, -1.0,
        1.0, -1.0, 0.0, 1.0, -1.0, -1.0, -1.0],
    [-1.0, 1.0, -1.0, 1.0, 1.0, 1.0, -1.0, 1.0, 1.0, -1.0, 1.0, 1.0, 1.0, 1.0, -1.0,
        1.0, 0.0, -1.0, 1.0, 1.0, 1.0],
    [-1.0, 1.0, -1.0, 1.0, 1.0, 1.0, -1.0, 1.0, 1.0, -1.0, 1.0, 1.0, 1.0, 1.0, -1.0,
        1.0, 0.0, -1.0, 1.0, 1.0, 1.0],
    [1.0, -1.0, 1.0, -1.0, -1.0, -1.0, 1.0, -1.0, -1.0, 1.0, -1.0, -1.0, -1.0, -1.0,
        1.0, -1.0, 0.0, 1.0, -1.0, -1.0, -1.0],
    [-1.0, 1.0, -1.0, 1.0, 1.0, 1.0, -1.0, 1.0, 1.0, -1.0, 1.0, 1.0, 1.0, 1.0, -1.0,
        1.0, 0.0, -1.0, 1.0, 1.0, 1.0],
    [-1.0, 1.0, -1.0, 1.0, 1.0, 1.0, -1.0, 1.0, 1.0, -1.0, 1.0, 1.0, 1.0, 1.0, -1.0,
        1.0, 0.0, -1.0, 1.0, 1.0, 1.0],
    [-1.0, 1.0, -1.0, 1.0, 1.0, 1.0, -1.0, 1.0, 1.0, -1.0, 1.0, 1.0, 1.0, 1.0, -1.0,
        1.0, 0.0, -1.0, 1.0, 1.0, 1.0],
    [-1.0, 1.0, -1.0, 1.0, 1.0, 1.0, -1.0, 1.0, 1.0, -1.0, 1.0, 1.0, 1.0, 1.0, -1.0,
        1.0, 0.0, -1.0, 1.0, 1.0, 1.0],
    [1.0, -1.0, 1.0, -1.0, -1.0, -1.0, 1.0, -1.0, -1.0, 1.0, -1.0, -1.0, -1.0, -1.0,
        1.0, -1.0, 0.0, 1.0, -1.0, -1.0, -1.0],
    [-1.0, 1.0, -1.0, 1.0, 1.0, 1.0, -1.0, 1.0, 1.0, -1.0, 1.0, 1.0, 1.0, 1.0, -1.0,
        1.0, 0.0, -1.0, 1.0, 1.0, 1.0],
    [0.0, 0.0, 0.0, 0.0, 0.0, 0.0, 0.0, 0.0, 0.0, 0.0, 0.0, 0.0, 0.0, 0.0, 0.0, 0.0,
        1.0, 0.0, 0.0, 0.0, 0.0, 0.0],
    [1.0, -1.0, 1.0, -1.0, -1.0, -1.0, 1.0, -1.0, -1.0, 1.0, -1.0, -1.0, -1.0, -1.0,
        1.0, -1.0, 0.0, 1.0, -1.0, -1.0, -1.0],
    [-1.0, 1.0, -1.0, 1.0, 1.0, 1.0, -1.0, 1.0, 1.0, -1.0, 1.0, 1.0, 1.0, 1.0, -1.0,
        1.0, 0.0, -1.0, 1.0, 1.0, 1.0],
    [-1.0, 1.0, -1.0, 1.0, 1.0, 1.0, -1.0, 1.0, 1.0, -1.0, 1.0, 1.0, 1.0, 1.0, -1.0,
        1.0, 0.0, -1.0, 1.0, 1.0, 1.0],
    [-1.0, 1.0, -1.0, 1.0, 1.0, 1.0, -1.0, 1.0, 1.0, -1.0, 1.0, 1.0, 1.0, 1.0, -1.0,
        1.0, 0.0, -1.0, 1.0, 1.0, 1.0]
  ]
  },
{
  "Name": "QuadOSTagging",
  "Values": [0.0, 0.0, 0.0, 0.0, 0.0, 0.0, 0.0, 0.0, 0.0, 0.0, 0.0, 0.0, 0.0002, 0.0,
      0.0, 0.0, 0.003, 0.001, 0.001, 0.0, 0.001],
  "SystematicCorrelationMatrix": [
    [1.0, 0.0, 0.0, 0.0, 0.0, 0.0, 0.0, 0.0, 0.0, 0.0, 0.0, 0.0, 0.0, 0.0, 0.0, 0.0,
        0.0, 0.0, 0.0, 0.0, 0.0, 0.0],
    [0.0, 1.0, 0.0, 0.0, 0.0, 0.0, 0.0, 0.0, 0.0, 0.0, 0.0, 0.0, 0.0, 0.0, 0.0, 0.0,
        0.0, 0.0, 0.0, 0.0, 0.0, 0.0],
    [0.0, 0.0, 1.0, 0.0, 0.0, 0.0, 0.0, 0.0, 0.0, 0.0, 0.0, 0.0, 0.0, 0.0, 0.0, 0.0,
        0.0, 0.0, 0.0, 0.0, 0.0, 0.0],
    [0.0, 0.0, 0.0, 1.0, 0.0, 0.0, 0.0, 0.0, 0.0, 0.0, 0.0, 0.0, 0.0, 0.0, 0.0, 0.0,
        0.0, 0.0, 0.0, 0.0, 0.0, 0.0],
    [0.0, 0.0, 0.0, 0.0, 1.0, 0.0, 0.0, 0.0, 0.0, 0.0, 0.0, 0.0, 0.0, 0.0, 0.0, 0.0,
        0.0, 0.0, 0.0, 0.0, 0.0, 0.0],
    [0.0, 0.0, 0.0, 0.0, 0.0, 1.0, 0.0, 0.0, 0.0, 0.0, 0.0, 0.0, 0.0, 0.0, 0.0, 0.0,
        0.0, 0.0, 0.0, 0.0, 0.0, 0.0],
    [0.0, 0.0, 0.0, 0.0, 0.0, 0.0, 1.0, 0.0, 0.0, 0.0, 0.0, 0.0, 0.0, 0.0, 0.0, 0.0,
        0.0, 0.0, 0.0, 0.0, 0.0, 0.0],
    [0.0, 0.0, 0.0, 0.0, 0.0, 0.0, 0.0, 1.0, 0.0, 0.0, 0.0, 0.0, 0.0, 0.0, 0.0, 0.0,
        0.0, 0.0, 0.0, 0.0, 0.0, 0.0],
    [0.0, 0.0, 0.0, 0.0, 0.0, 0.0, 0.0, 0.0, 1.0, 0.0, 0.0, 0.0, 0.0, 0.0, 0.0, 0.0,
        0.0, 0.0, 0.0, 0.0, 0.0, 0.0],
    [0.0, 0.0, 0.0, 0.0, 0.0, 0.0, 0.0, 0.0, 0.0, 1.0, 0.0, 0.0, 0.0, 0.0, 0.0, 0.0,
        0.0, 0.0, 0.0, 0.0, 0.0, 0.0],
    [0.0, 0.0, 0.0, 0.0, 0.0, 0.0, 0.0, 0.0, 0.0, 0.0, 1.0, 0.0, 0.0, 0.0, 0.0, 0.0,
        0.0, 0.0, 0.0, 0.0, 0.0, 0.0],
    [0.0, 0.0, 0.0, 0.0, 0.0, 0.0, 0.0, 0.0, 0.0, 0.0, 0.0, 1.0, 0.0, 0.0, 0.0, 0.0,
        0.0, 0.0, 0.0, 0.0, 0.0, 0.0],
    [0.0, 0.0, 0.0, 0.0, 0.0, 0.0, 0.0, 0.0, 0.0, 0.0, 0.0, 0.0, 1.0, 0.0, 0.0, 0.0,
        1.0, 1.0, 1.0, 0.0, 1.0],
    [0.0, 0.0, 0.0, 0.0, 0.0, 0.0, 0.0, 0.0, 0.0, 0.0, 0.0, 0.0, 0.0, 1.0, 0.0, 0.0,
        0.0, 0.0, 0.0, 0.0, 0.0, 0.0],
    [0.0, 0.0, 0.0, 0.0, 0.0, 0.0, 0.0, 0.0, 0.0, 0.0, 0.0, 0.0, 0.0, 0.0, 1.0, 0.0,
        0.0, 0.0, 0.0, 0.0, 0.0, 0.0],
    [0.0, 0.0, 0.0, 0.0, 0.0, 0.0, 0.0, 0.0, 0.0, 0.0, 0.0, 0.0, 0.0, 0.0, 0.0, 1.0,
        0.0, 0.0, 0.0, 0.0, 0.0, 0.0],
    [0.0, 0.0, 0.0, 0.0, 0.0, 0.0, 0.0, 0.0, 0.0, 0.0, 0.0, 0.0, 0.0, 1.0, 0.0, 0.0,
        1.0, 1.0, 1.0, 0.0, 1.0],
    [0.0, 0.0, 0.0, 0.0, 0.0, 0.0, 0.0, 0.0, 0.0, 0.0, 0.0, 0.0, 0.0, 1.0, 0.0, 0.0,
        1.0, 1.0, 1.0, 0.0, 1.0],
    [0.0, 0.0, 0.0, 0.0, 0.0, 0.0, 0.0, 0.0, 0.0, 0.0, 0.0, 0.0, 0.0, 1.0, 0.0, 0.0,
        1.0, 1.0, 1.0, 0.0, 1.0],
```

```
            [0.0, 0.0, 0.0, 0.0, 0.0, 0.0, 0.0, 0.0, 0.0, 0.0, 0.0, 0.0, 0.0, 0.0, 0.0, 0.0,
                0.0, 0.0, 0.0, 1.0, 0.0],
            [0.0, 0.0, 0.0, 0.0, 0.0, 0.0, 0.0, 0.0, 0.0, 0.0, 0.0, 0.0, 1.0, 0.0, 0.0, 0.0,
                1.0, 1.0, 1.0, 0.0, 1.0]
          ]
        }
      ]
}
,
{
      "ResultSetLabel": "2012-JPsiPiPi",
      "Description" : [
         "Contains the 2011-2012 2fb results for phis et. al. from polarisation independent
             nominal fit"
      ],
      "Parameter": [
        {
          "Name": "phis",
          "Value": 0.075,
          "Error": 0.065
        },
        {
          "Name": "lamb",
          "Value": 0.898,
          "Error": 0.051
        }
      ],
      "StatisticalCorrelationMatrix": [
        [ 1.0, 0.025],
        [0.025,  1.0 ]
      ],
      "SystematicErrors": [
        {
          "Name": "DecayTimeEfficiencyStatRun1",
          "Values": [0.0006, 0.0008 ]
        },
        {
          "Name": "AngEfficiencyStatpipi",
          "Values": [0.0003,     0.0003 ]
        },
        {
          "Name": "BackgroundTimepipi",
          "Values": [0.0002,     0.0011 ]
        },
        {
          "Name": "ResonanceModelling",
          "Values": [0.0060,     0.0100 ]
        },
        {
          "Name": "ResonancePar",
          "Values": [0.0007,     0.0007 ]
        },
        {
          "Name": "ProdAsym",
          "Values": [0.0058,     0.0017 ]
        },
        {
          "Name": "DecayTimeResolutionPromptpipiRun1",
          "Values": [0.0088,     0.0066 ]
        },
        {
          "Name": "Taggingpipi",
          "Values": [0.0052,     0.0014 ]
        },
        {
          "Name": "DeltaMs",
          "Values": [0.0038,     0.0024 ]
        },
    {
          "Name": "Gamma_L",
          "Values": [0.0004,     0.0004 ]
        },
    {
        "Name": "OtherFixedPars",
        "Values": [0.0004,      0.0009 ]
    },
    {
```

```
        "Name": "BackgroundMass",
        "Values": [0.0006,      0.0016 ]
    }
    ]
}
,
{
    "ResultSetLabel": "2016-JPsiPiPi",
    "Description" : [
       "Contains the 2015-2016 2fb results for phis et. al. from polarisation independent
           nominal fit"
    ],
    "Parameter": [
      {
        "Name": "ghgd",
        "Value": -0.050,
        "Error": 0.004
      },
      {
        "Name": "lamb",
        "Value": 1.01,
        "Error": 0.08
      },
      {
        "Name": "phis",
        "Value": -0.057,
        "Error": 0.060
      }
    ],
    "StatisticalCorrelationMatrix": [
      [ 1.0 , 0.022,  0.038],
      [ 0.022,   1.0, 0.065],
      [ 0.038, 0.065,  1.0 ]
    ],
    "SystematicErrors": [
      {
        "Name": "DecayTimeEfficiencyStatRun2",
        "Values": [0.0020, 0.0000, 0.0003 ]
      },
      {
          "Name": "AngEfficiencyStatpipi",
          "Values": [0.0002,      0.0001,      0.0000 ]
      },
      {
          "Name": "BackgroundTimepipi",
          "Values": [0.0030,      0.0027,      0.0006 ]
      },
      {
          "Name": "ResonanceModelling",
          "Values": [0.0005,      0.0289,      0.0090 ]
      },
      {
          "Name": "ResonancePar",
          "Values": [0.0006,      0.0019,      0.0008 ]
      },
      {
          "Name": "ProdAsym",
          "Values": [0.0003,      0.0006,      0.0034 ]
      },
      {
        "Name": "DecayTimeResolutionPromptpipiRun2",
        "Values": [0.0000,     0.0043,          0.0040 ]
      },
      {
          "Name": "Taggingpipi",
          "Values": [0.0000,      0.0022,      0.0023 ]
      },
      {
          "Name": "DeltaMs",
          "Values": [0.0003,      0.0046,      0.0025]
      },
      {
          "Name": "Gamma_L",
          "Values": [0.0003,      0.0004,      0.0004 ]
      },
      {
        "Name": "DecayTimeResolutionMean",
```

```
        "Values": [0.0003,     0.0012,          0.0003 ]
      },
    {
        "Name": "Bc",
        "Values": [0.0005, 0, 0]
      }
    ]
}
,
{
    "ResultSetLabel": "2012-highKK",
    "Description" : [
       "Contains the 2011-2012 2fb results for phis et. al. from polarisation independent
            nominal fit in the high KK mass region"
    ],
    "Parameter": [
      {
        "Name": "gsgd",
        "Value": -0.0080,
        "Error": 0.0058
      },
      {
        "Name": "deltaGammas",
        "Value": 0.066,
        "Error": 0.020
      },
      {
        "Name": "phis",
        "Value": 0.118,
        "Error": 0.111
      },
      {
        "Name": "lamb",
        "Value": 0.994,
        "Error": 0.019
      },
      {
        "Name": "dms",
        "Value": 17.807,
        "Error": 0.076
      }
    ],
    "StatisticalCorrelationMatrix": [
      [  1.0,  0.54,  0.02, -0.03, -0.03],
      [ 0.54,  1.00,  0.04, -0.06, -0.05],
      [ 0.02,  0.04,  1.00, -0.14, -0.01],
      [-0.03, -0.06, -0.14,  1.00, 0.17],
      [-0.03, -0.05, -0.01, 0.17, 1.00]
    ],
    "SystematicErrors": [
    {
        "Name": "DecayTimeEfficiencyStatRun1",
        "Values": [0.0028, 0.0022, 0.0, 0.0, 0.0 ]
      },
      {
        "Name": "DecayTimeResolutionPromptKKRun1",
        "Values": [0.0002, 0.0003, 0.0011, 0.0002, 0.0]
      },
      {
        "Name": "ProdAsym",
        "Values": [0.0003, 0.0001, 0.0040, 0.0014, 0.0 ]
      },
      {
        "Name": "ResonantBackground",
        "Values": [0.0008, 0.0005, 0.0015, 0.0004, 0.0]
      },
      {
        "Name": "MassFactorisationCosThMu",
        "Values": [0.0001, 0.0011, 0.0214, 0.0005, 0.0]
      },
      {
        "Name": "Bc",
        "Values": [0.0005, 0.0, 0.0, 0.0, 0.0 ]
      }
    ]
}
,
```

```
{
    "ResultSetLabel": "2012-psi2S",
    "Description" : [
        "Contains the 2011-2012 2fb results for phis et. al. from polarisation independent
            nominal fit to psi(2S)phi. gsgd=gamma-0.65789"
    ],
    "Parameter": [
      {
        "Name": "gsgd",
        "Value": 0.010,
        "Error": 0.011
      },
      {
        "Name": "deltaGammas",
        "Value": 0.066,
        "Error": 0.044
      },
      {
        "Name": "AperpSqPsi2SKK",
        "Value": 0.264,
        "Error": 0.024
      },
      {
        "Name": "AzeroSqPsi2SKK",
        "Value": 0.422,
        "Error": 0.014
      },
      {
        "Name": "dpaPsi2SKK",
        "Value": 3.67,
        "Error": 0.18
      },
      {
        "Name": "dpePsi2SKK",
        "Value": 3.29,
        "Error": 0.43
      },
      {
        "Name": "FSPsi2SKK",
        "Value": 0.061,
        "Error": 0.026
      },
      {
        "Name": "deltaSPsi2SKK",
        "Value": 0.03,
        "Error": 0.14
      },
      {
        "Name": "phis",
        "Value": 0.23,
        "Error": 0.29
      },
      {
        "Name": "lamb",
        "Value": 1.045,
        "Error": 0.069
      }
    ],
    "StatisticalCorrelationMatrix": [
      [ 1.00,  -0.40,  0.35, -0.27,  -0.08,  -0.02,  0.15,   0.02,  0.02, -0.04],
      [-0.40,   1.00, -0.66,  0.60,   0.02,  -0.04, -0.10,  -0.02,  0.19,  0.03],
      [ 0.35,  -0.66,  1.00, -0.54,  -0.31,  -0.05,  0.08,   0.03, -0.02, -0.02],
      [-0.27,   0.60, -0.54,  1.00,   0.05,  -0.02, -0.15,  -0.02,  0.07,  0.03],
      [-0.08,   0.02, -0.31,  0.05,   1.00,   0.26, -0.26,  -0.01,  0.00,  0.08],
      [-0.02,  -0.04, -0.05, -0.02,   0.26,   1.00, -0.21,  -0.25, -0.06,  0.59],
      [ 0.15,  -0.10,  0.08, -0.15,  -0.26,  -0.21,  1.00,   0.02,  0.05, -0.25],
      [ 0.02,  -0.02,  0.03, -0.02,  -0.01,  -0.25,  0.02,   1.00,  0.07, -0.09],
      [ 0.02,   0.19, -0.02,  0.07,   0.00,  -0.06,  0.05,   0.07,  1.00,  0.04],
      [-0.04,   0.03, -0.02,  0.03,   0.08,   0.59, -0.25,  -0.09,  0.04,  1.00]
    ],
    "SystematicErrors": [
      {
        "Name": "MassFactorisationCosThMu",
        "Values": [0.003, 0.002, 0.001, 0.001, 0.02, 0.0, 0.003, 0.01, 0.01, 0.001]
      },
  {
        "Name": "MassModelPsi",
```

```
        "Values": [0.001, 0.001, 0.0, 0.0, 0.0, 0.0, 0.0, 0.0, 0.0, 0.001]
      },
      {
        "Name": "AngEfficiencyPsi",
        "Values": [0.0, 0.001, 0.001, 0.002, 0.02, 0.03, 0.005, 0.02, 0.01, 0.006]
      },
      {
        "Name": "AngularResolution",
        "Values": [0.0, 0.0, 0.001, 0.0, 0.01, 0.01, 0.0, 0.0, 0.0, 0.0]
      },
      {
        "Name": "DecayTimeResolutionPsi",
        "Values": [0.0, 0.001, 0.0, 0.0, 0.0, 0.02, 0.002, 0.0, 0.02, 0.002]
      },
      {
        "Name": "DecayTimeResolutionStatPsi",
        "Values": [0.0, 0.0, 0.0, 0.0, 0.0, 0.02, 0.0, 0.0, 0.0, 0.002 ]
      },
  {
        "Name": "DecayTimeEfficiencyStatPsi",
        "Values": [0.005, 0.003, 0.001, 0.001, 0.0, 0.0, 0.002, 0.0, 0.0, 0.0 ]
      },
  {
        "Name": "DecayTimeEfficiencyModelPsi",
        "Values": [0.001, 0.001, 0.0, 0.0, 0.0, 0.0, 0.0, 0.0, 0.0, 0.0 ]
      },
      {
        "Name": "Bc",
        "Values": [0.001, 0.0, 0.0, 0.0, 0.0, 0.0, 0.0, 0.0, 0.0, 0.0]
      },
      {
        "Name": "FitBias",
        "Values": [0.001, 0.006, 0.0, 0.001, 0.01, 0.0, 0.003, 0.0, 0.0, 0.0]
      }
    ]
}
,
{
    "ResultSetLabel": "2012-DsDs",
    "Description" : [
       "Contains the 2011-2012 2fb results for phis et. al. from polarisation independent
            nominal fit to DsDs"
    ],
    "Parameter": [
      {
        "Name": "phis",
        "Value": 0.02,
        "Error": 0.17
      },
      {
        "Name": "lamb",
        "Value": 0.91,
        "Error": 0.18
      }
    ],
    "StatisticalCorrelationMatrix": [
      [  1.0, 0.03],
      [ 0.03, 1.00]
    ],
    "SystematicErrors": [
      {
        "Name": "DecayTimeResolutionDsDs",
        "Values": [0.016, 0.0164 ]
      },
      {
        "Name": "AngEfficiencyModelDsDs",
        "Values": [0.0047, 0.0044 ]
      },
      {
        "Name": "AngEfficiencyStatDsDs",
        "Values": [0.0023, 0.0023 ]
      },
      {
        "Name": "MassModelDsDs",
        "Values": [0.0075, 0.0016 ]
      },
      {
```

```
            "Name": "MassFactorisationDsDs",
            "Values": [0.0013, 0.0075 ]
          }
        ]
}
,
{
   "ResultSetLabel": "GammaD",
   "Description" :  ["GammaD"],
   "Parameter": [
      {
         "Name": "gammaD",
         "Value": 0.65833,
         "Error": 0.00173
      }
   ]
}
  ]
}
```

Appendix H

Total Correlation Matrices

This appendix shows the total correlation matrices including statistical and systematic uncertainties. The Run 1 $B_s^0 \to J/\psi K^+K^-$ numbers are from Ref. [56] and private communication. The Run 2 $B_s^0 \to J/\psi K^+K^-$ dataset refers to the analysis presented in Ref. [1], which analyses data recorded by the LHCb detector in the years 2015 and 2016. Table H.1 shows the correlations for the Run 1 and Run 2 $B_s^0 \to J/\psi K^+K^-$ measurements for the main parameters. The correlations between the Run 2 main and S-wave parameters are $\leq$ 0.15. Table H.2 and Table H.3 present the correlation matrices obtained after performing the combination for the Run 1 and Run 2 $B_s^0 \to J/\psi K^+K^-$ analyses, and for all LHCb ϕ_s measurements, respectively.

	Γ_s Run 1	$\Delta\Gamma_s$ Run 1	$\lvert A_\perp\rvert^2$ Run 1	$\lvert A_0\rvert^2$ Run 1	$\delta_\parallel - \delta_0$ Run 1	$\delta_\perp - \delta_0$ Run 1	ϕ_s Run 1	$\lvert\lambda\rvert$ Run 1	Δm_s Run 1	$\Gamma_s - \Gamma_d$ Run 2	$\Delta\Gamma_s$ Run 2	$\lvert A_\perp\rvert^2$ Run 2	$\lvert A_0\rvert^2$ Run 2	$\delta_\parallel - \delta_0$ Run 2	$\delta_\perp - \delta_0$ Run 2	ϕ_s Run 2	$\lvert\lambda\rvert$ Run 2	Δm_s Run 2	Γ_d
Γ_s Run 1	1.00	-0.30	0.27	-0.11	-0.07	-0.02	0.00	0.01	0.03	0.00	0.00	0.01	-0.02	0.00	0.00	0.00	0.00	0.00	0.00
$\Delta\Gamma_s$ Run 1		1.00	**-0.58**	0.36	-0.02	-0.05	-0.08	0.04	-0.00	0.00	0.00	0.00	0.00	0.00	0.00	0.00	0.00	0.00	0.00
$\lvert A_\perp\rvert^2$ Run 1			1.00	**-0.70**	-0.07	0.09	0.05	-0.04	0.03	0.00	0.00	0.06	-0.10	0.01	0.00	0.00	0.01	0.00	0.00
$\lvert A_0\rvert^2$ Run 1				1.00	-0.26	-0.28	-0.05	0.04	-0.07	-0.01	-0.01	-0.07	0.14	-0.02	-0.01	-0.00	-0.02	0.00	0.00
$\delta_\parallel - \delta_0$ Run 1					1.00	0.45	0.02	0.03	0.06	0.00	0.00	0.01	-0.02	0.01	0.00	-0.00	0.00	0.00	0.00
$\delta_\perp - \delta_0$ Run 1						1.00	0.15	-0.17	**0.64**	0.00	0.00	0.00	0.00	0.00	0.01	0.00	0.00	0.00	0.00
ϕ_s Run 1							1.00	-0.02	0.09	0.00	0.00	0.00	0.00	0.00	0.00	0.00	0.00	0.00	0.00
$\lvert\lambda\rvert$ Run 1								1.00	-0.19	0.00	0.00	0.02	-0.03	0.01	0.01	0.01	0.06	0.00	0.00
Δm_s Run 1									1.00	0.00	0.00	0.01	-0.01	0.00	0.00	0.00	0.00	0.01	0.00
$\Gamma_s - \Gamma_d$ Run 2										1.00	-0.46	0.36	-0.23	0.05	0.04	-0.05	0.06	0.06	0.00
$\Delta\Gamma_s$ Run 2											1.00	**-0.66**	0.48	-0.03	-0.10	0.01	-0.09	-0.05	0.00
$\lvert A_\perp\rvert^2$ Run 2												1.00	**-0.64**	0.09	0.07	-0.02	0.04	0.01	0.00
$\lvert A_0\rvert^2$ Run 2													1.00	-0.03	-0.03	0.00	-0.02	0.01	0.00
$\delta_\parallel - \delta_0$ Run 2														1.00	0.25	-0.01	0.03	0.00	0.00
$\delta_\perp - \delta_0$ Run 2															1.00	0.01	0.14	**0.61**	0.00
ϕ_s Run 2																1.00	0.17	-0.02	0.00
$\lvert\lambda\rvert$ Run 2																	1.00	0.05	0.00
Δm_s Run 2																		1.00	0.00
Γ_d																			1.00

Table H.1 *Overall correlation matrix of the Run 1 and Run 2 $B_s^0 \to J/\psi K^+K^-$ samples used for the combination. The correlations larger than 0.50 are highlighted in bold. For Run 2 only the main parameters are presented.*

	ϕ_s	$\lvert\lambda\rvert$	Γ_s	$\Delta\Gamma_s$	Δm_s	$\lvert A_\perp\rvert^2$	$\lvert A_0\rvert^2$	$\delta_\perp - \delta_0$	$\delta_\parallel - \delta_0$	F_{S1}	F_{S2}	F_{S3}	F_{S4}	F_{S5}	F_{S6}	$\delta_{S1} - \delta_\perp$	$\delta_{S2} - \delta_\perp$	$\delta_{S3} - \delta_\perp$	$\delta_{S4} - \delta_\perp$	$\delta_{S5} - \delta_\perp$	$\delta_{S6} - \delta_\perp$	Γ_d
ϕ_s	1.00	0.11	-0.02	-0.03	0.02	0.01	-0.02	0.06	0.00	0.01	-0.01	0.02	-0.02	-0.01	-0.03	0.02	-0.03	-0.02	-0.00	0.01	0.01	0.01
$\lvert\lambda\rvert$		1.00	0.03	-0.03	-0.06	0.03	-0.02	-0.01	0.03	-0.00	0.03	0.08	-0.04	0.02	0.03	0.03	-0.14	-0.12	-0.04	-0.02	0.04	-0.00
Γ_s			1.00	-0.35	0.04	0.28	-0.17	0.01	0.01	0.00	0.01	0.01	0.02	0.05	0.04	-0.03	-0.00	-0.02	0.00	-0.01	-0.02	0.39
$\Delta\Gamma_s$				1.00	-0.01	**-0.62**	0.41	-0.05	-0.01	-0.01	-0.01	0.00	0.01	-0.06	-0.04	0.05	0.00	0.02	0.01	0.02	0.03	0.04
Δm_s					1.00	0.01	-0.01	**0.62**	0.02	-0.03	0.00	-0.04	0.08	0.06	-0.00	-0.06	-0.05	0.06	0.02	0.03	-0.06	0.00
$\lvert A_\perp\rvert^2$						1.00	**-0.67**	0.04	0.01	-0.01	-0.09	-0.06	-0.00	0.02	-0.00	0.02	0.01	-0.04	0.02	-0.01	0.02	-0.02
$\lvert A_0\rvert^2$							1.00	-0.06	-0.07	-0.02	0.02	0.00	-0.00	-0.02	0.01	-0.03	-0.00	0.03	0.02	0.01	0.00	0.01
$\delta_\perp - \delta_0$								1.00	0.28	-0.04	0.05	0.05	0.03	0.04	-0.01	-0.13	-0.09	0.02	-0.07	-0.01	-0.16	-0.00
$\delta_\parallel - \delta_0$									1.00	0.01	0.16	0.17	0.00	0.05	0.05	-0.12	-0.05	0.02	-0.13	-0.04	-0.12	-0.01
F_{S1}										1.00	0.01	-0.00	0.00	0.00	0.04	0.07	-0.01	0.01	0.02	0.03	0.01	-0.00
F_{S2}											1.00	0.21	-0.00	0.05	0.04	-0.08	0.06	0.09	-0.16	-0.05	-0.08	-0.01
F_{S3}												1.00	-0.03	0.02	0.01	-0.06	-0.02	**-0.58**	-0.16	-0.05	-0.07	-0.01
F_{S4}													1.00	0.08	0.03	0.01	0.02	-0.01	0.46	0.02	0.03	-0.01
F_{S5}														1.00	0.07	-0.02	0.01	-0.02	0.02	0.43	0.01	-0.01
F_{S6}															1.00	-0.24	-0.01	-0.00	0.02	0.02	0.14	-0.01
$\delta_{S1} - \delta_\perp$																1.00	0.02	-0.02	0.07	0.04	0.40	0.02
$\delta_{S2} - \delta_\perp$																	1.00	0.01	0.02	0.00	0.03	0.00
$\delta_{S3} - \delta_\perp$																		1.00	-0.05	-0.01	-0.02	0.00
$\delta_{S4} - \delta_\perp$																			1.00	0.07	0.09	0.00
$\delta_{S5} - \delta_\perp$																				1.00	0.05	0.00
$\delta_{S6} - \delta_\perp$																					1.00	0.01
Γ_d																						1.00

Table H.2 *Correlation matrix for the results in Table 8.1 taking into account correlated systematics between the Run 1 and Run 2 $B_s^0 \to J/\psi K^+K^-$ measurements as described in Section 8.3. The correlations larger than 0.50 are highlighted in bold.*

	ϕ_s	$\lvert\lambda\rvert$	Γ_s	$\Delta\Gamma_s$	Δm_s	$\lvert A_\perp\rvert^2$	$\lvert A_0\rvert^2$	$\delta_\perp - \delta_0$	$\delta_\parallel - \delta_0$	F_{S1}	F_{S2}	F_{S3}	F_{S4}	F_{S5}	F_{S6}	$\delta_{S1} - \delta_\perp$	$\delta_{S2} - \delta_\perp$	$\delta_{S3} - \delta_\perp$	$\delta_{S4} - \delta_\perp$	$\delta_{S5} - \delta_\perp$	$\delta_{S6} - \delta_\perp$	Γ_d	$\left\lvert A_\perp^{\psi(2S)}\right\rvert^2$	$\left\lvert A_0^{\psi(2S)}\right\rvert^2$	$\delta_\parallel^{\psi(2S)}$	$\delta_\perp^{\psi(2S)}$	$\left\lvert A_S^{\psi(2S)}\right\rvert^2$	$\delta_S^{\psi(2S)}$
ϕ_s	1.0	0.06	-0.02	-0.03	0.02	0.01	-0.01	0.05	0.0	0.0	-0.01	0.01	-0.01	-0.01	-0.02	0.02	-0.02	-0.01	0.0	0.01	0.0	0.0	0.01	-0.01	0.0	-0.0	0.0	0.01
$\lvert\lambda\rvert$		1.0	0.02	-0.02	0.01	0.02	-0.01	0.02	0.02	-0.0	0.02	0.06	-0.03	0.02	0.02	0.02	-0.11	-0.09	-0.03	-0.01	0.03	0.0	0.0	0.0	0.01	0.11	-0.04	-0.01
Γ_s			1.0	-0.16	0.03	0.15	-0.08	-0.0	0.0	0.0	0.0	0.0	0.02	0.03	0.02	-0.02	-0.0	-0.01	0.0	-0.0	-0.01	0.49	0.03	-0.02	-0.01	0.0	0.01	0.0
$\Delta\Gamma_s$				1.0	-0.01	**-0.51**	0.32	-0.05	-0.0	-0.01	-0.01	0.01	0.02	-0.03	-0.02	0.03	0.0	0.01	0.01	0.01	0.02	-0.03	-0.09	0.07	0.0	-0.01	-0.01	-0.0
Δm_s					1.0	0.0	-0.01	**0.57**	0.01	-0.03	0.0	-0.03	0.07	0.06	0.0	-0.05	-0.05	0.05	0.02	0.03	-0.05	0.0	0.0	-0.0	-0.0	0.0	0.0	0.0
$\lvert A_\perp\rvert^2$						1.0	**-0.64**	0.03	0.01	-0.01	-0.1	-0.07	-0.01	0.0	-0.02	0.04	0.02	-0.03	0.02	-0.0	0.03	0.03	0.05	-0.04	-0.0	0.0	0.01	0.0
$\lvert A_0\rvert^2$							1.0	-0.05	-0.07	-0.02	0.02	0.01	-0.0	-0.01	0.02	-0.04	-0.01	0.02	0.01	0.01	-0.01	-0.01	-0.03	0.03	0.0	-0.0	-0.0	-0.0
$\delta_\perp - \delta_0$								1.0	0.29	-0.04	0.05	0.06	0.02	0.04	-0.01	-0.13	-0.09	0.01	-0.07	-0.02	-0.15	-0.0	0.0	-0.0	0.0	0.0	-0.0	0.0
$\delta_\parallel - \delta_0$									1.0	0.01	0.16	0.17	0.0	0.05	0.04	-0.12	-0.05	0.02	-0.13	-0.04	-0.12	-0.01	0.0	-0.0	0.0	0.0	-0.0	-0.0
F_{S1}										1.0	0.01	-0.0	0.0	0.0	0.04	0.07	-0.01	0.01	0.02	0.03	0.01	-0.0	0.0	-0.0	-0.0	-0.0	0.0	0.0
F_{S2}											1.0	0.21	-0.0	0.05	0.04	-0.08	0.06	0.09	-0.16	-0.05	-0.08	-0.01	0.0	-0.0	0.0	0.0	-0.0	-0.0
F_{S3}												1.0	-0.03	0.02	0.01	-0.06	-0.02	**-0.58**	-0.16	-0.05	-0.08	-0.01	-0.0	0.0	0.0	0.01	-0.0	-0.0
F_{S4}													1.0	0.08	0.04	0.01	0.02	-0.02	0.45	0.02	0.03	-0.01	-0.0	0.0	-0.0	-0.0	0.0	0.0
F_{S5}														1.0	0.07	-0.02	0.01	-0.02	0.02	0.43	0.01	-0.01	0.0	-0.0	-0.0	0.0	0.0	-0.0
F_{S6}															1.0	-0.24	-0.01	-0.0	0.02	0.02	0.15	-0.01	0.0	-0.0	-0.0	0.0	-0.0	-0.0
$\delta_{S1} - \delta_\perp$																1.0	0.02	-0.02	0.07	0.04	0.4	0.01	-0.0	0.0	0.0	0.0	-0.0	-0.0
$\delta_{S2} - \delta_\perp$																	1.0	0.01	0.02	0.0	0.03	0.0	-0.0	-0.0	-0.0	-0.01	0.0	0.0
$\delta_{S3} - \delta_\perp$																		1.0	-0.06	-0.01	-0.02	0.0	-0.0	0.0	-0.0	-0.01	0.0	0.0
$\delta_{S4} - \delta_\perp$																			1.0	0.07	0.09	0.0	-0.0	0.0	-0.0	-0.0	0.0	0.0
$\delta_{S5} - \delta_\perp$																				1.0	0.05	0.0	-0.0	0.0	-0.0	-0.0	0.0	0.0
$\delta_{S6} - \delta_\perp$																					1.0	0.01	-0.0	0.0	0.0	0.0	-0.0	-0.0
Γ_d																						1.0	-0.0	0.0	0.0	0.0	-0.0	0.0
$\left\lvert A_\perp^{\psi(2S)}\right\rvert^2$																							1.0	-0.24	-0.38	-0.11	0.0	0.01
$\left\lvert A_0^{\psi(2S)}\right\rvert^2$																								1.0	0.04	-0.01	-0.1	-0.0
$\delta_\parallel^{\psi(2S)}$																									1.0	0.26	-0.23	-0.0
$\delta_\perp^{\psi(2S)}$																										1.0	-0.08	-0.24
$\left\lvert A_S^{\psi(2S)}\right\rvert^2$																											1.0	-0.01
$\delta_S^{\psi(2S)}$																												1.0

Table H.3 *The correlation matrix for the results in Table 8.2 taking into account the systematic correlations between the Run 1 and Run 2 LHCb results as described in Section 8.4. The correlations larger than 0.50 are highlighted in bold.*

Bibliography

[1] R. Aaij et al. Updated measurement of time-dependent *CP*-violating observables in $B_s^0 \to J/\psi K^+K^-$ decays. *Eur. Phys. J.*, C79(8):706, 2019.

[2] Planck Collaboration. Planck 2015 results - i. overview of products and scientific results. *A&A*, 594:A1, 2016.

[3] A. D. Sakharov. Violation of CP Invariance, C asymmetry, and baryon asymmetry of the universe. *Pisma Zh. Eksp. Teor. Fiz.*, 5:32–35, 1967. [Usp. Fiz. Nauk161,no.5,61(1991)].

[4] J. H. Christenson, J. W. Cronin, V. L. Fitch, and R. Turlay. Evidence for the 2π decay of the K_2^0 meson. *Phys. Rev. Lett.*, 13:138–140, Jul 1964.

[5] M. Kobayashi and T. Maskawa. CP Violation in the Renormalizable Theory of Weak Interaction. *Prog. Theor. Phys.*, 49:652–657, 1973.

[6] A. J. Bevan et al. The Physics of the B Factories. *Eur. Phys. J.*, C74:3026, 2014.

[7] R. R. Wilson. The Tevatron. *Phys. Today*, 30N10:23–30, 1977.

[8] H. Fritzsch, M. Gell-Mann, and H. Leutwyler. Advantages of the color octet gluon picture. *Physics Letters B*, 47(4):365 – 368, 1973.

[9] S. L. Glashow. Partial-symmetries of weak interactions. *Nuclear Physics*, 22(4):579 – 588, 1961.

[10] E. S. Abers and B. W. Lee. Gauge Theories. *Phys. Rept.*, 9:1–141, 1973.

[11] S. Abachi et al. Observation of the top quark. *Phys. Rev. Lett.*, 74:2632–2637, 1995.

[12] F. Abe et al. Observation of top quark production in $\bar{p}p$ collisions. *Phys. Rev. Lett.*, 74:2626–2631, 1995.

[13] K. Kodama et al. Observation of tau neutrino interactions. *Phys. Lett.*, B504:218–224, 2001.

[14] G. Aad et al. Observation of a new particle in the search for the Standard Model Higgs boson with the ATLAS detector at the LHC. *Phys. Lett.*, B716:1–29, 2012.

[15] S. Chatrchyan et al. Observation of a new boson at a mass of 125 GeV with the CMS experiment at the LHC. *Phys. Lett.*, B716:30–61, 2012.

[16] P.W. Higgs. Broken symmetries, massless particles and gauge fields. *Physics Letters*, 12(2):132 – 133, 1964.

[17] Various contributors. *Standard Model of Elementary Particles*. Wikimedia Commons, 2006-2017. Taken from `https://commons.wikimedia.org/wiki/File:Standard_Model_of_Elementary_Particles.svg` under Creative Commons licence. The source cites PBS, FermiLab and the PDG.

[18] M. Gell-Mann. A Schematic Model of Baryons and Mesons. *Phys. Lett.*, 8:214–215, 1964.

[19] S. Weinberg. A model of leptons. *Phys. Rev. Lett.*, 19:1264–1266, Nov 1967.

[20] A. Salam and J. C. Ward. Weak and electromagnetic interactions. *Il Nuovo Cimento (1955-1965)*, 11(4):568–577, Feb 1959.

[21] N. Cabibbo. Unitary symmetry and leptonic decays. *Phys. Rev. Lett.*, 10:531–533, Jun 1963.

[22] L. Wolfenstein. Parametrization of the kobayashi-maskawa matrix. *Phys. Rev. Lett.*, 51:1945–1947, Nov 1983.

[23] J. Charles et al. Current status of the standard model ckm fit and constraints on $\Delta f = 2$ new physics. *Phys. Rev. D*, 91:073007, Apr 2015. updated results and plots available at `http://ckmfitter.in2p3.fr/`.

[24] M. Tanabashi et al. Review of particle physics. *Phys. Rev. D*, 98:030001, Aug 2018. 2019 update at `http://pdglive.lbl.gov/`.

[25] A. Lenz. Lifetimes and heavy quark expansion. *International Journal of Modern Physics A*, 30(10):1543005, 2015.

[26] M. Kirk, A. Lenz, and T. Rauh. Dimension-six matrix elements for meson mixing and lifetimes from sum rules. *Journal of high energy physics.*, 2017(12):068, December 2017.

[27] G. Borissov M. Artuso and A. Lenz. CP violation in the B_s^0 system. *Rev. Mod. Phys.*, 88:045002, Oct 2016.

[28] T. Aaij et al. Measurement of CP violation and the B_s^0 meson decay width difference with $B_s^0 \to J/\psi K^+K^-$ and $B_s^0 \to J/\psi \pi^+\pi^-$ decays. *Phys. Rev.*, D87(11):112010, 2013.

[29] C. Chiang et al. New physics in $B_s^0 \to J/\psi\phi$: a general analysis. *Journal of High Energy Physics*, 2010(4):31, Apr 2010.

[30] W. Wang X. Liu and Y Xie. Penguin pollution in $B \to J/\psi V$ decays and impact on the extraction of the $B_s - \overline{B}_s$ mixing phase. *Phys. Rev. D*, 89:094010, May 2014.

[31] R. Fleischer S. Faller and T. Mannel. Precision physics with $B_s^0 \to j/\psi\phi$ at the lhc: The quest for new physics. *Phys. Rev. D*, 79:014005, Jan 2009.

[32] R. Aaij et al. Measurement of CP violation parameters and polarisation fractions in $\mathrm{B_s^0 \to J/\psi \overline{K}^{*0}}$ decays. *JHEP*, 11:082, 2015.

[33] E. Mobs. The CERN accelerator complex. Complexe des acclrateurs du CERN. Jul 2016. General Photo.

[34] G. Aad et al. The ATLAS experiment at the CERN large hadron collider. *Journal of Instrumentation*, 3(08):S08003–S08003, aug 2008.

[35] S. Chatrchyan et al. The CMS experiment at the CERN LHC. *Journal of Instrumentation*, 3(08):S08004–S08004, aug 2008.

[36] A. Augusto et al. The LHCb detector at the LHC. *Journal of Instrumentation*, 3(08):S08005–S08005, aug 2008.

[37] K. Aamodt et al. The ALICE experiment at the CERN LHC. *Journal of Instrumentation*, 3(08):S08002–S08002, aug 2008.

[38] R. Aaij et al. Design and performance of the LHCb trigger and full real-time reconstruction in Run 2 of the LHC. *JINST*, 14(04):P04013, 2019.

[39] LHCb Online. Lhcb operations plots webpage. `https://lbgroups.cern.ch/online/OperationsPlots/index.htm`. Accessed: 2019-12-17.

[40] C. Elsässer. $\bar{b}b$ production angle plots. `https://lhcb.web.cern.ch/lhcb/speakersbureau/html/bb_ProductionAngles.html`. Accessed: 2019-05-05.

[41] R. Arink et al. Performance of the LHCb Outer Tracker. *JINST*, 9(01):P01002, 2014.

[42] R. Aaij et al. LHCb Detector Performance. *Int. J. Mod. Phys. A*, 30(LHCB-DP-2014-002. CERN-PH-EP-2014-290. LHCB-DP-2014-002. CERN-LHCB-DP-2014-002):1530022. 73 p, Dec 2014.

[43] W. D. Hulsbergen. Decay chain fitting with a kalman filter. *Nuclear Instruments and Methods in Physics Research Section A: Accelerators, Spectrometers, Detectors and Associated Equipment*, 552(3):566 – 575, 2005.

[44] M. Adinolfi et al. Performance of the LHCb RICH detector at the LHC. *Eur. Phys. J.*, C73:2431, 2013.

[45] R. Antunes-Nobrega et al. LHCb computing: Technical Design Report. Technical report, CERN, Geneva, 2005. Submitted on 11 May 2005.

[46] G. Barrand et al. Gaudi a software architecture and framework for building hep data processing applications. *Computer Physics Communications*, 140(1):45 – 55, 2001. CHEP2000.

[47] A. Morris. *Measurements of charmless B_s^0 meson decays at LHCb.* PhD thesis, The University of Edinburgh, Edinburgh, 2017.

[48] I. Belyaev et al. Handling of the generation of primary events in gauss, the LHCb simulation framework. *Journal of Physics: Conference Series*, 331(3):032047, dec 2011.

[49] S. Mrenna T. Sjöstrand and P. Skands. PYTHIA 6.4 physics and manual. *Journal of High Energy Physics*, 2006(05):026–026, may 2006.

[50] S. Mrenna T. Sjöstrand and P. Skands. A brief introduction to pythia 8.1. *Computer Physics Communications*, 178(11):852 – 867, 2008.

[51] D. J. Lange. The evtgen particle decay simulation package. *Nuclear Instruments and Methods in Physics Research Section A: Accelerators, Spectrometers, Detectors and Associated Equipment*, 462(1):152 – 155, 2001. BEAUTY2000, Proceedings of the 7th Int. Conf. on B-Physics at Hadron Machines.

[52] J. Allison et al. Geant4 developments and applications. *IEEE Transactions on Nuclear Science*, 53(1):270–278, Feb 2006.

[53] S. Agostinelli et al. Geant4a simulation toolkit. *Nuclear Instruments and Methods in Physics Research Section A: Accelerators, Spectrometers, Detectors and Associated Equipment*, 506(3):250 – 303, 2003.

[54] LHCb Collaboration. LHCb Trigger and Online Upgrade Technical Design Report. Technical Report CERN-LHCC-2014-016. LHCB-TDR-016, CERN, May 2014.

[55] R. Brun and F. Rademakers. Root an object oriented data analysis framework. *Nuclear Instruments and Methods in Physics Research Section A: Accelerators, Spectrometers, Detectors and Associated Equipment*, 389(1):81 – 86, 1997. New Computing Techniques in Physics Research V.

[56] R. Aaij et al. Precision Measurement of CP Violation in $B_s^0 \to J/\psi K^+K^-$ Decays. *Phys. Rev. Lett.*, 114:041801, Jan 2015.

[57] A. Höcker et al. TMVA - Toolkit for Multivariate Data Analysis. 2007.

[58] R. A. Olshen L. Breiman, J. H. Friedman and C. J. Stone. *Classification and regression trees.* CERN, Belmont, California, USA, 1984.

[59] Y. Freund and R. E. Schapire. A decision-theoretic generalization of on-line learning and an application to boosting. *Journal of Computer and System Sciences*, 55(1):119 – 139, 1997.

[60] L. Anderlini et al. The PIDCalib package. Technical Report LHCb-PUB-2016-021. CERN-LHCb-PUB-2016-021, CERN, Geneva, Jul 2016.

[61] A. Rogozhnikov. Reweighting with Boosted Decision Trees. *J. Phys. Conf. Ser.*, 762(1):012036, 2016. `https://github.com/arogozhnikov/hep_ml`.

[62] S. Benson et al. Measurement of the *CP*-violating phase ϕ_s using $B_s^0 \to J/\psi K^+K^-$ decays in Run 2. Private communication.

[63] M. Pivk and F. R. Le Diberder. SPlot: A Statistical tool to unfold data distributions. *Nucl. Instrum. Meth.*, A555:356–369, 2005.

[64] T. Skwarnicki. *A study of the radiative CASCADE transitions between the Upsilon-Prime and Upsilon resonances*. PhD thesis, INP. Cracow, 1986.

[65] L. Kish. Survey sampling. *Biometrische Zeitschrift*, 10(1):88–89, 1968.

[66] Y. Amhis et al. Averages of b-hadron, c-hadron, and τ-lepton properties as of summer 2016. *Eur. Phys. J.*, C77(12):895, 2017. Updated results and plots available at `https://hflav.web.cern.ch`, last visited on 30/12/2019.

[67] D. Martnez Santos and F. Dupertuis. Mass distributions marginalized over per-event errors. *Nuclear Instruments and Methods in Physics Research Section A: Accelerators, Spectrometers, Detectors and Associated Equipment*, 764:150 – 155, 2014.

[68] S. Stemmle. *CP violation and lifetime measurements in the decay $B_s^0 \to J/\psi\phi$ with the LHCb experiment*. PhD thesis, Universitat Heidelberg, Heidelberg, 2019.

[69] T. du Pree. *Search for a Strange Phase in Beautiful Oscillations*. PhD thesis, Vrije Universiteit, Amsterdam, 2010.

[70] R. Aaij et al. Measurement of the polarization amplitudes in $B^0 \to J/\psi K^*(892)^0$ decays. *Phys. Rev.*, D88:052002, 2013.

[71] H. G. Moser and A. Roussarie. Mathematical Methods for $B^0\overline{B}^0$ Oscillation Analyses. *Nucl. Instrum. Methods Phys. Res., A*, 384(CERN-OPEN-99-030. CERN-ALEPH-PUB-96-005. 2-3):491–505. 27 p, May 1996.

[72] E. Cohen, R. F. Riesenfeld and G. Elber. *Geometric Modeling with Splines: An Introduction*. A. K. Peters, New York, 2001.

[73] G. Raven T. Karbach and M. Schiller. Decay time integrals in neutral meson mixing and their efficient evaluation. Technical Report LHCb-INT-2013-043. CERN-LHCb-INT-2013-043, CERN, Geneva, Jul 2013.

[74] R. Aaij et al. Opposite-side flavour tagging of B mesons at the LHCb experiment. *Eur. Phys. J.*, C72:2022, 2012.

[75] R. Aaij et al. B flavour tagging using charm decays at the LHCb experiment. *JINST*, 10(10):P10005, 2015.

[76] R. Aaij et al. New algorithms for identifying the flavour of B^0 mesons using pions and protons. *Eur. Phys. J.*, C77(4):238, 2017.

[77] R. Aaij et al. A new algorithm for identifying the flavour of B_s^0 mesons at LHCb. *JINST*, 11(05):P05010, 2016.

[78] Scheme of tagging algorithms. `https://twiki.cern.ch/twiki/bin/view/LHCb/FlavourTaggingConferencePlots`. Accessed: 2019-10-15.

[79] D. Fazzini. *Proceedings, 6th Large Hadron Collider Physics Conference (LHCP 2018)*, volume LHCP2018. SISSA, 2018.

[80] R. Aaij et al. Measurement of *CP* asymmetry in $B_s^0 \to D_s^{\mp} K^{\pm}$ decays. *JHEP*, 11:060, 2014.

[81] F. James and M. Roos. Minuit - a system for function minimization and analysis of the parameter errors and correlations. *Computer Physics Communications*, 10(6):343 – 367, 1975.

[82] F. James. *The interpretation of errors*. CERN, 2004. `http://lmu.web.psi.ch/docu/manuals/software_manuals/minuit2/mnerror.pdf`.

[83] C. Langenbruch. Parameter uncertainties in weighted unbinned maximum likelihood fits. nov 2019.

[84] R. Aaij et al. Determination of the sign of the decay width difference in the B_s system. *Phys. Rev. Lett.*, 108:241801, 2012.

[85] R. Aaij et al. Amplitude analysis and the branching fraction measurement of $\bar{B}_s^0 \to J/\psi K^+ K^-$. *Phys. Rev.*, D87(7):072004, 2013.

[86] R. Aaij et al. Measurement of resonant and CP components in $\overline{B}_s^0 \to J/\psi \pi^+ \pi^-$ decays. *Phys. Rev. D*, 89:092006, May 2014.

[87] G. Breit and E. Wigner. Capture of slow neutrons. *Phys. Rev.*, 49:519–531, Apr 1936.

[88] R. Aaij et al. Resonances and CP violation in B_s^0 and $\overline{B}_s^0 \to J/\psi K^+ K^-$ decays in the mass region above the $\phi(1020)$. *JHEP*, 08:037, 2017.

[89] R. Currie. *CP-Violation in Beautiful-Strange Oscillations at LHCb*. PhD thesis, The University of Edinburgh, Edinburgh, 2014.

[90] R. Aaij et al. Measurement of the CP-violating phase β in $B^0 \to J/\psi \pi^+ \pi^-$ decays and limits on penguin effects. *Phys. Lett.*, B742:38–49, 2015.

[91] R. Aaij et al. Observation of the decay $B_c^+ \to B_s^0 \pi^+$. *Phys. Rev. Lett.*, 111:181801, Nov 2013.

[92] V. V Kiselev. Decays of the B_c meson. 2003.

[93] R. Aaij et al. Precision measurement of the $B_s^0 \to \overline{B}_s^0$ oscillation frequency with the decay $B_s^0 \to D_s^- \pi^+$. *New Journal of Physics*, 15(5):053021, may 2013.

[94] R. Aaij et al. Measurement of the CP-violating phase ϕ_s in $B_s^0 \to J/\psi\pi^+\pi^-$ decays. *Physics Letters B*, 736:186 – 195, 2014.

[95] R. Aaij et al. Measurement of the CP-violating phase ϕ_s from $B_s^0 \to J/\psi\pi^+\pi^-$ in 13 TeV pp collisions. *Physics Letters B*, 797:134789, 2019.

[96] R. Aaij et al. Resonances and CP violation in B_s^0 and $\overline{B}_s^0 \to J/\psi K^+K^-$ decays in the mass region above the $\phi(1020)$. *Journal of High Energy Physics*, 2017(8):37, Aug 2017.

[97] R. Aaij et al. First study of the CP -violating phase and decay-width difference in $B_s^0 \to \psi(2S)\phi$ decays. *Phys. Lett.*, B762:253–262, 2016.

[98] R. Aaij et al. Measurement of the CP-violating phase ϕ_s in $\bar{B}_s^0 \to D_s^+ D_s^-$ decays. *Phys. Rev. Lett.*, 113(21):211801, 2014.

[99] R. Aaij et al. Physics case for an LHCb Upgrade II - Opportunities in flavour physics, and beyond, in the HL-LHC era. Technical Report LHCB-PUB-2018-009. LHCC-G-171, CERN, Geneva, Aug 2018.

[100] V. Chobanova. Expected precision on ϕ_s for B_s^0 meson decays using LHCb data. Private communication.

[101] Heavy Flavor Averaging Group. Averages of b-hadron, c-hadron, and -lepton properties as of summer 2014, 2014. updated results and plots available at `https://hflav.web.cern.ch/`.

[102] T. Aaltonen et al. Measurement of the bottom-strange meson mixing phase in the full cdf data set. *Phys. Rev. Lett.*, 109:171802, Oct 2012.

[103] V. M. Abazov et al. Measurement of the CP-violating phase $\phi_s^{J/\psi\phi}$ using the flavor-tagged decay $B_s^0 \to J/\psi\phi$ in 8 fb^{-1} of $p\overline{p}$ collisions. *Phys. Rev. D*, 85:032006, Feb 2012.

[104] G. Aad et al. Measurement of the CP-violating phase ϕ_s in $B_s^0 \to J/\psi\phi$ decays in ATLAS at 13 TeV. 2020. `https://arxiv.org/abs/2001.07115`.

[105] CMS Collaboration. Measurement of the CP-violating weak phase phi-s and the decay width difference DeltaGamma-s using the Bs to J/psiPhi(1020) decay channel. 2014. `https://arxiv.org/abs/1507.07527`.

[106] O. Leroy. World averages for B_s^0 decays by the Heavy Flavor Averaging Group. Private communication.

[107] G. Raven T. Karbach and M. Schiller. Using splines to describe decay time acceptance. Private communication.